In-vitro quantitative assessment of ultrasonic contrast agents

Vassilis Sboros

Degree of Doctor of Philosophy

University of Edinburgh

1999

Declaration

I declare that the work contained in this thesis is my own, and that the thesis has been composed by myself.

Vassilis Sboros

To my parents Katerina and Paris

Acknowledgements

It is difficult to remember all those that contributed in many different ways during these years. It is difficult however to forget some of them.

Especially Norman and Carmel that fulfilled every possible role I could ever expect. Thank you for being always there for me, patient and understanding. I don't know of any students being granted so much initiative and freedom, as well as attention. I consider myself lucky to have met you, and I consider your presence almost as important as the thesis itself. Thank you for showing me the way.

Not easy to forget Tom either! Always there to materialise what was and especially what was not in my mind. Always having time to spare for me and show off his telepathic qualities with people. Thanks Tom.

Difficult to forget Steve too! Thank you Steve for being my ally (as wisely put by Carmel), and always willing to share my scientific worries (which happened quite often!).

I almost forgot Irene, maybe because I take our relationship for granted! Thank you Irene for making everything so simple for me and for being my friend.

What someone should never forget is his mentor. Thank you Mike for your sweating dedication, and hard work (even when it was in the pub).

Thanks also to Rab and Bob for building all my unfinished designs and turning them into something useful (for my work of course!).

I almost forgot Dr Soares and Dr Shao Feng Li! Thank you guys for taking my initiation in this job more seriously than I did. I wouldn't prefer dancing or chinese cooking lessons, honest!

Cannot forget Luk either because he is next to me while I am writing this. Thanks for all your input and unconditional help, never mind the sugar for my "early morning" coffees.

I am not allowed to forget Alistair, because he would never forget. As he modestly put it, I always came out with something when I needed him. Even if that is degassing!

Thank you Aline and Mike for doing it for me when I was useless.

Not easy to forget the help, such as the one I got from Ian, Bill, Iain, Bill, Kumar, Pete, Calum, Robin, Scott, Catriona, and Gillian.

I shouldn't forget to thank my Greek friends Kostas, George, Sandra, Dimitris, Yannis, Yannis, Panos, and Thanasis because I might need them in the future!

Impossible to forget Jill's smile too.

Table of Contents

Abbreviations

CA(s)	Contrast agent(s)
TGC	Time Gain Compensation
ROI	Region of Interest
BMF	Blood Mimicking Fluid
NB	Normalised Backscatter
OB	Overall Backscatter
HSA	Human Serum Albumin
MI	Mechanical Index
POP	Percent Output Power

List of Tables

Abstract

Contrast agents are new to the field of diagnostic ultrasound. Their use has been shown to have potential in the diagnosis of different pathological conditions. The prospect of quantitatively assessing perfusion also seems promising. Contrast agents in ultrasound, like in other imaging modalities, aim to enhance the signals reflected from the areas of interest, therefore improving the sensitivity and specificity of new diagnostic techniques and physiological indices.

One of the novel features of ultrasonic contrast agents is that they interact with the beam in a versatile way. In-vitro work in recent years has been focussed on the understanding of the interaction of the contrast agents with the ultrasonic beam. Two main areas of research have evolved through that effort. The first aims in improving the scanning technology in order to optimise the contrast imaging, and the second to assess the physical properties of the agents. It is important to have an accurate understanding of how the agents interact with the transmitted beam and how they are affected by their environment. This thesis aims to be a contribution to this understanding.

The agents Levovist, Quantison™, Myomap™, and DMP115 were used in the various investigations. The experiments were based on acquiring the ultrasonic echoes created by the agents in water suspensions. Radiofrequency echo data frames were collected with an ATL Ultramark 9 Scanner (UM9). The normalised mean backscatter intensity of a region of interest in the image was calculated and formed the basis of the quantitative analysis. Normalisation was carried out using tissue or blood mimicking material as the reference target.

Levovist displayed a diminished backscatter when introduced into degassed water. An extended stability study varying the acoustic pressure showed that Quantison™ and Myomap™ exhibited accelerated decay at higher acoustic pressures in a degassed environment. The backscatter properties changed with time and varied amongst agents in continuous imaging, and the feasibility of quantitative measurements using this imaging approach was fully explored in-vitro. A newly defined physical quantity called Overall Backscatter that equals the integral of the

decay of the normalised backscatter intensity over time, showed that it could optimally describe the properties of the agents in in-vitro imaging.

A new imaging approach had to be implemented in order to isolate the scattering properties of the contrast agent from its destruction process. To achieve this, individual scan sweeps were performed at defined intervals. The normalised backscatter of the agents was modelled as a function of the bubble concentration and the peak negative pressure. Using very low concentrations, individual bubbles were studied, and it was found that contrast agents scatter proportionally to the 3rd order of acoustic pressure. The results also suggested that above 0.6MPa peak negative pressure, free bubbles were formed for Quantison™ and DMP115.

Further work using an advanced version of the system assessed the optimal setting for imaging DMP115 in-vitro. A wide range of settings was provided: pulses between 2-10 cycles, frequency range 1-4.5MHz transmit and 1-8MHz receive, and acoustic pressure 0.08-2MPa. This allowed the extraction of the fundamental, 2nd and 3rd harmonic components of the signal. This agent displayed a dominant resonant frequency between 1.5 and 1.8MHz. A peak normalised backscatter for the harmonic signals was also found at acoustic pressures of around 0.5MPa. The length of the pulse also proved important at low acoustic pressures, which strongly suggested that the bubbles remained encapsulated at those pressures.

Using this novel and efficient system, it has been possible to elucidate the properties of microbubble contrast agents in-vitro.

1 Chapter One: Introduction

Contrast media were introduced in diagnostic imaging modalities to improve the sensitivity and specificity in clinical investigations. A wide range of pathology is diagnosed using contrast agents in computerised tomography (CT) and magnetic resonance imaging (MRI).

The attenuation caused to the X-ray beam varies approximately as the fourth power of the atomic number of a material (Webb, 1988). X-ray imaging (including transmission computed tomography, CT) is based upon the principle of mapping the transmitted energy through tissue. Contrast media have been used extensively in X-ray imaging. The purpose of these agents is to increase the atomic number in a targeted area, and therefore reduce the transmission of the beam. Clinical applications include angiography, as well as different types of intravascular or oral CT investigations.

Another major diagnostic tool is magnetic resonance imaging (MRI). Images obtained using this imaging technique map proton spin density and relaxation time. Contrast agents for MRI, which are paramagnetic, are used in order to enhance the relaxation times of protons which are close to them (Carr, 1988).

Diagnostic ultrasound imaging maps the reflection of ultrasound in tissue. The reflection of ultrasound is caused mainly by the acoustical impedance (similar to the refraction index in optics) mismatch of neighbouring tissues, and therefore outline different anatomical structures (McDicken, 1991). Ultrasound is a mechanical wave, and if the reflecting structure is a few times larger than the wavelength then the interaction is called specular reflection. If the reflecting structure is of a similar or smaller size than the wavelength then the interaction is called scattering. Contrast agents in ultrasound aim at enhancing the scattering from tissue. In general ultrasonic contrast agents are coated gas bubbles the majority of which are subcapillary in size. Even though the discovery of ultrasonic contrast agents dates back to the late sixties (Gramiak and Shah, 1968 and 1969), it is only in recent years that the potential of ultrasound contrast imaging is being realised. Contrast agents are starting to be routinely used in diagnostic ultrasound.

All the above major modalities of diagnostic imaging use contrast agents in order to improve image contrast. However ultrasonic contrast agents offer a versatility of interaction with the ultrasonic beam which does not occur with X-ray or MRI contrast agents. Microbubbles oscillate when subjected to an ultrasonic beam (Medwin, 1977). Their scattering properties, and subsequently the enhancement of ultrasound images, can alter depending on the nature of the oscillation. This varied interaction between contrast agents and the ultrasonic beam has created a research area in ultrasound in the pursuit of the explanation of the acoustical behaviour of those bubbles and their interaction with ultrasound.

1.1 The story so far

1.1.1 Development of ultrasonic contrast imaging

The discovery of contrast ultrasonography dates back to the late sixties (Gramiak and Shah, 1968). However the materials, indocyanine green solution and saline, did not produce stable microbubbles, which were not able to pass through the lungs. It was not until 1991 that Echovist (Schering AG, Berlin, Germany) first became commercially available in Germany (Nanda and Schlief, 1993). It is a galactose-based agent enclosing air microbubbles which does not withstand pulmonary passage, and therefore limited to the enhancement of the right heart (Albrecht and Bromley, 1997), and nonvascular cavities such as in hysterosalpingography (Ayida et al, 1996). The first agent that achieved pulmonary passage and produced echo enhancement in the left ventricle of the heart was Albunex (Molecular Biosystems, San Diego, US). This agent consisted of air microbubbles coated by an albumin shell (Feinstein et al, 1990). Evaluation of that agent showed that it did not behave like an ordinary Rayleigh scatterer but resonated at frequencies within the range of frequencies used in diagnostic ultrasound (Bleeker et al, 1990). The agent that achieved clinically useful vascular enhancement was the successor of Echovist, called Levovist (Schering AG, Berlin, Germany). This agent was more stable in the vascular bed than the previous two. Albunex and Levovist were the first two agents which revealed the potential application for ultrasonic

contrast imaging in monitoring vascularity and perfusion (Wilson et al, 1993; Schlief, 1991).

The need to understand the properties of contrast agents became apparent. In-vitro work showed that the oscillatory motion of these bubbles was non-linear (Schrope et al, 1992; de Jong et al, 1994), and it was demonstrated that the harmonics generated might provide a more sensitive way of imaging the contrast agents (Schrope and Newhouse, 1993; Burns, 1994). The contrast microbubbles emit the harmonic signal at twice the transmitted frequency, and therefore the signals received at the 2^{nd} harmonic frequency window, would significantly improve the contrast to tissue signal ratio.

In an attempt to assess the potential of myocardial perfusion measurements using contrast echocardiography, it was discovered that the bubbles can be destroyed in the ultrasonic field (Porter and Xie, 1995). Consequently, if the imaging was not continuous but triggered in every cardiac cycle, it was discovered also that the contrast enhancement of the myocardium was greatly improved. Triggered imaging allows time for contrast microbubbles to be introduced into the field of view and be visualised in a single frame before being destroyed.

The great improvement of sensitivity produced by these discoveries and the potential applications in the assessment of perfusion boosted the field of contrast imaging. The development of several new, more sophisticated and chemically stable contrast agents followed (Table 1.1). Less soluble gases like fluorocarbons were introduced, which further increased the stability of these agents within the vascular bed.

At the same time, major advances were also achieved in imaging technology. It was shown that Doppler intensity measurements provided an imaging tool with the same dynamic range as the radiofrequency data which has a wider dynamic range than ordinary B-mode imaging (Schwarz et al, 1995). Combined harmonic Doppler intensity in triggered mode proved to be one of the most sensitive approaches in detecting the echoes from contrast agents (Tiemann et al, 1997). With this technique arterioles of the size of 40μm were visualised, which was an improvement of more than 10 times in the spatial resolution of the image (Burns, 1996). Colour Doppler,

which is based on correlation of consecutive Doppler signals, benefited due to the collapse of microbubbles in one frame at high acoustic pressures. Consequently consecutive Doppler signals were not well correlated resulting in a new imaging method of detecting contrast agents using the Doppler technique LOC- (loss of correlation) imaging (Uhlendorf and Hoffman, 1994; Bauer et al, 1997). Further improvement in the detection of the harmonic signals was achieved by transmitting a pulse sequence modified by inverting every second transmit pulse (Simpson et al, 1999). The technique is referred to as Pulse Inversion Doppler. Received consecutive signals are subtracted and/or added in order to isolate the fundamental frequency component from the second harmonic, which is primarily generated by the contrast agent. The technique promises both improved resolution and sensitivity of 3 to 10 dB when compared to the ordinary harmonic mode.

Table 1.1 *The new generation of contrast agents*

Agent	Coating	Gas	Mean Size (μm)
Infoson™	HSA	Air	3
Echogen	(phase shift)	Dodecafluoropentane	2-5
Sonovue™	Lyophile	SF_6	2.5
FSO69	HSA	Perfluoropropane	3
Imagent	(not available)	SF_6	6
DMP115	Liposome	Perfluorocarbon	2.5
BY963	Phospholipid	Air	3.8
Sonovist	Cyanocrylat polymer	Air	2
Quantison™	Albumin	Air	3.2
Optison	HSA	Perfluoropropane	3.2
NC100100	(not available)	(not available)	(not available)

Phase shift in the case of Echogen is the shift from the liquid phase to the gas phase (i.e. formation of contrast microbubbles) at body temperatures. HSA: human serum albumin. Further information for NC100100 is not available

1.1.2 Clinical applications

1.1.2.1 Qualitative investigations

The first published report on contrast ultrasound imaging came from Gramiak and Shah in 1968, which reported enhancement of cardiac structure identification using indocyanine green dye. Today contrast agents are beginning to be used in stress echocardiography. Visualisation of myocardial vascularisation and ischaemic tissue in animal as well as human studies have been reported (Kaul et al, 1989; Villanueva et al, 1992; Villanueva et al, 1993; Porter and Xie, 1995; Porter et al, 1996; Lindner et al, 1998, Wei et al, 1998).

The contrast agents which reached the vascular system led to amplification of Doppler signals. The visualisation of the renal arteries was greatly improved, the Doppler intensity was amplified by 20dB, and as a result the sensitivity and specificity of renal artery stenosis detection was increased (Missouris et al, 1996). The visualisation of the circle of Willis was almost impossible without the use of contrast agents. Their use showed potential applications in the detection of intra-cranial aneurysms and of some intra-cranial tumours (Bauer et al, 1996).

The use of contrast agents in colour Doppler enhanced the irregular and chaotic vascularisation of tumours. Published investigations deal with breast, and liver cancers (Albrect and Bromley, 1997; Leen et al, 1994; Solbiati et al, 1996).

1.1.2.2 Quantitative investigations

The great enhancement of signals in early in-vivo work (35dB) showed potential in the assessment of myocardial perfusion (Burns et al, 1994). Perfusion may be broadly defined as the nutrient delivery from blood to tissue. Oxygen delivery to aerobic tissue is regarded to be representative of perfusion (Lindner and Kaul, 1995). It has also been shown that oxygen consumption in the myocardium correlates with coronary blood flow (Rubio and Berne, 1975). Therefore measuring myocardial blood flow could approximately assess myocardial perfusion. Contrast echocardiography and the assessment of myocardial perfusion is perhaps the most prolific area of research in ultrasonic contrast imaging. Comparisons with other imaging modalities have favoured contrast echocardiography in the assessment of myocardial perfusion (Lindner and Kaul, 1995), mainly because ultrasound contrast agents are good indicators of flow, since their kinetics were similar to red blood cells.

Ex-vitro as well as animal studies illustrated the potential of quantitating myocardial perfusion using mathematical modelling in order to extract useful indices that differentiate abnormal from normal tissue (Kaul et al, 1989; Villanueva et al, 1992). Infusion of contrast showed that myocardial perfusion studies can be reproducibly simulated (Wei et al, 1998).

Other potential applications for quantitative ultrasonic contrast imaging involve renal artery stenosis assessment (Correas et al, 1996), and differentiation of tumours from benign lesions (Albrecht and Bromley, 1997).

1.2 The physics of contrast

It is important to review briefly the physics of scattering from ultrasonic contrast agents, and explore the existing understanding of the interaction of the contrast agent microbubbles with the ultrasonic beam. The scattered intensity of ultrasound from a single scatterer is:

$$I_s = I_i \, \sigma \tag{1.1}$$

where I_s is the scattered intensity, I_i is the incident intensity of sound, and σ is the scattering cross-section, which is a measure of the scattering strength of the scatterer.

The scattering cross-section σ for a scatterer that is much smaller than a wavelength (Rayleigh scatterers) is given by (Morse and Ingard, 1968):

$$\sigma = \left(\frac{4}{9} \pi \alpha^2 (k\alpha)^4 \right) \left(\left(\frac{\kappa_s - \kappa}{\kappa} \right)^2 + \frac{1}{3} \left(\frac{3(\rho_s - \rho)}{2\rho_s - \rho} \right)^2 \right) \tag{1.2}$$

where α is the radius of the scatterer ($<<\lambda$), λ is the wavelength, $k = 2\pi/\lambda$ is the wavenumber, κ_s is the compressibility of the scatterer, κ is the compressibility of the surrounding medium, ρ_s is the density of the scatterer, and ρ is the density of the surrounding medium.

Simple calculations by Ophir and Parker (1989), for a liquid environment showed that the scattering cross-section is very large for a gas scatterer compared to a solid or liquid scatterer. This is because the gradients of compressibility and density become very large for a gas particle (de Jong et al, 1991).

If the bubble is compressible it would oscillate when subjected to a mechanical wave like an ultrasound wave. The maximum amplitude of oscillation is exhibited at the natural frequency (called the resonant frequency) of the oscillator. Anderson and Hampton (1980) observed resonance phenomena in microbubble scatterers. Their theoretical predictions agreed with their measurements. The scattering cross-section σ for an air bubble in a liquid has been shown to approximate to (Anderson and Hampton (1980)):

$$\sigma \approx \frac{4\pi\alpha^2}{\left[\left(\frac{f_0}{f}\right)^2 - 1\right]^2 + \left(\frac{f_0}{f}\right)^4 \delta^2} \tag{1.3}$$

where α is the radius of the air bubble, f is the insonating frequency, f_0 the resonant frequency, and δ is the damping constant given by (Medwin, (1977)):

$$\begin{aligned} \delta &= \delta_{th} + \delta_{vis} + \delta_{rad} \\ \delta_{rad} &= k\,\alpha \\ \delta_{vis} &= 4\eta/\rho\omega\, a^2 \\ \delta_{th} &= B\,\omega_r^2 / \omega^2 \end{aligned} \tag{1.4}$$

where δ_{th} is the thermal damping, δ_{vis} the viscous damping, δ_{rad} the re-radiation damping, k the wave number, η the viscosity, ρ the density of the surrounding liquid, ω the applied angular frequency, ω_r the angular resonant frequency:

$$\omega_r^2 = \omega_{ri}^2 + 8\pi Et/(1-\nu) \tag{1.5}$$

where ω_{ri} is the resonant frequency of an ideal gas bubble, E the shell elasticity, t the wall thickness, and ν the Poisson ratio (de Jong et al., 1992).

Using this model de Jong and Hoff (1993) calculated the backscatter from Albunex, and found that it was in good agreement with their measurements. Another important outcome was that the backscatter spectrum did not have a maximum value at any frequency, mainly due to the wide size distribution of the Albunex microbubbles.

The resonant bubble might also undergo a non-linear oscillation, which is responsible for emission of harmonic signals. Even at low incident power of incident wave harmonic emission was detected (Miller, 1981). De Jong et al (1994a)

attempted the first numerical calculation of the harmonic behaviour of Albunex scatterers using a linear model. The result showed peak amplitude for the harmonic signals around 2MHz. The amplitude of the 2^{nd} harmonic was slightly underestimated, as shown by experiment (de Jong et al, 1994b), and it was speculated that a linear model of the motion might be inadequate.

More recent experimental work has shown several different acoustical characteristics of the bubbles. The 2^{nd} harmonic signals have been measured to increase linearly with the square of the acoustic pressure amplitude for Albunex, while the relationship was more complicated for FSO69 (Krishna and Newhouse, 1997). Morgan et al (1998) have found that the intensity ratio of 2^{nd} harmonic to fundamental did not increase at high acoustic pressures (>0.5MPa), a behaviour displayed at low acoustic pressures. This was accompanied by the observation that at high acoustic pressures, bubble destruction usually occurs during single frame exposures. Chin and Burns (1997) calculated that at high acoustic pressures the energy is transferred to higher harmonics. The bubble oscillation and destruction has also been microscopically investigated recently (Dayton et al, 1999). This study witnessed gas diffusion, shell deformation, shell destruction, or bubble fragmentation.

The in-vitro work with contrast agents does not yet provide sufficient background information to build a solid mathematical model that explains the bubble motion in the ultrasonic field. The understanding of this oscillation for each agent is a fundamental requirement essential for optimising ultrasonic imaging settings.

1.3 Ideal requirements for ultrasonic contrast agents

The ideal contrast agent needs to fulfil several requirements. It is however difficult to categorise them efficiently in order to review the work that has been carried out so far, and highlight the gaps of knowledge in the field. Wiencek et al (1993) have presented them in a concise manner. A similar approach is followed here. Firstly the agents must be safe. Secondly the flow of the agents in the vascular bed must be representative of the existing flow. Thirdly a consistent relationship

must exist between the number of bubbles and the backscatter intensity, and an adequate dynamic range of enhancement must be produced. Fourth the agent must not recirculate. Fifth the agent must not alter any of the haemodynamic or any other parameters that it is attempting to measure, and sixth the agent must not decay or must decay in a predictable manner.

1.3.1 Safety

It is obvious that the agents must have no significant side effects and no toxicity. The concern mainly arises by the biological damage induced via the mechanism of acoustic cavitation, the size of the microbubbles that might occlude the blood circulation, and also the toxicity of the agent materials. All agents undergo tests in order to qualify for commercial and clinical approval.

Safety precautions also involve the interaction of ultrasound and the contrast bubbles. Cavitation induced hazard has attracted the attention of many investigators. It has been suggested that the presence of contrast agents act as cavitation nuclei and lower the cavitation thresholds (Miller and Thomas, 1995). Heamolysis, which is one of the most important bio-effect of cavitation in diagnostic ultrasound, was shown to be induced at peak positive pressures around 10MPa in the presence of contrast agents (Miller and Thomas, 1996). More modern agents with non-soluble gases like FSO69, have shown that they enhance the potential of cavitational effects (Miller and Gies, 1998). In general, at diagnostic imaging settings the presence of contrast agents has been shown to be safe (Brayman et al, 1995; Dalecki et al, 1997). Contrast manufacturers recommend avoiding lithotripsy for at least 24 hours after administration of the agent, since contrast bubbles can provide cavitation nuclei in the blood stream for several hours after administration.

1.3.2 Rheological properties

It is very important for all contrast agents to have similar flow characteristics to the system they are trying to characterise. Therefore if injected intravenously they must cross the lungs in order to be distributed in the blood pool. This property has been demonstrated for most of the agents in Table 1.1 (Mor-Avi et al, 1993; Goldberg et al, 1993; Unger et al, 1994; Correas and Quay, 1996; Broillet et al,

1998), while similar experiments are due for the rest. It is also desirable for the agents to have a flow pattern similar to red blood cells. It has been demonstrated, microscopically, that the rheology of sonicated albumin is very similar to that of red blood cells (Keller et al, 1989) and a high correlation between myocardial transit rate of contrast bubbles and flow has been established (Jayaweera et al, 1994), despite the differences in shape and size distribution between contrast bubbles and red blood cells.

1.3.3 Backscatter relationship and dynamic range

To perform either a qualitative or a quantitative assessment of contrast enhancement it is desirable to have a constant relationship between the backscatter intensity and the concentration of bubbles. Scattered intensity from different agents has been shown to be linearly proportional to the number of bubbles at low bubble concentrations (de Jong and Hoff, 1993). Further increase of the concentration does not provide a linear increase in backscatter intensity (Wiencek et al, 1993). Moreover, in an in-vivo situation, artefacts and varying attenuation patterns across an image will distort the relationship between backscatter intensity and bubble concentration (Rovai et al, 1997).

The dynamic range of the echoes received from contrast agents must be sufficiently wide to provide high sensitivity and specificity for diagnostic assessment. Significant improvements with the introduction of triggered, power Doppler and 2nd harmonic imaging, have been noted. Triggered imaging is based on the acquisition of frames at specific time intervals, usually one ultrasound frame acquired per cardiac cycle or multiple cardiac cycles. Exposure to ultrasound is known to destroy the contrast bubbles, and triggering allows time for the agent to re-perfuse the vascular bed (Porter and Xie, 1995). 2nd harmonic imaging was initially reported to increase contrast to tissue enhancement by 35dB (Burns et al, 1994). Bubbles insonated at a particular frequency will oscillate non-linearly and emit harmonic signals. These harmonic signals are much larger in amplitude than those produced by tissue, since tissue exhibits less non-linearity (Burns, 1996). Power Doppler imaging has been shown to provide maximum dynamic range provided only be the raw signal in B-

mode (Schwartz et al, 1995), and has been shown to improve the sensitivity of contrast imaging (Burns, 1996). An improved combined imaging modality was created and called pulse inversion 2nd harmonic Doppler and has demonstrated further enhancement of sensitivity (Simpson et al, 1999).

1.3.4 Recirculation

Although some agents such as Albunex do not recirculate (Wiencek et al, 1993), the more modern agents are expected to recirculate for several minutes after the injection, as in the case of Levovist (Goldberg et al, 1993). For the quantitative assessment of perfusion, recirculation can distort the indicator dilution measurements at first pass, when the agent is injected intravenously.

A new approach that uses infusion of the agent provides a quantitative assessment of perfusion without requiring the agent to have some of the basic tracer kinetics (Wei et al, 1998). The principle of the technique is based on the destruction mechanism of the bubbles due to exposure to the ultrasonic field. Frames were triggered at different time intervals. Assuming the ultrasound exposure of one frame is enough to destroy all the contrast bubbles in the field of view, and the time interval between triggered frames is too short to allow contrast to be distributed across the field of view, the enhancement of backscatter provided by the contrast would be very small. Increase of the enhancement was associated with increase of the time interval between triggered frames. When the field of view is filled with contrast agent, further increase of the time interval would not increase the enhancement. The function describing the relationship between the enhancement of backscatter and the time interval at a particular region of interest contains parameters that highly correlate with the flow at that region, and can accurately and reproducibly illustrate it.

1.3.5 Haemodynamic effects

It is also important that the injected agent does not alter any of the physiological parameters that are measured in contrast imaging. Albunex was the first agent to prove that there were no significant physiological adverse effects related to it (Feinstein et al, 1990; Christiansen et al, 1994). Most modern agents have published data on safety as well as possible effects on the circulation (Goldberg,

1997, Lindner et al 1998). Levovist has been reported to alter, though not significantly, some haemodynamic parameters in dogs (Schwarz et al, 1996).

1.3.6 Stability

There are several parameters that might affect the stability of the bubble. Contrast agents must exhibit chemical stability, since they are subjected to a chemically variable environment when injected in-vivo. Only the new generation of agents (Table 1.1) overcome such problems, and chemical stability is no longer a concern.

Reduced gas concentration in a suspension of contrast diminished the acoustic enhancement of Albunex microbubbles (Wiencek et al, 1993; Wei et al, 1997). A more modern agent, FSO69, did not show a reduced acoustic enhancement in a degassed environment (Wei et al, 1997). This area is explored further in chapter 4.

Inspection of Albunex microbubbles subjected to 160mmHg hydrostatic pressure showed that the bubbles deform and disappear (De Jong et al, 1993). This was in agreement with Vuille et al (1994) who noticed that the constant application of increasing hydrostatic pressure would proportionally reduce the reflectivity of the bubbles of both Levovist and Albunex in an irreversible way. Destruction and accelerated diffusion of the bubbles were suggested to be responsible for this effect. Pulsatile pressure induced a cyclic variation as well as an overall decrease in backscatter for hand agitated Angiovist (diatrizoate meglumine and diatrizoate sodium; Berlex Laboratories, Wayne, NJ, USA) which suggested accelerated diffusion as the likely mechanism to explain the decay of the agent (Padial et al, 1995).

Increased viscosity is related to reduction of the size of bubbles. An experiment that included Renograffin 76, solutions of sorbitol, and dextrose, showed that increased viscosity in-vitro offers stability to bubbles small enough to pass the capillaries (Koenig and Meltzer, 1986).

Reduction of temperature increased the lifetime of microfoam solutions (Sebba, 1971). Increased temperature reduced the number of bubbles in suspension

for Aerosomes MRX115 (ImaRx Pharmaceuticals), and Imagent (Alliance Pharmaceuticals) (Sahn et al., 1997).

The application of ultrasound has been shown to be responsible for the decay of backscatter from contrast agents (Wei et al, 1997; Wu and Tong, 1998; Moran et al, 1998). Microscopic investigation showed that contrast bubbles are destroyed due to the ultrasonic field (Wu and Tong, 1998; Dayton et al, 1999). Diffusion of the gas out of the shell occurs at low acoustic pressures. At higher pressures fragmentation of Optison into sub-μm size bubbles was observed, while Albunex displayed an ejection of fragments. Formations of defects in the shell have also been observed microscopically.

Continuous imaging is therefore responsible for low echoes from contrast due to bubble destruction. Triggered imaging allows time for new bubbles to appear into the field of view and therefore provide with enhanced image contrast (Porter et al, 1996).

All the above parameters affect the stability of contrast bubbles in-vivo. Little has been reported in the literature about the behaviour of the different agents, and little is known of their usefulness on quantitative measurements. Further research work is awaited to improve knowledge on the stability of contrast agents, and also to create reproducible imaging approaches.

1.4 Aims of the project

There are several fronts of active research in the field of ultrasonic contrast agents. New applications for the agents are being devised and their potential evaluated. All the requirements stated above for contrast agents constitute the basic areas of research in the field of ultrasonic contrast agents.

This thesis aims to improve the understanding of the interaction of the contrast microbubbles with the ultrasonic beam as used in medical diagnosis. The understanding of this interaction can be divided into two categories. The first involves measurement of the backscatter from the contrast bubbles, and the second involves the decay or destruction of the microbubbles caused by the beam.

Another parameter that affects the stability of contrast bubbles, and about which little is known, is the gas concentration of the suspension environment. It is also vital to explore this area for this thesis, since in-vitro studies are based on suspensions in liquids. Hydrostatic pressure, viscosity and temperature are more or less constant in an in-vitro set-up, but the dissolved gas varies and might affect the contrast bubbles.

1.4.1 Aims of the thesis

The aim of this thesis is to develop reproducible techniques for the qualitative and quantitative use of contrast agents by carrying out the following investigations:

1) Investigate and discuss the stability of bubbles due to:
   a) The suspension environment
   b) The ultrasonic beam
2) Investigate the physical properties of contrast agents
3) Investigate the settings that optimise contrast imaging
4) Assess the potential of continuous and triggered imaging in quantitative measurements
5) Understand bubble behaviour in the ultrasonic field

1.4.2 Layout of the thesis

Chapter 2: Introduction and evaluation of the in-vitro set up. Introduction of the physical quantity of normalised backscatter.

Chapter 3: Preliminary experiments and introduction to the contrast agents.

Chapter 4: Stability study of contrast agents in a degassed environment.

Chapter 5: Stability study of contrast agents in a degassed environment, and a range of acoustic pressures. Investigation of the destruction of bubbles. Introduction to backscattering properties of different contrast agents. Definition of the term 'Overall Backscatter' for quantitative measurements in continuous imaging.

Chapter 6: Reproducibility study in continuous imaging with contrast agents. Investigation of the potential of continuous imaging to perform quantitative measurments. Evaluation of the Overall Backscatter.

Chapter 7: Acoustic saturation of contrast agents. Acoustic behaviour of a cloud of contrast agent scatterers.

Chapter 8: Study of the properties of individual contrast agent scatterers.

Chapter 9: Introduction and evaluation to an advanced in-vitro set-up.

Chapter 10: Assessment of the optimal settings for contrast imaging. Investigation on the bubble motion.

Chapter 11: General conclusions and future research.

2 Chapter Two: The experimental set-up

2.1 Introduction

The aims of this thesis were set-out in the previous chapter. The need for a robust in-vitro experimental set-up would allow the identification of the individual imaging machine settings required for each agent so as to optimise their performance under different physical environments and imaging conditions. This chapter presents and evaluates the system used in the main part of the thesis. The system was based on a water filled anechoic test tank into which a quantity of ultrasonic contrast agent is introduced. The resulting suspension is then scanned and echo signals are collected by means of a radiofrequency (RF) data capture system, which enables quantification of the backscatter information of an insonated Region Of Interest (ROI) (Moran et al. 1994). This avoids the limitations introduced by videodensitometric techniques as discussed by Bijnens et al (1994), and Rovai et al (1993).

2.2 Materials and methods

2.2.1 Acquisition of data

2.2.1.1 The tank

The perspex tank used in the experiments was lined with an acoustic absorber (CERAM AB, Lund, Sweden) which according to the manufacturer, for 3MHz ultrasound, produces an echo 32dB below that of a perfect reflector. The size of the tank was 9cm high by 9cm long by 5cm wide. The tank was filled with 200ml of sterile water, in order to ensure high chemical purity and avoid possible chemical interaction with the contrast agents. The distance of the scanning surface of the ultrasound imaging probe from the bottom of the tank was fixed at 4.3cm. As described below, the ultrasound field in the tank was measured using a calibrated needle hydrophone.

The contrast agents were introduced into the tank using positive displacement pipettes (Microman®, Gilson Medical Electronics, France). The range of volumes

was from 1μl-1ml, with variable standard errors that never exceeded 6% (for 1μl) according to the manufacturer's specification. A comparative test, by means of triggered frames, was performed to check the accuracy of two pipettes in terms of injected contrast. Two pipettes, one with range 1μl-10μl and the other with range 10μl-100μl, were used to introduce the same quantity of contrast in the tank. At 5μl the average backscatter of 5 batches of 5 frames was significantly different for the two pipettes, but above 7μl the two pipettes did not provide contrast volumes with significantly different average backscatter ($p<0.05$). This was strongly suggestive of the high accuracy of the second pipette at volumes below the recommended by the manufacturer range.

After the introduction of the agent, the suspension was agitated by means of a variable speed magnetic stirrer (B211 Bibby Science products Ltd, UK). Also there was a choice of different magnetic bars such as oval or pivot ring of variable sizes. This proved to be of great importance to the accuracy and reliability of the measurements. For example, an oval bar needed higher speed than the pivot ring to give a homogeneously mixed suspension. The homogeneity of mixing of the suspension was also related to the size of the bar. However the pivot ring was more likely to create air bubbles in the suspension which would increase the standard error of the measurement. Thus an oval bar was preferably used for the experiments with contrast agents.

2.2.1.2 The scanner

An ATL Ultramark 9 (UM9) scanner (Advanced Technology Laboratories, Bothell, WA, USA) was used to scan the resulting contrast agent suspension contained in the tank. A phased array probe was used with a centre frequency of 3MHz, and 1.8MHz bandwidth at 6dB down from the peak amplitude. Figure 2.1 illustrates the experimental set-up.

The acoustic output power of insonation was controlled via the scanner console and could be varied from 2.24% to 100% of maximum, as displayed on the scanner's monitor. The calibration was performed using a PVDF needle hydrophone with an active area of 0.2mm (Precision Acoustics Ltd, England), calibrated by the National Physical Laboratory. Table 2.1 shows in detail the measurements of peak negative pressure (P^-), peak positive pressure (P^+) and rms acoustic pressure

amplitude at 3cm distance from the probe face. Those measurements are estimated to be within 5% accurate. Using a spectrum analyser (TF2370, Marconi Instruments Ltd) the amplitude of the fundamental frequency of the transmitted pulse, as well as the second harmonic, were measured and are shown in Table 2.1. The calculation of the spatial peak pulse average intensity was performed using the formula $I_{SPPA} = P_{rms}^2 / \rho c$,where P_{rms} is the spatial peak rms pressure, ρ is the density of water, and c is the speed of sound in the water (Preston 1991). The pulse length was measured using the IEC (International Electrotechnical Commission) definition, as described by Livett and Preston (1985).

A personal computer (PC) was used to download the acquired data and to record the values of scanner overall gain and time gain compensation (TGC) settings. All experiments were carried out at fixed gain and TGC.

Table 2.1 *Ultrasonic field measurements at 3cm distance from probe face*

Percent output power (%)	P^- (MPa)	P^+ (MPa)	rms (mV)	Intensity (W/cm^2)	Fundamental (μV)	2nd Harmonic (μV)
2.24	0.27	0.25	5.64	0.86	63	0
12.59	0.58	0.54	12.5	4.23	123	9
17.78	0.69	0.66	14.7	5.83	150	12
25.12	0.83	0.77	18.4	9.12	174	18
35.48	0.96	0.90	21.3	12.3	210	27
50.12	1.15	1.05	26.4	18.9	240	36
70.79	1.37	1.24	33.6	30.4	300	50
100	1.52	1.37	35.3	33.6	320	60

Percent output power (%) is the percent output power of the transmitted beam as indicated on the scanner's monitor, P^- is the peak negative pressure in MPa, P^+ is the peak positive pressure in MPa, rms is the root mean square voltage of a pulse in mV, Intensity is the spatial peak pulse average intensity in W/cm^2, Fundamental is the amplitude of the signal for the fundamental frequency as measured by a spectrum analyser in μV, 2nd Harmonic is the amplitude of the 2nd harmonic signal as measured by the spectrum analyser in μV.

2.2.1.3 The data acquisition system

A proprietary data acquisition module (DAM) manufactured by ATL was used to acquire the RF data from the scanner. Each frame of data consisted of 128 lines by 1024 pixels of RF data digitised to 12 bits at 12MHz. Each frame thus

occupied approximately 0.25Mbyte of stored data. A maximum of 15 frames could be acquired using the DAM. Data is transferred from the DAM to the PC (Storage in Figure 2.1) in the form of 16 bit words. Only the 12 most significant bits hold valid data. The 12 bit samples provide a theoretical dynamic range of 72dB.

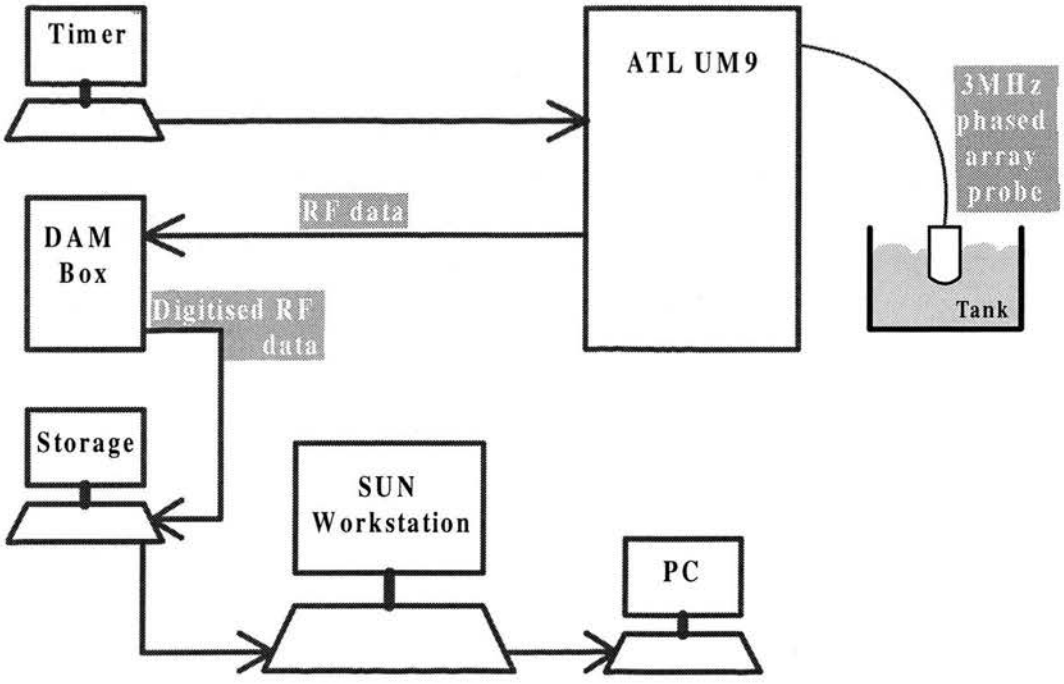

Figure 2.1 The data acquisition and analysis system.

This PC was also used for monitoring both overall gain and time gain compensation (TGC) values, and to initialise the acquisition of the frames. The software controlled the number of frames, the digitisation rate, the selection and number of lines, as well as the choice between cine-loop frames or individual frames. Data were transferred from the PC to a Sun Workstation, over a local area network. Image reconstruction and analysis were performed on the Sun Workstation.

The time, during which the imaging system was frozen or scanning, was controlled through the scanner's foot switch socket, which was connected to a second PC (Timer in Figure 2.1). The timer precision of ±1 millisecond was much shorter than the response time of the foot switch of the scanner.

In the Sun Workstation the data was rectified and an image was constructed using an 11 point moving average algorithm. Figure 2.2 shows a reconstructed image of the tank filled with water at 35.48% percent output power. The algorithm used for

this as well as the analysis package were developed in the Department of Medical Physics and Medical Engineering, University of Edinburgh. The analysis package is capable of calculating pixel intensities in multiple regions of interest (ROI).

Our assessment of backscatter intensities is based on the definition of integrated backscatter (Landini et al. 1987; Rijsterborgh et al. 1993). The intensities are always referred to a reference backscatter intensity (Moran et al. 1994). After rectification the image data are subjected to an 11 point moving average filter, and therefore have slightly reduced absolute backscatter values. Using a reference backscatter intensity, calculated in the same way, the effect of the moving average filter was cancelled out. This was confirmed in a pilot study designed to check whether the reconstructed image data distorted the results.

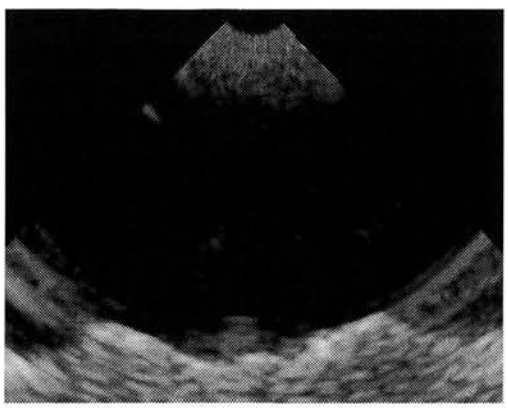

Figure 2.2 Scan converted image of RF data collected from the tank filled with water at 35.48% percent output power (Table 2.1). The image is log compressed. The base of the tank is the brightest feature at the bottom of the image.

2.2.2 Experimental protocol

2.2.2.1 Linearity of system

The method of signal collection and analysis aimed in being a linear process, and can be extended to assess the ultrasonic backscatter from individual scatterers. To establish the linearity or otherwise of the system, instead of evaluating each stage separately, the system was treated as a single process. By this means its transfer function could be established relatively simply. Instead of assessing the linearity range of each individual component in the acquisition system as well as the image reconstruction process, it was found more practical and efficient to assess the linearity range in terms of average pixel intensity of the final image. The average

pixel intensity is the actual image reconstructed ultrasonic intensity collected by the probe and refers to the average pixel amplitude squared.

A reticulated foam (Lerski et al. 1982) immersed in degassed water in the tank was used to assess the range of pixel intensities over which the entire system remained linear. The material was not expected to simulate the scattering properties of contrast agents, or even behave as Rayleigh scatterers. However, the selection of appropriate gain settings, for scattered ultrasound signal amplitudes, was possible. Five different gain settings were used, and measurements were performed for all the acoustic output pressures referred to in Table 2.1.

In the analysis of the image reconstructed data a ROI was placed 0.5cm above the bottom of the tank. The ROI was 2.92±0.03cm long and 1.41±0.03cm wide. A second ROI was placed over the brightest echo within the previous ROI, and its size was enough to cover the area of this echo (0.5cm by 0.5cm). The intention was to see whether the high backscatter signals would be responsible for a possible non-linear range of average backscatter from the large ROI.

2.2.2.2 Acoustic test materials

Standard acoustic materials were used to evaluate this system. Also they provide a reference for the normalised backscatter of contrast agents described in the following section. An acoustic grey scale phantom (Cardiff grey scale test object, Diagnostic Sonar, Livingston, Scotland), a blood mimicking fluid (BMF)(Ramnarine et al. 1998), and a suspension with Orgasol®, were insonated using the same frame rate, focal range, TGC and gain (Gain 2, in Figure 2.3). The BMF was made using: sterile water (85.41% weight), pure glycerol (10.25%), Sigma D4876 dextran of average molecular weight 185000D (3.42%), ICI synperonic N surfactant (0.92%), and 5μm diameter Orgasol® particles (ELF Atochem, France). The suspension of Orgasol® was based on the composition of the BMF. The ingredients dextran and glycerol were omitted, and replaced with water, since dextran and glycerol are responsible for the increased viscosity of the BMF. This suspension aimed in having similar wave propagation properties to contrast suspensions. Scanning gel was used to couple the acoustic grey-scale object to the transducer. When each of the two suspensions was used, 200ml of it was introduced into the tank and the probe was then immersed. The percent output power varied in the range stated in Table 2.1. The

three materials were compared in terms of pixel intensity of a ROI, placed in the same position, in the reconstructed images.

The measurement for each one of the three materials was repeated six times in order to assess reproducibility. For the grey scale phantom this meant repositioning of the probe on a different day, while for the suspensions it meant a new preparation of each suspension and then reintroduction of it into the tank. The two solutions were compared in terms of *t-tests* of two samples assuming equal variances to assess whether there was a statistically significant difference in backscatter at each of the pressure amplitudes used in this experiment.

2.2.2.3 Contrast agents

The use of this system with contrast agents can be illustrated by considering a study of two agents. Myomap™ (Andaris Ltd, Nottingham, UK) is an arterial agent and DMP115 (DuPont Pharmaceutical Co, Massachusetts, USA), an intravenous one. The intravenous agents are of subcapillary size in order to successfully cross the lungs. Arterial agents have larger size distributions and are used as depository agents. Table 3.1 describes the physical characteristics of the two agents. The volumes used for the two agents were 1ml for Myomap™ and 3μl for DMP115, as determined in the following chapter. These concentrations were within the linear range of backscatter. This means that the backscattered ultrasound is linearly proportional to the number of bubbles in the suspension. The difference in the concentrations used for the two agents was based on the difference in concentration of microbubbles in each vial, and the availability of the agents.

The peak negative pressure used for this experiment was 0.27MPa (Table 2.1). The agents were introduced into the tank and mixed with the 200ml of sterile water for 29.5sec, insonated for 0.5sec (frame rate 61Hz), then kept mixing for another 29.5sec in frame freeze and again insonated for 0.5sec and so on for a total of 15 periods of insonation. Verification that ultrasound was not emitted during frame freeze was performed using the needle hydrophone. The last frame of every insonation was acquired resulting in 15 frames of data. Those frames were downloaded and image reconstructed as described above. The average pixel intensity of a ROI was calculated on the Sun Workstation. The average pixel intensity of the same ROI calculated for the suspension of Orgasol® was taken from the Results'

Section of Acoustic test materials (p. 25) and used as reference backscatter intensity at each acoustic pressure, and to calculate the normalised backscatter intensity (N). Therefore:

$$N = I_i / (NI)_i \qquad (2.1)$$

where I_i is the backscatter intensity of a suspension of contrast for a specific combination of scanner settings (i), and $(NI)_i$ is the backscatter intensity of the suspension of Orgasol® under the same settings.

The definition of integrated backscatter (IB) as used by Moran et al. (1994), applies in our case as follows.

$$IB = 10 \log_{10} N \qquad (2.2)$$

IB is measured in decibels (dB) with 0dB referring to the contrast agent suspension that gives equal backscatter intensity to the solid scatterer suspension. Assuming that each one of the 15 values of N were representative of the backscatter of the suspension in the tank an exponential curve is fitted to the 15 values of N, to model its decay with time t(sec)

$$N = a\, e^{-bt} \qquad (2.3)$$

and the parameters of decay b(sec^{-1}) and intercept were calculated. Ideally **b** describes the decay rate of the contrast agent, and **a** the normalised backscatter of the contrast suspension at t=0. This converts according to (2.2) to

$$IB = 10 \log_{10} a - 10\, b\, t \log_{10} e \qquad (2.4)$$

2.2.3 Statistical Analysis

Analysis of the contrast agents was performed in order to assess the reproducibility of the system. The experiment is repeated three times for each agent and a comparison was performed between the curves.

The analysis of covariance performed for equation (2.4) can identify significantly different slopes or intercepts between two experiments. Equation (2.4) can be rewritten:

$$IB_i = A_i + B_i\, t \qquad (2.5)$$

where $A_i = 10 \log_{10} a_i$, and $B_i = -10\, b_i \log_{10} e$, with i = 1, 2, 3 for the three sets of experiments. Instead of using this equation and performing an analysis of covariance,

an equivalent approach was implemented which was a multiple regression analysis performed on the equation:

$$y = a + b\,t + c\,index + d\,tindex \qquad (2.6)$$

where y is the IB_i for two sets of data, t is the corresponding time t, ***index*** equals 1 for the first set of data and -1 for the second set of data, and ***tindex*** = t * ***index***. For each coefficient an *F-test* was performed and the probability values (Pr) were extracted. Using equation (2.6) the test of significance for c is a test of significance for the intercepts between the two sets of data, and a test of significance for d is a test of significance for the slopes between the two sets of data. In other words if c is significant, the difference between the two intercepts in equation (2.5) would be $2c$. Similarly a significant d would give a difference of $2d$ between the slopes of equation (2.5). For each agent 3 comparisons were done, which corresponded to comparing 3 sets of data between each other. The tests were performed using the SAS statistical package available on the university network. Two types of tests were carried out. The first is a step by step significance test (Type I), which means for example that the null hypothesis is checked for b for the equation $y = a + b\,t$, then the null hypothesis is checked for c for the equation $y = a + b\,t + c\,index$, and then the null hypothesis is checked for d for the equation $y = a + b\,t + c\,index + d\,tindex$. In the second type (Type III) of tests the null hypothesis is checked for each variable in the presence of all the other variables in equation (2.6). In the case d is not significant in the level of 0.1 $d = 0$ was replaced in equation (2.6) and repeat the null hypothesis test for b and c (Armitage and Berry, 1996).

2.3 Results

2.3.1 Linearity of the system

Figure 2.3a is a plot of the average pixel intensity, of the large ROI of the reticulated foam, against spatial peak pulse average intensity (I_{SPPA}) for the five different gain settings. Gain settings 0, and 1, provide pixel intensities that are linear with I_{SPPA}. Gain 2 is linear up to above $5x10^7$ pixel intensity. For increasing acoustic intensity at Gain 3 linearity is lost and the pixel intensities start to saturate. The same applies for Gain 4 for even smaller acoustic intensities. It is evident from these

graphs that up to approximately the $5x10^7$ pixel intensity value the plots remain linear and then show signs of saturation. This appears to indicate that the system has a 77dB ($10Log_{10}5x10^7$) linear dynamic range. However if we take into account that these decimal numbers are based on 16 bit format, and that only the most significant 12 bits are useful, then the linear range for this ROI is 53 dB (section 2.2.1.3, page18).

In Figure 2.3b the graphs correspond to the small and bright ROI inside the large ROI. Here Gain settings 0, and 1, provide pixel intensities that are linear with I_{SPPA}, but saturation starts at Gain 2 at high I_{SPPA}. Also Gain 3 and 4 are saturating the pixel intensities with increasing I_{SPPA}. These graphs suggest that for this ROI the linear range extends up to $1.1x10^8$ of pixel intensity, and that corresponds to more than 56dB linear range, including of course the previous considerations (section 2.2.1.3, page 18).

Comparing the graphs for Gain 2 at both Figure 2.3a and *b* it can be seen that the small region, which contains the brightest echoes inside the large ROI, induces a slight tendency for saturation, which is apparent for Gain 3 and 4. Saturation occurs at high values of pixel intensities, and affects the pixel intensities of the bigger ROI. In this experiment the backscatter of the ROI presented in Figure 2.3a seems to be affected by bright small regions inside it, presented in Figure 2.3b.

2.3.2 Acoustic test materials

The backscatter intensities of the acoustic grey scale phantom and the blood mimicking fluid are plotted against pulse average intensity in Figure 2.4a, while in Figure 2.4b the blood mimicking fluid is compared with the suspension of Orgasol®.

The Cardiff acoustic grey scale phantom had significantly higher backscatter intensities than the two fluids. Also the maximum backscatter intensity of the phantom did not exceed $4x10^6$ which is well within the linear region of the system. The *t-tests* performed to compare each pair of data points in the two graphs in Figure 2.4b showed that there is no significant difference, at 95% significance level, between the blood mimicking fluid and the suspension of Orgasol® at any of the pressure amplitudes used.

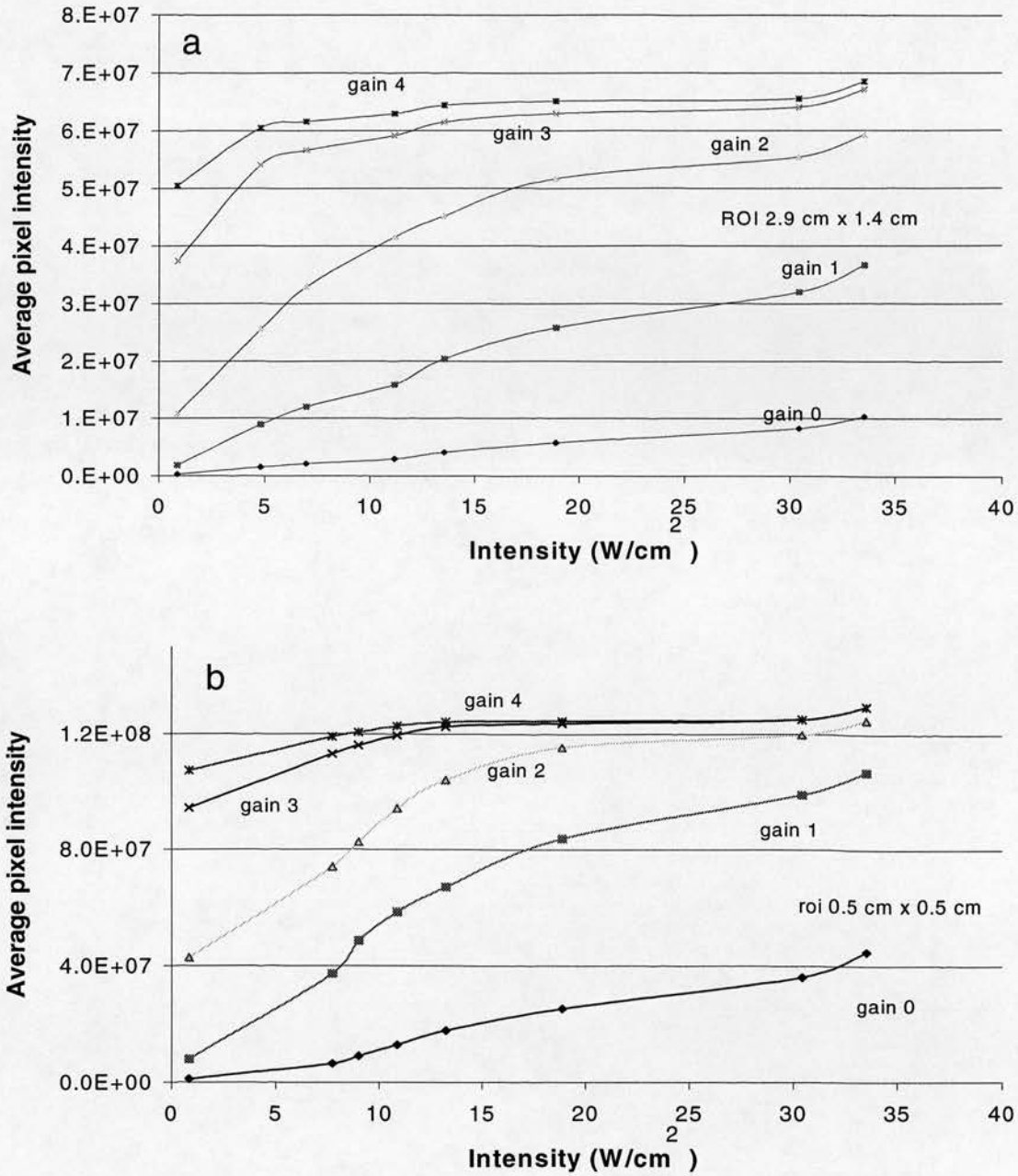

Figure 2.3 a Backscatter of a ROI of reticulated foam immersed into water for different gain settings, that are at the top range of gain of the scanner. Note that Gains 0 (r^2=0.99), 1 (r^2=0.97), and 2 (r^2=0.97) for the 5 initial points of the curve provide a linear variation of pixel intensity with spatial peak pulse average intensity (I_{SPPA}). Saturation of pixel intensity seems to occur for high I_{SPPA} at Gain 3 and at Gain 4. For pixel intensities at least up to $5x10^7$ the system is linear. **b** Backscatter of a small ROI inside the big ROI of reticulated foam immersed into water for different gain settings. This small ROI is selected to be the brightest region in image. Note that Gains 0 (r^2=0.98), and 1 (r^2=0.92) provide a linear variation of pixel intensity with I_{SPPA}, but saturation of pixel intensity seems to start for high I_{SPPA} at Gain 2 and of course at Gain 3, and 4. For values at least up to $1.1x10^8$ the average pixel intensity of the ROI is linear. Linearity is preserved in both graphs for the same settings of gain and acoustic intensity, which is suggestive of the influence of the small bright ROI to the big one.

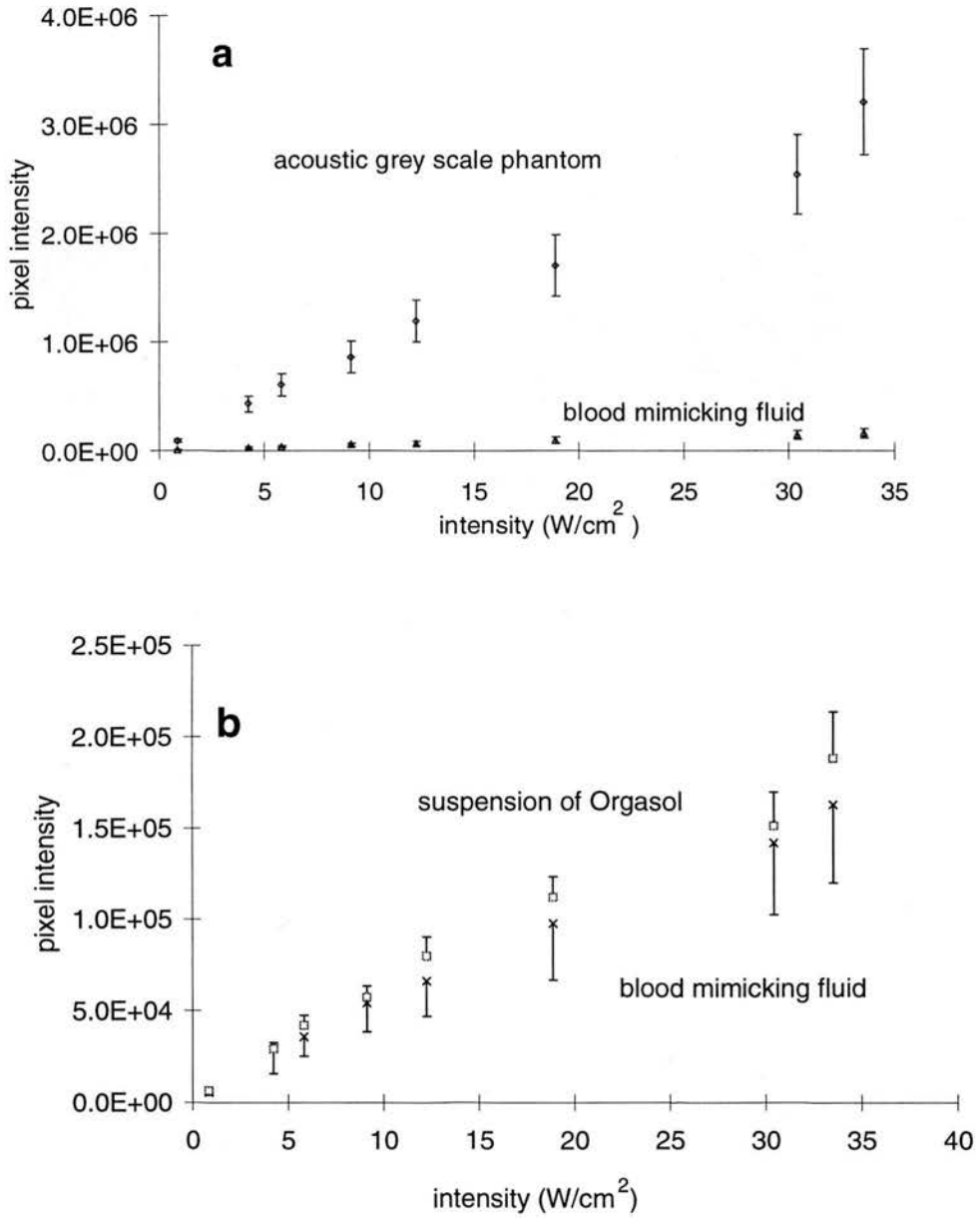

Figure 2.4 a The pixel intensities of the acoustic grey scale phantom and the blood mimicking fluid of the same ROI vs. I_{SPPA} of the scanner in a plane 3cm from the probe face. ***b*** The blood mimicking fluid and the suspension of Orgasol® pixel intensity are plotted against the pulse average intensity. The difference between the two curves is not significant.

2.3.3 Contrast agents

The scatter plots of integrated backscatter against time for DMP115 and Myomap™ are shown in Figure 2.5a and b respectively. The results of the multiple regression analysis are shown in Table 2.2. Each row refers to a pair of data sets. The calculated Pr values for the null hypothesis $\boldsymbol{d} = 0$ are under the column ***d***. Since ***d*** is

non-significant at the 0.1 level, for all comparisons $d = 0$ was substituted in equation (2.6) and the Pr values referring to the null hypothesis for b, and c are under the consecutive columns in Table 2.2. It can be seen that the b coefficients are highly significant, while c, and d are not significant, which indicates no difference in slope or intercept between the sets of data for both agents.

Table 2.2 *Significance test between repeated sets of measurements*

Pair of data \ Pr	*d*	*b*	*c*
DMP115 1 with 2	0.69	0.0001	0.53
DMP115 2 with 3	0.30	0.0117	0.41
DMP115 1 with 3	0.39	0.0005	0.17
Myomap™ 1 with 2	0.31	0.0001	0.12
Myomap™ 2 with 3	0.52	0.0041	0.37
Myomap™ 1 with 3	0.16	0.0002	0.87

Results of the multiple regression analysis applied on equation *2.6*. The numbers 1, 2, and 3 refer to the acquired data sets for each contrast agent. Each line of the table refers to a comparison between two data sets. **Pr** are the probability values for the variables in that column. The analysis performed by the SAS statistical software showed that ***d*** was statistically insignificant ($p>0.05$) for all the pairs of data sets and therefore was rejected (i.e. $d=0$ was replaced in equation *2.6*). A multiple regression analysis was performed on the new equation and gave the probability for ***b*** and ***c***. The ***b*** variable was highly significant ($p<0.01$) for most pairs of data sets, while ***c*** was insignificant ($p>0.05$). This shows according to section 2.2.3 that all three data sets compared in this table were insignificantly different for both contrast agents.

Table 2.3 *Performance of system with contrast agents*

	DMP115	Myomap™
correlation	0.960	0.972
decay constant (sec^{-1})	0.0573	0.0590
intercepts (dB)	27.73	8.31
max. standard deviation	3.4%	12.7%
mean standard deviation	2.2%	8.0%
IB_1 - IB_{15} (dB)	1.97	1.91

All three data sets were averaged for each contrast agent. The correlation coefficient (Integrated Backscatter vs. Time) to the linear fit was high (note that dB scale refers to 10x the logarithm of backscatter intensities). The decay constant and the intercept were significant for this fit. The maximum and mean standard deviation at each time value is stated, and also the overall average decay in dB.

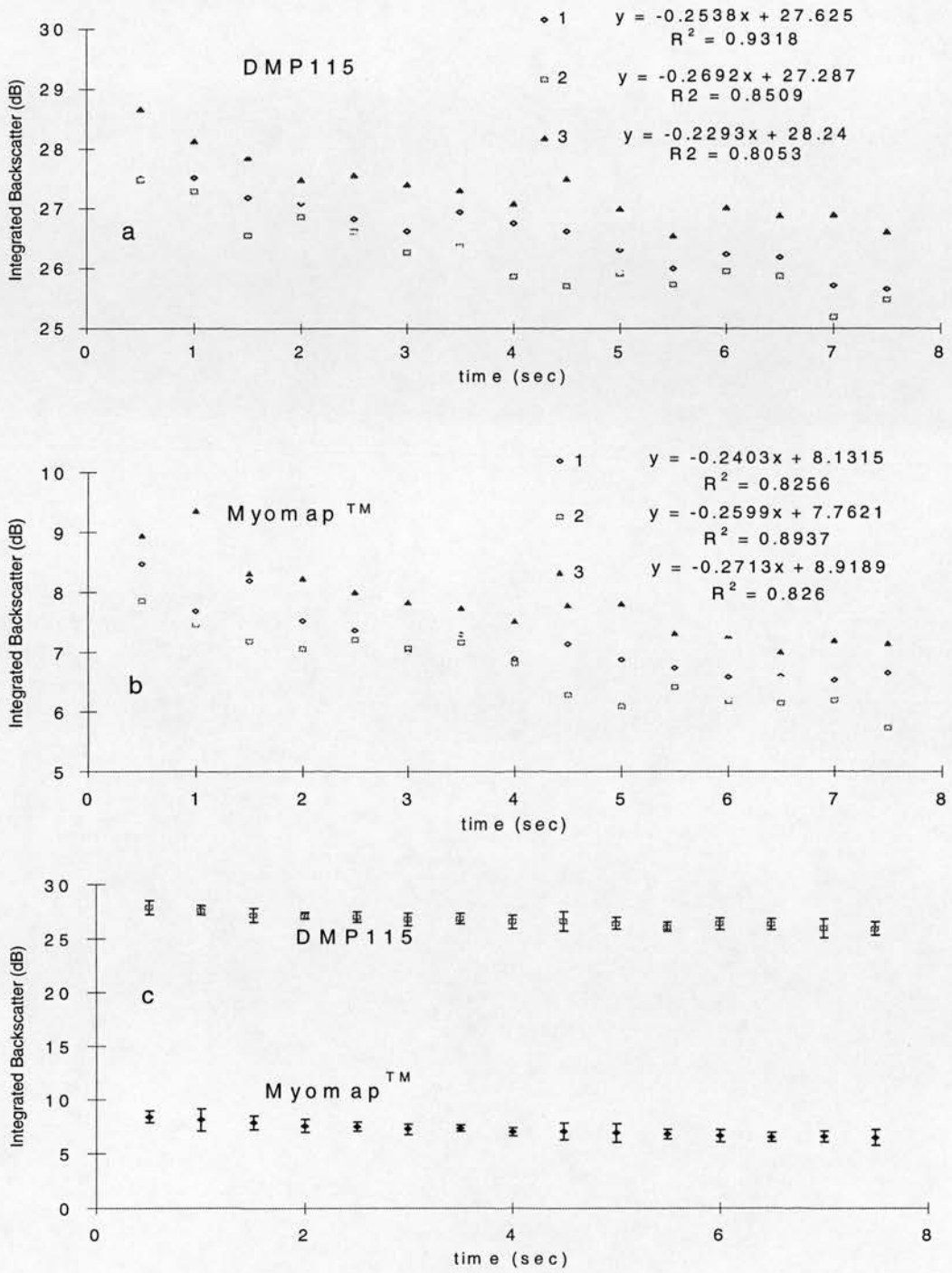

Figure 2.5 Integrated backscatter for DMP115 (***a***), and Myomap™ (***b***) against time of insonation. The experiment is repeated 3 times. The 3 equations and regression coefficients are also stated. According to Table 3 the three plots are not significantly different in terms of intercept and slope, which means that the system is highly reproducible. **c** Integrated backscatter of two contrast agents (DMP115, and Myomap™) against time of insonation. The level of backscatter for the two agents is not indicative of their relative ability to scatter ultrasound, since the bubble concentrations were different. This level was kept different in order to observe the ability of our system to detect decay. Even though the decay is very slow for both agents (overall less than 2dB), the linear fit provided a high correlation coefficient in both cases.

Also in Figure 2.5a and b the equations and regression coefficients of each data set are stated. Figure 2.5c plots the average integrated backscatter measurement against time of insonation for the two agents. The resulting figures from the two graphs are listed in Table 2.3. The decay constants refer to equation (2.3), i.e. the constant b. The intercept equals 10 $\log_{10}$a in equation (2.4). The difference between the first and the last IB value for each contrast agent was less than 2dB, as seen in Table 2.3. The difference in percent standard deviations between DMP115 and Myomap™ was expected due to the difference in the level of backscatter, and the difference in particle concentration. Myomap™ has also a wider size distribution of bubbles than DMP115 and is expected to give more variable backscatter.

2.4 Discussion

The objective of this chapter was to establish a reproducible system to use for contrast agent studies. It has been shown first that the system described is linear over a suitable dynamic range. The first areas of the image to saturate are highly backscattering regions within the ROI under investigation. By examining the RF signal from the small bright ROI it was not observed that any parts of the waveform were clipped, which would be a sign of electronic saturation. Instead the very large amplitudes in the signal did not increase, or increased non-linearly, with acoustic pressure and retained a sinusoidal waveform. Contrast agents are even "finer" and more uniform as scatterers than the fine foam utilised here, it is expected that the limits of linearity for the system, as set by the foam, would be wider for the case of a suspension with contrast agents. Operating between the linearity limits for foam should guarantee a linear system when contrast agents are used.

The backscatter intensities of an acoustic test object, a blood mimicking fluid, and a suspension of Orgasol® were then measured. This last suspension is aimed at being a reference in order to assess the integrated backscatter of contrast agent solutions and is thus different from that used by Moran et al. (1994). Nevertheless the method used follows the same concept of using a reference of similar acoustic nature as the material under investigation. In the following contrast agent studies the suspensions contain mainly water and therefore are more likely to behave

acoustically similar to a liquid like blood mimicking fluid. In addition the suspension of Orgasol® with a lower viscosity is expected to have similar non-linear characteristics to the suspending medium used for contrast agents. However both the acoustic grey scale phantom and the suspension of Orgasol® were used in the following chapters as a reference to contrast backscatter.

In the experiment that involved solutions with contrast agents the normalised backscatter was calculated, and from that the integrated backscatter. The quantity of normalised backscatter is considered as more appropriate for contrast agent studies. Using pixel intensity alone would not be representative as an assessment of backscatter intensity since it involves contributions from all the different components of an ultrasonic system, like the transducer, and the reconstruction of the images from the RF data. To eliminate all these a normalised pixel intensity value was calculated, using the suspension of Orgasol®, with exactly the same scanning settings, as a reference. This quantity is more suitable than integrated backscatter since it can be proportionally related to backscatter intensity, and therefore to scattering cross-section. This provides an accurate tool for quantification of the backscatter of contrast agent and will be used in future studies.

The sources of error were several in this set-up, and some only became apparent late in the project:

1) The non-uniform mixing with the magnetic stirrer gave a large variability between frames and provided either low correlation with the exponential decay or lower reproducibility. A lot of experience had to be gained in order to produce uniform mixing and carry out the experiments of this thesis.
2) The introduction of contrast to the tank using either a syringe or a pipette was another source of variability. The pipettes were used within the guidelines suggested by the manufacturer. Careful visual inspection for air cavities in their content before the introduction of the agent into the tank is necessary to avoid errors in the volume of agent injected.
3) Even when degassed suspensions were used there was a great risk of production of air bubbles since the mixing was done with the help of a magnetic stirrer. Care was taken in order to avoid such circumstances.

4) The ultrasound scanner was evaluated for stability in terms of transmit power and gain, and was found to require a 2 hour warm up period before stability was achieved. During the first 2 hours of operation the transmitted power is usually increasing and reaches a reproducible plateau after 2 hours.

5) The image of the tank was assessed to check for air bubbles identified by bright echoes. Possible cavities in the walls of the tank would reflect sound, and therefore distort the backscatter of the suspension. The bottom and walls of the tank were cleaned regularly in order to achieve optimal sound absorbing performance. This was very important since an accumulation of debris would add background echoes to the collected signals. Background subtraction of signal is common in contrast studies. Since the tank was anechoic, the necessary care described herein was sufficient to almost nullify the background signals. Thus background subtraction was not employed in the course of the work, even though tested in chapters 5 and 8.

This study showed that all these factors that had the potential to affect the accuracy of the system could be controlled and minimised. The results of the ultrasound backscatter from the same agent were inspected for consistency. Instances of inconsistent results were few in this thesis. In each chapter the result of that inspection is reported in the discussion. The statistical analysis suggested that a single acquisition of data set was reproducible. The accurate assessment of the decay constant for the two contrast agents, when the overall decay is less than 2dB, shows that this system is suitable for these studies.

2.5 Conclusion

The evaluation of a system for the in-vitro study of ultrasonic contrast agents has been described in this chapter. The system proved accurate and highly reproducible in an investigation using contrast agents. The practical aspects also raised in this chapter contribute useful knowledge, which will be necessary for the following chapters.

3 Chapter Three: Preliminary experiments

3.1 Introduction

The previous chapter explored the experimental set-up and introduced the reader to the experimental system's capabilities. This chapter is an introduction to contrast agent studies. First the contrast media used in all the experiments will be introduced, then some practical issues that were important in the experiments will be raised, and lastly some preliminary experiments will introduce the investigation on contrast agents.

The need for an in-vitro investigation has already been outlined in a brief literature review in chapter 1. The goal of such an investigation is the quantification of contrast in-vivo. At each separate in-vitro experiment in this thesis quantification of contrast should be feasible. For example in the previous chapter it was shown that the system was linear for most of the dynamic range of the scanner.

Contrast agents were created to improve the sensitivity of an ultrasonic investigation, in other words enhance the brightness of a grey-scale image. It is obvious that an increase in concentration does not always relate to a linear increase in backscatter. The experiments undertaken in this chapter assess the range of bubble concentrations that provide linear backscatter for each agent, and their data will be used in the following chapters.

Part of these early experiments was also to learn how to handle a particular agent and to assess its performance after it has been produced. It is important to know how stable the agent was in the vial, and for how long.

Based on the existing theory that explains the behaviour of gas bubble scatterers, a basic understanding of the properties of these agents is also attempted.

3.2 Materials and methods

3.2.1 Contrast Agents

Four contrast agents: Levovist (Schering), DMP115 (DuPont), Quantison™ (Andaris), and Myomap™ (Andaris) were studied in this series of experiments. Their characteristics are given in Table 3.1. These agents provided a range of different characteristics. A comparison of their relative properties would hopefully help to understand the contribution of individual characteristics (such as size, shell thickness, gas etc.) to the magnitude of the scattering cross-section.

The manufacturer's recommended preparation method was followed in each case. 1g of Levovist contains 999mg of galactose and 1mg palmitic acid, and each vial contains 4g of Levovist. To prepare the agent 17ml of sterile water were inserted in the vial, which then was vigorously shaken for 10 seconds. The suspension is then allowed 2 minutes to equilibrate before use. It was also advised by the manufacturer that the suspension should be used not later than 10 minutes after preparation. As explained by Schlief et al (1993) the microparticles of galactose and palmitic acid will dissolve until equilibrium is reached and the rest of them that remain in solid state will be stabilised by the equilibrium. The bubbles are trapped on sites within the galactose macrostructure. This structure dissolves in blood releasing free bubbles.

DMP115 comes in smaller vials of 1.5ml of suspension. A shaker supplied by the company (Capmix®) is used for vigorous shaking of the vial for 60 seconds. The vial is then allowed to equilibrate for 10 minutes as advised by the company. The resulting bubbles are perfluorocarbon-filled lipid bilayer about 20 nanometers thick composed of dipalmitoylphosphatidylchloine (Unger et al 1994).

Quantison™ comes in vials as formed bubbles and 5ml of sterile water are inserted to the vial and mixed gently. The bubbles contain air and the coating is human serum albumin of about 300 nanometre thickness.

Myomap™ is similar to Quantison™, only the bubbles are greater in size as stated in Table 3.1, and instead of sterile water, 5ml of a 10mg/ml Polysorbate 80 solution are inserted in the vial and mixed gently.

During the experiments the agent remaining in the vials was constantly agitated with a mixer.

Table 3.1 *Characteristics of contrast agents*

	Levovist	**DMP115**	**Quantison™**	**Myomap™**
Nature	galactose +fatty acid	Liposomes	Human serum albumin	Human serum Albumin
Gas	air	Perfluorocarbon	Air	Air
Thickness of coating (nm)	Not relevant	5	300	1000
mean diameter(μm)	3	2.5	3.2	12
Concentration (bubbles/ml)	$4x10^7$	10^9	$1.5x10^9$	$1.5x10^7$

3.2.2 Acquisition of data

3.2.2.1 The set-up

The full description of the set-up is given in chapter 2. The transmit power was set at 2.24% on the scanner console which corresponds to 0.27MPa peak negative pressure at 3cm distance from the probe, focusing at 4.25cm from the transducer (measured using a needle hydrophone). This was also the distance of the probe from the bottom of the tank. Gain and Time Gain Compensation (TGC) were kept constant throughout the whole experiment.

The time during which the system was in "freeze" and "scanning" position, was controlled through the foot switch connector using a PC.

3.2.2.2 Practical considerations

Before proceeding with the experimental protocol it is necessary to raise the practical issues that concern the experimental investigations carried out with this set up, which was also used for the experiments in chapters 4, 5, 6, 7 and 8.

The injections of contrast in the tank were done with Microman positive displacement pipettes (Gilson®, France). The three models used are a) M10 for volumes between 1μl-10μl, b) M100 for volumes between 10μl-100μl, and c) M1000 for volumes between 100μl-1ml. These are high precision pipettes and the highest

relative error is stated to be 6% for M10 at 1μl volume. Care should be taken to avoid inserting air in the pipette at the time an agent is inserted.

The agitation of the suspensions was done with a magnetic stirrer (B211 Bibby Science products Ltd, UK) that had a variable speed facility. However the choice of the magnetic bar was a significant one. There were different shapes of magnetic stirrers, and pivot ring and oval stirrers of different sizes were tested. An oval one 15x6mm (Merck Ltd, UK), and a pivot ring 25x10mm were finally used. The stirrer must spin at a sufficiently rapid speed to give a homogeneous distribution of the contrast in the tank. Images taken with slow stirring showed clouds of contrast that of course would give a very variable contrast and would almost certainly influence the statistics of the experiment. If the spin is very fast then there are two risks: firstly the stirrer is likely to be displaced from the spinning centre which practically means that the mixing became unreliable and inhomogeneous, and secondly air bubbles that are created by the resulting turbulence would again significantly affect the measurements. Taking into account also that each agent gives images of different texture, which made it difficult to assess the different problems, it was a very difficult task to optimise the stirring, but the general concept was to adopt a fast stirring that would also avoid the problems mentioned above.

The tank was built with notches every 0.5cm that were used as location divisions in order to place the scanner's probe accurately and reproducibly in the required position. Also, the distance of the tip of the probe from the bottom of the tank, as measured using the scanner, was used to assess accurately the vertical positioning. The scanning must be performed in a reproducible and highly controllable manner. It was also important to rinse the tank carefully after use. Any remainder of the suspensions on the surface of the acoustic absorber would alter the reflectivity of the walls, and especially the bottom, of the tank, and as a result alter the ultrasonic environment of the suspension or cause undesirable multiple reflections.

3.2.3 Experimental protocol

3.2.3.1 Backscatter vs. bubble concentration

In this study 200ml of sterile water were introduced in the tank, and different volumes of agents were injected into the tank. They were allowed to mix for 28sec with the help of a magnetic stirrer, and then insonated for 2sec from which the last image frame of digitised RF echo data was collected. Table 3.2 gives full details of the injection doses for each agent. For DMP115 the injections ranged from 0.0005ml to 0.005ml, with a 0.0005ml step (overall 10 injections). For Quantison™ the injections ranged from 0.05ml to 0.65ml, with a 0.05ml step (overall 13 injections). For Myomap™ the injections ranged from 0.3ml to 2.7ml, with a 0.3ml step (overall 9 injections). For Levovist the injections ranged from 0.2ml to 1.6ml, with a 0.2ml step (overall 8 injections). Also in Table 3.2 the amount of bubbles per millilitre is shown derived from the concentrations of bubbles in the vials as given in Table 3.1.

Table 3.2 *Dose range of contrast agents*

	Levovist	**DMP115**	**Quantison™**	**Myomap™**
Minimum dose*	0.2/40000	0.0005/2500	0.05/375000	0.3/22500
Maximum dose*	1.6/320000	0.005/25000	0.65/4875000	2.7/202500
Step*	0.2/40000	0.0005/2500	0.05/375000	0.3/22500
Number of injections	8	10	13	9
Number of repetitions	4	5	6	2

(* ml of contrast agent per 200ml of suspension/number of bubbles per ml of suspension)

For DMP115 the experiment was repeated 5 times, for Quantison™ 6 times, for Levovist 4 times, and for Myomap™ 2 times. The purpose of this repetition was to assess how reproducible this study was. This experiment is repeated for Quantison™ more than the other agents because it returned the lowest signal, and therefore the lowest signal to noise ratio. The measurements were considered reproducible when the average backscatter values gave a standard deviation below 20%.

3.2.3.2 Lifetime in the vial

In this experiment the echogenicity of the agents was tested over a long period of time. Table 3.3 illustrates the protocol followed. After a measurement, the tank

was cleaned and prepared for the next measurement. The agent was kept in the vial until just prior to acquisition of data. DMP115, Quantison™, and Myomap™ were tested for 5 hours, starting with a measurement 10 minutes after preparation. A measurement was repeated for those agents every 20 minutes, and the bubble concentrations were chosen to be in the linear region of the "Backscatter vs. Concentration" (arrows in Figure 3.1) plots of the previous experiment (Table 3.3). Levovist has a shorter lifetime in the vial, and therefore was tested for 30 minutes, starting 2 minutes after its preparation, as advised by the manufacturer. It is very important to note that some vials of Levovist were starting to lose their milky appearance, and thus excluded from the measurements. The experiment was repeated twice for all agents apart from Levovist where it was repeated 4 times.

Table 3.3 *Protocol for assessing the lifetime of contrast agents in the vial*

	Levovist	**DMP115**	**Quantison™**	**Myomap™**
Dose (bubbles/ml)	160000	12500	2250000	75000
First measurement (min after preparation)	2	10	10	10
Last measurement (min after preparation)	30	290	290	290
Time between measurements (min)	2	20	20	20

The imaging protocol used to check the lifetime of the agents in the vial is deduced after several pilot experiments and it is the same for all agents apart from Levovist. The concentrations used for this were the outcome of the first experiment in this chapter and are seen in Table 3.4.

3.2.4 Statistical analysis

All the sets of frames were transferred to the Sun Workstation where image reconstruction took place. As described in chapter 2 (paragraph 2.2.1.3) the backscatter intensity of a region of interest above the bottom of the tank was calculated using the available software. This backscatter intensity was referenced to

the acoustic test grey scale object (Cardiff grey scale test object, Diagnostic Sonar, Livingston, Scotland). This is the Normalised Backscatter NB_i as defined in equation 2.1, and explained in chapter 2. By referring the backscatter intensity of contrast agents to that of the acoustic grey scale test object, the resulting normalised backscatter illustrates quantitatively the difference between tissue and contrast agent at the particular settings.

3.3 Results

3.3.1 Backscatter vs. Concentration

The graphs of results are plotted in Figure 3.1. All the agents have a distinct linear portion for the lower concentrations. For Levovist Figure 3.1a, and DMP115 Figure 3.1b there is a distinct shoulder in the curve for higher values of concentrations, which implies self-attenuation effects for those values (de Jong and Hoff, 1993). For Quantison™ Figure 3.1c this shoulder is less distinct. Table 3.4 shows the maximum bubble concentrations for this linear part of each curve, and the regression coefficient that corresponds to the linear fit. The maximum bubble concentrations were a subjective estimate and were based on the visual inspection of the graphs, and these bubble concentrations were used in the following experiments (chapters 5, 6, and 7). For example for Quantison™ it could be claimed that the graph was approximately linear in its whole. The concentrations used for Myomap™, due to limited availability of the agent from the company, were not high enough to show where this shoulder starts. The concentration of bubbles in the vial is considerably lower (~100 times), and therefore more vials were needed, than the ones available at the time, to reach "shoulder-concentrations" for Myomap™. Thus the bubble concentration in Table 3.5 refers to the one used in the following experiments, and the r^2 to the linear fit that contains all the values of the plot. The average standard deviations for all the measurements for each agent shown in Figure 3.1, were: for Levosist 11%, for DMP115 18%, for Quantison™ 19%, and for Myomap 15%.

Table 3.4 *Bubble concentrations of contrast agents*

	Bubble concentration (bubbles/ml of suspension)	r^2
Levovist	$1.6*10^5$	0.90
DMP115	$1.5*10^4$	0.96
Quantison™	$2.25*10^6$	0.98
Myomap™	$7.5*10^4$	0.96

The values of bubble concentration correspond to the arrows in Figure 3.1, and the regression coefficients refer to the linear fit applied to the plots in Figure 3.1 for bubble concentrations that range up to that value. For Myomap™ the linear fit refers to the whole plot.

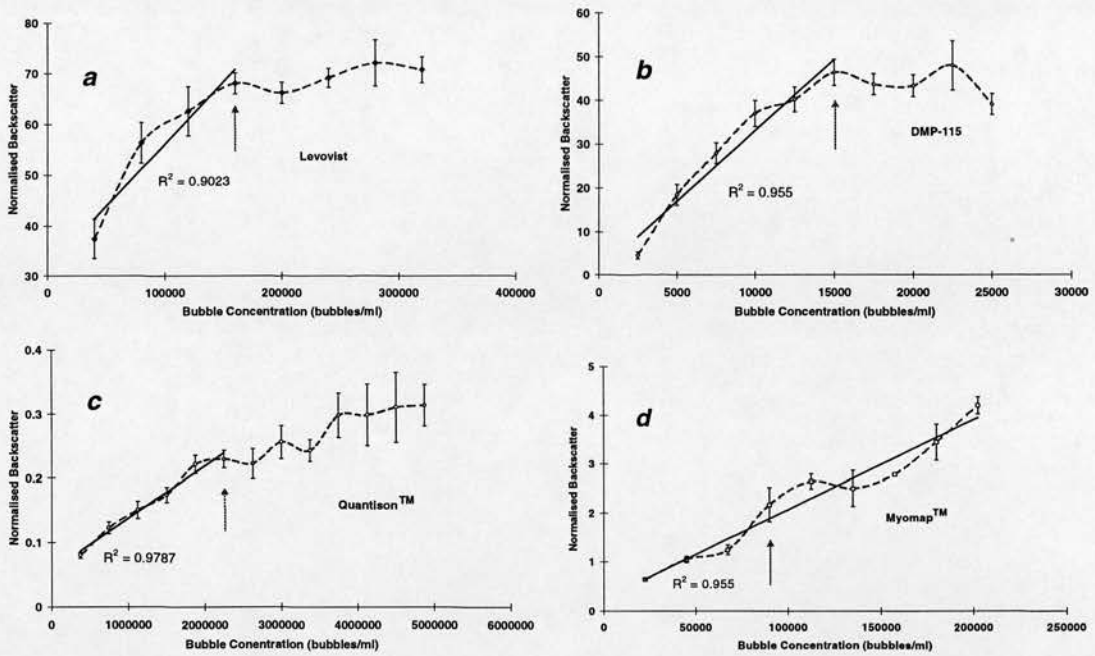

Figure 3.1 The normalised backscatter is plotted against bubble concentration for (**a**) Levovist, (**b**) DMP115, (**c**) Quantison™, and (**d**) Myomap™. For all agents apart from Myomap™ the initial increase of backscatter is followed by a plateau at the value of 160,000 bubbles/ml of suspension for Levovist, 15,000 bubbles/ml for DMP115, and 2,250,000 bubbles/ml for Quantison™ (arrows in each chart). For Myomap™ a plateau was not achieved, due to the availability of the agent. The concentration used for the following experiments (unless stated differently) was 75,000 bubbles/ml (arrow in chart d).

Although the regression coefficients of the linear fit look satisfactory for each agent, visual inspection of Figure 3.1, for the cases of Levovist and DMP115 in particular, gives the impression that the two agents do not have a completely linear relationship between bubble concentration and backscatter up to the bubble concentrations stated in Table 3.4. A more detailed investigation on the nature of this relationship is explored in a separate chapter (chapter 7). For the purpose of the

experiments in the following chapters, a linear relationship between bubble concentration and backscatter was considered satisfactory. This means that all the measurements of backscatter were considered to be proportionally related to the number of bubbles in the suspension.

Using these results an estimate of the acoustic properties of the four agents is attempted. Using this linearity assumption the gradients of the resulting trendlines (Table 3.5) should be proportional to the scattering cross-section of the bubbles. In the second row of Table 3.5 the ratio of the square of the radius to the slope (α^2 / slope) is calculated, and in the next row the resonant frequencies (f_0) are stated for Levovist and DMP115 (Unger et al 1997, Schlief et al 1993). This information was not available for Quantison™ and Myomap™. Hence from equation 1.3 the ratio α^2 / σ, which is equal to $\left(\left(\left(\frac{f_0}{f}\right)^2 - 1\right)^2 + \left(\frac{f_0}{f}\right)^4 \delta^2\right) / 4\pi$, is proportional to α^2 / slope, and can be used in an attempt to understand the acoustic nature of the above agents.

Table 3.5 *Characteristics of Figure 3.1*

	Levovist	**DMP115**	**Quantison™**	**Myomap™**
Slope of linear part of curves in Figure 3.1 (arbitrary units)	$8*10^{-5}$	$1.1*10^{-4}$	$3*10^{-8}$	$6*10^{-6}$
α^2 / slope	$1.1*10^{-7}$	$5.7*10^{-9}$	$3.4*10^{-4}$	$2.4*10^{-5}$
f_0 (MHz)	~2.5	~2.5	-	-

The slope of the linear part of Figure 3.1 is proportionally related to the scattering cross-section. The calculation α^2 / slope in the 2nd row is proportional to $\left(\left(\frac{f_0}{f}\right)^2 - 1\right)^2 + \left(\frac{f_0}{f}\right)^4 \delta^2$, and the last row gives the resonant frequencies of the agents quoted in the literature.

3.3.2 Lifetime in the vial

Over the time of 5 hours after preparation DMP115, Quantison™, and Myomap™, showed no decay in the vial (Figure 3.2a) in terms of backscatter. Levovist had a shorter lifetime, but showed considerably stability up to 30 minutes after preparation (Figure 3.2b). The average standard deviations for DMP115,

Myomap™ and Quantison™, that were repeated only twice, were 15%, 41%, and 26% respectively, while for Levovist, that was repeated 4 times, 21%.

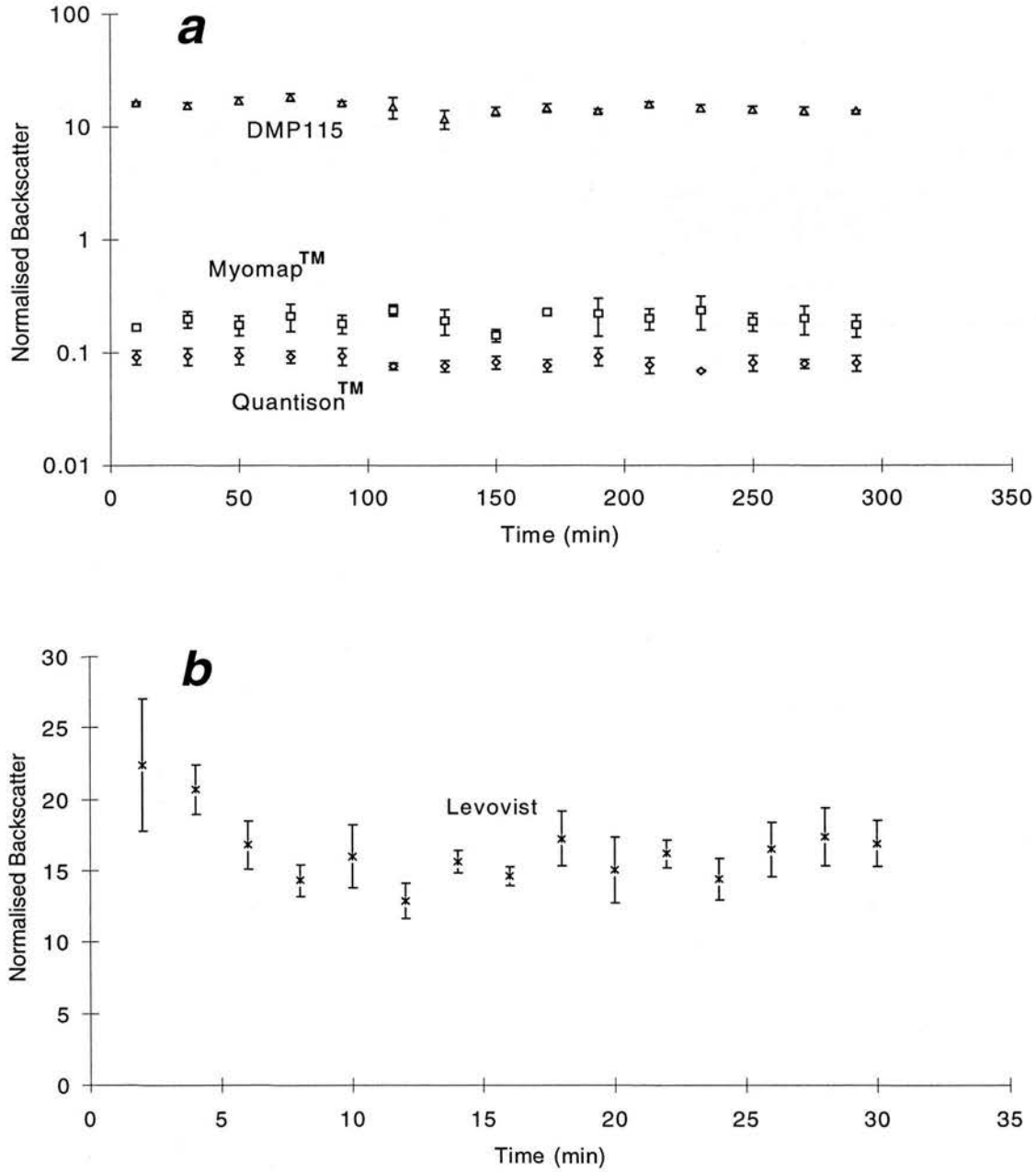

Figure 3.2 a Lifetime in the vial for DMP115, Myomap™, and Quantison™. All three agents retained their backscatter level for over 5 hours. The average standard deviations were consecutively 15%, 41%, and 26%. ***b*** Lifetime in the vial for Levovist. The backscatter level remained stable for 30 minutes and the standard deviation averaged to 21%.

3.4 Discussion

3.4.1 Backscatter vs. Concentration

At the lower range of bubble concentrations it was shown that the normalised backscatter had a linear relationship with bubble concentration. Since the normalised backscatter is proportional to the average scattering cross-section of the bubbles, then it is proportional to the number of bubbles. The experiments performed in chapters 4, 5, and 1 use the same concentration protocol, and therefore these graphs (Figure 3.1) can be used for quantification purposes (Ophir and Parker 1989, Wiencek et al. 1993). If for example in an experiment the measured normalised backscatter, was such that it was within the plateau of these curves, then possible destruction or decay of the bubbles, would not be evident as proportionally reduced backscatter power. The backscatter power would remain in the plateau region until the amount of backscattering bubbles reduced sufficiently so that the linear portion of the curve was reached. Without the preliminary results of this chapter such results would be misleading.

Experimenting in the linear range of backscatter also allowed comparisons between agents, assuming that all the agents were exposed to the same ultrasonic field. As evident from Table 3.5, not all the resonant frequencies of the agents were found in the literature. De Jong and Hoff (1993) simulated successfully the backscatter spectrum of Albunex®, which did not appear to peak at any particular frequency. The resonant frequency for Levovist in Table 3.5 was taken from the measured attenuation spectrum (Schlief et al 1993). DMP115 displayed peak backscatter intensities between 2 and 3MHz with a probable peak around 2.5MHz, but the beam characteristics in this investigation remained unknown (Unger et al 1997). Even though all the bubbles within a contrast agent preparation would have a resonant frequency, the preparation may not exhibit a clear resonance, simply because of the wide size distribution of bubbles that the contrast agent consists of, and their variable contribution to the average scattering cross-section. This was the outcome of the study done by De Jong and Hoff (1993), that is expected to apply to intravenous agents which have similar size distributions. Furthermore, a commercial scanner in B-mode, like the one used in this set up, would transmit one or two-cycle

pulses (in order to allow image reconstruction with acceptable axial resolution) which give a broad frequency bandwidth for the ultrasonic beam. For bubbles that resonate at a particular frequency inside the emitted band, it would be expected not to express that resonance when they are subjected to a broad range of frequencies. Moreover each contrast agent contains a range of bubble sizes with different resonant frequencies and as a result an agent might not have a dominant resonance for a population of bubbles and therefore not express a peak in the backscatter spectrum. It is therefore clear that equation 1.3, because it is applicable for a specific bubble size, can not be used directly in the present study, and only a qualitative discussion would be appropriate. The α^2 / slope ratios as well as the proximity of the graphs in Figure 3.1 may be used for such comparisons. Levovist and DMP115 could not be compared, taking into account that the calculation of slope for Levovist was based on only 4 points that had the lowest regression coefficient (Table 3.4), and also their graphs almost overlap in Figure 3.1. The difference between Quantison™ and Myomap™, is also not pronounced to lead to a qualitative conclusion. However, Quantison™ and Myomap™ provided distinctively higher α^2 / slope ratios than the previous two agents. In the case of Quantison™, acoustical saturation was reached at much lower values of normalised backscatter than those of any of the other three agents. This suggests a much greater motion damping, δ, for Quantison™ and Myomap™ for the particular beam settings. This was in agreement with equations (1.4) and (1.5) where the contribution of the wall thickness t, to the damping constant δ is shown. Increased wall thickness means increased damping and therefore from equation (1.3) decreased scattering cross-section σ.

The range of normalised backscatter values of these agents showed that Levovist and DMP115 had higher backscatter values than the tissue phantom (Cardiff grey scale test object), while the other two seemed that they could not be used as backscatter enhancers of blood echoes for the specific settings. However it must be borne in mind that this applied for the specific insonation settings, and did not imply that the first two agents were in general "brighter" than the latter. A change in acoustic output power would possibly alter the appearance of the Figure 3.1, suggesting the need for a reassessment for every combination of settings. The

following chapter deals also with that, while chapter 8 deals with the backscatter of individual contrast agent scatterers.

3.4.2 Lifetime in the vial

It was important to test all agents in terms of stability in their vial environment, in order to estimate the allowable time scale for experiment with each agent. The performance of DMP115, Quantison™, and Myomap™ showed that they could be used for almost 5 hours after preparation (Figure 3.2a). However, Levovist was less stable and therefore better used in the first 30 minutes after preparation (Figure 3.2b). The backscatter for the first 4 minutes after preparation showed an increased variability and was considerably higher than the rest of the time. It is therefore suggested to use this agent after 4 minutes of preparation, which are 2 minutes more than the manufacturer's suggestion. The high reproducibility achieved with both DMP115 and Myomap™ in the previous chapter, was largely due to their high stability, which set the standards for the experimental set-up.

3.5 Conclusion

The outcome of this chapter established the concentrations that should be used in experiment with each agent, to ensure a linear relationship between backscatter power and scatterer concentration. It was also shown that an *in vitro* investigation with contrast agents should start with experiments similar to the ones performed in this chapter. It remains to be seen, in the following chapter, whether the suspensions used to investigate the agents would be a source of variability for the experiments.

As a side outcome of this chapter, a rough idea of the scattering cross-section of the contrast agents was deduced, and also an introductory effort in understanding their properties was performed using the existing theory presented in chapter 1. The experiments in this chapter suggested not only the ones in the following chapter to complete the understanding of the handling of the agents, but also the need to investigate the behaviour of the bubbles in different acoustical fields. The investigation carried out so far raised questions as to whether or not the contrast agents perform differently under different acoustic fields, and how they could be

optimised for in-vivo studies. The need for an *in vitro* investigation of contrast agents is evident, and this thesis aims to contribute towards the understanding of their properties.

4 Chapter Four: The influence of the suspension environment on contrast agents

4.1 Introduction

In chapter 1 the requirements for the ideal contrast agent were stated. Amongst them it was mentioned that the agent should be stable *in vivo* during the course of the clinical examination. This means that the agent must remain stable first in terms of chemical interactions, and second in terms of physical interactions. In the latter category, one of the most important interactions is that between the contrast agent and the ultrasonic beam. This constitutes one of the main research areas in contrast ultrasonography.

In a less favourable situation, where the agent is not stable, it is necessary to be able to predict and quantify its degradation. By doing so it may be possible to assess the relationship between the concentration of the agent and its backscatter, which may lead to reproducible images and accurate calculation of flow or perfusion.

In this chapter the physical environments that may affect the stability of contrast agents are examined, and the effect of the gas content of the suspending solution on the stability of four different contrast agents is evaluated. Chapter 3 has allowed the choice of an appropriate bubble concentration. Also by determining the lifetime of the agents in the vial after preparation, valuable information is provided to ensure the reproducibility of the following experiments.

4.2 Physical interactions of contrast agents

4.2.1 Gas concentration in a liquid

The pressure within a free bubble at rest is greater than the pressure of the liquid surrounding the bubble because of surface tension forces (Leighton, 1994). Therefore the internal pressure of a bubble p_i equals:

$$p_i = p_l + p_\sigma \tag{4.1}$$

where p_l is the pressure in the liquid and p_σ is the surface tension. The internal pressure also equals:

$$p_i = p_g + p_v \tag{4.2}$$

where p_g is the pressure of the gas in the bubble and p_v is the pressure of the liquid vapour. Combining (4.1) and (4.2) we get:

$$p_g = p_l - p_v + p_\sigma \tag{4.3}$$

which means that the gas pressure in the bubble is greater than $p_l - p_v$. Consequently even in a saturated solution the gas pressure inside the bubble is greater than that in the liquid, and therefore the bubble will tend to dissolve. Epstein and Plesset (1950) calculated the dissolution times of air bubbles in water and also their change in size. Their calculations showed that if surface tension is neglected then a bubble would not dissolve in a saturated solution, while taking into account the surface tension would result in a finite dissolution time for the bubble. Of course dissolution of a bubble means shrinkage and therefore decrease of the scattering cross-section (resonance is not accounted for). Epstein and Plesset set the variable $f = C/C_s$ where C is the concentration of the gas in the liquid and C_s is the concentration when the solution is saturated. For $f = 0$ the dissolution time t is calculated to be 1.17sec for a 10μm air bubble in a water solution. For $f = 0.5$, $t = 1.96$sec and for $f = 1$, $t = 6.63$sec. Using these calculations de Jong et al (1991) extended this theory to show that larger bubbles disappear slower than the smaller ones.

A simulation of exchanges of multiple gases in-vivo shows the complexity of the problem. Burkard and Van Liew (1994) have shown that gases interact with each other and after an injection of contrast the bubble may take in several gases that are present in-vivo. Calculations based on this model showed that exchanges of O_2, CO_2, and N_2 between the bubble and the blood might affect the size of the bubble (Van Liew and Burkard, 1995a).

The case of stabilised microbubbles can also be examined (Van Liew and Burkard, 1995b). Surface films or surfactant monolayers are considered to behave as mechanical stabilisers and cancel out the surface tension that is responsible for the diffusion of the bubble as discussed above. Their permeability is however high enough to allow the exchange of gases. It must be noted however that this

permeability can only be speculated. Moreover the necessary stabilising pressure can not be accurately predicted and therefore the role of the stabilising process is not yet clear. Wiencek et al. (1993) observed in their laboratory that a degassed saline solution diminished the acoustic enhancement of Albunex microbubbles. This chapter is dedicated to such an investigation with four different CAs.

4.2.2 Hydrostatic pressure

Boyle's law states that the gas pressure inside a bubble p_g is:

$$p_g V = (B / M) m T \tag{4.4}$$

where V is the volume of the bubble, B is the universal gas constant, M is the molecular weight of the gas, m is the mass of the gas in the bubble, and T the temperature. If we assume that the right hand side term of this equation is constant, then an increase in hydrostatic pressure in the liquid from (4.3) would increase the gas pressure in the bubble, and this would proportionally reduce the volume V. In other words the bubble would compress.

De Jong et al (1993) applied 160mmHg hydrostatic pressure to Albunex microbubbles and apart from compression he noticed microscopically that the bubbles deform and disappear. This is in agreement with Vuille et al (1994) who noticed that the constant application of increasing pressure would proportionally reduce the reflectivity of the bubbles in an irreversible way, i.e. the release of pressure application would not recover the reflectivity of the bubbles. This result suggests that compression is not the sole mechanism for the decay of the agents. Vuille et al, in attempting to explain this irreversibility, suggested that destruction and/or accelerated diffusion of the bubbles could be responsible. However destruction was an unlikely explanation since a big initial decay of reflectivity would be expected after the application of pressure. Instead the results tended to fit a sigmoid function, which is more compatible with a slower process such as diffusion.

This leaves accelerated diffusion as the more likely mechanism. Decompression sickness can occur to deep-sea divers when the ascent is rapid. In that situation exposure to lower pressure oversaturates nitrogen in the blood resulting in bubble formation. The opposite happens in a rapid descent (West 1985). A gas saturated solution can become undersaturated under the application of pressure, the

gas concentration gradient is increased across the wall of the bubble and may be the cause for the accelerated diffusion. The parameter f, introduced by Epstein and Plesset (1950), decreases, due to increase of C_s, and therefore the dissolution time is decreased. This argument is supported further when pulsatile pressure is applied to the contrast agents. Hand agitated Angiovist (diatrizoate meglumine and diatrizoate sodium; Berlex Laboratories, Wayne, NJ, USA) when subjected to pulsatile pressure showed a cyclic variation as well as an overall decrease in backscatter, while Albunex did not show any recovery and decayed continuously (Padial et al, 1995). Destruction could be considered responsible for the decay of the Albunex echoes, but for Angiovist the cyclic variation of reflectivity showed that increase in pressure is partially recoverable and therefore accelerated diffusion is the likely mechanism to explain the decay of the agent.

4.2.3 Other parameters

It has been suggested that the half-life of microbubbles can be increased by reducing the temperature or by increasing the viscosity (Sebba, 1971).

Viscosity is a parameter inversely related to the size of the bubbles. An experiment that included Renograffin 76, solutions of sorbitol, and dextrose, showed that increased viscosity in-vitro offers stability in bubbles small enough to pass the capillaries (Koenig and Meltzer, 1986). The variability of viscosity in the blood is significant in several pathological conditions. However the role of viscosity in the performance of contrast agents has yet to be investigated.

Temperature also affects the size and properties of contrast agents. Reduction of temperature is reported to increase the lifetime of microfoam solutions (Sebba, 1971). In another study with Aerosomes MRX115 (ImaRx Pharmaceuticals), and Imagent (Alliance Pharmaceuticals) 58% of the bubbles survived after 1 hour in a water bath at 37°C, while at 20°C 81% survived (Sahn et al., 1997). Although for modern contrast agents temperature does appear to have an effect on their stability, within the time scale of an examination with contrast agents it is not considered to have such a large effect.

Experimental in-vitro investigations have been carried out to assess the impact of the hydrostatic pressure on the stability of the agents, but little has been reported on the role of the gas content of the suspending solution (section 1.3.6). The variation of oxygen content in the blood might significantly affect the stability of the contrast bubbles. In this chapter, four agents are tested in terms of relative decay in solutions with different oxygen concentrations. Traditional methods of degassing like boiling were not used and instead the introduction of Helium to the solution is employed prior to introduction of the agent. This is a highly accurate and reproducible approach for degassing used routinely in chromatography (Williams and Miller, 1962). Moreover it provides a simple, fast and effective tool with great versatility compared to other techniques. The results should be suggestive of the tolerance of the agents in the arterial and venous blood environments.

4.3 Materials and methods

The full description of the experimental set-up is given in chapter 2, but paragraph 2.2.1 (p.16) is most relevant. The exact settings used in these experiments are described in paragraph 3.2.2.1 (p. 35). Also the handling of agents is covered in paragraph 3.2.2.2 (p. 35).

4.3.1 Helium degassing

Sterile water was used as the suspending medium for all the agent suspensions. Different air concentrations were achieved by putting the sterile water in a 3 litre Total Parenteral Nutrition plastic bag (KabiBag™, Kabi Pharmacia), and introducing either helium or air. Helium degassing is considered as the most reliable, efficient, and particularly fast (Williams and Miller 1962). Stripping liquids with an inert gas, which is used as a carrier gas, has long been known. Henry's Law explains that the ratio of concentration of a dissolved gas in a liquid, to its partial pressure is constant (Atkins 1994). Helium is essentially insoluble so it simply acts as a carrier in degassing. If there is any dissolved gas it will distribute itself into the helium bubbles according to Henry's law. Thus the helium progressively removes the dissolved gas. The concentration of air in the liquid should fall exponentially with time. The solubility of helium is very low at about 1% of the volume in water (at

room temperature), while for nitrogen is slightly higher at 1.6%, and oxygen which is considered as a soluble gas at 3% ("the Merck index" 1968). Helium was introduced by a cylinder, maintained under high pressure, to 3 litres of sterile water for 20 minutes using a narrow tube that could release the gas into the water. After the preparation the bag was sealed.

Air-saturated solutions were also prepared by introducing air to 3 litres of sterile water for 15 minutes.

The assessment of air content in the suspending medium was done by measuring the partial pressure of oxygen (pO_2) in it. Oxygen is the most soluble atmospheric gas that could dissolve in the water, and therefore its measurement stands as the gas with the maximum concentration. Thus a degassed solution can be best characterised by assessing the concentration of oxygen. The measurement of pO_2 was taken using a blood gas manager (model 1312, Instrumentation Laboratories (UK) Ltd, Warrington, UK). A 10ml sample was collected from the bag with a syringe. Because the objective of this measurement is to assess the pO_2, the solution was pulled gently into the syringe from the bag in order not to corrupt the measurements. The measurement of pO_2 was done immediately after the preparation, and randomly in the course of five hours after preparation.

After the introduction of the degassed sterile water into the tank, it is expected that air dissolves in the course of an experiment, and the pO_2 increases. The measurement of pO_2 was repeated 20 minutes after the introduction of the degassed water into the tank.

4.3.2 Experimental protocol

The contrast agents used in this study are: Levovist (Schering), DMP115 (Dupont-Merck), Quantison™ (Andaris), and Myomap (Andaris). Paragraph 3.2.1 (p.34) describes in detail the preparation protocol as well as the properties of these agents.

In this experiment the agents underwent two sets of measurements, 1) a long experiment, and 2) a short experiment.

1) Long experiment. After the production of the suspending medium in the bag, the pO_2 was measured and then the agent was injected into the bag, and stirred for 5

minutes. The concentrations for the different agents were decided after the completion of the first experiment, and chosen to be in the linear range of the resulting curves (arrows in Figure 3.1, and Table 3.5). A 200ml sample was taken from the bag and introduced into the measuring tank. The solution was stirred for 29.5sec with a magnetic stirrer and then insonated for 0.5sec, and the last frame was acquired. The solution was disposed of and after 10 minutes a new 200ml sample was placed in the tank, and the procedure repeated. In this way a frame was acquired every 10 minutes until a total of 15 frames was reached, and at the end of the experiment the pO_2 was measured in the remaining liquid in the bag. This experiment was repeated for two solutions with different gas levels as mentioned previously. One solution was degassed and the other was air saturated. For Quantison™ this experiment was repeated three times, since the level of backscatter for this agent was low. Levovist did not undergo this set of measurements since it was not designed to remain echogenic for the above time ranges.

2) Short experiment. The suspending medium was produced in the bag and then the pO_2 was measured. Instead of injecting the agent into the bag, 200ml of the suspending medium in the bag were placed in the tank and then the agent was injected in the tank. The new solution was continuously mixed, and every 29.5sec a 0.5sec of insonation took place and the last frame of the insonation was acquired. This was repeated until 15 frames were acquired. The complete experiment was repeated as previously for the degassed and the air-saturated suspension, but it was also repeated three times for every suspension, to assess the variability of the experiment.

For Levovist the protocol for the short term experiment was altered. Levovist is more short lived in suspension and the protocol was designed not to allow the same time of mixing, as for the other agents, before acquisition. After the introduction of the 200ml to the tank, Levovist was injected into the tank and stirred for 9.5sec and then insonated for 0.5sec, and the last frame was acquired. The same was repeated until 15 frames were acquired. The complete experiment was repeated 6 times, for each of the above two oxygen levels, to reduce the variability of the experiment.

The concentrations of contrast used in this experiment are given in the section (a) of the results.

4.3.3 Statistical analysis

All the sets of frames were transferred to the Sun Workstation where image reconstruction took place. As described in chapter 2 (paragraph 2.2.1.3) the backscatter intensity of a ROI above the bottom of the tank was calculated using the available software. This backscatter intensity was referred to the acoustic test grey scale object (Cardiff grey scale test object, Diagnostic Sonar, Livingston, Scotland). This is the Normalised Backscatter NB_i as defined in equation 2.1 (p. 23), and explained in chapter 2.

For every set of 15 frames of either the short or the long experiment, an exponential fit was applied to the 15 values of normalised backscatter and the decay constant and the intercept were derived. The mean value and standard deviation of these values, were calculated for each pO_2, and a t-test with equal variances was performed to compare the two gas saturation levels. The 5% level of significance was considered and the probability of the t-test was calculated.

Correlation with the exponential fit was performed by extracting the linear correlation r between time and the natural logarithm (ln) of normalised backscatter. Correlation to the exponential fit was considered acceptable when $r>0.9$, and when $r<0.7$ the exponential fit is not considered satisfactory.

4.4 Results

4.4.1 Degassing

For the short experiments the degassed sterile water suspensions achieved 1.50±0.36kPa and the air-saturated one 25.12±0.88kPa oxygen partial pressures (pO_2) respectively. Table 4.1 demonstrates the results of the introduction of helium and air in the solutions. Maximum, minimum, and average pO_2 as well as its standard deviation are shown for the solutions prepared for each agent. After the preparation, with either gas, the bag was sealed. The oxygen level remained constant within a range of 0.2kPa for more than 5 hours.

The solution finally produced in the bag was used in two different ways. 1) The agent was injected into the bag and then batches of 200ml were introduced in the measuring tank (see long experiment), and 2) 200ml of the solution were introduced, using the tubing supplied with the bag, into the measuring tank and the agent was injected in that tank (see short experiment). As explained in the experimental protocol the performance of the contrast agents for variations of backscatter in a short period of time (2), and also for several hours (1) was investigated.

Table 4.1 *Oxygen partial pressures in the solution in the short experiment*

Contrast agent	Repetition degassed/ saturated		pO_2 maximum (kPa)		PO_2 minimum (kPa)		pO_2 average (kPa)		pO_2 st.dev. (kPa)	
Levovist	6	6	1.8	26.0	1.0	25.2	**1.23**	**25.7**	0.37	0.45
DMP115	3	3	1.9	26.4	1.4	24.7	**1.70**	**25.4**	0.26	0.89
Quantison™	3	3	1.8	24.3	1.6	23.7	**1.70**	**23.9**	0.10	0.32
Myomap™	3	3	2.0	25.7	1.3	24.3	**1.63**	**24.8**	0.35	0.78

It should be noted that by the end of the measurements the degassed solution picks up atmospheric air and as a result pO_2 increases. This pO_2 for all the short experiments averaged to a final 8.36±0.48kPa before disposal. The time between the introduction of the degassed water in the tank and the measurement of the pO_2 at the end of each experiment was about 20 minutes. The pO_2 was also checked for the air saturated solutions. It was noticed that the values remained the same or changed by 0.1kPa at most. The fact that air dissolves in the degassed solution during the course of the experiment was not considered a problem since even after the end of the experiments the suspension was still degassed having a significantly different pO_2 than the air-saturated suspension. As shown in Table 4.1 the production of degassed and saturated solutions was reproducible. This can be seen from the maximum and minimum values, as well as the standard deviations of the average value which are small. Also the air that dissolves during the experiments in the degassed solutions gives a standard deviation of only 5.7% from the average value, showing that this parameter of the experiment is also highly predictable.

The long experiment averaged 1.67kPa±0.14kPa (pO_2) for the degassed solution, and 25.0kPa±0.7kPa for the saturated solution. These are average values taken in the beginning of each experiment, but, as mentioned earlier, in the course of 5 hours an increase in pO_2 higher than 0.2kPa was not observed.

4.4.2 Long experiment

After the completion of the experiment "backscatter vs. bubble concentration" (paragraph 3.3.1 p. 39) the concentrations of the three contrast agents were chosen. Table 4.2 shows the concentrations that were used in this experiment. Myomap™ and Quantison™ showed similar behaviour when injected into the bag with different pO_2. Both agents showed little correlation between the normalised backscatter and time for both pO_2 (Figure 4.1c and b), which is explained as lack of decay in the solution environment. Table 4.2 shows this in more detail. DMP115 on the contrary showed remarkable correlation with the exponential decay (Figure 4.1a), but no significant change in the decay constant existed between the two solutions. This implied that these bubbles diffuse in solution without however being affected by the presence of other gases. After 145 minutes in two different solutions the DMP115 gave backscatter that was almost at the noise level of the experiment.

Table 4.2 *Long experiment results*

		DMP115	**Quantison™**	**Myomap™**
Concentration (ml of contrast /3lit suspension)		0.05	4	10
Low air level	pO_2 (start in kPa)	1.8	1.9±0.5	1.7
	Decay constant (min^{-1})	0.037 ±0.001	0.0004 ±0.0003	0.0012 ±0.0005
	r	-0.99	-0.21±0.16	-0.54
	pO_2 (end in kPa)	2.5	4.8±1.2	1.9
High air level	pO_2 (start in kPa)	25.5	26.1±0.1	24.7
	decay constant (min^{-1})	0.045 ±0.003	-0.0024 ±0.0025	0.0011 ±0.0013
	r	-0.98	0.50±0.22	0.24
	pO_2 (end in kPa)	25.1	25.1±0.3	24.7

For all three agents the pO_2 at the start (0min) and at the end (145min) of the measurements, the decay constants, and also the correlation coefficient to the exponential decay are stated. The experiment was repeated 3 times for Quantison™ and the mean decay constant ± the standard deviation are given. The experiment was not repeated for DMP115 and Myomap™ and therefore the standard deviation of the decay constant is a standard deviation of the mean calculated by the regression analysis.

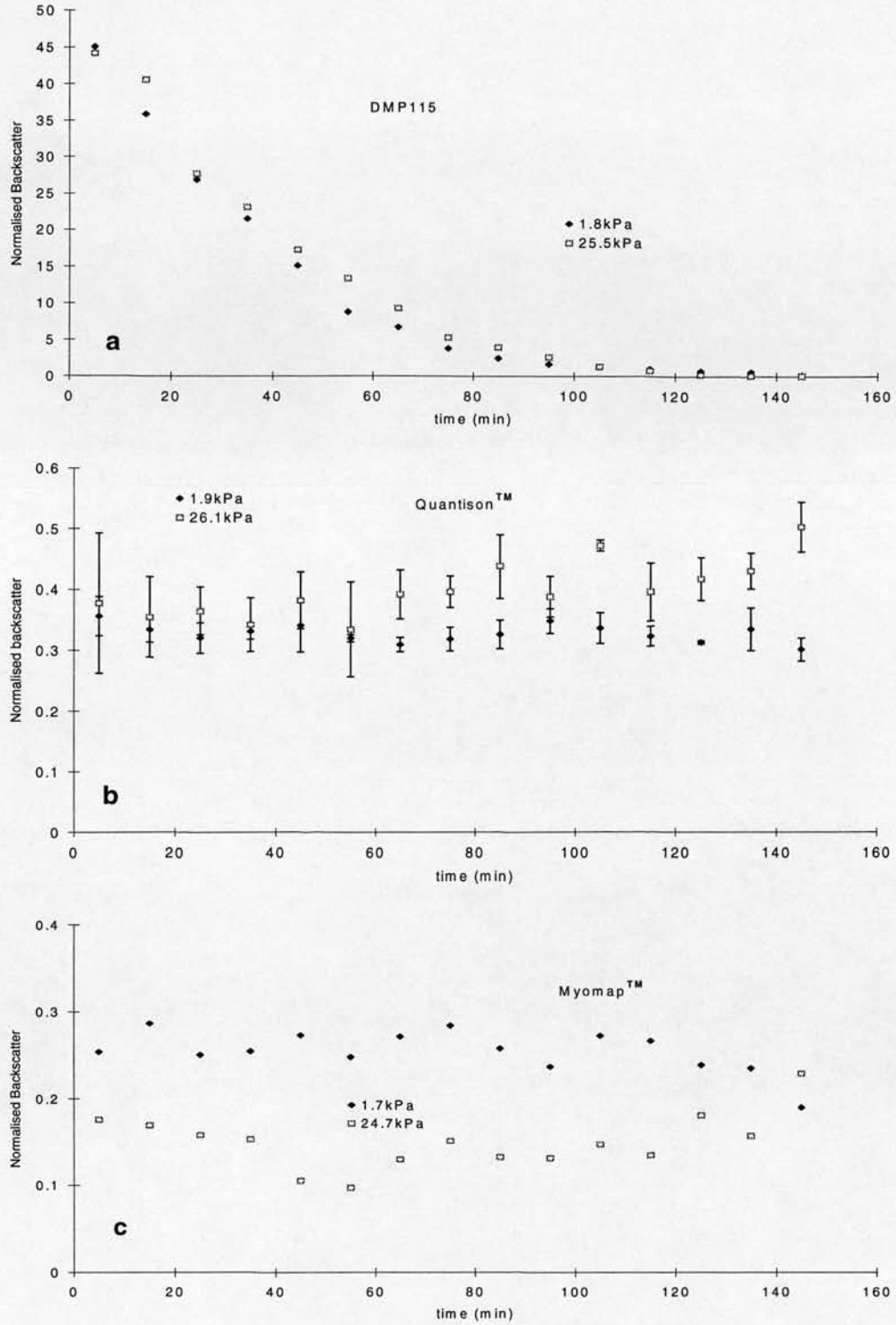

Figure 4.1 a Decay of DMP115 in the bag at 1.8kPa and 25.5kPa partial oxygen pressure. No significant difference between the two graphs is noticed. ***b*** No decay for either pO_2 for Quantison™, and no significant difference between the two graphs is noticed. ***c*** There is no decay of contrast for Myomap™ in the bag at either 1.7kPa and 24.7kPa partial oxygen pressure. No significant difference between the two graphs is noticed either. Correlation coefficients with the exponential fit from all graphs are in Table 4.2. The experiment was only performed once for DMP115 and Myomap™ due to their high reproducibility (section 2.3.3).

4.4.3 Short experiment

The bubble concentrations used for this part of the experiments are stated in Table 4.3. Some examples of curves produced in these experiments are shown in Figure 4.2. For DMP115, Myomap™, and Quantison™, for each value of air level in the suspension, the measurements were repeated 3 times, while for Levovist 6 times. Averaging of the repeated measurements of the same experiment was not performed since it is not statistically correct to average normalised backscatter values that are not independent from the previous or the following measurement. The variation in the data appeared from both within and between measurements, i.e. the decay constant, the intercept and the correlation of the data to the exponential fit. Hence the averaging between these curves was applied to the intercepts and decay constants of the exponential fit. Table 4.3 provides that analysis. For each solution and contrast agent the correlation coefficients of the exponential fit to the data were calculated and in the table the number of times this was lower than 0.7 and higher than 0.9 are shown. Average values of intercepts and decay constants are also stated and the result, i.e. the probability, of a t-test with equal variances between the two solutions are found in the bottom of the table. It was also important to measure the pO_2 at the end of the experiments that were done in the degassed solutions. These measurements are also in Table 4.3.

Quantison™ was the only agent that did not have good correlation with the exponential fit, probably also due to the lack of decay in the plots (Figure 4.2c). The best correlation with the exponential fit was exhibited by DMP115 with values very close to one (Figure 4.2b). Levovist and Myomap™ also showed good correlation in all measurements (Figure 4.2a and d). Quantison™, Myomap™ and the DMP115 exhibited no difference in the decay constants, and intercepts deduced from the exponential fits, for the two pO_2 of the solution. Levovist was the only agent that exhibited significantly different values for the two solutions. However all the Levovist curves had the characteristic of their first data point standing out as an outlier. Since this happened for almost all of the measurements with Levovist, it can not be rejected from the plots as a false value. Thus the exponential fit was not an accurate representation of the decay of Levovist. It was noticed that indeed the

oxygen-saturated solution gave a higher normalised backscatter value, for these outliers than the degassed one. However performing a t-test for the mean values, for each of the two pO_2 in the solution, there was no significant difference between the two solutions (p=0.057). Performing also a t-test for the decays and intercepts, when the plots exclude the outliers, it was realised that both these characteristics of the curves still were highly significantly different for the two solutions (p<0.001).

Table 4.3 *Short experiment results*

		Levovist	**DMP115**	**Quantison™**	**Myomap™**
Concentration (ml/200ml of suspension)		0.8	0.0025	0.3	1
Low air level	pO_2 (start in kPa)	1.3±0.2	1.5±0.3	1.7±0.1	1.6±0.3
	r<0.7	0	0	3	0
	r>0.9	5	3	0	2
	pO_2 (end in kPa)	6.4±0.7	8.5±0.5	8.7±0.6	8.3±0.6
	Intercept	33±18	49±5	0.51±0.04	0.48±0.04
	Decay constant (min^{-1})	1.23±0.25	0.07±0.02	0.01±0.02	0.06±0.00
High air level	pO_2 (start in kPa)	25.1 ±1.0	25.4±0.9	23.9 ±0.3	24.8 ±0.7
	r<0.7	0	0	2	0
	r>0.9	3	2	0	3
	Intercept	81±17	43±5	0.44±0.10	0.49±0.07
	Decay constant (min^{-1})	0.31 ±0.07	0.058 ±0.005	0.030 ±0.027	0.059 ±0.004
Comparison	degrees of freedom	10	4	4	4
Intercepts	p	0.003	0.201	0.343	0.933
Decays	p	0.0005	0.493	0.404	0.806

The slight difference in concentration between this and the long experiment only lies in the availability of the agents. For all four agents the correlation coefficients r is compared with 0.7 and 0.9. If greater than 0.9 it is considered that the exponential fit is representative of the decay of the contrast agents, and if smaller than 0.7 it is considered that the behaviour of the agent is not following the exponential decay. Intercepts and Decay constants derived from the fit are also averaged and stated in the table, and the p values are the result of the t-test with equal variances between the two solutions. 0.05 was the significance level of this comparison.

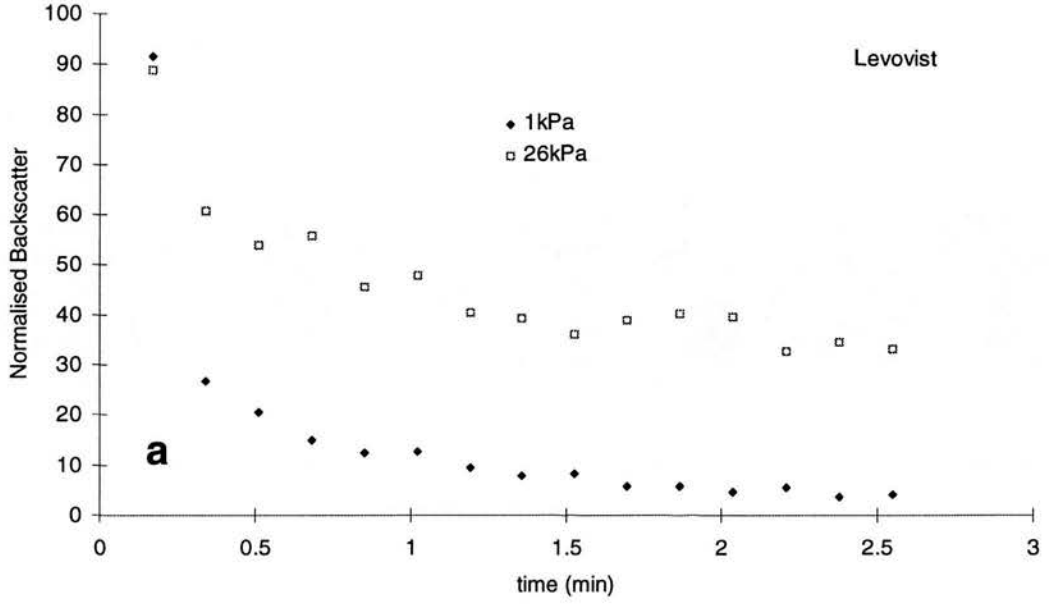
Levovist
1kPa
26kPa
a
Normalised Backscatter
time (min)
0
10
20
30
40
50
60
70
80
90
100
0
0.5
1
1.5
2
2.5
3

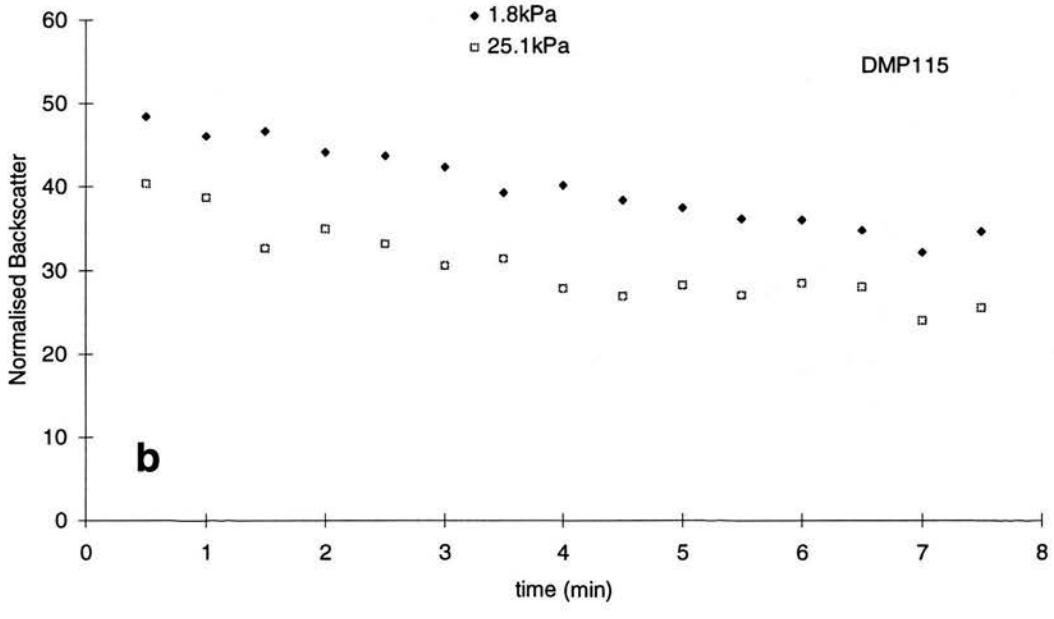
1.8kPa
25.1kPa
DMP115
b
Normalised Backscatter
time (min)
0
10
20
30
40
50
60
0
1
2
3
4
5
6
7
8

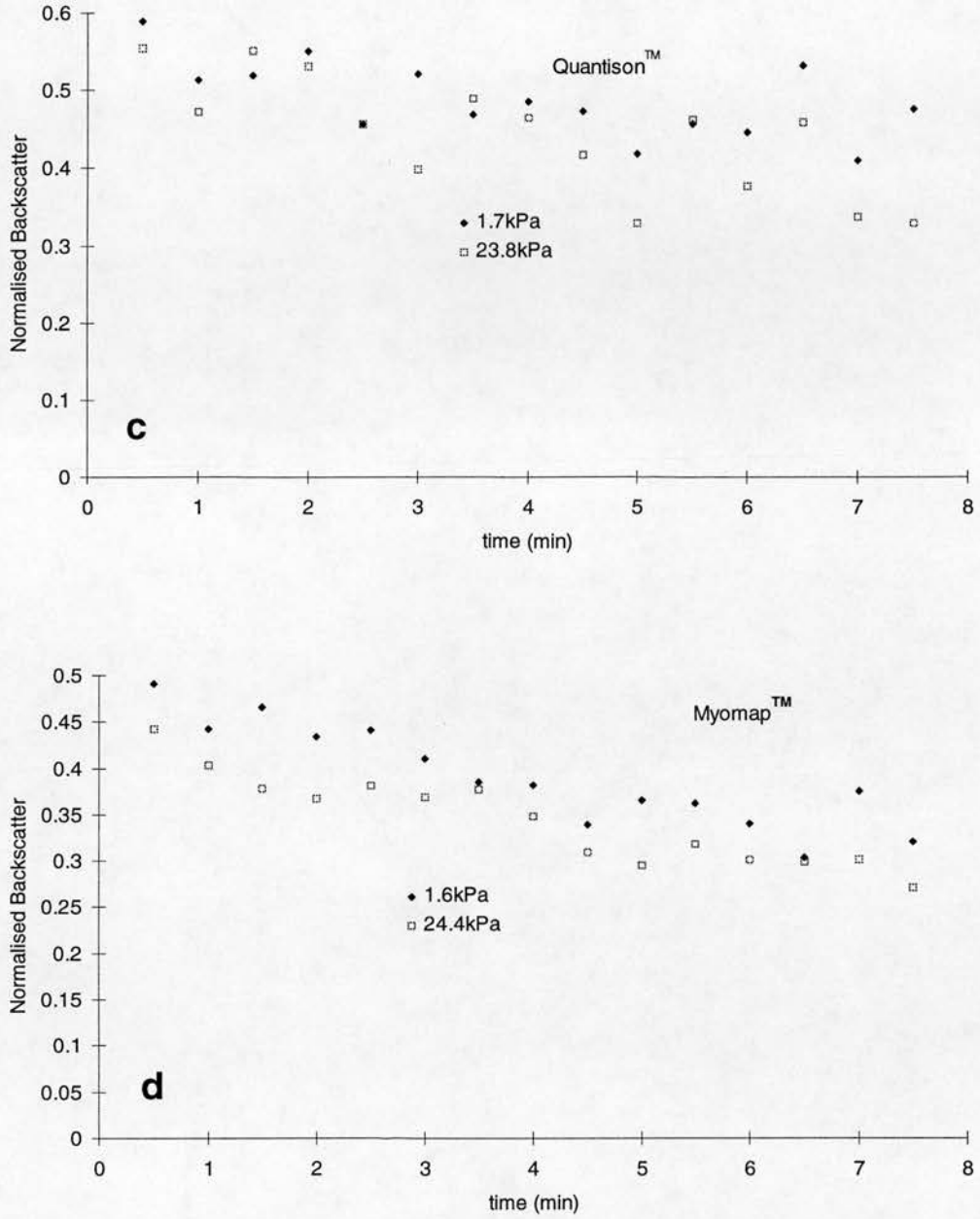

Figure 4.2 The two curves for each graphs were randomly selected. The experiment was repeated 3 times (6 for Levovist) and the results are in *Table 4.3* ***a*** Decay of contrast against time for Levovist. The degassed solution (pO_2=1kPa) provides a faster decay for the agent than the air-saturated solution (pO_2=26kPa). ***b*** Decay of contrast against time for DMP115. The agent decays in both degassed (pO_2=1.8kPa), and the air-saturated solution (pO_2=25.1kPa). There is no difference between the decay rate of the two solutions. ***c*** Decay of contrast against time for Quantison™. There is no sign of decay in either degassed (pO_2=1.7kPa), and the air-saturated solution (pO_2=23.8kPa). ***d*** Decay of contrast against time for Myomap™. The agent decays in both degassed (pO_2=1.6kPa), and the air-saturated solution (pO_2=24.4kPa). There is no difference between the decay rate of the two solutions.

4.5 Discussion

4.5.1 Degassing

The method of degassing presented here is routinely used in high-pressure liquid chromatography (Altech, Illinois, USA). The technique applied provided a tool which was faster, and much more efficient than any of those used for previous ultrasonic measurements (Fowlkes and Carson 1991). This provides remarkable reproducibility of the suspension's pO_2, as well as a wide range of gas concentrations. Moreover it was possible to carry out a study that could assess the tolerance of different contrast media in degassed suspensions.

4.5.2 Significance of the preliminary experiments

The two experiments presented in chapter 3 are considered necessary not only for this chapter's investigation, but also for in-vitro or in-vivo investigations that aim at reproducible images and the quantitation of contrast enhancement.

The "lifetime in the vial" experiment (paragraph 3.3.2) is important because the outcome of this would define a) whether the agent is sufficiently stable in the vial to give reproducible enhancement for a defined period of time, and if not b) whether the acoustic backscatter is decaying in a reproducibly predictable fashion, so the measurements taken at any time after the preparation of the agent suspension could be compensated for it. Where neither of these two conditions prevails then it is not possible to use the agent for a quantitative analysis. Levovist proved to be most unstable. The company's instructions for Levovist dictate "...vigorous shaking for about 5-10 seconds. Then allow the suspension to equilibrate before use (up to 2 minutes). The resulting homogeneous suspension is to be administered not later then 10 minutes after preparation...". The phrase "resulting homogeneous suspension", was of utmost importance. A few times after the preparation a vial failed to have a homogeneous appearance and when tested it showed a very low level of backscatter. Vials like these were rejected for use in the experimental procedure. Because they were easy to visually distinguish and consequently discarded, they did not affect the outcome of the experiments. Despite this the vials that were used showed a large

variation in backscattering performance compared to the other agents and therefore the number of repetitions for each experiment were doubled. However the standard deviations for decays and intercepts remained higher than for the rest of the agents.

The results from chapter 3 suggested that Levovist would not survive the long term experiment, and the short term experiment, was modified in order to obtain comparable plots of backscatter with time.

Another important issue raised in chapter 3 through the "Backscatter vs. Concentration" experiment, was highly valued here. The results were in the form of Normalised Backscatter, and with the help of the results of chapter 3 these extrapolated to bubble concentrations. This made the experimental procedure highly reliable and quantifiable, and provided a check of reproducibility. The results in this chapter proved statistically reproducible.

4.5.3 Effect of the gas levels

For Quantison™ and Myomap™ there was no sign of decay, in the long experiment, which suggested great tolerance of the agents of the specific in-vitro situation (Figure 4.1b and c). DMP115 had a positive decay constant but there was no sign of difference in decay between the two pO_2 levels. After 2 hours in both environments the backscatter level of the agent was close to noise levels (Figure 4.1a).

The short experiment showed also that Quantison™ did not exhibit any significant decay, and therefore did not show strong correlation with the exponential fit (Table 4.3). Quantison™ proved to be the most robust agent. Myomap™ and DMP115 showed little or no decay in the long term experiment (Table 4.2), while they showed higher decay rates in the short term experiment (Table 4.2). This indicated that even a low acoustic pressure, which was used in this experiment, was enough to reduce the backscattering performance of those two agents. Also both agents showed that they were tolerant under different pO_2 levels.

Levovist was substantially different from the other agents, and was destroyed much faster when subjected to a low pO_2. Levovist is composed of air microbubbles, and is stabilised with palmitic acid. Its permeability allows different gas levels to affect its rate of diffusion. Even though the first values of the plot were not

significantly different with level of significance p=0.05, it was obvious that there was a significantly higher drop in backscatter and an increase in decay when the agent was suspended in the degassed solution. From this it cannot be concluded whether the pO_2 of the suspension was alone responsible for the destruction of Levovist, or it was both the pO_2 and the acoustic power applied to the agent that act as a combined parameter to the destruction. To determine which of these possibilities were responsible, another experiment was performed where the agent was maintained in the suspension for 30sec instead of 10sec before insonation. The first measurements were significantly different for the two suspensions, which proved that a low pO_2 alone was destructive for Levovist. Another observation, already noticed in the results' section, was that the first point of each plot was an outlier to the exponential fit, and therefore this model cannot explain the decay of Levovist (Figure 4.2a). This outlier suggested that there was a population of bubbles that were less stable, than the rest of the bubbles which showed a good correlation with the exponential fit.

Similar findings were demonstrated in an experiment, where Albunex bubbles were insonated at 1MPa peak negative pressure (Wu and Tong, 1998). That study also showed, on a different time scale, that after an initial drop in the number of scatterers after insonation, a subsequent less pronounced decrease of the remaining number followed. The authors suggested that there were two different populations of bubbles. One "weak" population easily destroyed by the insonation, and a "stronger" one more resistant to the particular acoustic pressures.

It was difficult however from all the results to point to the responsible mechanism for the decay of the different agents. Quantison™ showed no sign of decay in any environment at this acoustic pressure. The results suggested that its coating is non-permeable since its gas is diffusable (compared to DMP115) and would obviously tend to dissolve at least in a degassed environment.

Myomap™ showed some decay when exposed to ultrasound. This agent is similar to Quantison™ in structure, and the main difference is that it has a bigger bubble. Decay due to exposure to ultrasound suggested that its coating tends to become permeable, perhaps due to rupture. The lack of difference in decay between

the two environments suggested that the ultrasonic beam probably affected the permeability of the coating, and was responsible for the diffusion of the bubble.

DMP115 decayed without the assistance of ultrasound (Figure 4.1a). The permeability of its lipid bilayer coating, being similar to that of a red blood cell, is expected to be high enough to allow exchange of gases between the bubble and the surrounding liquid (Van Liew and Burkard, 1995b). Gas flux towards the microbubble would not occur in a degassed environment due to the inherent lack of gases in suspension. However, when the environment is gas-saturated, the volume of the bubble is expected to increase due to the diffusion of gases from the bubble environment (Van Liew and Burkard, 1995a). According to this study a subsequent diffusion from the bubble depending on the concentrations of the different gases in the suspension would be expected. However, it was found that there was no difference in the decay in the two different solutions, which suggests that any influx of gases into the bubble was negligible, and therefore the decay was dictated by the diffusivity of perfluorocarbon. It is also believed that this was the rate observed in the long experiment. It could be suggested that the bubbles that might grow would not be stabilised by the existing coating, and it seems unlikely that this coating would expand to follow the initial growth of the bubble (due to the suggested influx of gases from its environment) and have the necessary elasticity.

4.5.4 Limitations of the study

An in-vitro experiment can only be suggestive of the in-vivo situation. Experiments in real blood and under more realistic conditions would give a better idea of the behaviour of the agents at different gas levels. The complexity of the problem relies on the fact that all the various parameters which contribute to altering the size of a bubble, can not be accounted for independently, and therefore can not be investigated separately.

Further, it was not clear what was the exact contribution of the ultrasonic beam in the decay process of the agents. This lead to the experiments described in the next chapter.

4.5.5 Clinical implications

Venous blood has 6-9kPa pO_2, and the arterial 11-14kPa pO_2 in physiological subjects. The pO_2 values in this study were arranged to have values below and above that range. Despite these extremes the role of gas content in different vascular spaces is outlined. Moreover it is difficult to predict the behaviour of an unstable agent in a pathological situation related to the alteration of pO_2.

This chapter has shown that it is necessary for contrast agents to be tested for their stability in different environments. Manufacturers (Schneider et al. 1992, Unger et al. 1994) have reported hydrostatic pressure tests for agents. The effects of the gas content in the suspending medium is reported in the literature.

Levovist may be unsuitable for quantitative studies, while the other three agents seem to offer a reproducible and stable backscatter level. The slight decay of DMP115 in suspension suggested that experiments with DMP115 should be performed over a shorter time scale.

It is also very important to carry out comparative studies. This study included one commercially available agent, and another three that expect FDA approval in the near future. As pointed out previously, the benefit was not only the comparison between the agents, but also the understanding of the properties of the contrast agents individually. The literature is limited in comparative studies of such a variety of contrast agents.

4.6 Conclusion

This chapter presented a novel degassing technique, previously not used in the field of ultrasound, and tested the stability of four contrast agents. Levovist was the only contrast agent that was unstable in degassed water, while DMP115, Quantison™, and Myomap™ proved stable. The following chapter aims to clarify the stability of the above agents for a wider range of scanner settings.

5 Chapter Five: The influence of pO_2 and acoustic pressure on contrast agents

5.1 Introduction

The previous chapter concluded the testing of the experimental set-up and handling of the contrast agents. It also initiated the investigation into the physical properties of contrast agents. However, it included an important assumption that the mixing of the contrast agent within the suspension using the magnetic stirrer was such that the backscatter was linearly related to the concentration of contrast bubbles in the whole suspension. This assumed that if the acoustic field caused destruction of the microbubbles within the acoustic field the number of destroyed bubbles would be very small compared to the total number of microbubbles. It also assumed that sufficient mixing would occur between frames to ensure that a completely uninsonated set of microbubbles were scanned each time a frame was acquired.

Even though it was concluded that Levovist was sensitive to the variation of pO_2, and the other agents were not, it did not become clear whether or not the acoustic field was responsible for the observed decay, and whether or not the above assumptions were valid. In the previous chapter a simple way of determining the effect of oxygen concentration on the lifetime of contrast agents was explored.

The study of the stability of the agents is taken a step further in this chapter. The influence of the acoustic pressure on the stability of the bubbles was investigated in addition to the gas content of the suspensions. The aim was to isolate the different parameters that influence the stability and behaviour of contrast agents, and to assess how these parameters affect the backscatter. Furthermore, it was considered valuable to investigate the independence of these parameters. A natural outcome for this chapter would also be the assessment of the performance of different agents in different acoustic pressures during continuous ultrasonic imaging mode, and thus this chapter is a step from stability studies to the assessment of contrast enhancement.

5.2 Materials and methods

5.2.1 The set-up

The full description of the experimental set-up is given in chapter 2, but paragraph 2.2.1 (p.16) is an easier reference. Also the handling of agents is covered in paragraph 3.2.2.2 (p. 35). The settings that were not used in chapters 3 and 4 are outlined here.

The transmit power ranged from 2.24% to 100% output power on the scanner console which corresponds to the range of 0.27MPa to 1.52MPa peak negative pressure. The details of the beam characteristics are in Table 2.1. All acoustic pressures, except for the third lowest (0.69MPa peak negative pressure), listed in that table were used and the focus was located at 4.25cm from the transducer. This was also the distance of the probe from the bottom of the tank.

5.2.2 The contrast agents and the suspensions

Three contrast agents were used in this study, DMP115 (DuPont), Quantison™ (Andaris), and Myomap™ (Andaris). Levovist (Schering) was not used in this study since it did not exhibit sufficient backscatter reproducibility in comparison with the other agents (paragraph 4.5.3, p.63). Paragraph 3.2.1 (p.34) describes in detail the preparation protocol in addition to the nature of these agents.

The suspending mediums were produced in the same manner as in chapter 4 (paragraph 4.3.1, p. 51). Sterile water was placed into a 3-litre Total Parenteral Nutrition plastic bag (KabiBag™, Kabi Pharmacia), and either Helium for 20 minutes or air for 15 minutes were introduced to produce either a degassed or an air saturated suspension.

Overall 9 bags of degassed and air saturated suspensions were produced. The pO_2 for the degassed suspension was 1.43±0.10kPa, with maximum and minimum values 1.6 and 1.3kPa respectively. The content of each bag was used for approximately 2 hours, and random checks proved pO_2 stable.

5.2.3 Experimental protocol

The tank was filled with 200ml of the suspension medium from the bag. The agent was then injected in the tank. The quantities of contrast in the different suspensions were: 3μl for DMP115, 0.3ml for Quantison™, and 1ml for Myomap™. The choice of bubble concentrations in the tank was given in Table 3.4. Consequently after the injection of contrast there were approximately 15000 bubbles/ml (ml refers to the suspension) of DMP115, 2250000 bubbles/ml of Quantison™, and 75000 bubbles/ml of Myomap™ in the respective suspensions in the tank. Continuous mixing was applied for 28sec, and insonation was applied for 2sec (mixing continued). The RF data of the last frame of the 2-second insonation period was acquired. This routine was repeated until 15 frames were acquired. The only substantial difference between this protocol and the "short experiment" of the previous chapter was that the insonation time was increased from 0.5sec to 2sec. This was done in order to assess more reproducibly any possible decay. This measurement was repeated, for each agent, again for the two concentrations of oxygen, but it was also repeated three times for each concentration of oxygen, to reduce the variability of the experiment. In addition to the RF data being collected, all measurements were recorded on video for visual inspection.

5.2.4 Statistical analysis

All the analysis was based on normalising the backscatter intensity of the contrast agents as explained in paragraph 2.2.2.3 (equation 2.1). Unlike the last chapter in which the backscatter of the agents was referred to the acoustic test object, in this chapter the normalising factor was the scattering suspension based on the BMF (Figure 2.4b). This suspension was assumed to propagate and scatter the ultrasound beam in a similar manner to that of the contrast suspensions. The backscatter from the suspension was almost identical to that of the BMF (Figure 2.4b), but the preparation aimed at a suspension that would allow similar wave propagation to that obtained in sterile water. Therefore it was preferred as a backscatter reference, rather than the previously used acoustic test object.

Comparisons between contrast agents with different scanner settings are discussed in this chapter. In the previous chapters the normalised backscatter, with

reference to the acoustic test object, served as a comparison of the backscatter of contrast agents to that of a tissue mimicking material, and the scanner's setting remained unaltered (2.24% output power).

Also in this chapter background subtraction was used and its significance was assessed. A background frame was captured at the start of each set of acquisitions (suspension without contrast), and its backscatter intensity was subtracted from the backscatter intensity of each acquired frame from the contrast suspension. Normalisation was performed on the background-subtracted contrast intensity.

For each one of 18 sets of normalised data an exponential fit was applied, and the linear correlation coefficient, the decay constant in minutes^{-1}, and the intercept on Y-axis of normalised backscatter were calculated. The decay constant represents the decay rate of the bubbles in suspension in terms of backscatter, and the intercept is the normalised backscatter of the contrast suspension when no insonation has occured. The correlation coefficient was calculated after the natural logarithm of the data was plotted against time.

An arbitrary criterion was used in order to assess whether the exponential decay was followed. Correlation coefficients lower than 0.7 were considered as poor correlation to the exponential curve, and correlation coefficients higher than 0.9 were considered a satisfactory correlation to the exponential decay. Each combination of contrast agent, pO_2, and acoustic pressure, was repeated 3 times. Both decay constants and intercepts were averaged and a *t-test* assuming equal variances was performed in order to assess the difference between the two levels of pO_2.

5.3 Results

All backscatter intensities, except three for DMP115, were within the linear range of pixel intensities (<50,000,000) as this was set for the system in paragraph 2.3.1 and Figure 2.3. An experiment similar to that described in paragraph 3.2.3.1 and Figure 3.1, which would define each agent's concentration regime, was not carried out before these experiments for each different setting, since it was assumed that the concentrations used, were within the linear range of backscatter intensities.

Chapter 7 re-evaluates the relationship between normalised backscatter and the concentration of the agent, and also tests the validity of this assumption.

Even though all the data were background subtracted, it was realised that the importance of that calculation was insignificant, since the background never exceeded 5% of the lowest intensity measurement. All the agents showed decay when exposed to ultrasound at different acoustic pressures, perhaps with the exception of Quantison™ at the lowest acoustic pressure setting. Moreover, none of the highest backscatter intensity points (usually first in each data set) fell outwith the exponential trendline on its left side (see Figure 5.1), which suggested that these backscatter values were linear to the concentration of bubbles. Overall 126 decay curves were produced, and fitted to exponential models. This figure is composed of results from 3 agents, and the combinations of 7 acoustic pressures, 2 pO_2 suspensions, and 3 repetitions of each of the above combinations. Table 5.1 illustrates these in detail.

Table 5.1 *Behaviour of contrast agents when insonated at different acoustic pressures and pO_2 values*

	DMP-115	***Quantison™***	***Myomap™***
Number of acoustic pressures	7	7	7
Number of pO_2 levels	2	2	2
r < 0.7	0/42	24/42	1/42
r > 0.9	40/42	2/42	24/42
Number of non-significant intercepts	5/7	5/7	1/7
number of non-significant decays	6/7	6/7	3/7

3 data sets were collected for each (of 7) acoustic pressure, and each (of 2) pO_2 level. DMP115 and Quantison™ did not have significantly different decays (both 5 out of 7 non significantly different decay constants) and intercepts (both 6 out of 7 non significantly different intercepts) between the 2 pO_2 levels. The relationship of normalised backscatter versus time for Quantison™ had a rather poor correlation with the exponential decay (24 out of 42 fits had a correlation coefficient lower than 0.7) while DMP115 had a very high correlation (40 out of 42 fits had a correlation coefficient higher than 0.9). Myomap™ had a considerably good correlation with exponential decay but the 6 highest values of acoustic pressures provided significantly different intercepts. The same applied to 4 out of 7 decay constants.

Figure 5.1 shows a data set chosen at random with the acoustic pressure at maximum for (a) DMP115, (b) Quantison™, and (c) Myomap™. DMP115 demonstrated a very high correlation with the exponential model, while the correlation for Quantison™ was rather poor. Myomap™ demonstrated a behaviour

that was between the other two agents. The appearance of the captured frames at maximum acoustic pressures was similar to those obtained at 70.79% output power (Figure 5.2(2)). In Figure 5.2a2 DMP115 appeared as a homogeneous suspension of scatterers. In Figure 5.2b2 Quantison™ appeared very different and there seems to be two species of scatterers. Firstly a homogeneous low backscattering background and secondly a cloud of very bright scatterers. The same seems to apply in Figure 5.2c2 for Myomap™, except that the background seems enhanced.

The appearance of the data sets at the lowest acoustic pressure (2.24% output power) was similar to those shown in Figure 4.2 with the variability around the trendline being smaller for both Quantison™ and Myomap™. The correlation to the exponential decay was poor since there was negligible decay. All frames were relatively homogeneous (Figure 5.2(1)). According to the level set out in the statistical analysis for high/low correlations, the vast majority of the data sets for DMP115 highly correlate with the exponential fit, while for Quantison™ the correlation is considered poor. Almost half of the data sets (24) correlate highly with the exponential decay for Myomap™, but the rest of the sets provide a lower correlation coefficient, but not as poor as that of Quantison™. No tendency to higher or lower correlation coefficients was noticed for either different pO_2 or acoustic pressures. Looking at the VCR recordings of all the data, the suspensions of DMP115 appeared visually homogeneous, and when most bubbles were destroyed the frames provided almost identical backscatter intensity to the background. The appearance of Quantison™ and Myomap™ shown in Figure 5.2b2 and c2 respectively was observed at acoustic pressures higher than 0.83MPa (25.12% output power). For the two lowest acoustic pressures the suspensions for those agents looked homogeneous. The *t-tests* showed that the decays and intercepts were not significantly different for DMP115 and Quantison™ for the vast majority of acoustic pressures (Table 5.1). Myomap™ had significantly different intercepts for the 6 highest acoustic pressures, and 4 significantly different decays. Figure 5.3 illustrates the characteristics of the data sets versus the applied acoustic pressure. The solid lines correspond to the high pO_2 suspensions and the dashed lines to the low pO_2 suspensions. The decay constants are plotted in the left side (1) and the intercepts in the right side (2) of

Figure 5.3. Both parameters were in general lower at lower values of pO_2. For all agents there was a general increase in the decay constant with increasing acoustic pressure and increasing pO_2. The intercepts increased with acoustic pressure only for Quantison™ and Myomap™, while for DMP115 there was a small decrease. The poor correlation to the exponential decay resulted to an increased variability in the decay constant and intercept for Quantison™ (Figure 5.3b).

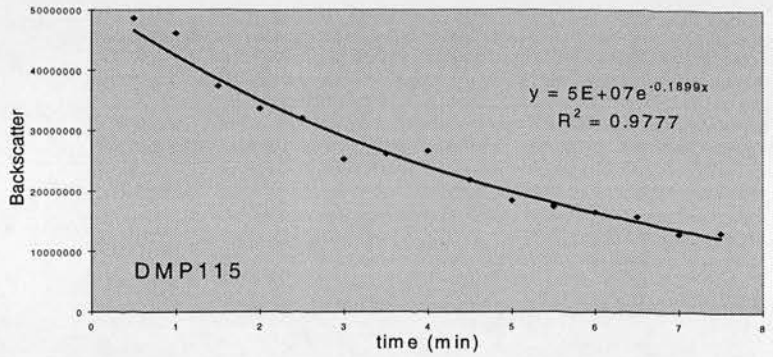

a

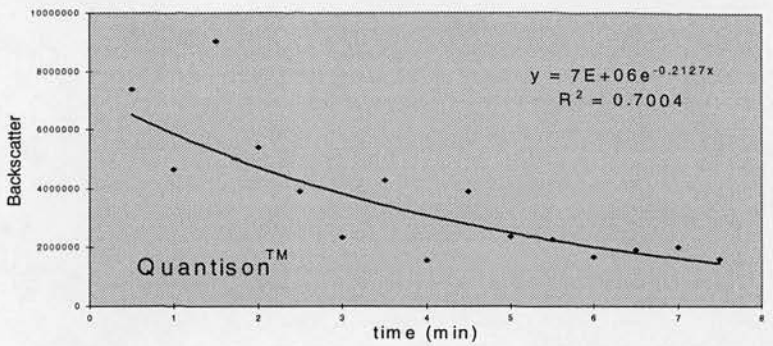

b

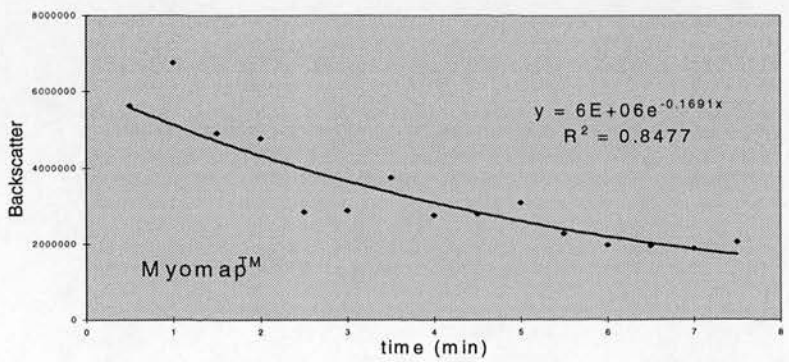

c

Figure 5.1 Backscatter vs. Time for ***a*** DMP115, ***b*** Quantison™ and ***c*** Myomap™. Note the difference in regression coefficients and the scattered values of the plots around the trends, as well as the decay constants and the intercepts.

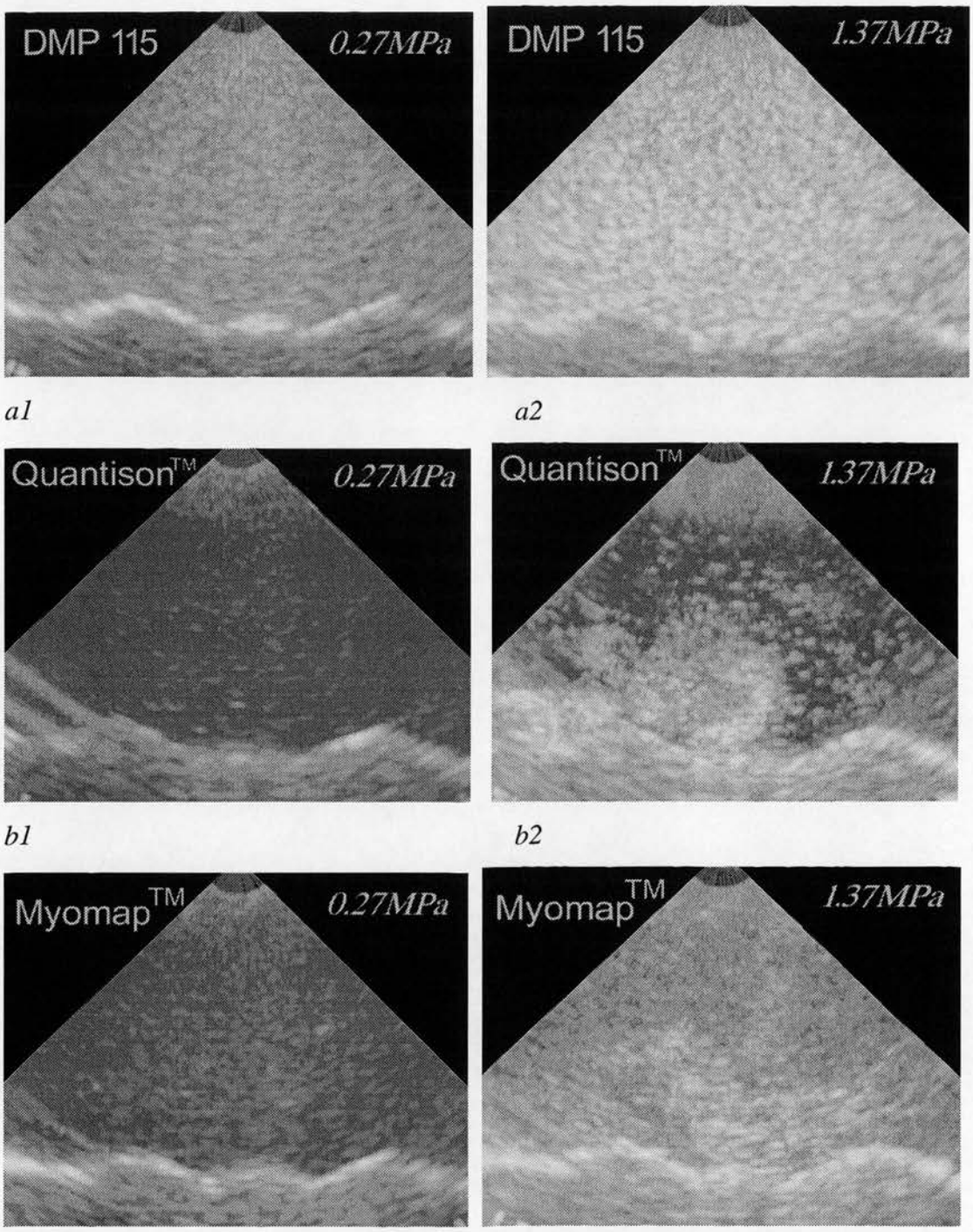

Figure 5.2 All the images refer to frames captured after 2 seconds of insonation. ***1)*** These images refer to the lowest acoustic pressure applied to the agents (0.27MPa), and ***2)*** refer to the second highest acoustic pressure (1.37MPa). Images ***a*** refer to DMP 115, ***b*** to Quantison™, and ***c*** to Myomap™.

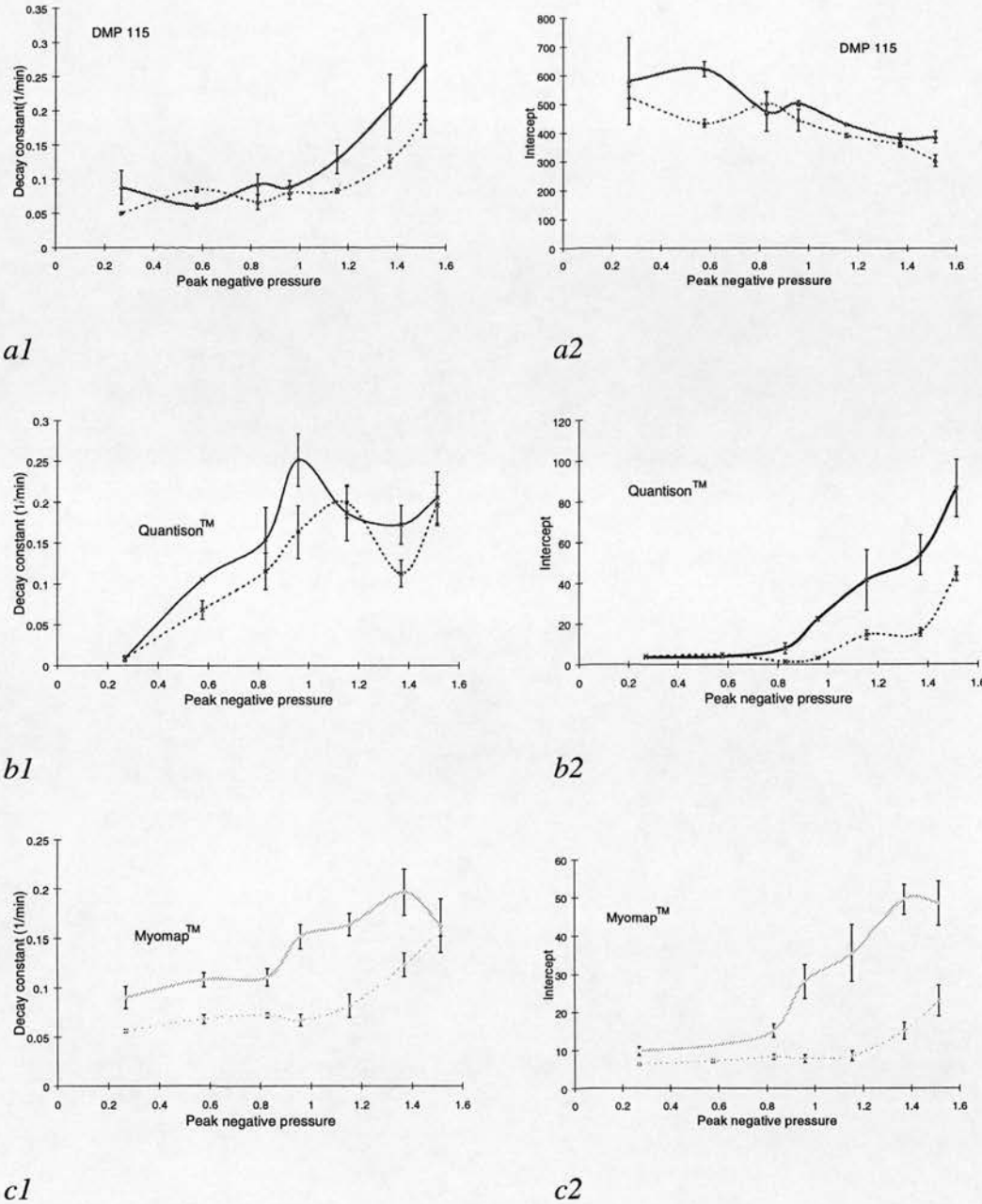

Figure 5.3 Applying an exponential trend to each set of data (normalised backscatter) the decay constant, and the intercepts were calculated (sets of graphs ***1*** and ***2*** respectively). Decay constants are measured in minutes^{-1}, and intercepts in normalised backscatter. The points are connected with lines to make the effect of different pO_2 and the relationship of the above parameters with peak negative pressure more distinguishable. The solid lines refer to air-saturated suspensions, and the dotted lines to degassed suspensions. It is also important to note that interpolation between points was performed only so that the tendencies of each curve can be observed, especially when the plot seem to overlap. DMP 115, Quantison™, and Myomap™, are referred to as ***a***, ***b***, and ***c*** pairs of graphs respectively.

5.4 Discussion

5.4.1 Destruction of bubbles

The images in Figure 5.2 gave some information on the nature of these agents, but the observation of sequences of frames recorded on videotape was valuable in understanding their behaviour. In Figure 5.2 all the *(1)* images referred to the lowest acoustic pressure, where the scatterers were homogeneously distributed. The differences in brightness of these images have been discussed (Figure 3.1 and Table 3.5).

Above 0.83MPa PNP it could be suggested that the background species of scatterers were the encapsulated bubbles and remained so after insonation, and the larger (than Quantison™) Myomap™ bubbles are expected to have higher backscatter. Both materials are reported to have robust shells, and would provide the same number of microbubbles after insonation (Johnson 1997, Frinking et al. 1999). This robustness restricts shell motion, which strongly suggested that the lower backscattering species of scatterers for both these agents have a behaviour closer to linear scatterers. For the same reason it also seems reasonable, at high acoustic pressures, that the bright species for both agents were free bubbles that leaked from their coating. The belief that these bright scatterers were free bubbles is further supported by their disappearance after one frame of insonation, which implies that they dissolve fast, highly likely for a highly soluble free air bubble (61Hz frame rate, i.e. dissolution time < 1/61 sec = 0.016 sec). Theoritical calculations and experiment agree with the above, and have shown that Quantison™ bubbles have a dissolution time about 11msec when exposed to 2MHz frequency (Finking et al. 1999). This study calculated that the dissolution time decreases with the increase of transmit frequency. Moreover, Frinking et al. (1999) calculated that about 1% of the entire population of bubbles is releasing free bubbles that are able to scatter ultrasound strongly, and therefore also suggested the existence of two different population of bubbles.

The behaviour of DMP115 is in agreement with the theory as well as observations of other studies. Dayton et al. (1999) observed that octafluoropropane

remained a free bubble for 280±180ms, while similar order dissolution times have been measured for sparingly soluble bubbles by Kablanov et al (1998b) in vivo. Dayton et al. also witnessed expansion (6% from bubble at rest) and contraction (9% from bubble at rest) for a phospholipid coated bubble (similar to the coating of DMP115), which did not occur for the albumin coated Optison. The behaviour of DMP115 is uniform across the range of acoustic pressures used in this study, and this is suggested to be related to the elasticity of the coating that perhaps is slightly dumping the bubble oscillation. This does not rule out the possibility of free bubble release at higher acoustic pressures, where the coating might not be able to withstand the oscillation amplitude or might be directly destroyed by the ultrasonic field.

5.4.2 The definition of the Overall Backscatter (OB)

Vigorous mixing would increase the number of fresh bubbles not previously in the field of view, and as a consequence the number of bubbles likely to release a free bubble, as discussed for Quantison™ and Myomap™. Morgan et al. (1998) have encountered a similar situation with a flow phantom, and found out that the increase of flow rate increased the backscatter intensity of contrast. Likewise lower frame rate would also increase that number. Therefore the frame rate and the mixing procedure determined the number of particles that gave free bubbles, for both agents. Taking into account that the mixing is not perfectly homogeneous the number of bubbles introduced in the field of view would vary significantly from frame to frame. This and the fact backscatter of the "bright" scatterers was significantly higher than the one from the "non bright" explained the poor correlation of Quantison™ with the exponential decay (Figure 5.1b, and Table 5.1). The same reasoning is behind the slightly improved correlation of the Myomap™ decay curves (Figure 5.1c, and Table 5.1), where the "non bright" scatterers have an enhanced backscatter when compared to the Quantison™ ones.

The finite slice width of the ultrasonic field (as supposed to infinitely small width) made the mixing inadequate in keeping the concentration of bubbles ("bright" scatterers at least) in the ultrasonic field equal to that of the rest of the suspension. It

was apparent for the case of Quantison™ that a single frame was sufficient to destroy almost all the scatterers (the "bright" species) in the scan plane, and that the scatterers that would appear in the next frame were those that were introduced into the scan plane by the mixing in 0.016sec (~1/61Hz). A near inverse relationship therefore exists between the frame rate and the magnitude of the backscatter intensity in each frame, and would be responsible for an underestimation of the intercept. Therefore, higher frame rate would decrease the amount of "bright" scatterers and the intercept, which suggests also that the intercept is no longer representative of the bubble concentration in suspension.

Although DMP115 seemed different compared the other two agents, it is rather unlikely, especially when the decay becomes larger, to assume that the concentration of scatterers in the ultrasonic field was equal to that of the rest of the suspension. Furthermore increasing acoustic pressure, which increases the decay, would lead to an increasing underestimation of the above intercept, which was probably the reason for the decreasing intercept in the case of DMP115 (Figure 5.3a2). Hence the intercept was affected by the decay process, and the decay constant was probably not accurately describing the decay process of the contrast agents. This may be the reason why for both Quantison™ and Myomap™, both parameters' graphs followed similar relative behaviour, i.e. both intercept and decay constant remained lower for the low pO_2 (Figure 5.3b and c). For Myomap™ this was a significant effect for all apart from the lowest acoustic pressure. It is also likely that a lower intercept was indicative of the effect of the low pO_2 on the agent. No conclusions however can be drawn knowing that continuous imaging mode cannot provide accurate assessment of decay and backscatter intensity representative of the concentration of scatterers in the tank.

Considering that at least the Quantison™ scatterers seemed to be destroyed much faster on the video, the underestimation of both parameters might be even greater. In search of a physical quantity that would solve this problem it could be suggested at this point that a quantity (roughly) inversely proportional to the intercept could be related to the decay of the each agent. The normalised backscatter $N(t)$ is assumed to follow the exponential model as a function of time. Hence:

$$N(t) = ae^{-bt} \tag{5.1}$$

The integral of normalised backscatter over time (***OB*** for Overall Backscatter) that represents the normalised backscatter intensity capacity of a particular suspension of scatterers would be:

$$\boldsymbol{OB} = \int_0^\infty N(t)dt = \int_0^\infty ae^{-bt}dt = -\frac{a}{b}e^{-bt}\Big|_0^\infty + \frac{a}{b}e^{-bt}\Big|_0^0 = \frac{a}{b} \tag{5.2}$$

which is the ratio of the intercept to the decay constant. Figure 5.4 plots this integral against PNP. There are several observations that can be made from this figure. 1) The variability of the points about each curve is significantly reduced. 2) The comparative effect of decay and backscatter of the agents to continuous imaging is demonstrated, and 3) the effect of the concentration of dissolved gas in suspension in the backscatter of the agents can be deciphered.

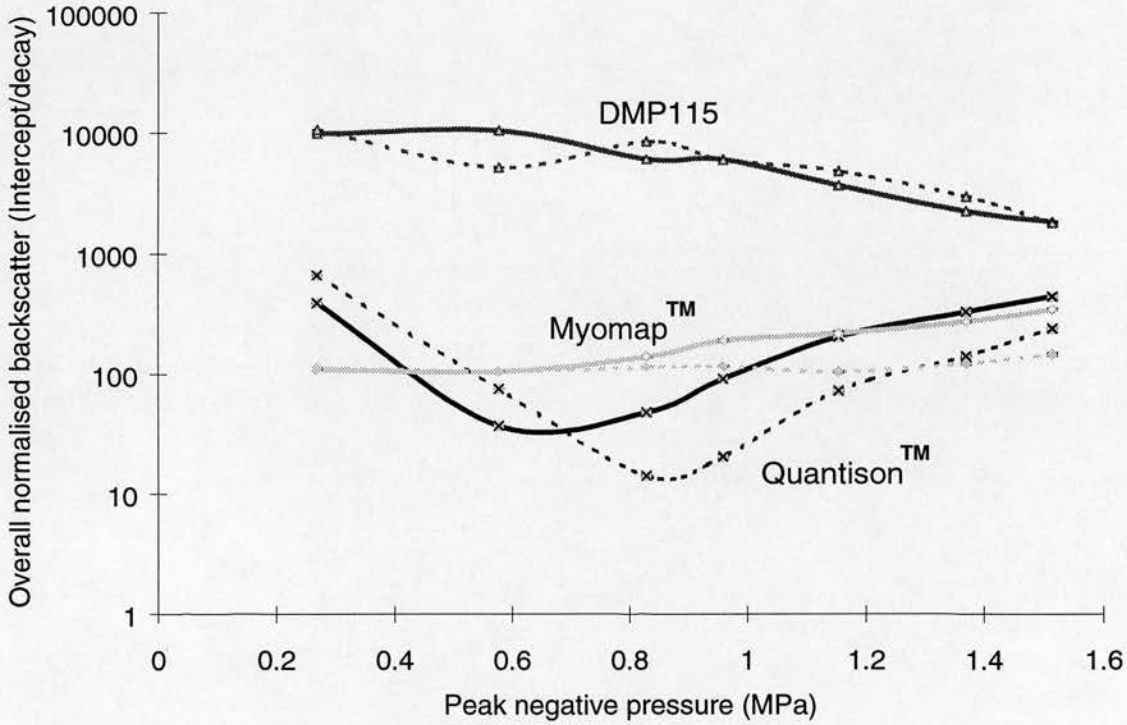

Figure 5.4 The ratio intercept/decay constant is plotted against peak negative pressure. Equation 5.1 proves that it represents the overall normalised backscatter (i.e. integrated over time). The dotted lines refer to low pO_2 (degassed suspension) and the solid ones to the high pO_2 (air-saturated suspension). The ratio is not significantly different for the two pO_2

levels for DMP115, while it becomes higher above 0.83MPa for the high pO_2 for the other two agents. (DMP115-triangles, Myomap™-diamonds, Quantison™-x).

A visual comparison of the overall backscatter plots (Figure 5.4) with the corresponding decay constant and intercept plots (Figure 5.3), demonstrated that the overall backscatter followed a less variable pattern with acoustic pressure. The considerably high standard deviation of decays and intercepts (Figure 5.3) were reduced for the overall backscatter. Errors were not plotted in Fig. 4 to make reading of the graphs easier. Moreover, there was also graphical evidence of significantly reduced variability in the overall backscatter. The curves that corresponded to the two different suspensions seemed to follow similar pattern (for Myomap™ and especially for Quantison™). The two lowest acoustic pressures seemed to provide no difference between the two suspensions, but further increase of acoustic pressure displayed a higher overall backscatter for the air-saturated suspension. This was consistent with both agents. A plot of the difference of the overall backscatter, between the two suspensions, against acoustic pressure was more illuminating (Figure 5.5). This difference correlated highly with acoustic pressure above 0.83MPa, and was similar for both agents. Both decay constants and intercepts were inadequate in following graphical patterns and provide subtle characteristics. The reduced variability of the overall backscatter justified also the reasoning behind its choice and stands as a proof of the fact that the decay constants and the intercepts were not independent of each other and did not stand as solid physical quantities that assess decay and tank concentration-representative backscatter respectively.

Fig. 4 was conclusive of the behaviour of the different agents. The decay of Quantison™ at very low acoustic pressures was negligible, and therefore the Overall Backscatter would be large. The increase of acoustic pressure increased dramatically the decay of Quantison™ (Figure 5.3b1) which causes the decrease of the Overall Backscatter. However the largely enhanced normalised backscatter of the Quantison™ (Figure 5.3b2), with the increasing acoustic pressure, was the reason for the increase of the Overall Backscatter after 0.83MPa seen in Fig. 4. For Myomap™ this enhancement was less pronounced (Figure 5.4), and the gradient of Overall

Backscatter increased (versus acoustic pressure) was lower. As argued earlier in this discussion the intercept is expected to be underestimated, and was probably the reason that DMP115 exhibits a decrease in the Overall Backscatter with the increase of acoustic pressure.

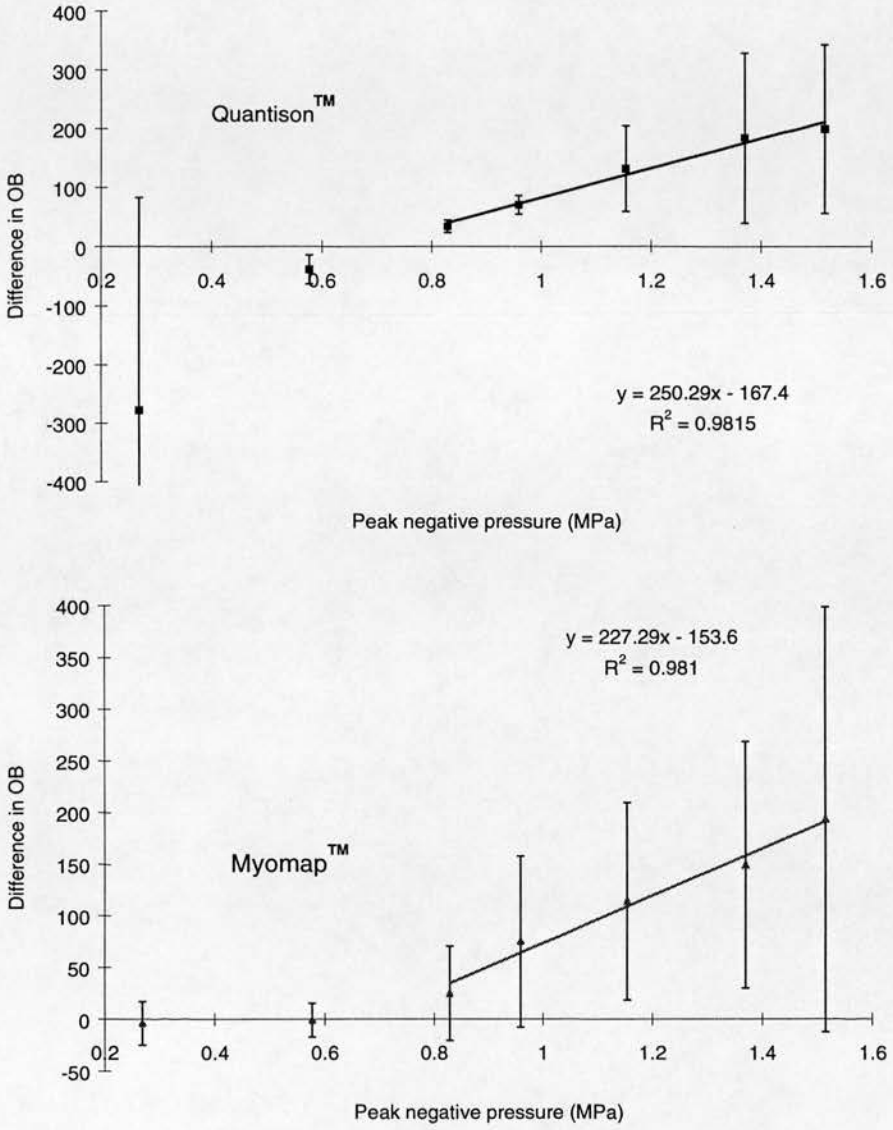

Figure 5.5 The difference of OB refers to the subtraction of the OB at the air-saturated suspension from that of the degassed one. The difference of OB is plotted against peak negative pressure for the Quantison™ and Myomap™. The two suspensions provided significantly different OB at 0.83MPa and higher acoustic pressures, for the two agents. As shown in the graphs, the difference of OB at those pressures highly correlated with acoustic pressure. Also, the slope and intercept of the resulting regression was less than 10% different between the two agents.

5.4.3 Acoustic pressure dependence of backscatter

DMP115 demonstrated a linear increase in backscatter intensity with the increase of incident intensity, that was illustrated as a slight decrease of normalised backscatter with acoustic pressure (Figure 5.3a2). This alone would suggest that DMP115 scatterers have a scattering cross-section independent of acoustic pressure. This property is met by linear scatterers like the ones used for normalising, and by contrast agents at very low acoustic pressure fields (Chang et al. 1996). As discussed above, the intercept did not provide an accurate measure of the backscatter of each agent. Strong suggestion of an increasing underestimation of the intercept with the increase of acoustic pressure is produced by the increase of decay. A higher order increase is therefore expected for the backscatter intensity of DMP115 with the increase of transmitted intensity.

The appearance of free bubbles for Quantison™ at 0.83MPa coincided with an increase of intercept and overall backscatter with the increase of acoustic pressure (Figure 5.3b2, Figure 5.4). Myomap™ showed similar behaviour, but less pronounced (Figure 5.3c2, Figure 5.4). Both agents demonstrated increasing decay with acoustic pressure, but the increase of overall backscatter above 0.83MPa with acoustic pressure suggested a higher-order non-linear dependence than DMP115 (order >1) of both agents' scattering cross-section to acoustic pressure. Frinking and de Jong (1997) speculated the release of free bubbles is the cause of this transient effect. It is however suspicious that the creation of free bubbles occurs at some acoustic pressure and not at all acoustic pressures. In other words gas is only allowed out of the shell, due to some rupture or leakage site, only at high acoustic pressures. It might be the case that a rupture in a shell is not a structural imperfection, but damage caused by exposure to ultrasound. Defects of the albumin shell of Optison that was followed by a free gas bubble release has been demonstrated microscopically when the bubbles were subjected to ultrasound at 2.25MHz transmit frequency (Dayton et al. 1999). If the latter occurs then the frequency of ruptures amongst the population of bubbles would probably be dependent on the amplitude of the incident wave. It seems logical to hypothesise that increase of acoustic pressure

would increase the proportion of free bubbles in a Quantison™ or a Myomap™ suspension. That way the enhancement was not only due to the free bubbles, but also to the increasing population of them with the increase of transmit intensity. However, there is no direct evidence to such an occurrence and further investigation is required to prove such a property for the two agents.

5.4.4 Stability in degassed and air-saturated suspensions

The decay constant and intercept were shown inadequate in describing decay and backscatter from the agents. The comparison in Table 5.1 was of limited value. Figure 5.4 showed that the overall backscatter can be used for detecting the effect of air level in the suspension to the agents. A paired *t-test* was performed in order to evaluate differences in overall backscatter between the degassed and the air-saturated suspension (dotted and solid lines respectively in Figure 5.4). There was no difference at 5% significance level for any of the pairs of lines. However if the first two points were omitted (i.e. the ratios that refer to the two lowest acoustic pressures) the paired *t-test* showed that both Myomap™ and Quantison™ had significantly lower Overall Backscatter at the degassed suspension ($p \sim 0.014$ in both cases). DMP115 demonstrated insignificant difference between the two pO_2 ($p=0.1$). This was strong evidence that the air from Myomap™ and Quantison™ dissolved more readily in the degassed suspension triggered by the ultrasonic field above 0.83MPa acoustic pressure. The difference of OB between the two suspensions was plotted against acoustic pressure for both agents (Figure 5.5). The propagated error was reasonably high due to the small sample size, but the correlation of this difference to acoustic pressure was near perfect above 0.83MPa PNP ($r = 0.99$ for both agents). The differences had also almost identical linear fits for the two agents (<10% difference in slope or intercept in the graph). This similarity suggests that Quantison™ and Myomap™ had identical dissolution behaviour. It is further suggested that the dissolution time reduced with increasing acoustic pressure. Due to the linear relationship between the difference of overall backscatter and the acoustic pressure, it could be speculated that the reduction of time of dissolution, in the

degassed suspension, is related to acoustic pressure. However, the difference in OB for two agents occurred only when free bubbles were present. If the above hypothesis of free-bubble concentration dependence on acoustic pressure is correct, then the dissolution time could be independent of acoustic pressure. Hence the dependence of the difference of OB between the two suspension on acoustic pressure could probably be related to the dependence of the number of free bubbles on acoustic pressure and a constant, for each suspension, dissolution time (smaller dissolution time for the degassed suspension). The latter seemed a more reasonable explanation for the difference in OB of the two agents.

5.5 Conclusion

This chapter concluded that continuous imaging is not of limited value in assessing the properties of contrast agents. Even though the decay constant and the intercept were proven not to have a solid physical meaning, the definition of the new physical quantity of the Overall Backscatter, as the integral of normalised backscatter over time, proved ideal in assessing subtle properties of the different agents. The contributions of the dissolved gas concentration in suspension and the acoustic pressure on the stability of the agents were clarified. It was shown that Quantison™ and Myomap™ release free bubbles at high acoustic pressure that also dissolve faster in degassed suspensions. The destruction of bubbles was dependent on acoustic pressure. The scattering cross-section of all agents was also related to acoustic pressure, but differences between DMP115 and the other two agents were strongly suggestive of a dependence between free-bubble formation and acoustic pressure for Quantison™ and Myomap™. Further investigation should be performed in microscopical level in order to assess this. At last it was shown that a degassed suspension accelerated the dissolution of the above free bubbles in a reproducible manner.

The next chapter aims to model the intercept and the decay constant, and explore the capability of continuous imaging for quantitative measurements.

6 Chapter Six: Modelling continuous imaging with contrast agents

6.1 Introduction

Chapter 2 and 3 included the description and validation of the set-up for in-vitro contrast work. Chapter 4 described a stability test for the contrast agents. The results from this chapter led to chapter 5 where the stability study was expanded to include variations of acoustic pressure. In all these chapters the experiments with contrast agents were performed using continuous imaging. In ultrasound diagnosis continuous imaging is the mode where the frame rate is higher than that which the eye can perceive as separate frames. It is now accepted that destruction of contrast microbubbles by the ultrasound beam is the main mechanism of decay of the agents. Consequently, only a limited number of recent publications deal with continuous imaging of contrast agents. In chapter 5, it was shown that the destruction process due to the ultrasound beam influences the backscatter from an agent. This suggested that the continuous imaging mode might have limited use in quantitative studies using contrast agents.

In chapter 5 the decay constant of the exponential fit was inadequate to determine the decay of the contrast agent in the tank. Visual observation of the frames, the videotapes, and the different plots of the data led to the conclusion that the intercept of the exponential fit was affected by the destruction of the contrast microbubbles. The integral of the backscatter of the agent over time (Overall Backscatter) was suggested as the physical quantity that quantifies all the (normalised) contrast enhancement "available in the tank" (equation 5.1).

In order to quantify the effect of different settings of the scanner (ATL UM9) on the agents, two experiments were performed and will be presented in this chapter. In the first, the time between insonations and the insonation time varied. In the second, the variables were the frame rate, the focal point, and the amplitude of the acoustic pressure in the ROI. The first experiment aimed to assess the reproducibility of contrast stability in in-vitro continuous contrast imaging, and the second to model

the behaviour of the agents in continuous imaging. This modelling does not intend to improve the understanding of the physical properties of the contrast agents, but to assess the capacity of continuous imaging for quantitative studies. Both experiments were performed at two different output power settings. One at 2.24% and one at 70.79% that exhibited different microbubble behaviour as shown in Figure 5.2. In the latter part of this chapter, the potential of continuous contrast imaging in quantitative measurements is assessed.

6.2 Materials and methods

The set-up used in the following experiments is described in 2.2.1 (p.16). DMP115, Quantison™, and Myomap™ were the agents used in these experiments. As stated in Table 3.4, the bubble concentrations in the tank were 2250000 bubbles/ml for Quantison™, and 75000 bubbles/ml for Myomap™, while for DMP115 the concentration was reduced to 10000 bubbles/ml in order to avoid having backscatter intensities that were close to the upper limit of the linear range for the system (see section 5.3). The general protocol again involved 15 consecutive insonations of the agent and capture of the last frame of insonation. 3 sets of data were collected at each different combination of settings.

6.2.1 Reproducibility test

6.2.1.1 Mixing time

The experiments were performed at 2.24% and 70.79% percent output power. The applied mixing time between insonations was 1sec, 5sec, 10sec, or 30sec. The insonation time was 2sec. There was also an initial mixing time of 30sec. Each experiment was repeated three times.

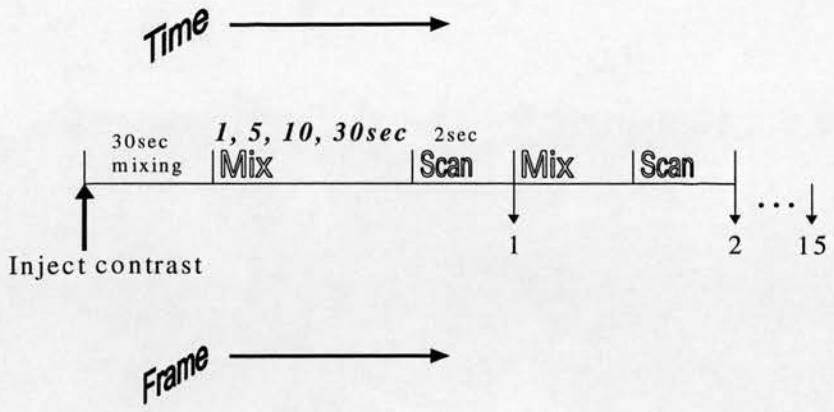

Figure 6.1 Insonation protocol for the reproducibility test that involved the mixing time.

6.2.1.2 Insonation time

The experiments were also performed at 2.24% and 70.79% percent output power. The applied insonation time was 0.5sec, 2sec, 5sec, or 10sec. The mixing time between insonations was 10sec. There was also an initial mixing time of 30sec. Each experiment was repeated 3 times.

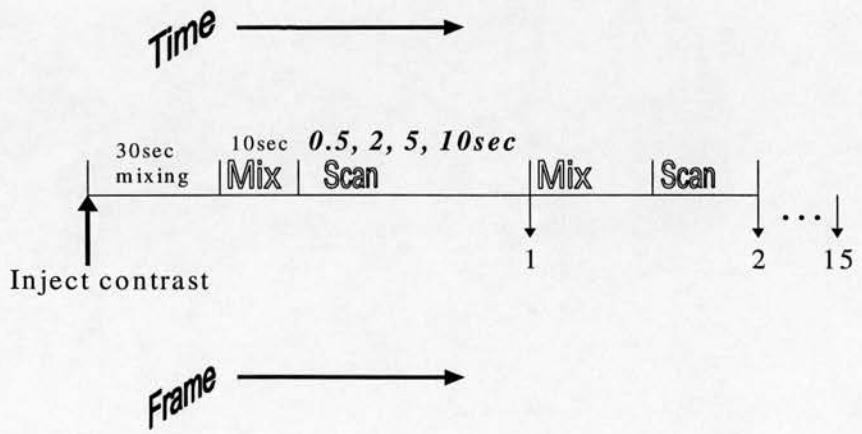

Figure 6.2 Insonation protocol for the reproducibility test that involved the insonation time.

6.2.2 Modelling continuous imaging

The insonation time was 2sec, the mixing time between insonation 10sec, and the mixing time before the first insonation 30sec. The focal length was positioned at 3cm, 4.3cm, 6.25cm, or 9cm. For each setting, there are three available frame rate settings in the scanner. A calibration similar to the one shown in Table 2.1 was performed for all 24 settings (2 output power settings) and was likewise repeated every 0.5cm across the ROI, in order to assess the acoustic pressure variations in the ROI. It was preferable to illustrate the results that were considered useful to the discussion graphically, which would otherwise form a large and probably confusing table. All the settings along with the peak negative pressure at 3cm are shown in Table 6.1. Two percent output powers were used, 2.24% and 70.79%.

Table 6.1 *Settings for continuous imaging modelling protocol*

Focus	***Frame rate***	***Peak negative pressure*** (in MPa at 3cm depth)	
		2.24%	70.79%
3cm	→ 47Hz	0.35	1.53
	→ 65Hz	0.29	1.39
	→ 78Hz	0.25	1.24
4.3cm	→ 45Hz	0.31	1.47
	→ 61Hz	0.27	1.36
	→ 78Hz	0.22	1.18
6.25cm	→ 37Hz	0.28	1.33
	→ 47Hz	0.28	1.33
	→ 66Hz	0.24	1.24
9cm	→ 33Hz	0.27	1.27
	→ 41Hz	0.27	1.27
	→ 55Hz	0.27	1.27

6.2.3 Statistical analysis

For both experiments (described in sections 6.2.1 and 6.2.2) all data sets contained 15 RF frames, to which an exponential decay model was fitted. From this the decay constants and the intercepts could be extracted. The data were plotted

against time of insonation. The previous chapter proved that the suspension environment had almost no effect on the decay of the agents for the time scale over which these experiments were performed. The previous chapter also showed that the effect of the background subtraction was insignificant when the necessary care was taken, as described in the discussion of chapter 2. Therefore it was not used in this analysis.

6.2.3.1 Reproducibility test

The data were analysed without the usual normalisation since quantitative comparisons between agents were not intended. The protocol aimed at exploring the effect of the following two variables in the study of contrast agents using continuous imaging.

Mixing time Backscatter intensity was plotted against time of insonation for each data set, and were similar to the graphs in Figure 5.1. An exponential trend was fitted to each data set, and the average intercepts and decay constants were extracted and plotted against mixing time for both acoustic pressures and all three agents. Furthermore the standard deviations of the intercept and the decay constant were assessed.

Insonation time Backscatter intensity was plotted against time of insonation for each data set (which were similar to the graphs in Figure 5.1), and exponential trend was fitted to each data set. The average intercepts and decay constants were then extracted and plotted against the time of insonation for both acoustic pressures and all three agents, and the standard deviations were also assessed. Moreover, decay curves were averaged in order to produce smoothed data sets that would allow investigation of different parts of the curve. As discussed in the previous chapter the exponential trend seemed to provide underestimated intercepts and decay constants at high acoustic pressures for Quantison™ and Myomap™. By varying the time of insonation and investigating the behaviour of different parts of the averaged data sets, a fuller explanation of the two populations of scatterers in the suspensions of the two agents was expected.

6.2.3.2 Modelling continuous imaging

Continuous imaging modelling was performed using normalised backscatter in order to compensate for the variations of the ultrasound field across the ROI.

Normalisation was implemented using the Cardiff acoustic grey scale phantom rather than the suspension of Orgasol®. The choice was dictated by the negligible variability in backscatter that could be achieved with the phantom. In Figure 2.4b, the standard deviation of the backscatter intensity for different preparations of the suspension of Orgasol® was just over 10%, while that of the phantom in Figure 2.4a was slightly higher, but this value came from those taken at different positions and times. It is difficult to improve the variability of the backscatter of a suspension, since it is subjected to variations due to the magnetic stirring. The backscatter intensities used here to normalise the contrast data sets were captured at a specific position on the phantom. This reduced the variability within these measurements to a negligible amount, and thus suited the comparison between the different settings which in these experiments were less differentiated than in the previous chapter (see the acoustic pressure differences within an output power setting in Table 6.1).

The calculation of the decay constant and intercept of each curve was accomplished creating a Visual Basic programme (macro). The facility is available in Excel 7.0 software (Microsoft). The same programme was used for plotting all the normalised data sets. The exponential equations and regression coefficients were also produced in order to examine whether the general behaviour of the agents was compatible with previous results.

The results of those calculations (i.e. decay constant and intercept) were statistically analysed using the SAS statistical package available via the Edinburgh University network. A multiple regression analysis was implemented in order to assess a statistically significant model, in terms of variance ratio F, which would include variables that were statistically significant in terms of a *t-test* (Armitage and Berry, 1996). The level of significance was set at 5%. The regression coefficient and the adjusted regression coefficient were also calculated for these models. The probability value produced by the variance ratio F of the model illustrates the strength of evidence (significance) that the particular model contains the specific variables. On the other hand, the regression coefficient illustrates the strength of association of the predicted value to the associated variables, hence the predictability of the model.

The decay constant and the intercept were modelled separately. A model for each combination of percent output power and contrast agent was produced for the corresponding decay constants and another for the corresponding intercepts. As illustrated in Table 6.1, each model had 12 samples, and the initial components were the frame rate, the focal length, and the acoustic pressure. These components in the first, second and third order, were the tested variables.

The statistical analysis was implemented in two steps using the SAS software. 1) Models were produced containing the 3 first orders of each variable (overall 9 variables). Using the command PROC RSQUARE, the regression coefficient was calculated and the variables were specified for all the models, which were optimal in terms of regression coefficient. This procedure was used as a guideline in building the best model for each case. For example, a large increase of the regression coefficient when using 4 instead of 3 variables would probably be important for the significance of the variables, i.e. the 3 variables might not be significant to a model, but the addition of the 4^{th} might make them, and the specific model, significant. 2) Using the command PROC GLM (general linear model), different models were tested in terms of significance of the model, significance of variables, and adjusted regression coefficient.

Residual plots were also produced versus each one of the initial 3 variables, the values predicted by the model, and also the 3 products of the pairs of initial variables, in order to judge whether there were irregularities and specific patterns as described by Armitage and Berry (1996, pp324-328), which would suggest a different model.

The simplest models, in terms of number of variables, were generally preferred from those with similar or slightly higher regression coefficients but with more variables. The behaviour of the agents shown in all the previous experiments, was also taken into consideration.

The above analysis was based on the comparison of the decay curves (normalised backscatter versus time of insonation) of different agents at different settings. However, the destruction of the contrast bubbles is highly dependant on the number of frames that the suspension was insonated for, and a "frame domain" could

also be used to analyse the data. The whole of the analysis was repeated replacing the time of insonation with number of frames. Decay constants, intercepts, and Overall Backscatter were calculated and modelled. The new decay constant would have dimensions of $frames^{-1}$ instead of sec^{-1}. It is easier to present the results in separate sections: One for the "time domain" and one for the "frame domain".

A multiple regression analysis was also performed for the new physical quantity of Overall Backscatter, as defined in the previous chapter, and occupied a different section of the results. Also, to allow comparisons between the two domains, normalised models were calculated using the maxima of the predicted values.

6.3 Results

6.3.1 Reproducibility test

6.3.1.1 Mixing time

All data lay within the linear range of backscatter as determined in chapter 2. Exponential trendlines were fitted to the data and the calculated intercepts and decay constants were plotted against the mixing time in Figure 6.3a and b respectively. Error bars were not plotted in Figure 6.3a because this would make the graph less clear. The graph showed that the intercepts were constant. Maximum variability 25% (standard deviation/average) was displayed by Quantison™ when insonated at 70.79% output power, while the variability averaged at 13% for all agents at all settings. In Figure 6.3b the error bars (± standard deviation) were plotted to illustrate the variability of the decay constant. Following an increase in mixing time, increase in decay constant was only observed by DMP115 over the range of mixing times, especially for the maximum value of 30sec between insonations. The other two agents did not show a significant change in decay constant when the mixing time varied.

The standard deviation of the two parameters was also calculated. Table 6.2 shows the calculated percent average standard deviation for the four mixing times for all the agents and both output powers. Even though this calculation does not represent a quantity with physical meaning, it aimed in illustrating the variability associated with the mixing time. The percent standard deviation for Quantison™ for

the decay constant at 2.24% output power ranged from 77% to 921%. This variation may well be due to the negligible decay at that setting. Thus those values were excluded from the calculations in the table.

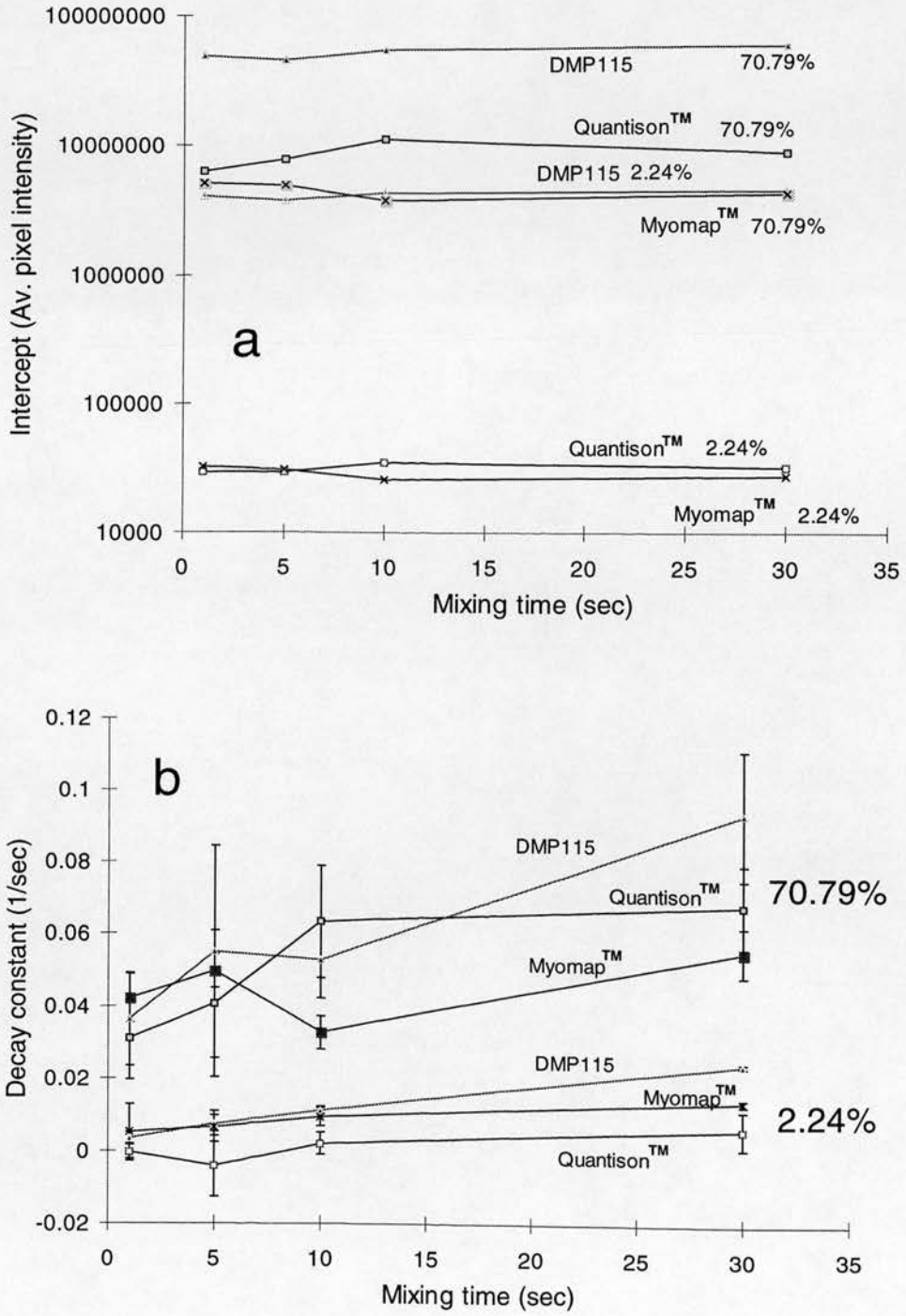

Figure 6.3 Intercept (**a**) and decay constant (**b**) plotted against mixing time. The intercept was stable with mixing time while the decay constant increased only for DMP115 with the increase of mixing time at both percent output powers. In graph **a** no error bars were plotted in order to improve its clarity.

Table 6.2 *Average percent standard deviations of the parameters of the exponential trend (Mixing time)*

Parameter\Mixing time	**1sec**	**5sec**	**10sec**	**30sec**
Intercept	16.7	23.7	24.3	15.0
Decay constant*	55.8	41.2	18.9	11.2

Average percent standard deviation of the mean intercept and decay constant for all agents. The variability of the decay constant is reducing with increasing mixing time (see discussion). (*) Quantison™ at 2.24% percent output power is excluded from the calculation because the standard deviation was very high due to negligible decay.

6.3.1.2 Insonation time

All data were well within the linear range of backscatter vs concentration, as specified in chapter 2. Exponential trendlines were fitted to the data and the calculated intercepts and decay constants were plotted against the insonation time in Figure 6.4a and b respectively. Error bars were omitted from the graph to maintain clarity. Instead, the standard deviations of the mean intercept and decay constant are shown in Table 6.3. The standard deviation of the decay constant for Quantison™ at 2.24% output power ranged from 53% to 802%. This was due to the negligible decay. These values were not included in the calculation of the average standard deviation of the decay constant. Overall the standard deviations of the intercept and decay constant were low (with the exception of Quantison™) and therefore any conclusions that can be drawn from the observation of Figure 6.4, which did not plot error bars for convenience, should be considered valid.

Table 6.3 *Average percent standard deviations of the parameters of the exponential trend (Insonation time)*

Parameter\Insonation time	**0.5sec**	**2sec**	**5sec**	**10sec**
Intercept	17.0	15.0	18.7	12.5
Decay constant*	9.1	13.6	14.6	15.5

Average percent standard deviation of the mean intercept and decay constant for all agents. The variability of the insonation time is reduced for the decay constant at low insonation times (see discussion) (*) Quantison™ at 2.24% percent output power is excluded from the calculation because the standard deviation was very high due to negligible decay.

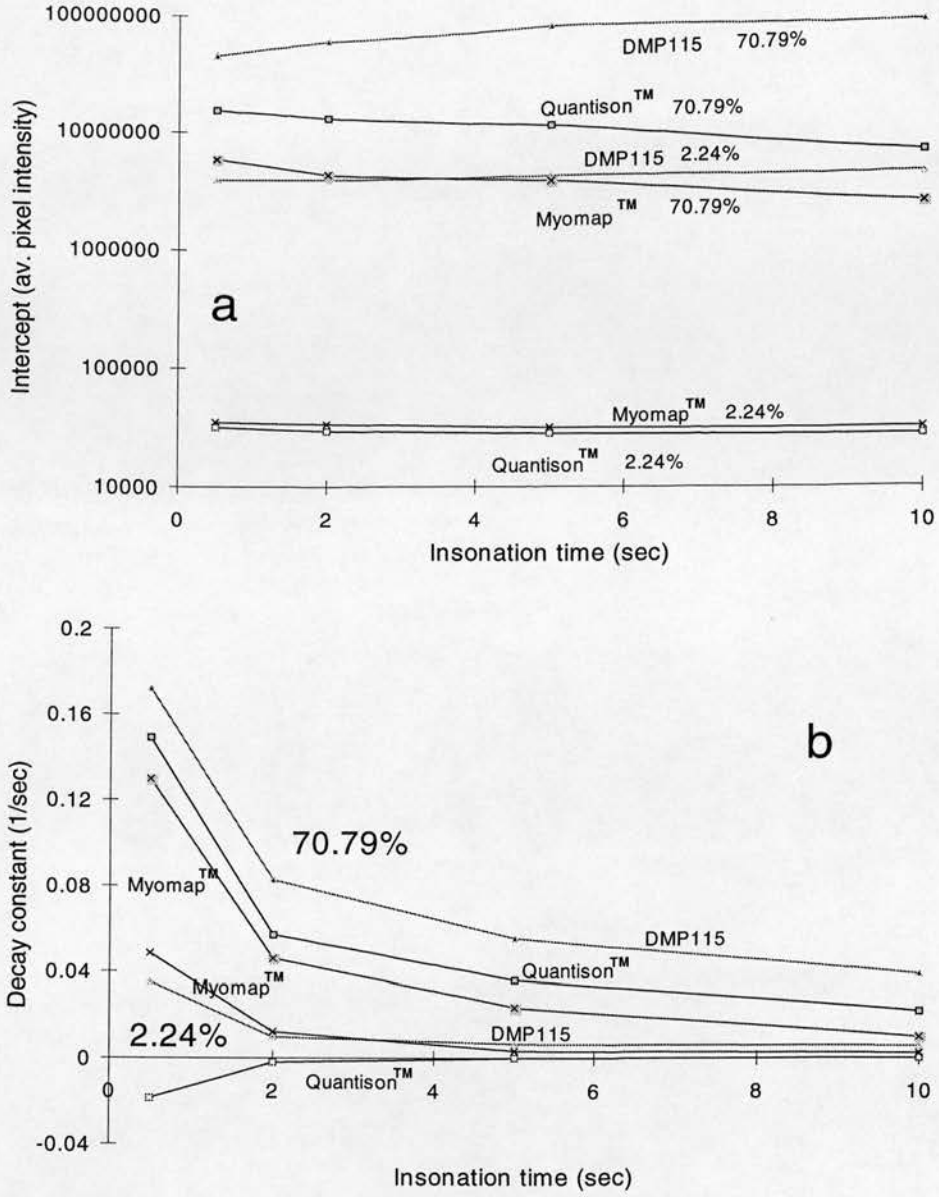

Figure 6.4 Intercept (**a**) and decay constant (**b**) plotted against insonation time. The intercept was stable at 2.24% output power, while it decreased for increasing insonation time for Quantison™ and Myomap™, and increased up to 5sec insonation time for DMP115. The decay constant decreased with increasing insonation time for all agents at both acoustic pressures, apart from Quantison™ at 2.24% output power. Standard deviations were not plotted since they would affect the clarity of the graphs.

It is evident from this graph that the intercepts were constant only for the low acoustic pressure setting. At the high acoustic pressure Quantison™ and Myomap™ exhibited a decrease of intercept with the increase of insonation time, while DMP115 seemed to have highly stable intercept.

The decay constants for all agents decreased with increasing insonation time at both acoustic pressures, except for Quantison™ at 2.24% output power (Figure 6.4b).

For the three captured data sets that correspond to each contrast agent, acoustic pressure and insonation time, the average curve was produced in order to smooth out the variability of individual data sets (Figure 6.5). An investigation followed to assess the variability within each average curve. An exponential model was fitted to the initial part of the curve (first 6-10 points), the remainder of the curve and finally to the whole curve. The initial part of the curve was chosen to be the one that fitted a different exponential model from the remainder of the curve. Figure 6.5 illustrates an example of this analysis at 10sec insonations and 70.79% output power. For DMP115, the exponential trend for insonation time up to 80sec (solid line in Figure 6.5a) provided a similar regression coefficient with the trend of the whole curve (dotted line in the same figure). Even though the trend for the first 80sec overestimated both intercept and decay constant, the difference was not significant.

Figure 6.5b and c showed the different behaviour of Quantison™ and Myomap™. In addition to giving a significant underestimation of the intercept and decay constant, the exponential fit of the whole curve (light grey line) in Figure 6.5b also gave a poorer regression coefficient, when compared with the trend of the first 80sec. The exponential curve provided a satisfactory description of the behaviour of the agent for the first 80sec of insonation. The same did not apply for the rest of the insonation time, as illustrated by the forecast of the exponential trend (of the 80sec) for the rest of the data points. In this case the agent showed a departure from its initial behaviour. This departure could be considered to happen earlier for Myomap™ (Figure 6.5c). The agent seemed to alter its initial behaviour after the first 60sec of insonation. In both agents, the data points at the end of the curve stand at higher values than those forecasted by the trends of their initial part, which also provided very high regression coefficients.

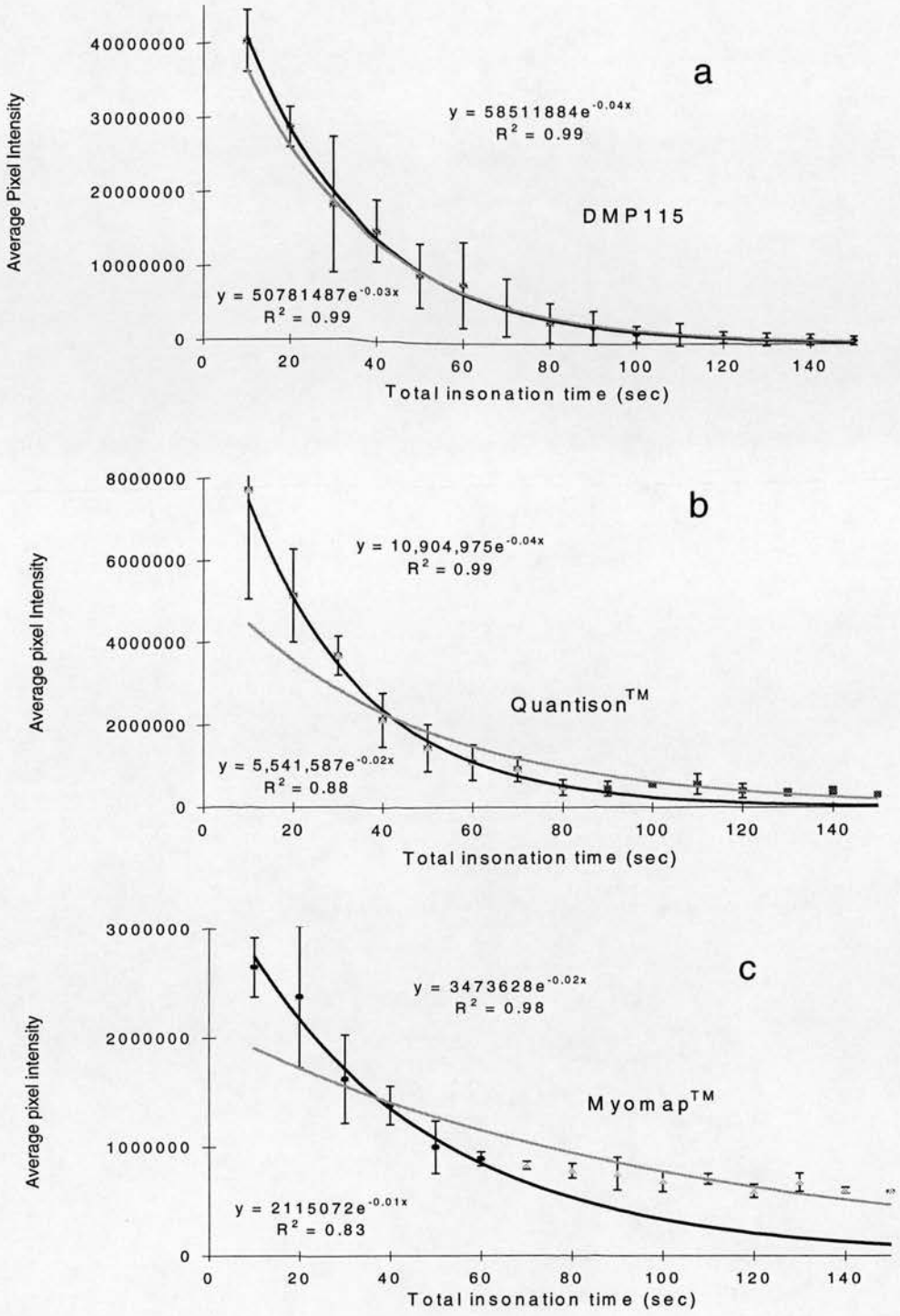

Figure 6.5 Curve of backscatter intensity against total insonation time produced by averaging 3 data sets at 70.79% output power for the 10sec insonation time. (**a**) DMP115, (**b**) Quantison™, and (**c**) Myomap™. The solid line is the exponential trend of the initial 80sec of insonation for **a**, and **b**, and for 60sec for **c**, which is also forecasting the following time of insonation. Its equation and regression coefficient is in the middle of each graph. The light grey lines are the exponential trends for the whole curve, and its equation and regression coefficient is in the left bottom corner of each graph. See text for further detail.

A summary of this analysis for 70.79% output power is illustrated by plotting the intercepts of both trends (referring to initial 80sec and whole) against insonation time (Figure 6.6). This figure contained data points included in Figure 6.4 (intercepts of the whole curve plotted as solid lines), and also the intercepts produced by the exponential trend of the first 80sec (dashed lines). It is evident that the differences were insignificant for DMP115, while the maximum insonation time provided significantly higher intercepts for the 80sec trends for the other two agents. A figure including the decay constant was not considered necessary, since it led to a similar outcome to that of the intercept analysis.

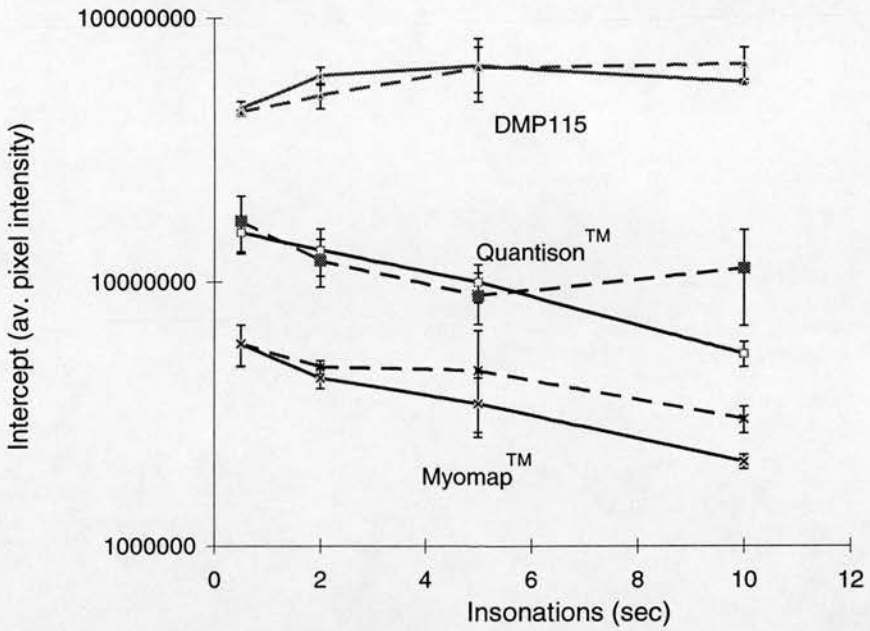

Figure 6.6 Intercept of exponential trend for the average curve for the different insonation times. The solid lines refer to the intercepts produced by the exponential trend applied to the whole decay curve, while the dashed lines refer to the intercepts produced by exponential trends applied for the first 8 insonations (out of 15). Note that at maximum insonation time (10sec) Quantison™ and Myomap™ have significantly different intercepts for the two ways of analysis.

6.3.2 Modelling continuous imaging

6.3.2.1 Time domain

After having captured and analysed all the data on the Sun Workstation, further analysis was performed in Excel spreadsheets using to the facility of Macro programming with Visual Basic. All normalised data sets were plotted against time, and the decay constant and intercept were calculated. The analysed data were similar to previous ones in terms of intercepts, decay constants, and regression coefficients.

The output of this analysis was used as input data for the statistical analysis in the SAS analysis package. A typical table used as an input file for SAS is Table 6.4 where in the first column was the focal length, the second column was the frame rate, the third was the peak negative pressure at 3cm from the probe, and the fourth column was the average decay constant for DMP115 at 70.79% output power (experiments were repeated 3 times at each setting). Two tables were produced separately for 2.24% and 70.79% output power level for each decay constant and intercept, hence overall 12 input files for all 3 contrast agents.

The initial SAS script (programme) shown in the right side of the page (Script 6.1) produced a model which included all 3 variables (focal length, frame rate, peak negative pressure) in the first, second, and third order. The underlined command PROC RSQUARE produced an output that gave the combinations of variables that produced models with high regression coefficients, for different number of variables (up to 9). This output was used as a guideline, as explained in section 6.2.3.2, to create the optimal model in each case.

The following SAS script (Script 6.2) was used to test the different models, in terms of significance of the variables and the model, and also in terms of high regression coefficient. This was done with the command PROC GLM. This command also produced the equation of the model. The command PROC PLOT was used to produce all the residual plots.

Table 6.4 SAS input file for DMP115 decay constant at 70.79% output power

```
3       47      1.53    0.0690108
3       65      1.39    0.0597669
3       78      1.24    0.0447605
4.3     45      1.47    0.0667496
4.3     61      1.36    0.0673268
4.3     78      1.18    0.0465029
6.25    37      1.33    0.0508115
6.25    47      1.33    0.0451032
6.25    66      1.24    0.0480154
9       33      1.27    0.0480891
9       41      1.27    0.0369482
9       55      1.27    0.0397094
```

Script 6.1 SAS programme for regression coefficient comparison

```
data temp;
infile 'dmp115db';
input focus 1-4 fr 6-7
        pnp 9-12 y 26-37;
sqfr=fr*fr;
sqpnp=pnp*pnp;
sqfocus=focus*focus;
cufr=fr*fr*fr;
cufocus=focus*focus*focus;
cupnp=pnp*pnp*pnp;
proc rsquare;
model y=fr sqfr cufr focus
sqfocus cufocus pnp sqpnp cupnp;
```

Script 6.2 SAS programme for model testing

```
data temp;
infile 'dmp115db';
input focus 1-4 fr 6-7
        pnp 9-12 y 26-37;
sqfr=fr*fr;
sqpnp=pnp*pnp;
sqfocus=focus*focus;
cufr=fr*fr*fr;
cufocus=focus*focus*focus;
cupnp=pnp*pnp*pnp;
infr=1/fr;
pfr=pnp*fr;
pfo=pnp*focus;
ffo=fr*focus;
proc glm;
model y=focus pnp;
output      out=new      p=predict
        r=resid;
proc plot;
plot resid*predict/vref=0;
plot resid*pnp/vref=0;
plot resid*fr/vref=0;
plot resid*focus/vref=0;
plot resid*pfr/vref=0;
plot resid*pfo/vref=0;
plot resid*ffo/vref=0;
```

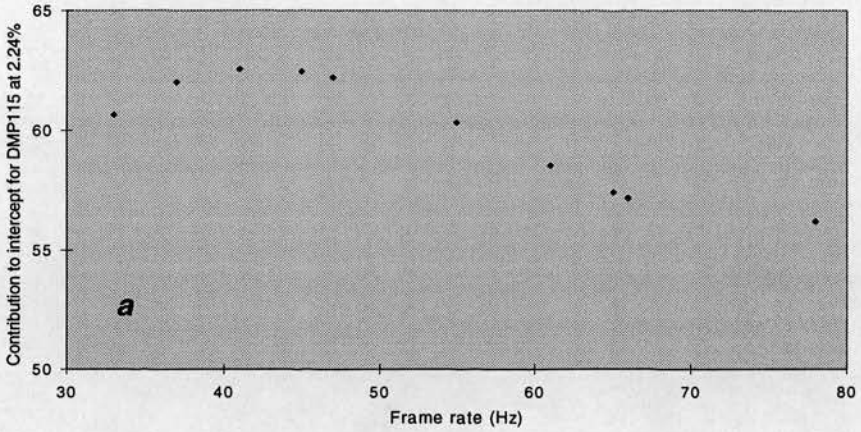
Contribution to intercept for DMP115 at 2.24%
65
60
55
50
30
40
50
60
70
80
Frame rate (Hz)
a

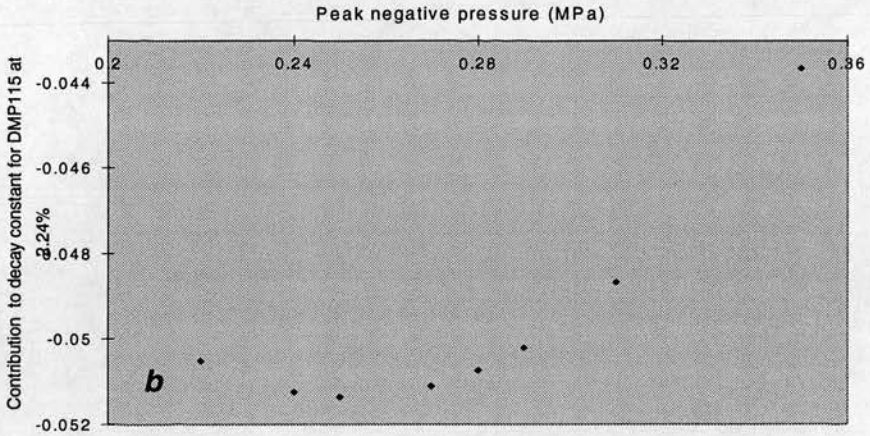
Peak negative pressure (MPa)
Contribution to decay constant for DMP115 at 2.24%
0.2
0.24
0.28
0.32
0.36
-0.044
-0.046
-0.048
-0.05
-0.052
b

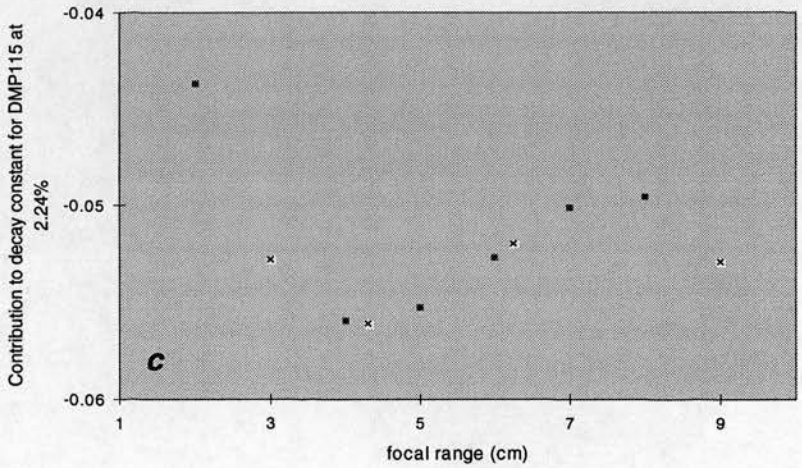
Contribution to decay constant for DMP115 at 2.24%
-0.04
-0.05
-0.06
1
3
5
7
9
focal range (cm)
c

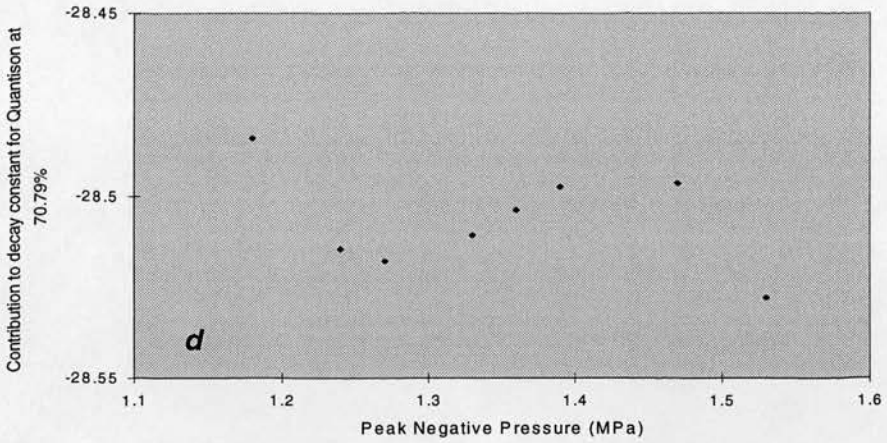

Figure 6.7 Four graphs that describe the contribution of different parameters to different models. **a** the increase of frame rate contributes to a decrease in the $I_{2.24\%}$ for DMP115 as shown in the graph, **b** the increase of peak negative pressure increases $D_{2.24\%}$ for DMP115 as shown in the graph, **c** the four different values of focal range has the effect shown in the graph (x points) to $D_{2.24\%}$ for DMP115, and **d** the peak negative pressure has the contribution to $D_{70.79\%}$ as shown in the graph for Quantison™.

The best models for each input file are shown in Table 6.5. The regression coefficient, the adjusted regression coefficient, the significance of the model, and the significance of its variables were also shown in this table. The adjusted regression coefficient equals $((n-1)R^2-p)/(n-p-1)$, where n is the sample size, p is the number of variables, and R^2 is the regression coefficient. The regression coefficient quantifies the predictability of a model, but can not be used for comparison between models with different number of variables. The adjusted regression coefficient is a direct comparison between regressions when the number of variables varies (Armitage 1996).

Since all the backscatter intensities were normalised using a grey scale phantom, the backscatter intensity from the phantom was modelled. At 2.24% and 70.79% output power, the best fit for the phantom's backscatter was:

$$B_{2.24\%}=339052p+24.8fr^2-0.29fr^3-4007fo \quad (6.1)$$

($r^2=0.975$, Pr=0.0001, $p<0.01$ for all variables)

$$B_{70.79\%}=-10594432+14832430p^2-6163096p^3+2fr^3+368860fo-25134fo^2 \quad (6.2)$$

($r^2=0.976$, Pr=0.0001, $p<0.05$ for all variables)

The models for the phantom suggest an overall linear relationship with peak negative pressure within each output power, a third order increase of $B_{70.79\%}$ with increasing frame rate and a more complicated relationship of $B_{2.24\%}$ with the frame

rate. Lastly, a negative linear relationship of $B_{2.24\%}$ with the focal length and a more complicated relationship of increase of $B_{70.79\%}$ with the focal length also appeared in the model. It was shown in chapter 2 that the backscatter from the phantom was linearly related to acoustic pressure. The above models therefore suggest that the acoustic pressure varies across the ROI, and this variation was dependent on the focal length and the frame rate.

As seen in Table 6.5, the intercept at 2.24% ($\mathbf{I_{2.24\%}}$) output power for DMP115 decreases linearly with the increase of peak negative pressure. However, it decreases with the frame rate in a more complicated fashion as illustrated in Figure 6.7a. For small values of frame rate there was probably no significant change in the intercept, while for higher values the intercept decreased. Models that included the frame rate in the first or second order had a low regression coefficient and the peak negative pressure was insignificant. The decay constant at the same output power ($\mathbf{D_{2.24\%}}$) was more complicated. The contribution of the peak negative pressure was small at low values, while for larger peak negative pressures the decay constant increased (Figure 6.7b). Highly significant ($p<0.01$) was the contribution of the focal range, which followed a third order pattern shown in Figure 6.7c. None of the orders of focal range were significant as individual variables. The same applies to the combinations of the pairs.

At 70.79% percent output power the model for both $\mathbf{I_{70.79\%}}$ and $\mathbf{D_{70.79\%}}$ was simpler for DMP115. The $I_{70.79\%}$ decreased linearly with the increase of peak negative pressure ($p=0.0036$), frame rate ($p=0.012$), and focal range ($p=0.001$). Moreover, only all three variables together were significant in modelling the $I_{70.79\%}$. No other combination of variables gave significance to those variables. The $D_{70.79\%}$ decreased with the increase of focal range ($p=0.047$), while it increased with the increase of peak negative pressure ($p=0.004$). In this case, the introduction of the second and third order of focal range to the model would be insignificant ($p\sim0.09$), but would provide a much higher regression coefficient and adjusted regression coefficient ($r^2=0.88$ and $r_a^2=0.81$).

For Quantison™ the $\mathbf{I_{2.24\%}}$ was very similarly modelled by the frame rate as for the case of DMP115 at the same output power, which is illustrated by Figure 6.7a.

The peak negative pressure had no effect. The decay constant was not significantly changed by any of the variables.

At 70.79% output power the intercept $\mathbf{I_{70.79\%}}$ for Quantison™ was again similar to the model seen at the same output power for DMP115. Peak negative pressure, frame rate and focal range were negatively linearly related to $I_{70.79\%}$. Again the model was significant only if all three variables were used together in the model. The peak negative pressure was only slightly insignificant ($p=0.07$), but its presence in the model made the other two variables significant ($p<0.05$). The contribution of peak negative pressure to the $D_{70.79\%}$ is illustrated in Figure 6.7d, and was included all three orders of peak negative pressure, all of which were highly significant ($p\sim0.0019$). None of those variables individually or in pairs had a significant effect on the decay constant.

The $\mathbf{I_{2.24\%}}$ for Myomap™ had a slightly significant inversely proportional relationship with the frame rate, but the low regression coefficient ($r^2=0.35$) suggests a low predictability for that model. No significant model was found to describe the $\mathbf{D_{2.24\%}}$.

Peak negative pressure and frame rate proved highly significant in describing the $\mathbf{I_{70.79\%}}$ ($p<0.01$) for Myomap™. Increase of peak negative pressure increased the intercept linearly, while increase of frame rate decreased it linearly. An alternative model order similar to that of $D_{2.24\%}$ for DMP115 (as illustrated in Figure 6.7b) was suggested. It included the peak negative pressure in first and second, the frame rate in second order and the focal range in all three orders in a similar way as illustrated in Figure 6.7c ($I_{70.79\%}$ in brackets in Table 6.5). This model had a very high regression coefficient and adjusted regression coefficient ($r^2=0.98$ and $r_a^2=0.96$). The $\mathbf{D_{70.79\%}}$ was negatively linearly related to the frame rate, and also related to the focal range as was illustrated by Figure 6.7c. An alternative model for $D_{70.79\%}$ replaced the frame rate with the first, second and third order of peak negative pressure, which contribute with a very fast increase $D_{70.79\%}$ with the increase of peak negative pressure, and provided a higher regression coefficient and adjusted regression coefficient ($r^2=0.92$ and $r_a^2=0.82$ comparing to $r^2=0.85$ and $r_a^2=0.76$ of the first model).

6.3.2.2 Frame domain

The same analysis procedure was followed to assess the best model for both intercept and decay constant. The intercepts were identical in both the time and the frame domain. Thus the resulting Table 6.6 includes only the decay constant at each setting and contrast agent. The decay constants in both domains were very similar regarding the variables that involve the peak negative pressure and the focal length, with the exception of $D_{70.79\%f}$ for DMP115, which was not related to the focal length, as it was in the time domain calculations.

The obvious difference between the models in the two different domains was the variables that involved the frame rate. All models of the decay constants provided first or second order negative relationship with the frame rate. All models provide a higher regression, and adjusted regression coefficient. The significance of each model was also improved.

6.3.2.3 Overall Backscatter

The multiple regression analysis for the Overall Backscatter produced Table 6.7. The regression coefficient and adjusted regression coefficient were very high, and most models were highly significant. For three models, the variables were not significant within the 5% level, but their presence in the model contributed to the significance of other variables.

A comparison of the investigation of the frame and time domains suggested that most models were similar in terms of variables. To allow more detailed comparisons between the two domains, the normalised models were produced. In the frame domain, increasing the frame rate increased the Overall Backscatter for DMP115 at both output powers, and decreased the Overall Backscatter for Quantison™ at 70.79%. Myomap™ had a more complex behaviour as shown in Table 6.7. As expected, the time domain showed less increasing (or more decreasing) Overall Backscatter with increasing frame rate. For example DMP115 at 2.24% output power demonstrated a positive linear relationship in the frame domain, while a negative relationship occurred in the time domain.

The differences of the variables involving the focal length and the peak negative pressure were mostly negligible between the two domains. DMP115 demonstrated a general decrease of Overall Backscatter with increasing acoustic

pressure. The contribution of acoustic pressure to the Overall Backscatter for Quantison™, and Myomap™ was less important.

Table 6.5 *Model of continuous imaging (time domain)*

		Model Equation	r^2	r_a^2	*Pr*	*Details*	
Intercept	**DMP115**	$I_{2.24\%} = -41\mathbf{p} + 3.6\mathbf{fr} - 0.068\mathbf{fr}^2 + 0.00038\mathbf{fr}^3$	0.87	0.80	0.003	<0.05	
		$I_{70.79\%} = 31 - 11.0\mathbf{p} - 0.063\mathbf{fr} - 0.65\mathbf{fo}$	0.80	0.73	0.003	<0.05*	
	Quantison™	$I_{2.24\%} = 0.026\mathbf{fr} - 0.00048\mathbf{fr}^2 + 0.00000279\mathbf{fr}^3$	0.80	0.73	0.004	<0.05	
		$I_{70.79\%} = 17.2 - 5.4\mathbf{p} - 0.098\mathbf{fr} - 0.40\mathbf{fo}$	0.86	0.81	0.001	<0.05*	apart
						Pr_p=0.07	
	Myomap™	$I_{2.24\%} = 0.1356 + 2.23/\mathbf{fr}$	0.35	0.29	<0.05	<0.05	
		$I_{70.79\%} = 2.07\mathbf{p} - 0.0127\mathbf{fr}$	0.89	0.87	<0.0001	<0.01	
		$(I_{70.79\%}=22.3-27.7\mathbf{p}+10.5\mathbf{p}^2-0.000195\mathbf{fr}^2-1.31\mathbf{fo}+0.233\mathbf{fo}^2-0.0131\mathbf{fo}^3)$	0.98	0.96	<0.0004	<0.05	
Decay	**DMP115**	$D_{2.24\%} = 0.117 - 0.41\mathbf{p} + 0.81\mathbf{p}^2 - 0.0323\mathbf{fo} + 0.0059\mathbf{fo}^2 - 0.000328\mathbf{fo}^3$	0.90	0.82	0.0061	<0.05	
constant		$D_{70.79\%} = 0.071\mathbf{p} - 0.00181\mathbf{fo}$	0.79	0.74	0.0008	<0.05	
	Quantison™	$D_{70.79\%} = 28.5 - 63.6\mathbf{p} + 47.1\mathbf{p}^2 - 11.6\mathbf{p}^3$	0.73	0.63	0.01	<0.005*	
	Myomap™	$D_{70.79\%} = 0.130 - 0.000253\mathbf{fr} - 0.049\mathbf{fo} + 0.0093\mathbf{fo}^2 - 0.00053\mathbf{fo}^3$	0.85	0.76	0.005	<0.05	
		$(D_{70.79\%}=9.7-21.1\mathbf{p}+15.6\mathbf{p}^2-3.8\mathbf{p}^3-0.103\mathbf{fo}+0.0196\mathbf{fo}^2-0.00111\mathbf{fo}^3)$	0.92	0.82	0.013	<0.05	

The equation of the model (time domain) of intercept and decay constant for each agent at 2.24% ($I_{2.24\%}$, and $D_{2.24\%}$ respectively) and 70.79%output power ($I_{70.79\%}$, and $D_{70.79\%}$) are shown in this table. The parameters are: the peak negative pressure (p), the frame rate (fr), and the focal length (fo). Also the regression coefficient (r^2), the adjusted regression coefficient (r_a^2), the significance of the model (Pr), and a summary of the probabilities of each of the variables in the model (Details), are also shown in separate columns. The * means that for the specific model all the variables have to be present in order to be individually significant. All the models shown in the table are significant (Pr<0.05), and all the variables in those models are significant too apart for $I_{70.79\%}$ where the peak negative pressure (p) is not significant (Pr=0.07) for Quantison™. The precision of the constants in each model is the first two digits of standard error. The intercepts are stated only when they are significant (Pr<0.05).

Table 6.6 *Model of continuous imaging (frame domain)*

	Model Equation for the Decay Constant	r^2	r_a^2	*Pr*	*Details*
DMP115	$D_{2.24\%f}=0.0034-0.0115\mathbf{p}+0.02\mathbf{p}^2-0.0000061\mathbf{fr}-0.00068\mathbf{fo}+0.00012\mathbf{fo}^2-0.0000067\mathbf{fo}^3$	0.97	0.93	0.0012	<0.05
	$D_{70.79\%f}=0.003+0.0023\mathbf{p}-0.000078\mathbf{fr}+0.0000006\mathbf{fr}^2$	0.91	0.88	0.0002	<0.05
Quantison™	$D_{70.79\%f}=0.54-1.2\mathbf{p}+0.89\mathbf{p}^2-0.22\mathbf{p}^3-0.00026\mathbf{fr}$	0.88	0.81	0.0026	<0.005
Myomap™	$D_{70.79\%f}=0.0045-0.000068\mathbf{fr}+0.00000043\mathbf{fr}^2-0.00089\mathbf{fo}+0.00017\mathbf{fo}^2-0.0000099\mathbf{fo}^3$	0.98	0.96	0.0001	<0.05 apart Pr_{fo}=0.05

The equation of the model (at the frame domain) of decay constant for each agent at 2.24% ($D_{2.24\%f}$) and 70.79%output power ($D_{70.79\%f}$) are shown in this table. The parameters are: the peak negative pressure (p), the frame rate (fr), and the focal length (fo). Also the regression coefficient (r^2), the adjusted regression coefficient (r_a^2), the probability which implies the significance of the model (Pr), and a summary of the probabilities of each of the variables in the model (Details), are also shown in separate columns. All the models shown in the table are significant (Pr<0.05), and all the variables in those models are significant too apart for $D_{70.79\%f}$ where the focal length (fo) is insignificant (Pr=0.05. The models for the intercepts were identical to the ones in Table 6.5.

Table 6.7 *Model of the Overall Backscatter*

	Model Equation	r^2	r_a^2	*Pr*	*Details*
DMP115	$O_{2.24\%} = -0.16\mathbf{fr}^2 - 27420\mathbf{p}^3 + 2095\mathbf{fo} - 391\mathbf{fo}^2 + 22\mathbf{fo}^3$	0.81	0.64	0.038	<0.05 apart Pr_{p3}=0.06
	$O_{2.24\%f} = -246815 + 855\mathbf{fr} + 145652\mathbf{fo} - 25075\mathbf{fo}^2 + 1347\mathbf{fo}^3$	0.86	0.78	0.0045	<0.05
	$O_{70.79\%} = -57\mathbf{p}^3 + 55\mathbf{fr} - 1.09\mathbf{fr}^2 + 0.0068\mathbf{fr}^3$	0.83	0.73	0.008	<0.05 apart Pr_{fr}=0.06
	$O_{70.79\%f} = -2664\mathbf{p}^3 + 3780\mathbf{fr} - 71\mathbf{fr}^2 + 0.45\mathbf{fr}^3$	0.95	0.93	0.0001	<0.05
Quantison™	$O_{70.79\%} = -15771 + 36474\mathbf{p} - 27608\mathbf{p}^2 + 6903\mathbf{p}^3 - 0.00022\mathbf{fr}^3 - 10\mathbf{fo}$	0.98	0.97	0.001	<0.01
	$O_{70.79\%f} = -753959 + 1695551\mathbf{p} - 1257493\mathbf{p}^2 + 309631\mathbf{p}^3 - 26\mathbf{fr} - 251\mathbf{fo}$	0.89	0.80	0.007	<0.05 apart Pr_{fr}=0.05
Myomap™	$O_{2.24\%} = 2303 - 119\mathbf{fr} + 2\mathbf{fr}^2 - 0.01\mathbf{fr}^3$	0.79	0.71	0.0046	<0.05
	$O_{2.24\%f} = 75954 - 3966\mathbf{fr} + 68\mathbf{fr}^2 - 0.38\mathbf{fr}^3$	0.72	0.62	0.013	<0.05
	$O_{70.79\%} = 129 - 213\mathbf{p}^2 + 121\mathbf{p}^3 - 0.133\mathbf{fr}$	0.97	0.96	0.0001	<0.05
	$O_{70.79\%f} = 29694 - 43092\mathbf{p} + 15164\mathbf{p}^2 + 167\mathbf{fr} - 1.66\mathbf{fr}^2 - 98\mathbf{fo}^2 + 7.9\mathbf{fo}^3$	0.99	0.98	0.0001	<0.05

Equation of the model of the Overall Backscatter at the two different domains. O refers to Overall Backscatter, and the subscript f denotes the frame domain. The parameters are: the peak negative pressure (p), the frame rate (fr), and the focal length (fo). Also the regression coefficient (r^2), the adjusted regression coefficient (r_a^2), the significance of the model (Pr), and a summary of the probabilities of each of the variables in the model (Details) with those that are insignificant, are also shown in separate columns. The intercepts of each model are stated only when they are significant (Pr<0.05).

6.4 Discussion

6.4.1 Reproducibility test

6.4.1.1 Mixing time

It was evident from the data generated that there was no significant change in the average values of the intercepts and decay constants for Quantison™ and Myomap™, and only DMP115 showed an increase of decay constant with the increase of mixing time. This was compatible with the decay that this agent showed when dissolved in sterile water (see Figure 4.1a). The assumption that the suspension environment has an insignificant role could not be considered valid for the maximum mixing time for this agent, and therefore mixing times of 10sec and lower were considered suitable for DMP115 for further experiments.

The standard deviations of DMP115 (13.4%) and Myomap™ (14.3%) increased in comparison with the experiment in chapter 2 as seen in Table 2.3 (2.2% and 8.0% respectively). The differences between the two experiments were that in this experiment: (a) the insonation time increased from 0.5sec to 2sec, (b) the use of different vials, and (c) the use of the scanner at different times (variability of scanner performance increases when the time interval is increased, even if it is still small). Even though all three factors were considered negligible in the discussion of chapter 2, their contribution is evident here, if it is assumed that all the other possible sources of variability were under control. The variability in these experiments was even greater, which indicated that a single data set was not reproducible, as shown by the experiment in chapter 2. Thus 3 data sets per setting can illustrate the behaviour of each contrast agent more effectively. Optimum (i.e. minimum) standard deviation was achieved for intercepts and decay constants for mixing times of 10sec and 30sec. Shorter mixing times showed very high variability in the decay constant most probably due to variability in the stirring. A mixing time of 10sec was taken for all the following experiments in this chapter.

6.4.1.2 Insonation time

For all agents at all output powers the decay constant decreased as the time of insonation increased, except for Quantison™ at 2.24% output power where there was

no detectable decay (Figure 6.4b). This means that the destruction of the bubbles per unit time was faster when shorter periods of insonation were applied, and suggests that the mixing of the suspension brings bubbles into the scan plane at a slower rate than the rate that they are destroyed by the ultrasonic beam. If the time of insonation becomes very long, the decay constant will become negligible, if it is assumed that the amount of contrast in the tank was finite. Similarly, when the insonation time approaches zero, the decay constant becomes very large. This suggests an inverse relationship between the two. It was found that the experimental data correlated with this relationship, which suggests that the above explanation is correct.

The intercepts were reasonably constant for DMP115, whereas for the other two agents they decreased with increasing insonation time at the high acoustic pressure (Figure 6.4a). It was found that the exponential decay could not explain the behaviour of the whole data set at large insonation times for Quantison™ and Myomap™ (Figure 6.5), and that the initial part of those data sets would give an increased intercept with the increase of insonation time (Figure 6.6). The exponential fit of the initial 80sec (first 8 points in the graph) was improved in terms of regression coefficient. The observation of two different populations of scatterers in the previous chapter (Figure 5.2), was further supported by this behaviour and Figure 6.5. In chapter 5 observation of the cineloop frames of the last few insonations for Quantison™ showed that the agent still had a low backscattering population of bubbles, but also a very small population of very high backscattering bubbles. Even though these bubbles mostly disappear in one frame, they were many still evident in the field of view for a long time after the last captured frame. If it is assumed that both populations were gas encapsulated bubbles, it is suggested that some bubbles probably need to be hit by the ultrasound beam several times before they provide a leaking site in the coating, thus liberating a free bubble, as was discussed in the previous chapter (section 5.4). If the background population of bubbles was deficient and did not containing gas inside their shells, then it is suggested that dissolved gases in the suspending medium might be eventually trapped inside the shell, and subsequently appear as bright scatterers. The above two suggested mechanisms that give bright scatterers for a long time of insonation might co-exist.

For Myomap™, the background species of bubbles appeared more enhanced and its behaviour was different to that of Quantison™. This population probably remains undestroyed after a long insonation, and is highly scattering due to the larger size of the agent. The earlier departure from the initial behaviour of the agent agrees with the above suggestion.

The initial part of each curve provided a similar exponential fit with the whole curve at low insonation times. This, along with the values of the standard deviations stated in Table 6.3, justifies the empirical choice of the 2sec insonation choice of the previous chapter, which proved optimal for calculating the parameters of decay constant and intercept, and therefore is the choice for the rest of the experiments that involve continuous imaging.

6.4.2 Model of continuous imaging

Modelling using multiple regression is a cumbersome procedure and "none of the selection methods provides infallible tactics in the difficult problem of selecting predictor variables" (Armitage and Berry, 1996). Therefore, even though the models stated in Table 6.5 provide high predictability ($r^2 > 0.8$ for most models), they can only be suggestive of the behaviour of the agents in continuous imaging. Furthermore, the narrow range of acoustic pressures, the shortage in the number of focal positions (four), and the small sample size of 12 of the data (although average of 3 measurements) do not allow detailed conclusive remarks. Yet even within these limitations the system proved to be capable of extracting useful information for the three agents. The previously gained knowledge in the first part of this chapter and the two previous to it was used in the modelling procedure as discussed in the statistical analysis section, and forms the basis of the following discussion. The results of the investigation in the time domain are first discussed.

Modelling the backscatter from the phantom showed a complicated relationship between a linear scatterer and the different variables affecting the beam. If it is assumed that the phantom is scattering linearly with acoustic pressure, these equations illustrate the complexity of the ultrasound field across the whole ROI that can be described by the three main parameters. However, it would be misleading to try to interpret the contribution of frame rate, focus, and peak negative pressure

separately. The difference in the two equations (6.1 and 6.2 in p101) suggested that the beam shape was different for the two output power levels.

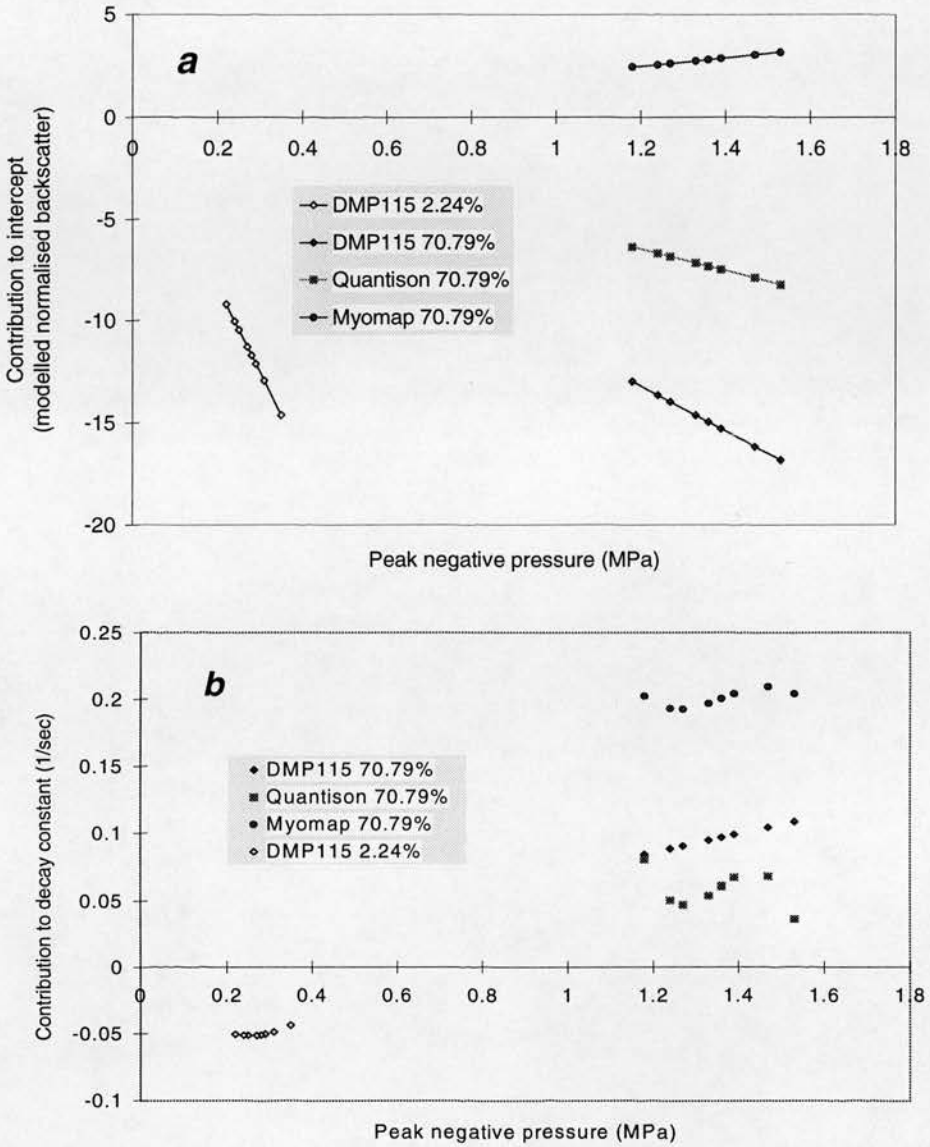

Figure 6.8 Contribution of peak negative pressure to the intercept (**a**), and to the decay constant (**b**) according to the models stated in Table 6.5. Because the contribution to the decay constant for Quantison™ could not be included in the graph due to its high magnitude, the model result was plotted instead. The acoustic pressure of the alternative model for the $D_{70.79\%}$ for Myomap™ was also plotted here. $D_{2.24\%}$ for both Quantison™ and Myomap™ did not provide any significant model due to the negligible decay of those two agents.

The acoustic pressure was present in most models in Table 6.5, apart from Quantison™ and Myomap™ at 2.24% output power. Those two agents have negligible decay at that particular setting as shown in the last two chapters. As a result the acoustic pressure affected neither the intercept nor the decay constant. Unlike Quantison™ and Myomap™, DMP115 showed a slight increase of decay

constant and decrease of intercept with the increase of acoustic pressure. This outcome generally agrees with the results of chapter 5 and Figure 5.3a1 and 2. It was suggested in the discussion of chapter 5 that the increase in decay would increase the underestimation of the intercept. Figure 6.8b shows that with the increase of acoustic pressure, the increase of decay constant was faster at 70.79% output power. This suggested that higher acoustic pressures have a higher destructive effect on the bubbles. If the underestimation of intercept should be larger at that output power, as proved in the previous chapter, the intercept should decrease faster with the increase of acoustic pressure at the high output power. However Figure 6.8a showed the opposite. The intercept decreased slower at 70.79% output power than at 2.24%, indicating that there must be a more complicated mechanism to explain the behaviour of the intercept. Apart from the effect of decrease on the intercept, the intercept reflects the backscatter level of the suspension, and therefore the scattering cross-section of the bubbles. The contribution of the bubble destruction and the relationship of the scattering cross-section with the acoustic pressure remain unclear, and it remains to be clarified in the following chapters.

Quantison™ and Myomap™ further contribute to this problem. Myomap™ has a third order relationship between the decay constant (in the alternative model Table 6.5) and the acoustic pressure (Figure 6.8b), and its intercept increased linearly with acoustic pressure (Figure 6.8a). A very similar relationship between the decay constant of Quantison™ and the acoustic pressure was shown in Figure 6.8b, while the intercept was decreasing linearly with acoustic pressure (Figure 6.8a) which did not agree at first glance with the results of the previous chapter (Figure 5.3b2). It is well known that the Quantison™ bubbles are destroyed by the ultrasonic beam. The appearance of very bright scatterers at 70.79% output power that did not exist at 2.24% raised another question: Does the amount of bright scatterers vary with acoustic pressure? The similar patterns in the decay constant for the two agents probably agrees with the similarity of their nature. However the increase of acoustic pressure for Myomap™ provided an increase in intercept, and a probable increasing tendency in the decay constant (i.e. increasing destruction with increasing acoustic pressure). On the other hand the intercept for Quantison™ slightly decreased and the

decay constant showed a decreasing tendency (i.e. decreasing destruction with increasing acoustic pressure). Note also that there were no other variables affecting that model, and none of the variables in this model were individually significant. Even though it has already been shown that the tendency in the one variable would be reflected in the other, the mechanism of destruction, and the relationship of the scattering cross-section with the acoustic pressure alone can not explain these models. The following two chapters aim in clarifying the problem and quantify the different components contributing in the behaviour of the bubbles.

Varying the focal length introduced an interesting factor in the modelling of the contrast agents. The region of interest (ROI) was positioned at a distance 2.12cm from the probe, and its axial length was 1.41cm. Increasing the focal length from 3cm to 9cm suggests a decreased overall level of acoustic pressure to the ROI, which probably explains the negative linear relationship between $I_{70.79\%}$ and focal length for both DMP115 and Quantison™ (Table 6.5).

It is also expected that an increase of focal length would increase the width of the beam at the location of the ROI (both in-plane and out-of-plane). Furthermore, the calibration at those settings showed that the acoustic pressures had different gradients across the ROI (Figure 6.9). In fact, the longer the focal length, the more pronounced the increase of acoustic pressure axially along the ROI. The third order contribution of focal length was similar to the $I_{70.79\%}$ and $D_{70.79\%}$ for Myomap™, and to $D_{2.24\%}$ for DMP115. This was suggestive of the distribution of acoustic pressures across the ROI, especially for low decay constants where the decay was negligible, as illustrated in Figure 6.9. For example in the above two models for the decay constants ($D_{70.79\%}$ for Myomap™, and $D_{2.24\%}$ for DMP115), the significance of a more subtle effect might become more discernible. It is worth mentioning that $D_{70.79\%}$ could be modelled for DMP115 including a similar function of focal length (r^2=0.88). However, each one of the orders of the focal length was slightly insignificant (p~0.09), suggesting that a larger sample size would be able to detect such a subtlety when the acoustic pressure is dominant in describing the destruction of bubbles. The contribution of the focal length to these models illustrated the complexity of the ultrasound field, and its effect on the contrast enhancement.

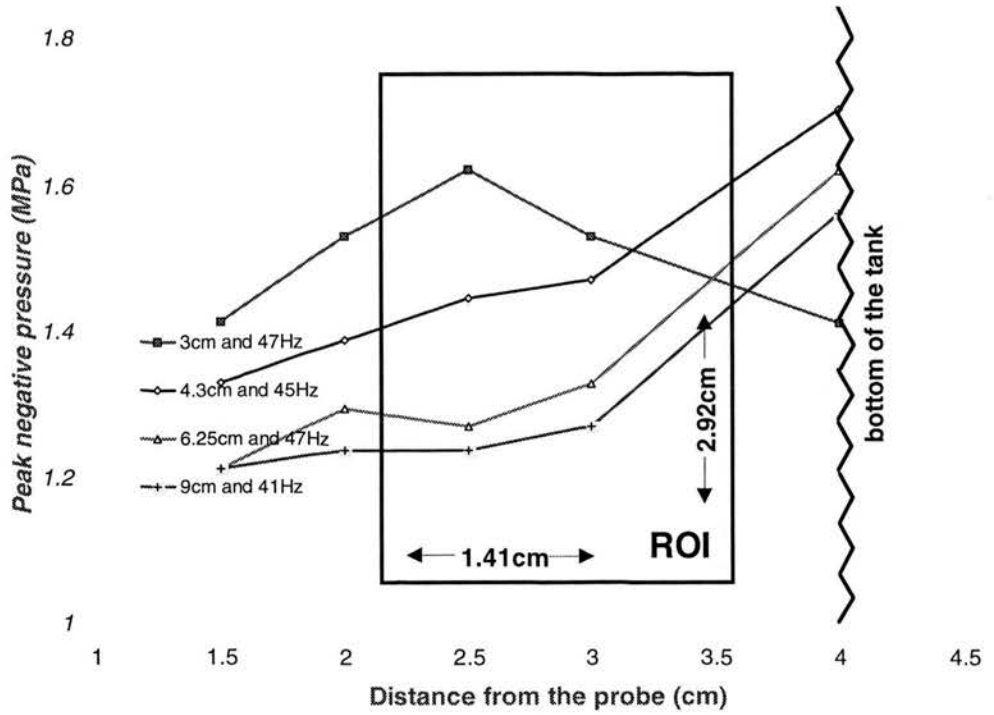

Figure 6.9 Illustration of the distribution of peak negative pressures at different distances from the probe, and inside the region of interest (ROI). The four different lines can only be suggestive of the acoustic pressure between the points, and refer to the four different focal lengths used in the experiment at similar frame rates. Note the increase of the gradient of peak negative pressure across the ROI with the increase of focal length.

The frame rate had similar effect on all intercepts, and had almost no effect on any of the decay constants. Figure 6.10 illustrates a comparative summary of the contribution of the frame rate to the models of intercepts of all the agents at both percent output powers as these shown in Table 6.5. The increase of frame rate resulted in a decrease of intercept with no exception. For Myomap™ the decrease in the intercept was small but significant at 2.24% output power, and became steeper and even more significant at 70.79%. DMP115 provided a higher difference between the two output powers and for Quantison™ this difference was even more pronounced.

It was discussed in the previous chapter that the frame rate could be highly significant for the level of backscatter in the field of view. The time between two frames, is the time that new contrast is introduced into the field of view, due to the magnetic stirring. At high acoustic pressures Quantison™ and Myomap™, as suggested in the previous chapter, had two different populations of scatterers, one very bright for both agents, and a second one less bright for Myomap™ and for

Quantison™ significantly darker. It was also observed that the bright scatterers disappear usually in one frame. Thus the number of new bright scatterers that were introduced in the next frame would be expected to be proportional to the amount of time between frames, up to a plateau that would be dictated by the bubble concentration. Hence the level of backscatter, represented by the intercept, would be expected to be inversely proportional to the frame rate. The negative linear relationship of frame rate and intercept at high output power for all three agents was a very close approximation of the inversely proportional relationship, especially when the range of frame rates was small (33 to 78Hz).

The fact that the frame rate contributes to the intercept to such a large extent for Quantison™, lower for DMP115, and lower again for Myomap™, was in agreement with the outcome of the previous chapter. The bright scatterers almost fully characterise the backscatter of Quantison™'s suspensions, and their almost immediate destruction shows that the intercept fully depends on the introduction of the agent to the scan plane, done by the mixing. For DMP115, the destruction of bubbles was not immediate and even though all the bubbles seem to behave the same, the fact that they are individually more tolerant to ultrasound results in the difference between the slopes of the curves in Figure 6.10 being small. The bright scatterers of Myomap™ probably display similar decay properties to those of Quantison™, but the background scatterers seem to give echoes at much higher level than the Quantison™ ones. Therefore the above difference in slope was very small.

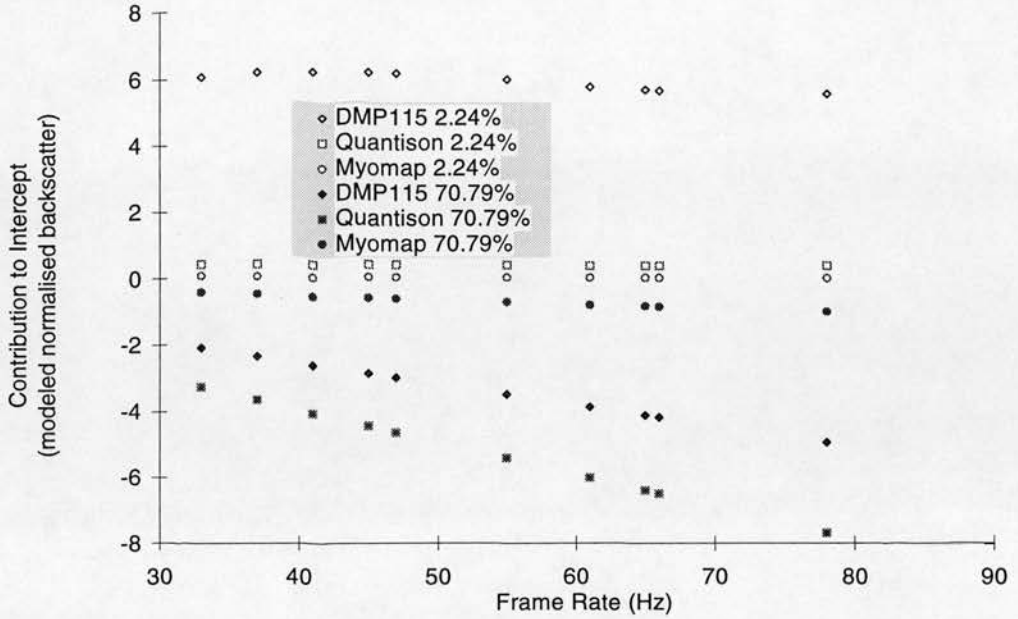

Figure 6.10 Contribution of the frame rate to the intercept. All agents showed a decrease of intercept with the increase of frame rate, which was even more pronounced at 70.79% output power. For Myomap™ the difference between the two output power was less pronounced, and for Quantison™ it was the largest compared to the other agents. The contribution to $I_{2.24\%}$ for DMP115 was divided by 10 for display purposes, since the slope and the shape of the curves were more important than their magnitude.

Further investigation in the frame domain showed that the decay constant decreased with the increase of frame rate (Figure 6.11). This was most pronounced for Quantison™, and less for Myomap™ at 70.79% output power. A saturation of this effect occurred for DMP115 at higher frame rates, while at low acoustic pressure the decay constant for DMP115 showed the slowest decrease with the increase of frame rate.

These results simply show that increasing the frame rate would cause less bubbles to be available for destruction in the field of view, as discussed previously, due to the constant mixing that would supply a constant amount of bubbles in the field of view. The higher the destruction due to the ultrasonic beam, the higher will be this negative effect of frame rate to the decay constant, which explains why Quantison™ shows the highest decrease of decay constant.

The effect of the frame rate generally did not appear in the equations in the time domain, which gave the impression that changing the frame rate did not have any effect on the destruction of the agents. The frame domain investigation showed in general that a slow frame rate was more effective in destroying the bubbles

compared to a faster one, but more importantly, it showed that the changes of frame rate result in changes of the bubble destruction, which differed amongst the contrast agents. Using the frame domain proved a more objective assessment, than the time domain, of the decay constant, and the parameters that change it.

The Overall Backscatter would therefore be better defined in the frame domain. This was also shown in Table 6.7. The time domain only showed a negative relationship between the frame rate and the Overall Backscatter, which gave the impression that the effect of frame rate would only be related to the time between frames that allows new contrast to be introduced in the ultrasonic field. The frame domain showed that the destruction was less effective with increasing frame rate. Furthermore, the Overall Backscatter clearly increases with the increase of frame rate in the case of DMP115 in the frame domain, which is further evidence that the same bubbles appear in the field of view for more than one frame. This was not the case for Quantison™, because the majority of bubbles were destroyed after one frame of insonation, and the Overall Backscatter decreased with the increase of frame rate.

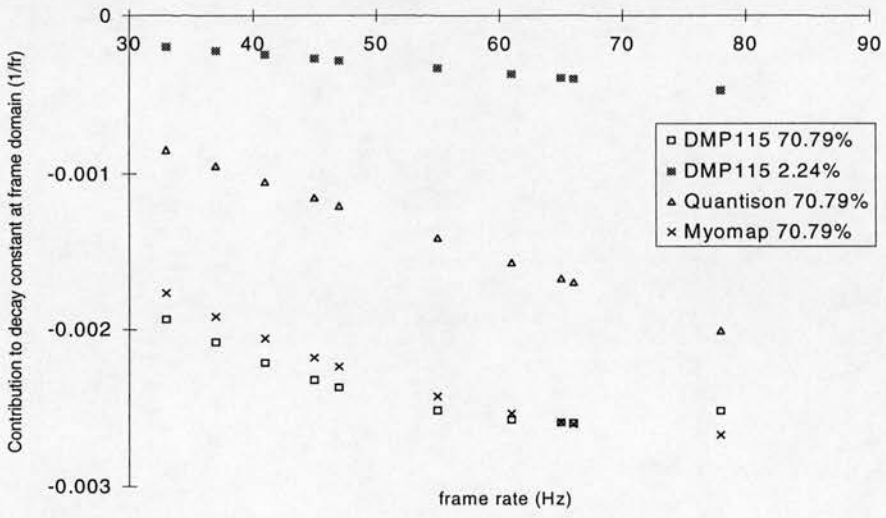

Figure 6.11 Contribution of frame rate to the decay constant at the frame domain. Increase of frame rate resulted in decrease of the decay constant at all models. At 70.79% output power Quantison™ showed the highest decrease of the decay constant, while Myomap™ was slightly less decreasing. At lower frame rates the decay constant of DMP115 also decreased, but seemed not to be affected at higher frame rates. The general decrease of the decay constant for DMP115 at 2.24% was the slowest amongst all data sets.

The Overall Backscatter is the physical quantity describing the amount of backscatter that can be witnessed over a period of time, and can be an objective quantity when defined in the frame domain. There are two major parameters that

affect its value: a) the nature of decay of the agent, and b) the general reflectivity of the agent. Both those parameters in general appear together in the equations of Table 6.7. At 2.24% output power Myomap™ and DMP115 display two completely different models. Their small decay at those acoustic pressures show that all the variables in these two equations were expressing the effect of the ultrasonic field across the ROI on each agent. A similar situation was also illustrated in the rest of the equations.

DMP115 at 2.24% showed the largest Overall Backscatter in Figure 6.12. However, Figure 6.5b and c illustrate that Quantison™ and Myomap™ do not probably have an Overall Backscatter equal to the ratio of the intercept to the decay constant. This is simply due to the fact that in those graphs it was shown that the decay of the agents could not be illustrated by the simple exponential decay. The dual nature of both those agents dictated perhaps two exponential terms explaining their behaviour, and therefore the solution of equation 5.2 is expected to be more complicated and give larger values of Overall Backscatter. In this section, the short insonation times allowed the simple exponential to be satisfactorily applied, since the bright population of scatterers was a dominant population.

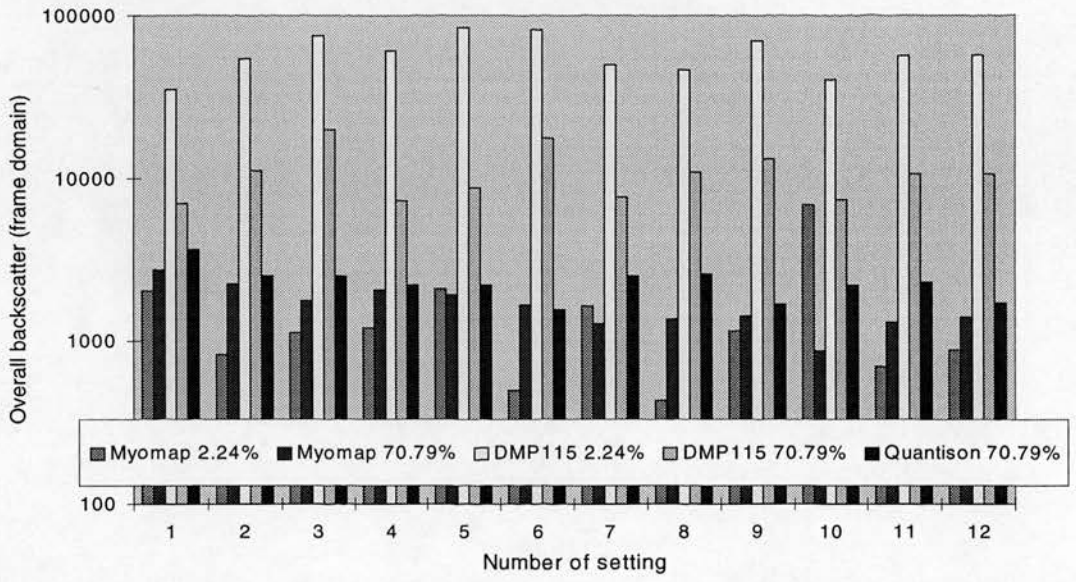

Figure 6.12 Overall Backscatter for all three agents at the 12 different settings of each output power level. DMP115 demonstrated the highest Overall Backscatter in 2.24% since it provided a combination of both high reflectivity and low decay constant. Quantison™ and Myomap™ might not follow the formula describing the Overall Backscatter, and therefore might be accurately illustrated in this graph. See text for details.

A comparison between the dynamic range achieved by the intercept and the Overall Backscatter is shown in Table 6.8. In this table the dynamic range (in dB) of each contrast agent at each percent output power (POP) provided by the intercept and the Overall Backscatter are calculated. In the last row the overall dynamic range provided by all the measurements is also calculated. The Overall Backscatter provided a larger dynamic range at all except one case (Quantison™ at 70.79%).

Table 6.8 *Comparison between intercept and Overall Backscatter*

Contrast agent +POP	***Dynamic range of Intercept (dB)***	***Dynamic range of Overall Backscatter (dB)***
Quantison™ 2.24%	1.99	12.43
Quantison™ 70.79%	5.21	3.67
Myomap™ 2.24%	2.04	12.04
Myomap™ 70.79%	4.42	4.98
DMP115 2.24%	1.82	3.76
DMP115 70.79%	1.61	4.57
All agents	22.30	37.44

6.5 Conclusion

This chapter was the last dealing with continuous imaging of contrast agents. The reproducibility and accuracy of all the experiments proved to be high. The models of the different agents at various insonation settings showed high predictability, despite the small sample size of the data and the small differentiation between settings. The knowledge and understanding of the behaviour of these agents also improved. The new physical quantity called Overall Backscatter, showed that it could optimally describe the properties of the agents in in-vitro imaging, and perhaps a similar physical quantity could be implemented in in-vivo studies for research purposes. However it was difficult to distinguish the different contributions of the scattering properties and destruction patterns of each agent. This implies that an approach other than continuous imaging should be implemented in order to avoid the effects of destruction in the quantification of contrast enhancement. The following chapters investigate the contrast agent bubbles in triggered imaging mode, in an effort to isolate the scattering properties of the agents from their decay.

7 Chapter Seven: Concentration and acoustic pressure effects on backscatter

7.1 Introduction

Attempting to quantitate the presence of contrast has been one of the main aims of contrast imaging. In the last two chapters it was assumed that the measured backscatter was linear to the concentration of bubbles in the suspension. This assumption was based on a preliminary experiment carried out in chapter 3. That experiment, which was done at 2.24% output power, decided the optimal concentration for the experiments in chapter 4. It was further assumed that the backscatter intensity at higher acoustic pressures would be linearly related to this concentration, and therefore this concentration was again used in the experiments in chapter 5. Chapter 5 also showed also that the backscatter from contrast agents was not linear to the incident intensity (Figure 5.5). Two agents showed enhanced backscatter with increased acoustic pressure (Quantison™ and Myomap™), while DMP115 showed a slightly decreased backscatter with increasing acoustic pressure. The differences in behaviour between agents also require an investigation that would clarify whether this was a difference in scattering properties or this difference was induced by the different bubble concentrations. There were three major questions about these relationships raised in the previous chapters.

1) In these three chapters, it was also assumed that the attenuation of the contrast agent suspensions was negligible. This assumption is tested in this chapter.
2) The relationship between the scattering cross-section (or the attenuation) and the acoustic pressure (peak negative pressure is used) could not be concluded from the experiments carried out so far.
3) The differences between contrast agents and the various scattering populations add a further complication in understanding the relationship between backscatter and concentration. In continuous imaging mode, DMP115 produced images of very similar uniform appearance throughout the range of acoustic pressures used

in chapter 5, while Quantison™ and Myomap™ demonstrated two different populations of scatterers. Figure 6.5 and the discussion paragraph 6.4.1.2 suggested two different mechanisms of destruction, and therefore a variable behaviour in the appearance of bright scatterers. This raised the question of whether the number densities the different populations of scatterers were dependent on the acoustic pressure.

The aim of this and the following chapter was to isolate the physical parameters contributing to the backscatter signal from contrast agents. The concentration of contrast will be varied in this chapter in high number density ranges close to acoustic saturation for the agent (backscatter reaches a plateau and does not further increase with concentration increase), and in the next chapter in very low number densities. It has also been shown in the last two chapters that continuous imaging was limited in accurately displaying backscatter, which would be representative of a suspension of contrast agent scatterers. It was shown that it is impossible to isolate the scattering properties from the decay process. The measured level of backscatter (intercept) was not representative of the true level of backscatter in the tank.

The use of triggered imaging was introduced in this chapter. A single frame acquisition is considered representative of the backscatter of a suspension of scatterers.

7.2 Materials and methods

7.2.1 The experimental set-up

The set-up used in the following experiments is described in 2.2.1 (p.16). This experiment however was done in triggered imaging mode. The scanner was set to trigger mode, and a pulse generator (Phillips PM5705) was connected to the ECG lead. The pulses generated and transmitted to the ECG lead were 1msec in duration, had 0.8sec repetition rate, and 5Volts amplitude. The triggered mode was activated using foot switch control. The PC, which was used as a timer (Figure 2.1) and controlled the number of captured frames. When the scanning was on and the foot switch pressed, a few triggered frames were scanned. The scanning time, and the

pulse repetition frequency, specified the number of acquired frames. In this experiment the suspensions were allowed to mix for 30sec (timer in freeze position), and were insonated for 1sec, which was enough to capture 1 triggered frame. All the output powers stated in Table 2.1 were used.

7.2.2 Contrast agents

In these experiments DMP115, and Quantison™ were studied. The protocol of concentrations was built with the aim of achieving acoustic saturation for the agent. Note that to reach a plateau similar to the ones in the graphs of Figure 3.1, it was not necessary to produce images with visually apparent attenuation across the tank. Furthermore, since the scanner's monitor displayed log-compressed images, it was almost impossible to judge whether a specific contrast concentration used in a suspension was providing linear backscatter. Therefore it was necessary to conduct a pilot study in order to decide the appropriate concentrations that would be able to produce backscatter that lies both in the linear and the saturated range.

Figure 5.3a2 and b2 showed that DMP115 had a small decrease in normalised backscatter, and Quantison™ a large normalised backscatter enhancement with increasing acoustic pressure. It was easy to derive the concentration regime for DMP115, which was composed of 15 injections to the tank from 0.3μl to 3.1μl, with 0.2μl difference between consecutive injections, and was the same for all acoustic pressures. The injection regime for Quantison™ varied at each acoustic pressure. Overall the injections varied from 0.5μl to 400μl. At each acoustic pressure a different concentration regime was implemented that had 15 different injections. With the help of Table 3.2, the volumes of contrast can be converted to number of bubbles per ml of suspensions. 1μl of introduced agent for DMP115 is 5000 bubbles per ml of suspension, while for Quantison™ it is 7500 bubbles per ml of suspension. The measurements at each output power setting were repeated 3 times.

7.2.3 Statistical analysis

After image reconstruction, the backscatter intensity of each frame was calculated on the same ROI used to date in this thesis. However since attenuation effects were also to be investigated, another 3 arbitrarily chosen ROIs were used to

analyse the data. These were all closer to the probe compared to the usual ROI. The backscatter intensities from the 4 ROIs were compared graphically.

The backscatter pixel intensity of the acquired contrast frames were normalised with respect to the suspension of Orgasol®. This technique was also used in chapter 5, and was described in section 2.3.2 and Figure 2.4b. Nonlinear regression analysis was performed, using the SAS statistical package, in order to model the normalised backscatter of the two agents. A simple model was considered for normalised backscatter:

$$NB = a_0 f_1(C, p) e^{-b_0 f_2(C,p)} \tag{7.1}$$

where **C** was the bubble concentration in number of bubbles per μl of suspension, and **p** the peak negative pressure in MPa at 3cm distance from the probe, $f_1(C,p)$ and $f_2(C,p)$ functions of concentration and acoustic pressure. The functions $f_1(C,p)$ and $f_2(C,p)$ are related to backscatter and attenuation respectively (Marsh et al. 1998), although they were not assumed to be related to acoustic pressure. If multiple scattering is considered to be negligible then both backscatter and attenuation are proportional to the bubble concentration:

$$f_1(C, p) = a_1 C f_{10}(p) \tag{7.2a}$$

$$f_2(C, p) = C f_{20}(p) \tag{7.2b}$$

Because there is limited knowledge to the nature of $f_{10}(p)$ and $f_{20}(p)$, it is assumed that:

$$f_{10}(p) = p^n \tag{7.3a}$$

$$f_{20}(p) = b_1 + b_2 p + b_3 p^2 \tag{7.3b}$$

If n=0 then a particular contrast agent is scattering just the incident beam in linear manner. Because there is evidence of bubble oscillation and change of bubble diameter with the increase of acoustic pressure, it is expected that n>0.

The dependence of the attenuation term to the acoustic pressure was illustrated as a 2nd order polyonym due to limitations induced by the nonlinear regression algorithms. More variables were tested in that model, and it was found that the convergence criteria were not met for the nonlinear regression analysis. However, a

2^{nd} order equation was considered adequate to describe the attenuation contribution on the collected signals. Equation 7.1 therefore becomes:

$$NB = aCp^{n}e^{-C(b_1+b_2p+b_3p^2)} \tag{7.4}$$

Modelling separate data subsets was considered.

7.3 Results

7.3.1 DMP115

All values of pixel intensity for DMP115 were lower than $5*10^7$, and according to chapter 2 (2.3.1), this was inside the linear region of backscatter intensities for the system.

Figure 7.1a illustrates the average pixel intensity for DMP115 (over the ROI, and three repeated acquisitions), while Figure 7.1b illustrates the normalised backscatter intensity by means of the suspension of Orgasol®. At low concentrations the normalised backscatter increases with increasing acoustic pressure, while at high concentrations it decreases with increasing acoustic pressure.

Errors bars would make Figure 7.1 difficult to read. For that reason Table 7.1 was created to demonstrate the variability, i.e. maximum and mean percent standard deviation of three measurements, at different acoustic pressures.

The measured pixel intensity was plotted against bubble concentration at three different acoustic pressures at 4 different regions of interest (ROIs). In Figure 7.2 *r0* is the ROI described in section 2.2.2.1. The other three ROIs were placed closer to the probe and had half the width of the first one. The closest to the original ROI was *r1* and the closest to the probe was *r3*. Figure 7.2a, b, and c illustrate the data at 0.27, 0.96, and 1.52MPa respectively. As expected, the pixel intensity was increased as the distance from the probe was increased, since the beam focuses at 4.3cm, a distance from the probe, which was close to the bottom of the tank.

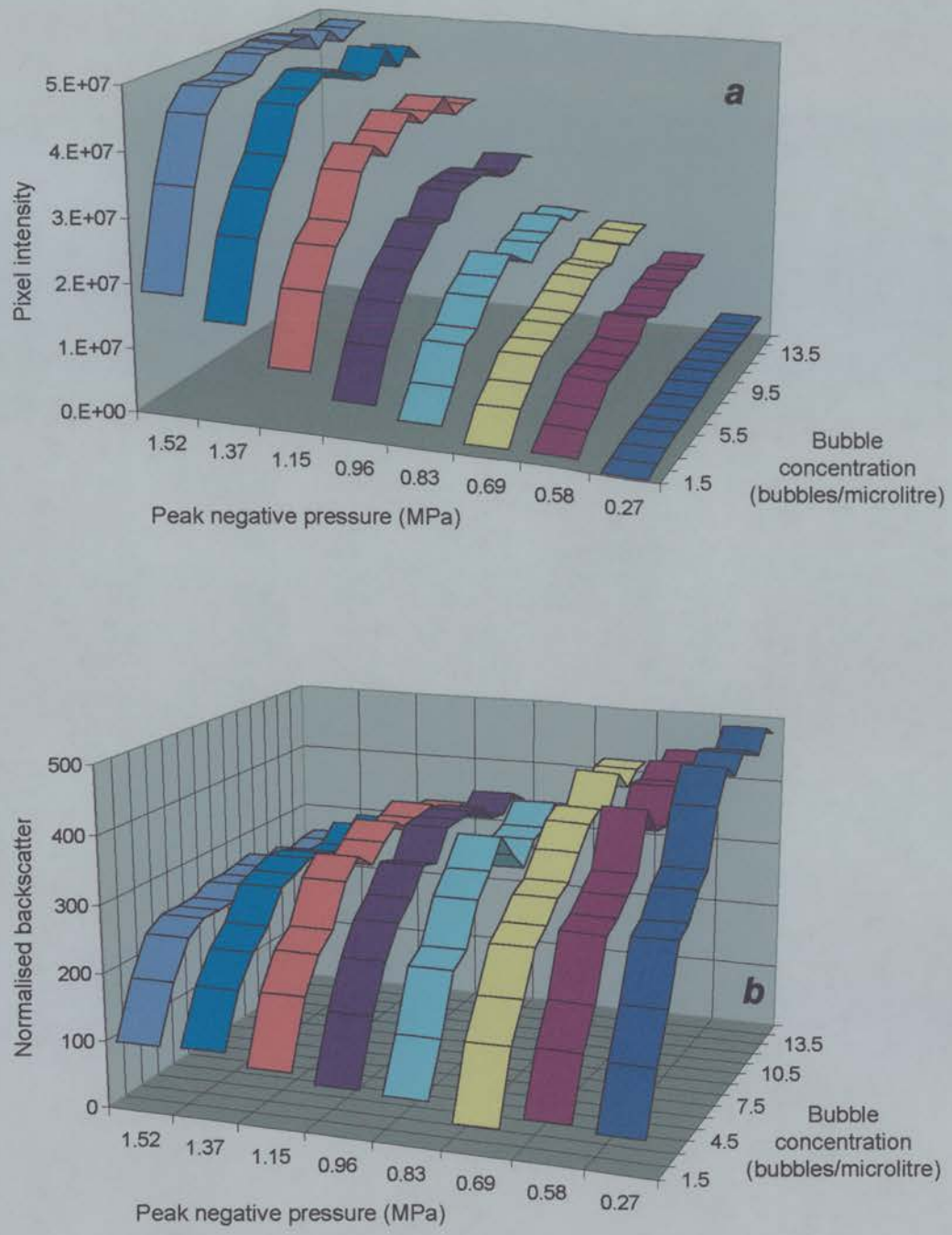

Figure 7.1 a Pixel intensity of DMP115 over original ROI at different bubble concentrations (number of bubbles/microlitre of suspension) and peak negative pressures (MPa) **b** Normalised backscatter intensity, referenced to an Orgasol® suspension, against bubble concentration and peak negative pressure. The scaling in the peak negative pressure axis is not linear.

Table 7.1 *Standard deviation of normalised backscatter for DMP115*

Peak negative pressure (MPa)	Max standard deviation (%)	Mean standard deviation (%)
0.27	36	22
0.58	30	14
0.69	38	17
0.83	51	22
0.96	47	11
1.15	44	14
1.37	32	10
1.52	60	12

These data were used as input to the SAS scripts similar to those in the previous chapter. The largest acoustic pressure provided backscatter values that seem to saturate the system above a certain concentration (Figure 7.2c). Thus, the optimal model for all the data sets was also fitted to all apart from the two highest acoustic pressure sets, i.e. data for 1.52 were excluded. It was also noticed that this model was also optimal for this reduced data set. The models for all the data (sample size=120), and those excluding the highest acoustic pressure (sample size=105) proved almost identical, but the latter displayed higher regression coefficient. The resulting model for the normalised backscatter of DMP115 was:

$$NB = 81.3Cp^{0.157}e^{-C(0.033+0.063p-0.0075p^2)} \tag{7.5}$$

The regression coefficient was 0.95, and the model as well as all the variables were highly significant at 5% level (p~0.0001). This equation predicted the normalised backscatter as illustrated in Figure 7.3a. A comparison between measured and predicted data was illustrated in Figure 7.3b. The correlation coefficient between the measured and predicted data was 0.88 for the highest acoustic pressure and 0.97 for the other two acoustic pressures.

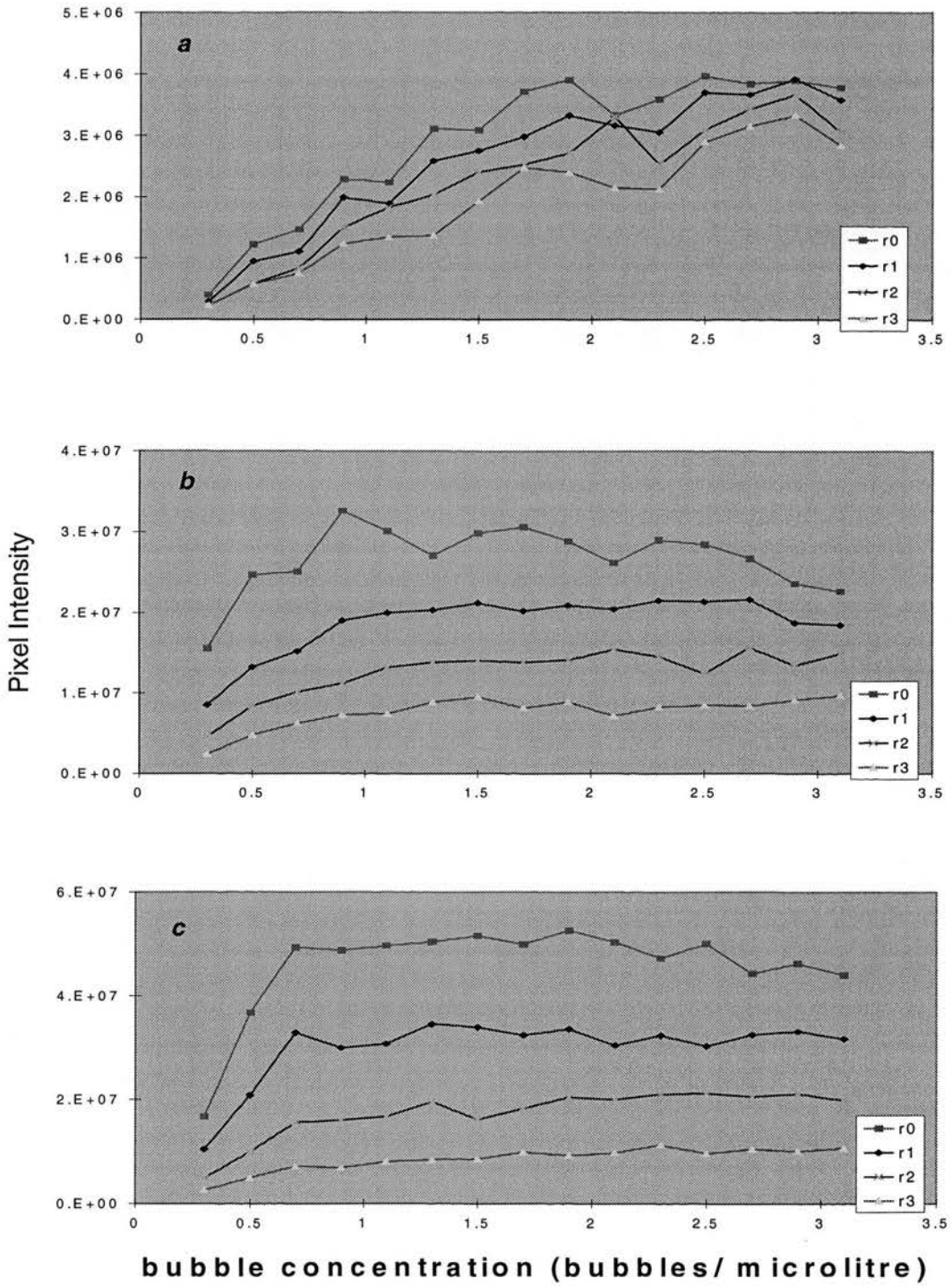

Figure 7.2 Pixel intensity against bubble concentration at 4 regions of interest (r0-r3). The r3 is located closer to the probe, r0 is the ROI used for all the thesis, r1 is closer to r0, and r2 is between r3 and r1. ***a*** 0.27MPa peak negative pressure at 3cm from the probe (inside r0), ***b*** 0.96MPa, and ***c*** 1.52MPa. There was no obvious sign of attenuation, but the r0 graphs are moving closer to the r1 curves at large bubble concentrations for all three figures (more apparent in ***b***).

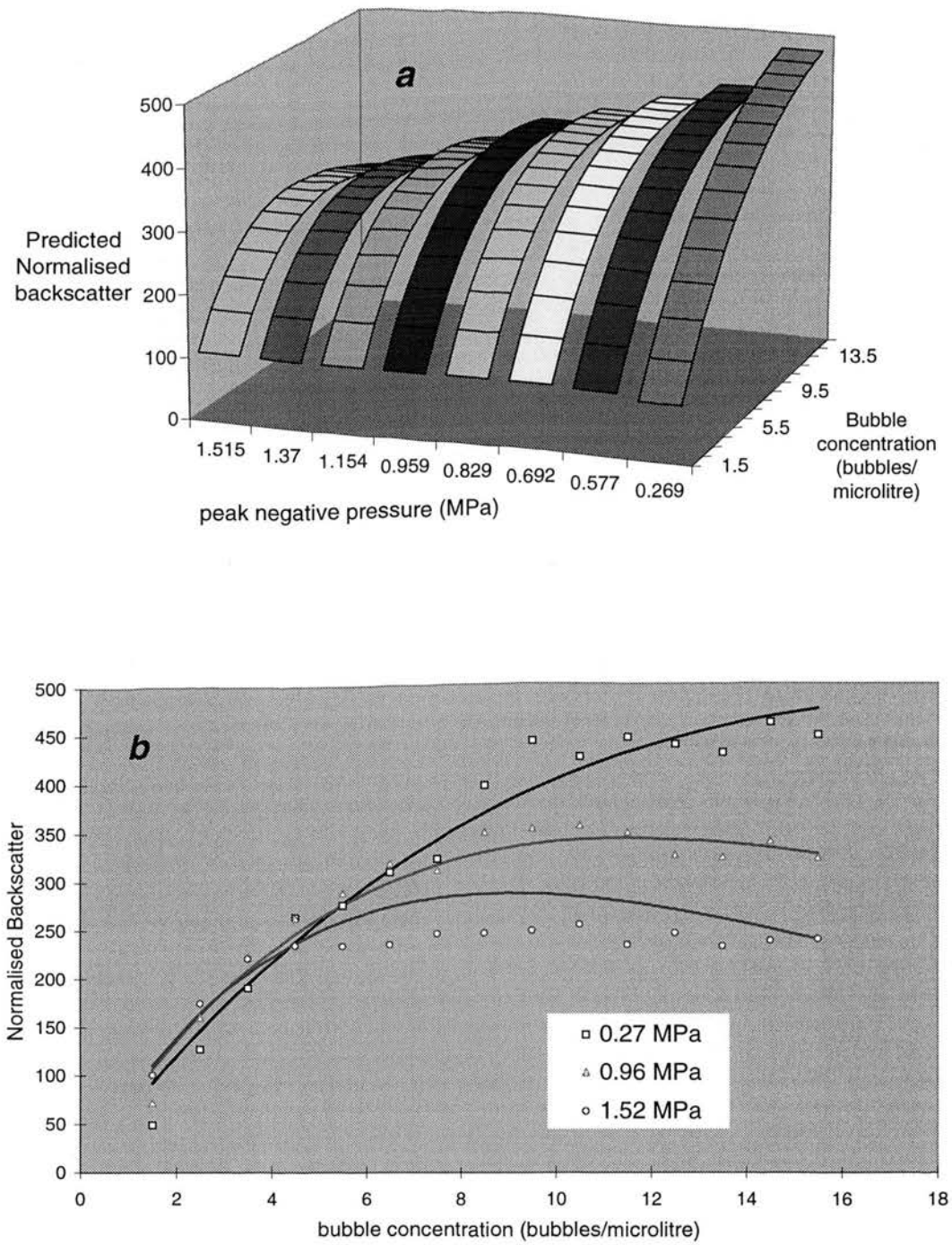

Figure 7.3 a Normalised backscatter predicted by the equation *7.5* plotted against peak negative pressure (MPa) and bubble concentration (number of bubbles per μl of suspension) ***b*** Comparison between the predicted (solid lines) and the measured data (points) at three different acoustic pressures (0.27, 0.96, and 1.52 MPa). The correlation coefficient between the measured and the predicted data at those three acoustic pressure was 0.97, 0.97, and 0.88 respectively.

7.3.2 Quantison™

The pixel intensity was higher than $5.5*10^7$ for 13 measurements for Quantison™, all at the highest acoustic pressure setting. The normalised backscatter was plotted against bubble concentration in Figure 7.4 for the different acoustic pressures. The concentration regime was wider than the one used for DMP115 as shown in Figure 7.1 and Figure 7.4. Likewise, the pixel intensities and consequently the normalised backscatter were spread on a wider range of values.

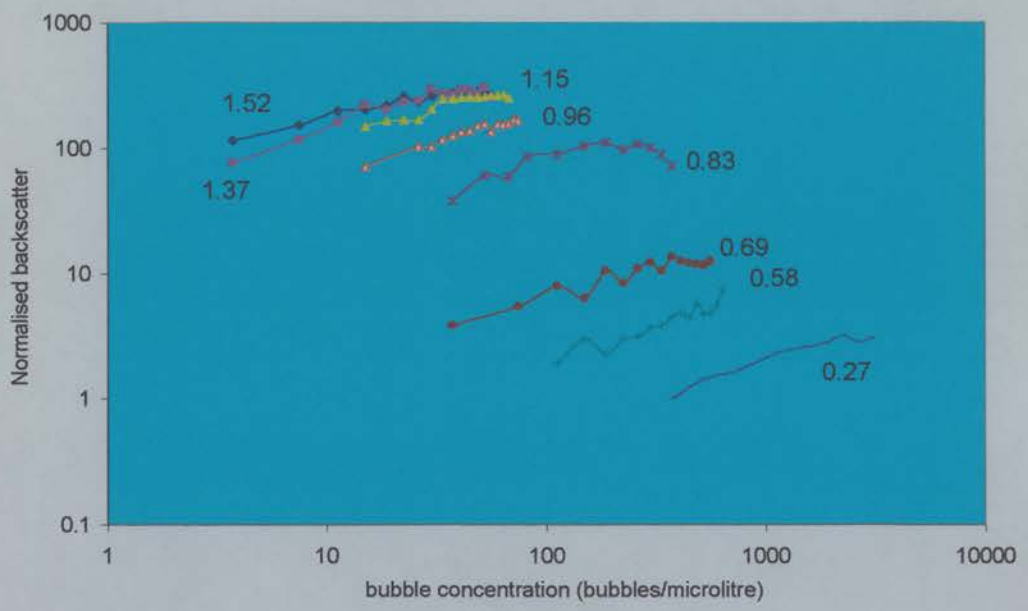

Figure 7.4 Normalised backscatter against bubble concentration (number of bubbles per μl of suspension) at different peak negative pressure. Both axes are in logarithmic scale.

Errors bars would make Figure 7.4 difficult to read. For that reason Table 7.2 was created to demonstrate the variability, i.e. maximum and mean percent standard deviation of three measurements, at different acoustic pressures.

Modelling the normalised backscatter of Quantison™ proved more difficult than that of DMP115. The data sets (sample size = 111) did not fit the model in equation 7.4 that dealt with the variables discussed at the statistical analysis section. Excluding the data acquired at the two lowest acoustic pressures, which did not demonstrate different populations of scatterers, a subset of data was created that fitted the model of equation 7.4 (see also chapters 5 and 1). The excluded data did

not form a subset since they belonged to two acoustic pressure settings, and therefore were unsuitable for modelling with respect to acoustic pressure. The resulting two models for Quantison™ were:

$$NB = 4.51Cp^{4.1}e^{-C(0.073-0.143p+0.077p^2)} \tag{7.6}$$

The regression coefficient was 0.95 for p>0.58. The model and all the variables were highly significant at 5% level (p~0.0001).

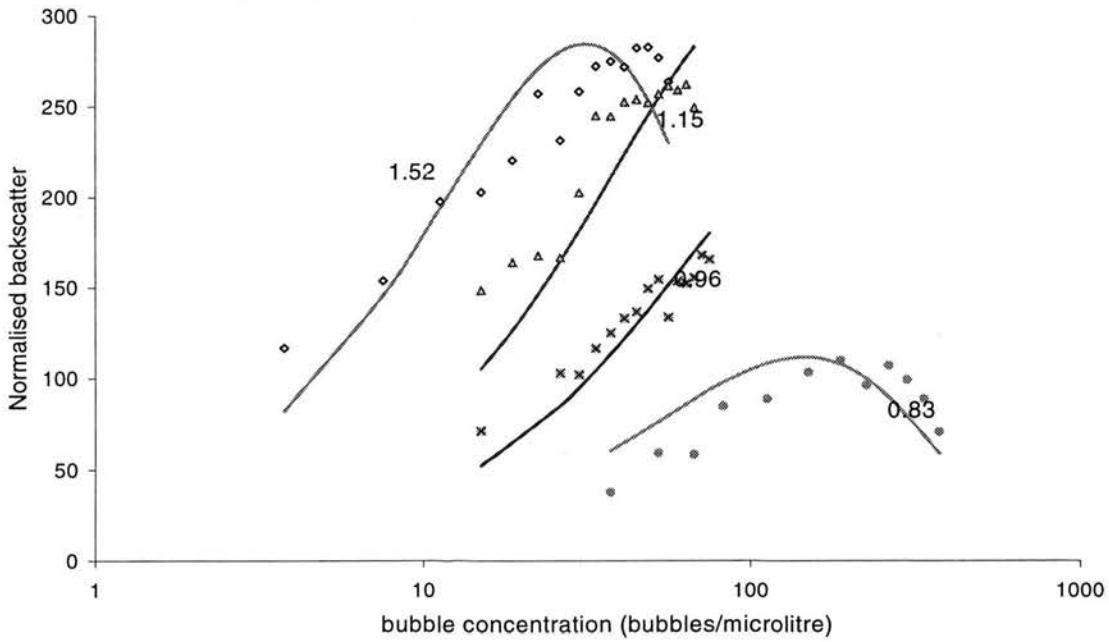

Figure 7.5 Normalised backscatter against bubble concentration (number of bubbles per µl of suspension) for Quantison™. The points are the measured data, and the lines are the predicted data by the model in equation *7.6*. The numbers on the graphs refer to peak negative pressure values.

7.4 Discussion

The following discussion is an attempt to interpret the above results and to extract the information displayed in the models. Overall the experiments proved highly reproducible, which was illustrated by the high regression coefficients. Also the initial assumption that there is no multiple scattering proved correct. The high regression coefficients exhibited by both models proved that both backscatter and attenuation were proportional to bubble concentration.

7.4.1 DMP115

Equation 7.5 demonstrated that the normalised backscatter increases at an order of 0.157 with respect to acoustic pressure, which suggests that the contrast agent did not scatter like a linear scatterer (i.e. independently of acoustic pressure).

The attenuation of normalised backscatter showed that the attenuation was nearly proportional to acoustic pressure (Figure 7.6). This confirms the previous conclusion that contrast bubbles are not linear scatterers of ultrasound, and also suggests that the absorption was not independent of acoustic pressure (as it would be expected by linear scatterers).

Table 7.2 *Standard deviation of normalised backscatter for Quantison™*

Peak negative pressure (MPa)	Max standard deviation (%)	Mean standard deviation (%)
0.27	29	22
0.58	65	23
0.69	79	33
0.83	41	22
0.96	35	17
1.15	22	9
1.37	25	10
1.52	34	10

7.4.2 Quantison™

Equation 7.5 demonstrated that the normalised backscatter increases at an order of 4.1 with respect to acoustic pressure, which demonstrates a large enhancement of backscatter with acoustic pressure for the agent. The difference in order between Quantison™ and DMP115 suggests that the free bubble creation, speculated in the previous chapters, is dependent on the acoustic pressure and in fact increases with the increase of acoustic pressure.

The attenuation of normalised backscatter showed that the attenuation a second order polynomial of acoustic pressure (Figure 7.6). This is a more complicated expression than the one met with DMP115. The attenuation increases

fast with the increase of acoustic pressure at high acoustic pressures, perhaps at an order of dependence similar to the one displayed by the backscatter term. However, the attenuation was also high at low acoustic pressures (especially at 0.69MPa) where the backscatter was low. This suggests that the free bubble creation was very low at this acoustic pressure, and the very high proportion of the other scatterers created the high attenuation (note the bubble concentrations were much higher at 0.69MPa).

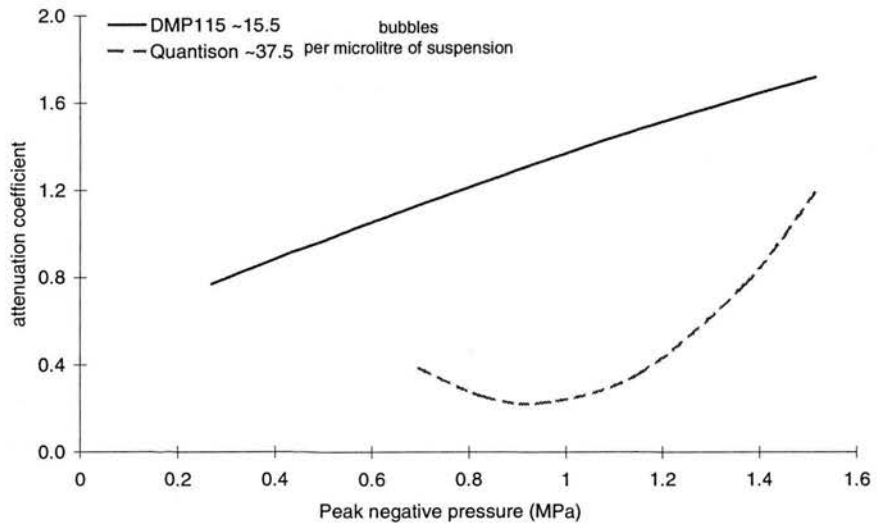

Figure 7.6 Suggested contribution of the attenuation to the model of normalised backscatter for high acoustic pressures for both agents. The plot is against acoustic pressure.

7.4.3 Limitations and general critique

There were several interesting conclusions from this chapter, and more knowledge has been gained about the interaction of the contrast agents and the ultrasonic beam. The components that contribute to the collected signal from the agents have been identified. The work in the next chapter aims to fully identify each of the components of the behaviour of Quantison™ and confirm the suggestions made in this chapter for the behaviour of DMP115. However, several limitations were also brought up in this study that need to be assessed.

The linearity of the system was examined in chapter 2, and the maximum linear average pixel intensity was set at $5*10^7$. DMP115 provided however much lower level of plateau for the two maximum acoustic pressures, and started at $4.5*10^7$ for 1.37MPa, and $4.7*10^7$ for 1.52MPa. This dictates a narrower linear

dynamic range for this agent than the one set in chapter 2. Examining all the data of the two previous chapters, Quantison™ and Myomap™ demonstrate much lower pixel intensity values than the above limits, and only DMP115 tended to have a few values above the limit. In 58 acquired data sets (15 average pixel intensity measurements each) in the maximum two acoustic pressures, there were 10 sets with one measurement exceeding the limit of $4.5*10^7$, 5 sets with two measurements exceeding the limit, and 5 exceeding the limit for more than two measurements. Considering that each set has 15 average pixel intensity measurements, one or two saturated measurements that might not be in the linear range of the set-up would not significantly affect the outcome of the calculated intercept and decay constant. The sets with more than two pixel intensities above the limit perhaps would. A closer look to the data shows that only on one occasion a high pixel intensity provided an outlier to the exponential decay fit to the data (which does not mean that it significantly alters the calculations). Furthermore, none of the groups of high intensities biased its curve on any occasion. It can therefore be concluded that this limit, even though advisable to be followed, did not affect the measurements in the previous chapters.

This experiment also revealed that the attenuation was of considerable magnitude, whether this occurs to the transmitted beam or the backscatter echoes, while in the previous chapter it was assumed negligible. Attenuation is defined as the intensity loss through a medium, which is practically the sum of scatter and absorption. However, visual inspection of Figure 7.2 strongly suggested that the attenuation was almost negligible, and was only apparent at large bubble concentrations which did not occur in the continuous imaging experiments, mainly due to the initial time of insonation (and therefore destruction of a large amount of bubbles) before a frame acquisition.

Moreover, in continuous imaging close to the probe, the concentration of bubbles was much lower than in the bottom of the tank. The introduction of contrast in the scan plane was faster at the bottom of the tank, because the magnetic bar was placed at the bottom of the tank and the mixing was more vigorous. The fast dissolution of contrast bubbles due to consecutive ultrasound frame exposure resulted

to images that had the appearance of Figure 5.2b2 for Quantison™ and of Figure 5.2c2 for Myomap™ with more contrast at the bottom of the tank. The cloud of bright scatterers appears in the bottom of the frame, and very few of them were found close to the probe. DMP115 did not show such an obvious pattern, but the destruction process is slower (hence the homogeneity of appearance of the captured frames) and most probably not visually apparent. Thus an attempt to perform an attenuation correction in previous chapters seems unnecessary.

At last the terms of backscatter and attenuation in both the models shown in equations 7.5 and 7.6 are subject to limitations induced by fitting a model to any set of data. This means that those terms separately, could not describe in a quantitative way the nature of the two contrast agents. Experimenting in conditions with negligible attenuation would give a good assessment approach for the backscatter of each of the agents. The following chapter focuses on this by using very low concentrations of contrast that enables visualisation of individual scattering events.

7.5 Conclusion

This was the first chapter where triggered imaging was used. The normalised backscatter of the agents was measured directly and modelled as a function of the concentration and the peak negative pressure, with high regression coefficients. This proved the triggered imaging mode is more accurate and reproducible at quantifying the backscatter from contrast than continuous imaging mode is. Both contrast agents showed that they scatter ultrasound nonlinearly. The complex nature of Quantison™ was not clarified in this chapter, although it strongly suggested that the creation of free bubbles was dependant on acoustic pressure. In order to describe the behaviour of the contrast agent scatterers, the concentration of bubbles must be very low and the resulting backscatter proportional to it. Consequently the next chapter aims to assess the behaviour of individual bubbles.

8 Chapter Eight: Detecting the behaviour of individual contrast agent scatterers

8.1 Introduction

The last chapter answered a few of the questions that arose in the previous chapters, by means of a statistical model of the normalised backscatter as a function of concentration and acoustic pressure. Most importantly it showed that since only one triggered frame was acquired, the destruction of the microbubbles was not a consideration of the model.

The contribution of the attenuation at different settings made the assessment of the scattering cross-section (or an equivalent physical quantity) difficult even in the case of DMP115, which provided the least complicated model. Although the modelling of contrast agent behaviour using a commercial ultrasonic scanner was considered successful, one question remained unanswered: What is the dependence of normalised backscatter on the acoustic pressure? It became obvious that an attempt to answer this question would involve an experiment that provides virtually no attenuation of the ultrasonic beam between the probe and the contrast agent scatterers, and most importantly the relationship between backscatter and bubble concentration should be linear.

This chapter aims to answer the question. The bubble concentration used was as low as needed to distinguish individual scatterers, and therefore count them and assess the normalised backscatter per scatterer.

8.2 Materials and methods

8.2.1 The set-up

The same experimental and acquisition set-up was used as in the previous chapter (section 7.2.1).

Part of the set-up, as described in chapter 2, was the analysis performed by a package developed in the Department of Medical Physics and installed on the Sun Workstation. The data was rectified and an image was constructed using a moving average algorithm. A new version of the package allowed the calculation of pixel intensities in sub-regions within a ROI, which were set by thresholding the pixel intensity. In other words the average pixel intensity of a ROI could be calculated only for those pixels that had higher intensity than a pre-set threshold. This for example could allow the calculation of the average intensities that would not include background noise. For the purposes of this study, the average pixel intensity was calculated for the contrast agent scatterers alone.

8.2.2 The experimental protocol

The contrast agents used in this experiment were DMP115, and Quantison™. The concentration was low enough to enable the distinction of individual scatterers ultrasonically, and high enough to obtain the highest possible number density that still allows the distinction of individual scatterers and would reduce the variability of the experiment.

In order to do that, both agents were diluted in a beaker. 3μl of DMP115 was introduced in a beaker with 100ml of sterile water, and mixed for 1min with the help of a magnetic stirrer. 50μl of that suspension were introduced into the tank which contained 200ml of sterile water, and 30sec of mixing was allowed before the acquisition of 5 triggered frames separated by 1sec. For Quantison™, 5μl were introduced into the beaker, and from that suspension after mixing, 250μl were introduced into the tank. The bubble concentration in the tank was derived from Table 3.1. DMP115 would have 7.5 bubbles per ml of suspension in the tank, and Quantison™ would have 93.75 bubbles per ml of suspension.

The experiment was repeated, at each acoustic pressure, 5 times for DMP115 and 6 times for Quantison™.

Both agents were shown in suspension under a phase microscope (Olympus IX50, Japan). Figure 8.1 is a microscopical view of DMP115 particles in suspension. All the particles were separated from each other and no clustering could be seen. Similar images were obtained for Quantison™.

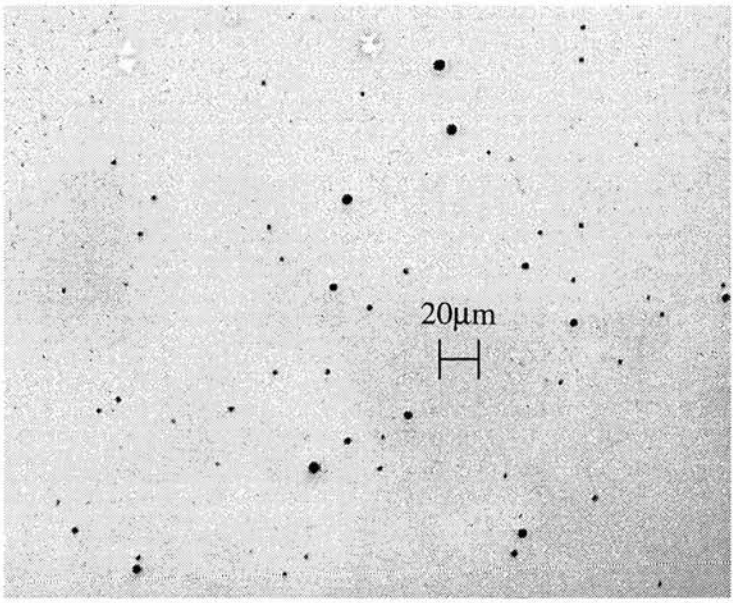

Figure 8.1 Image of DMP115 microbubbles in suspension using a phase microscope (Olympus IX50, Japan). The largest of the bubbles in the picture are approximately 7μm.

8.2.3 Analysis

8.2.3.1 Number of scatterers

The number of scatterers was counted manually in each image. The ROI used was identical to that used previously. As mentioned in 2.2.2.1, the ROI was 2.92±0.03cm long and 1.41±0.03cm wide. The tip of a 0.2mm needle hydrophone was used as a point scatterer in order to assess the slice width. The gain was adjusted in order to obtain an average pixel intensity from the tip of the hydrophone similar to the brightest air bubble. The slice width of the beam was equal to the distance (across the slice width) at which the tip of the hydrophone would be visible in the scanner's monitor. This distance was found to be 1.50±0.05cm. Therefore the volume of the ROI was 6.18±0.25cm^3. This allowed an approximate calculation of the number of scatterers per unit volume in the ROI. Also knowing the injected concentration of bubbles, a comparison between the expected number of bubbles and the counted number of scatterers was possible.

8.2.3.2 The measurement of backscatter

The average pixel intensity was calculated for the ROI used so far in this thesis. The analysis package installed on the Sun Workstation was modified to allow the selection of a threshold pixel amplitude in order to calculate the average pixel intensity of the pixels that had higher amplitude than that threshold. The pixel

intensity was measured using four different thresholds produced by the following procedure. The tank was filled with sterile water and was allowed to settle until no air bubbles or artefacts could be seen on the monitor. A frame similar in appearance to the one in Figure 2.2 was captured at each acoustic pressure. Three average pixel intensities from three different ROIs were calculated. The first one was from the usual ROI also seen in Figure 8.2a, and the square root of the magnitude of the backscatter intensity was set to be *threshold 1*. The second ROI was set over a low backscattering artefact appearing in each frame, and the third ROI was from a high backscattering artefact. The respective square roots of those intensities were *threshold 2*, and *threshold 3*. Both those artefacts were air bubbles, visualised in the wall of the tank. They provided very low echoes since they were almost outside the scan plane, but the echoes were large when compared to those from single scatterers. The fourth threshold was set to zero in order to include background noise in the average pixel intensity calculation (*threshold 4*). After having set the threshold amplitude, all the pixels that would be included in the average pixel intensity calculation became blue in colour in the image. Figure 8.2b shows the pixels that were included in the calculation of the average pixel intensity using *threshold 1*. Figure 8.2c and d show the pixels that had amplitudes above *threshold 2*, and *threshold 3*. It is obvious that *threshold 4* would create a completely blue image. The normalised backscatter was calculated as in the previous chapter. The four different thresholds were compared by the normalised backscatter values they produced.

The ratio of the normalised backscatter (for a specific threshold) to the number of scatterers in the ROI would give the normalised backscatter per scatterer. This calculation was averaged over all the frames at each acoustic pressure.

. Since the bubble concentration was very low, very large scatterers appeared in some of the images caused probably by impurities (usually air bubbles). Those frames could distort the calculation of the normalised backscatter per bubble. For this reason, those frames were not used in the calculation of normalised backscatter. The effect of this new approach was also assessed.

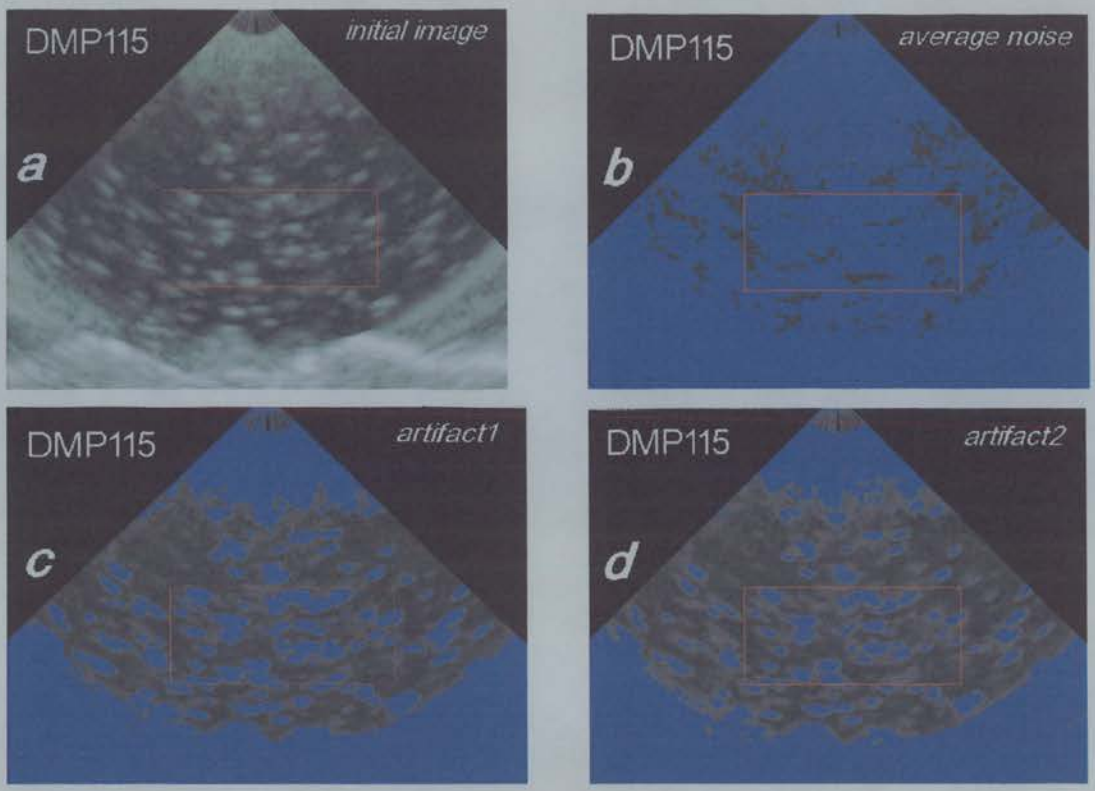

Figure 8.2 a Reconstructed image frame for DMP115. The pixel intensity was calculated for the rectangle ROI (which was also used in the rest of this thesis). **b** Threshold 1 was employed and most of the pixel in the frame became blue. Those pixels had higher amplitude than the threshold and the analysis package would calculate the average pixel intensity for the pixels inside the ROI. The threshold is the square root of the average pixel intensity (of an identical ROI) of a tank filled with sterile water. Similarly in **c** and **d**, where threshold 2 and 3 were used (square root of average pixel intensity of two different artefacts of the tank filled with sterile water). The images were the same frame at 0.58MPa peak negative pressure.

8.3 Results

Figure 8.3 shows reconstructed frames at two different acoustic pressures for DMP115, and Quantison™. The number of scatterers refers to the counts inside the rectangular ROI. The frames were chosen to have number of scatterers close to the average for that acoustic pressure.

The counts of scatterers in the ROI, at different acoustic pressures, is illustrated in Figure 8.4. DMP115 demonstrated a constant number of scatterers at all acoustic pressures, apart from the two lowest ones. Quantison™ did not have bright scatterers at the two lowest pressures, and demonstrated an increasing number of scatterers with the increase of acoustic pressure.

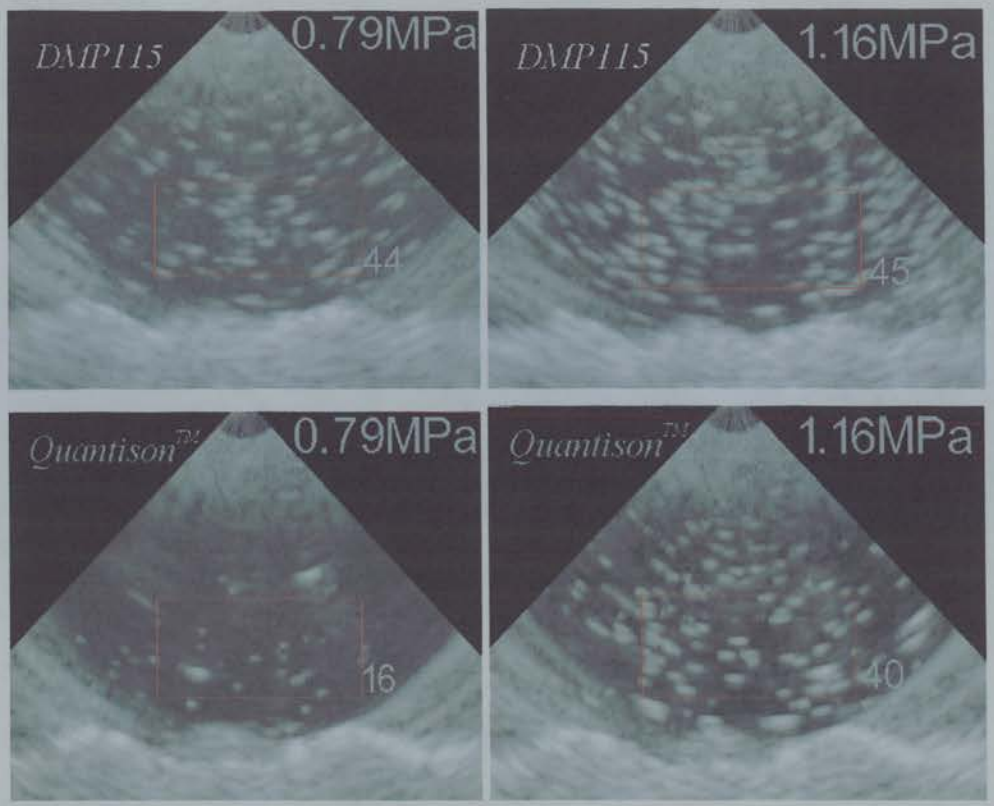

Figure 8.3 Reconstructed frames for scatterer counting. The number of scatterers inside the rectangular region of interest (ROI) is stated in each frame. The particular frames were chosen in order to have numbers of scatterers close to the average for all acquisitions in each peak negative pressure. DMP115 showed a particularly constant number of scatterers at different acoustic pressures, while Quantison™ showed an increasing number of scatterers with increasing acoustic pressure. Note that the number of microbubbles in the solution was 7.5microbubbles/ml for DMP115 (~46microbubbles in the ROI), and 93.75microbubbles/ml for Quantison™ (~580 in the ROI). Note also in 0.79MPa there are two larger scatterers, that are probably air bubbles.

The calculation of the volume of the ROI, allowed an approximate calculation of the concentration of observed scatterers per unit volume. The expected concentration of the introduced contrast was calculated, knowing the concentration of bubbles in the vial given by each manufacturer. Using this number, for the used dilution DMP115 would have 7.5 microbubbles per ml of suspension in the tank, and Quantison™ 93.75. The ratio of the concentration of scatterers (microbubbles that were seen to scatter and accounted for) to the expected concentration of microbubbles was shown versus the acoustic pressure in Figure 8.5a for DMP115 and in Figure 8.5b for Quantison™. The ratio for DMP115 was close to one for most acoustic pressures. This means that all of the bubbles of the agent were observed as scatterers. For Quantison™, not more than 8% of the bubbles were observed as scatterers.

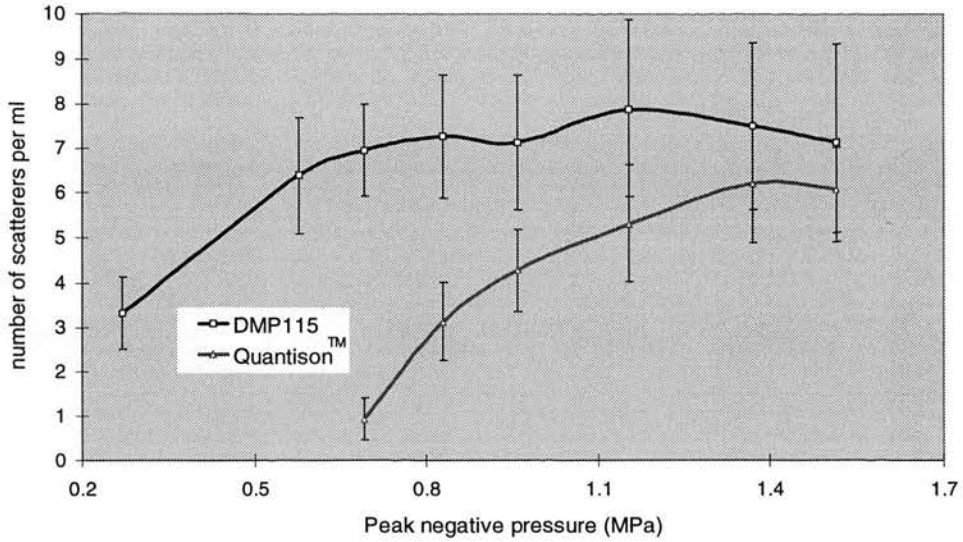

Figure 8.4 Number of scatterers counted in the ROI vs. Peak negative pressure. DMP115 provided considerably constant counts at most acoustic pressures, and only the two lowest acoustic pressures had lower counts. Quantison™ showed an increase of the number of scatterers with the increase of acoustic pressure that seem to settle at the two maximum acoustic pressures.

The calculated normalised backscatter per scatterer was plotted against acoustic pressure in Figure 8.6a for DMP115 and Figure 8.6b for Quantison™. 12 out of 200 frames for DMP115 were considered to have impurities (such as air bubbles shown in Figure 8.3 at 0.79MPa for Quantison™) and therefore they were not used in the calculation of the normalised backscatter per scatterer. For Quantison™ 52 out of 180 frames were considered to have similar problems, which is significantly more than the DMP115 frames. The difference in the gas content of those two agents might explain this occurrence. DMP115 vials contain perfluocarbon, while Quantison™ vials contain air, which might be the reason for the formation of big air-bubbles. The dashed lines were the average normalised backscatter per scatterer for all data, while the solid lines were the average normalised backscatter per scatterer for the data that did not seem to have any impurities.

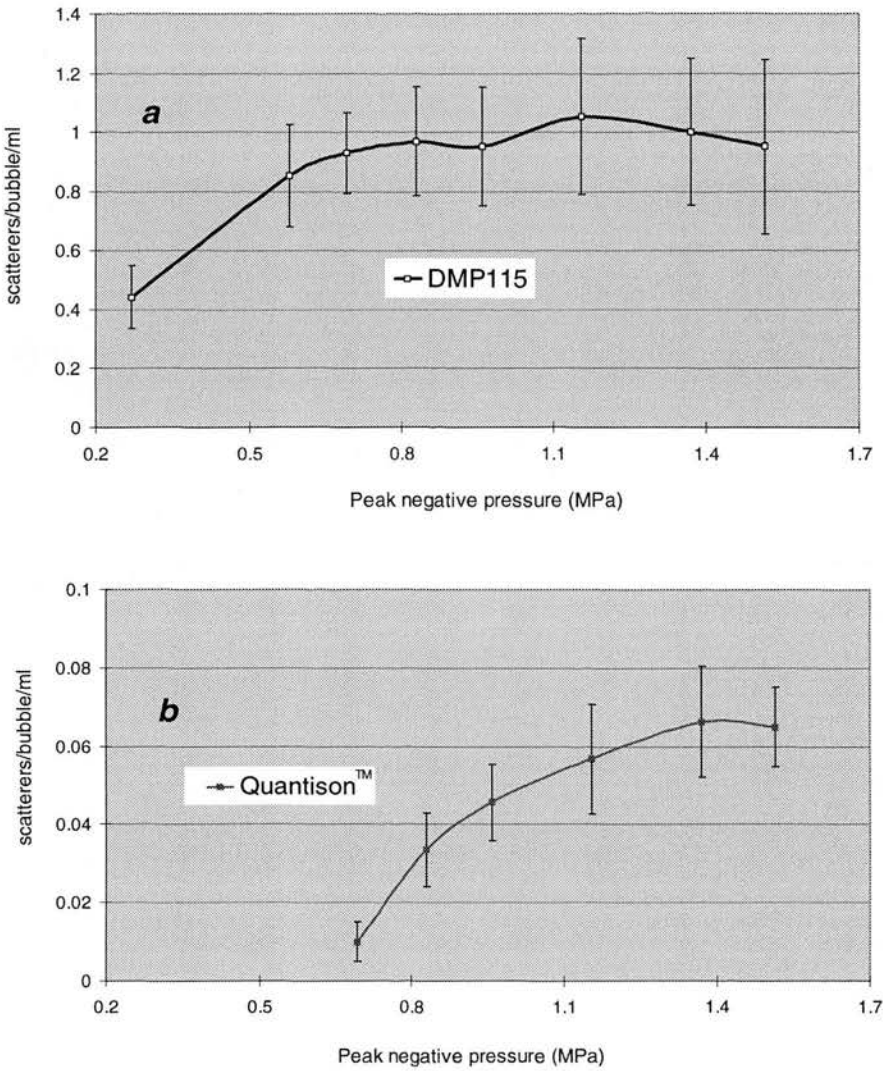

Figure 8.5 The ratio of observed scatterers per unit volume to the concentration of (micro)bubbles is plotted vs peak negative pressure ***a*** for DMP115, and ***b*** for Quantison™. This ratio was close to one for most acoustic pressures for DMP115, while it did not exceed 8% for Quantison™.

The display of error bars in Figure 8.6 would affect its clarity, and therefore the percent standard deviation of the normalised backscatter per scatterer was plotted in Figure 8.7. Dashed lines refer to the calculation that included all the data, and the solid lines refer to the calculation that excluded the data with impurities. The solid lines were definitely at lower values than the dashed ones. DMP115 did not show significant difference since the frames that were found to have impurities were only 6% of the total amount of frames. For Quantison™, the difference between the two curves was greater since the frames with impurities were almost 30% of the total number of frames. The standard deviation seemed to decrease with increasing

acoustic pressure for Quantison™, perhaps because the lower acoustic pressure provided lower number densities of scatterers. DMP115 showed a stable percent standard deviation over the range of acoustic pressures used.

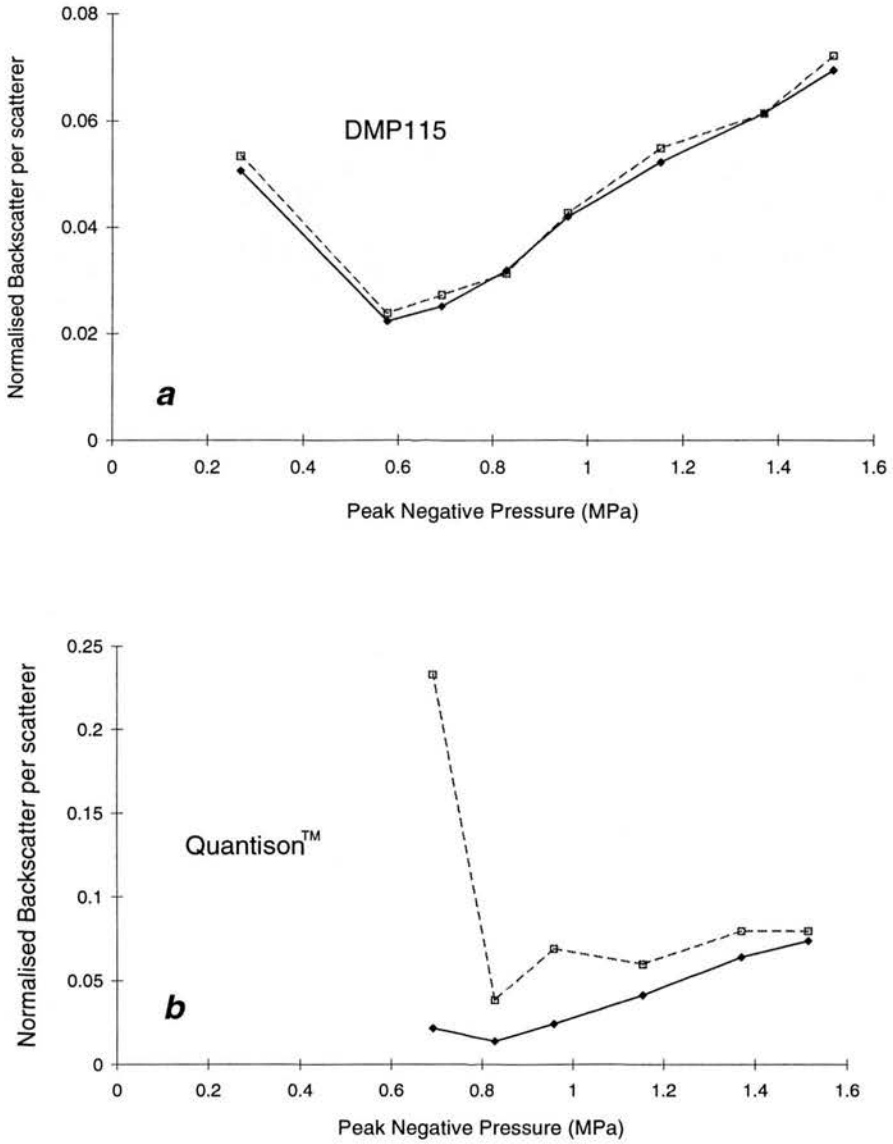

Figure 8.6 Average backscatter per scatterer plotted against peak negative pressure ***a*** DMP115, and ***b*** Quantison™. The dotted line refers to all the data, and the solid line refers to data after rejecting the frames that had impurities. 6% of the frames of the original data were rejected for DMP115, and 29% for Quantison™.

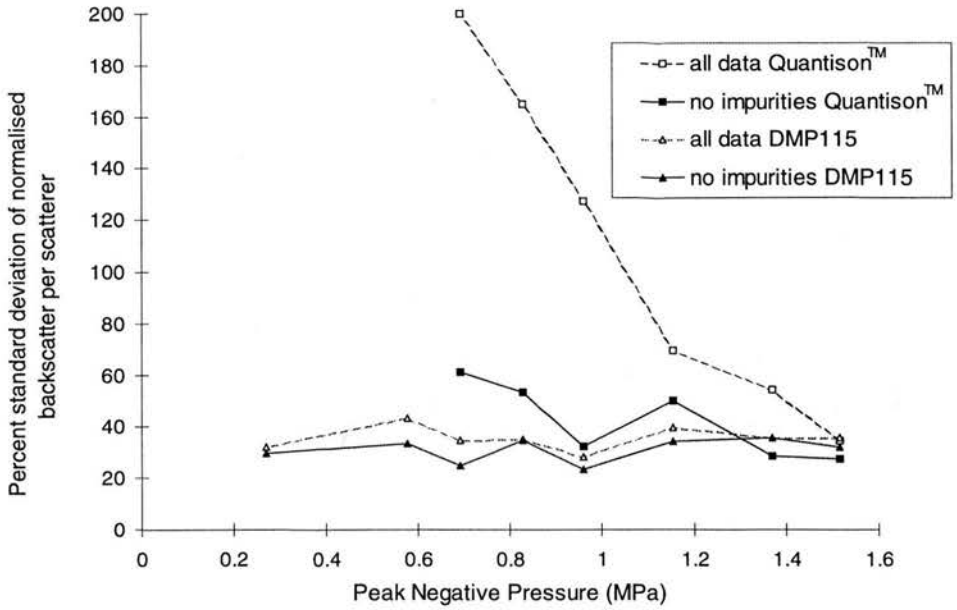

Figure 8.7 Percent standard deviation of the normalised backscatter per scatterer for the original data (dotted lines), and the data without any impurities (solid lines). The small number of rejected frames for DMP115 provided similar standard deviations at both data sets. Quantison™ showed a higher rejection rate, and therefore the deviations showed great improvement for the data without impurities. The decreasing tendency of percent standard deviation with increasing acoustic pressure for Quantison™ was perhaps associated with the increasing numbers of scatterers.

The results produced by using the 4 different thresholds were plotted in Figure 8.8a for DMP115, and Figure 8.8b for Quantison™. All the thresholds provided similar values of normalised backscatter per scatterer. For Quantison™ none of the thresholds produced significantly different values. DMP115 demonstrated a significantly lower level of normalised backscatter per scatterer for threshold 3 when compared with threshold 1 and 2. All the other comparisons demonstrated insignificant differences between them. The calculation of normalised backscatter per scatterer was optimal when threshold 2 was used. At the lowest acoustic pressure used for Quantison™, an elevation of the normalised backscatter per scatterer was observed in Figure 8.8b for threshold 1 and 0. This might be due to the very low count of scatterers (lowest in Figure 8.4), which make the contribution of the background dominant when, using those two thresholds. Figure 8.8 illustrated the insignificant contribution of the background to the vast majority of the calculations. For those reasons threshold 2 was considered optimal for the calculation of normalised backscatter per scatterer.

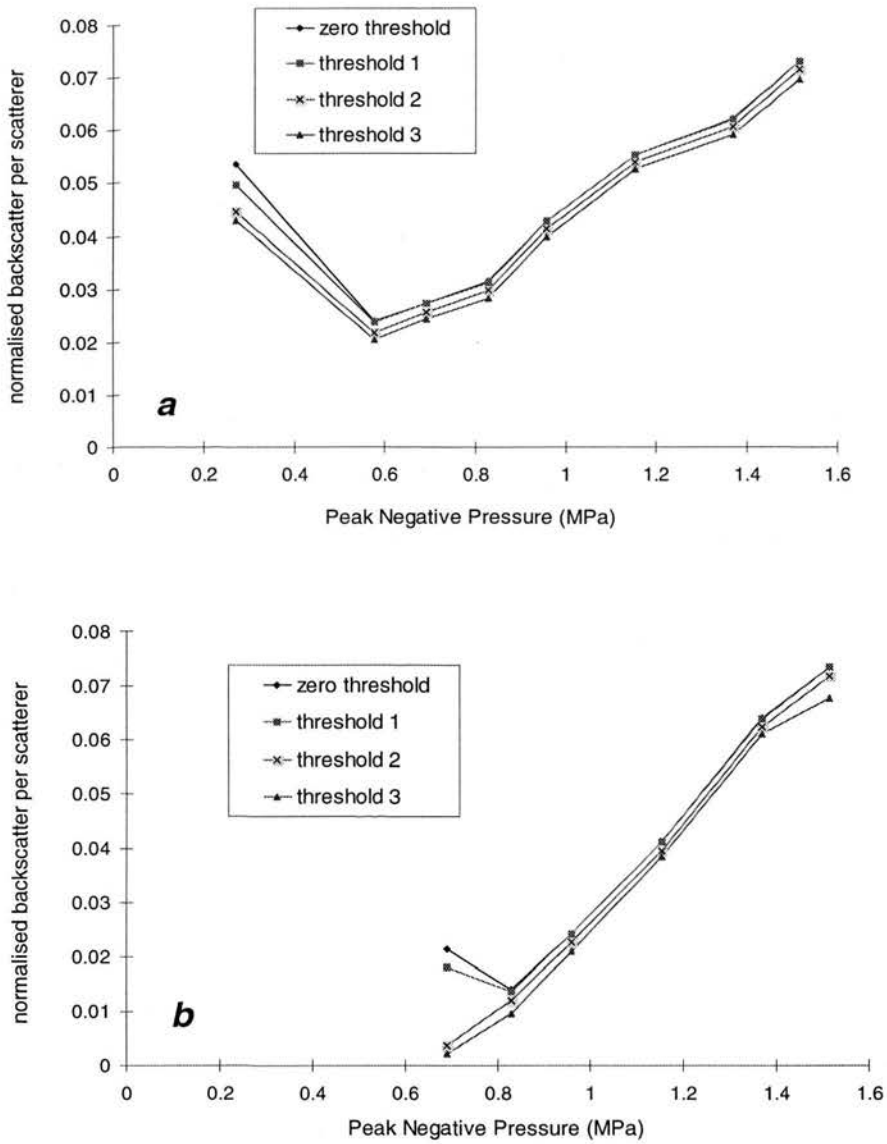

Figure 8.8 Normalised backscatter per scatterer plotted against acoustic pressure. The four threshold levels provided different levels of backscatter. ***a*** DMP115 and, ***b*** Quantison™. The difference between the thresholds was almost insignificant (perhaps with the exception of threshold 3 for DMP115) Threshold 2 was found to be optimal for extracting the normalised backscatter per scatterer.

The result of the previous analysis leads to Figure 8.9. The normalised backscatter per scatterer was plotted against peak negative pressure for the two agents, after the use of threshold 2 and rejecting the frames that had impurities. At low acoustic pressures, DMP115 seemed to have a higher normalised backscatter per scatterer. At high acoustic pressures both agents become almost identical. Both agents have a linearly increasing normalised backscatter with acoustic pressure.

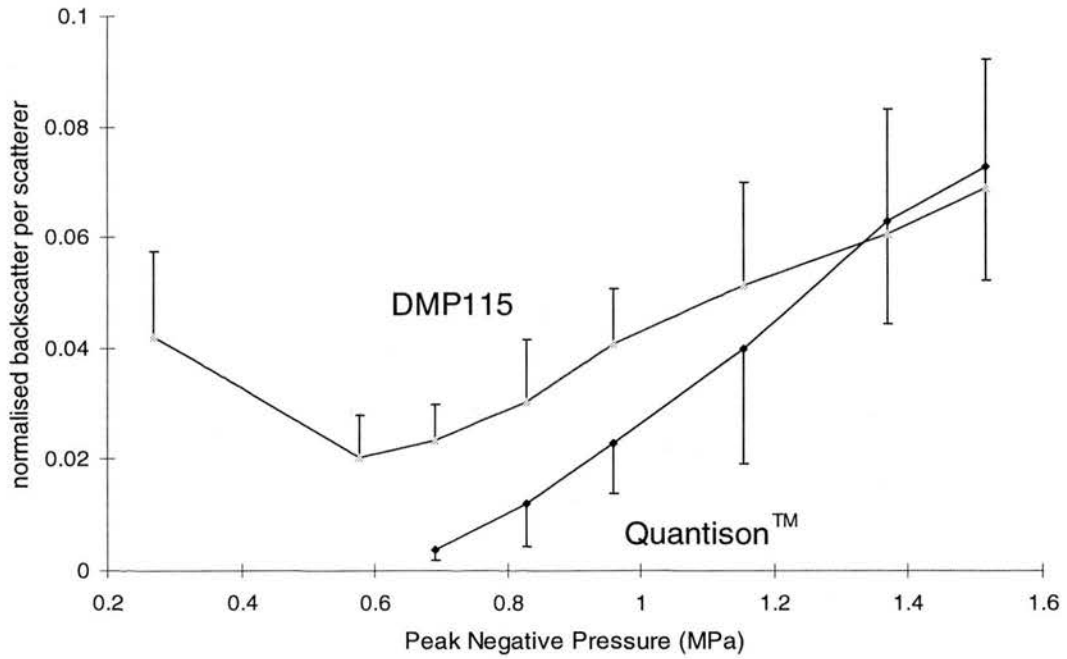

Figure 8.9 Normalised backscatter per scatterer against acoustic pressure. DMP115 showed higher values at low acoustic pressures, which became similar for both agents at high acoustic pressures.

8.4 Discussion

8.4.1 Number of scatterers

There was a large difference in the number of scatterers, counted using the manual technique, between DMP115 and Quantison™. The first agent provided an almost constant number of scatterers at the range of acoustic pressures used, while for Quantison™ scatterers appeared in the image at 0.69MPa peak negative pressure, and showed an increase in number with increasing acoustic pressure. A rough calculation showed that most bubbles were backscattering strongly for DMP115, while a small percentage of the Quantison™ bubbles appeared as scatterers (not more than 8%). It is already known that Quantison™ has a much thicker coating compared with DMP115 (Table 3.1), and that this coating was not destroyed after insonation (Johnson, 1997). This suggested that the gas might leak out of the coating to create a free bubble. The fact that more bubbles did that with increasing acoustic pressure agreed with this explanation, since higher acoustic pressures could cause leakage to bubbles with more robust coating. Furthermore, the creation of free bubbles might be

the case for DMP115 at high acoustic pressures, where the normalised backscatter per scatterer was almost identical to that of Quantison™. Those two agents are different in nature in both gas content and coating material. The similarity of the two agents at these high pressures could suggest that they release similar sized free bubbles.

8.4.2 The measurement of backscatter

It was difficult to provide an accurate assessment of the backscatter intensity of the scatterers. A few problems were tackled, but in a rather empirical way. Impurities, that were probably air bubbles, were difficult to define. The aim was to identify a scattering feature in the image, which was much larger in size than the rest of the scatterers (at least double). The rejection of those images significantly decreased the variability of the measurement of the normalised backscatter per scatterer. The reason for which Quantison™ showed a greater percentage of frames with impurities remained unknown. Whatever the reason, reconstruction of RF data proved crucial to the outcome of this study (by facilitating the detection of artefacts such as air bubbles), and would be perhaps necessary in studies that are intended to measure scattering cross-section.

Another important factor in the assessment of backscatter was the background signals introduced by the set-up. When the threshold was set high, a great proportion of the scatterers were not accounted for in the backscatter signal (Figure 8.2d), and some of the scatterers did not contribute to the calculated average pixel intensity. Note that only the blue regions inside the ROI in Figure 8.2 were included in the assessment of the average pixel intensity. A low threshold in Figure 8.2b would include background artefacts and noise in the calculation of the average pixel intensity, which would provide a distorted calculation of the normalised backscatter per scatterer at the lowest acoustic pressure used for Quantison™ (Figure 8.8b). The choice of threshold 2 proved best when compared visually to the other three. The four thresholds were also statistically compared. In general no significantly different calculations of normalised backscatter was given by any threshold, with the exception of *threshold 3* that gave a significantly lower normalised backscatter calculation for DMP115, and *thresholds 0* and *1* that gave an overestimation of the

normalised backscatter per scatterer for Quantison™ at the lowest peak negative pressure. Consequently *threshold 2* is the most suitable compared to the other three. It is difficult to suggest criteria that would determine the calculation of the threshold. Unfortunately background subtraction can not offer an alternative. Even though the background was at very low levels, the variability of the background echoes amongst different frames was high and the average background intensity could not be used for subtraction.

The procedure employed resulted in calculating the normalised backscatter per scatterer and plotting this against peak negative pressure. Figure 8.10 illustrates the linearity between acoustic pressure and normalised backscatter per scatterer. Hence:

$$N \cong c_X P^- \tag{8.1}$$

where N is the normalised backscatter per scatterer, c_X is the slope provided by the linear fit for the X agent, and P^- is the peak negative pressure.

Assuming the same field for the normalising and the contrast suspensions, and also that the backscatter intensity of the particles in the normalising suspension of Orgasol® (equation 1.1) was approximately equal to the product of their number (in the ROI), their scattering cross-section, and the incident ultrasound intensity. Equation 2.1 combined with equation 1.1 results in:

$$N = \frac{\mathrm{I}_i}{\mathrm{NI}_i} \cong \frac{n_{CA}\sigma_{CA}}{n_{nor}\sigma_{nor}} \tag{8.2}$$

where I_i is the backscatter intensity per scatterer from the contrast agent, NI_i is the backscatter intensity from the normalising suspension, n_{CA} is the number of counted contrast agent scatterers, n_{nor} is the number of scatterers in the normalising suspension, σ_{CA} is the average scattering cross-section of the contrast agent scatterers, and σ_{nor} is the average scattering cross-section of the particles of the normalising suspension. Combining 8.1 and 8.2 the average scattering cross-section of the contrast agent is:

$$\sigma_{CA} \approx \frac{n_{nor}}{n_{CA}} \sigma_{nor} c P^- \tag{8.3}$$

and because n_{nor}, n_{CA}, σ_{nor}, and c are constant, the average scattering cross-section of either contrast agents is proportional to the peak negative pressure.

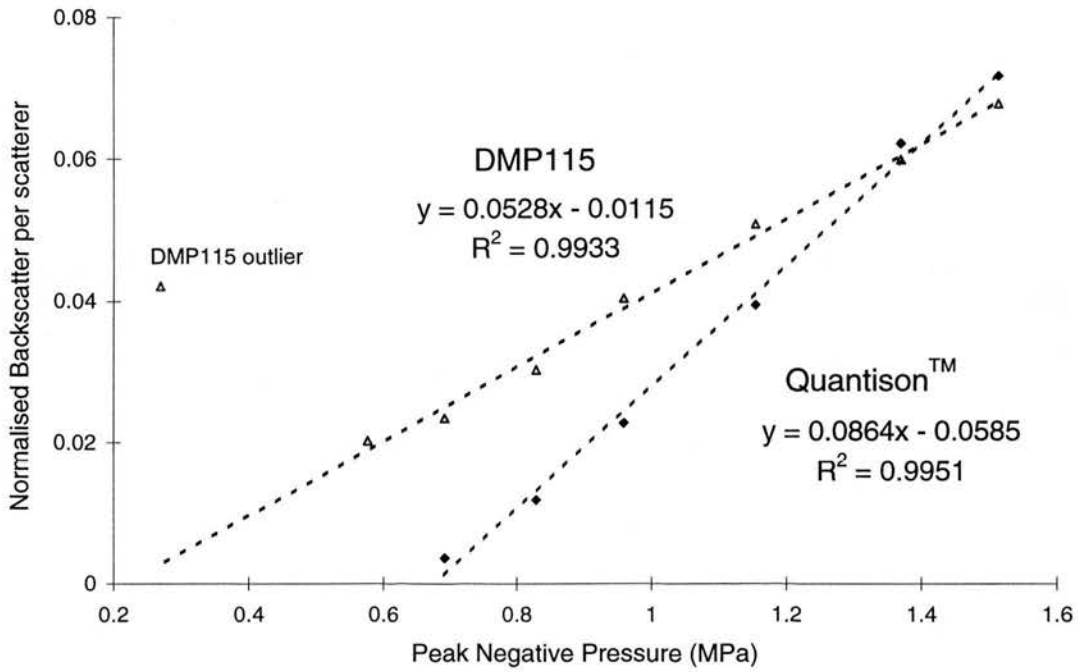

Figure 8.10 The relationship between normalised backscatter per scatterer and acoustic pressure was linear for both DMP115 and Quantison™. An outlier to the linear trend was found at the lowest acoustic pressure for DMP115. There is no indication of an overestimation of the normalised backscatter per scatterer at that pressure, but conclusions for the behaviour of the agent can not be drawn.

DMP115 provided an outlier to the linear trend at the lowest acoustic pressure. The concentration of scatterers was very similar to the concentration of bubbles (Figure 8.5a), which suggests that a systematic error in manually counting the scatterers was negligible at most acoustic pressures. Furthermore, the generally insignificant differences provided by the calculations of normalised backscatter by the different thresholds, strongly suggests that the manual counting of the scatterers was not underestimating their number. Therefore, the counted number of scatterers for the lowest acoustic pressure was correct, and is probably due to the lower sensitivity of the system at that pressure.

It is difficult to draw conclusions for the behaviour of DMP115 at low acoustic pressures, however, since only one point in the plot can not be used to suggest the behaviour of the agent at low acoustic pressures.

8.4.3 Reassessment of previous measurements

The work carried out in this chapter clarified the behaviour of DMP115 and Quantison™, and answered some of the questions raised by previous experiments. chapters 5 showed the differences in the echoes collected by DMP115 and Quantison™, but the outcome of the specific experiments could not suggest the nature of the two agents. Two populations of scatterers were identified for Quantison™. Equation 7.6 did not help in understanding the properties of the agent. Also the behaviour of Figure 6.5b, where an exponential fit was not sufficient to explain the decay of Quantison™, was resolved in this chapter. It became clear that a small percentage of Quantison™ scatterers were free bubbles. Even though these bubbles disappear in one frame, it needed more than one frame of insonation for the ultrasonic beam to cause the release of a free bubble in most bubbles, since not all the contrast in the field of view were bright scatterers. Perhaps the very low backscattering population of bubbles were those that had the gas inside the coating, and their thick coating damped the bubble oscillatory motion.

The suggestions for the behaviour of DMP115, in an effort to explain equation 7.5, proved valid in this chapter. However the specific equation did not predict accurately the backscatter behaviour for individual bubbles.

8.5 Conclusion

The general behaviour of two different contrast agents has been clarified in this chapter. The scattering cross-section of contrast agents is proportional to acoustic pressure, and has been shown to be the case for two agents with different composition. Furthermore, this chapter suggested that above a certain acoustic pressure (around 0.6MPa), formation of free bubbles occurred.

The experiments in this chapter epitomised all the efforts in understanding of the general behaviour of contrast bubbles in a typical diagnostic ultrasound field. Further work is needed in order to assess the optimal imaging conditions for specific contrast agents, and clarify the behaviour of the contrast microbubbles in the ultrasonic field. The next two chapters, attempt at finding these conditions for

DMP115 *in vitro*. An ultrasonic system that would provide a wider variety of beam shapes and settings is introduced. The experiments are expected to improve the current knowledge on the bubble motion.

9 Chapter Nine: A new system for the study of contrast agents

9.1 Introduction

Chapters 7 and 8 demonstrated the general behaviour of two different contrast agents in a diagnostic ultrasound field. However, this information is not adequate to fully describe the behaviour of a contrast bubble in an ultrasound field. Equation 1.3 (p7) describes the scattering cross-section for an ideal gas bubble as a function of the driving frequency. As discussed in the introduction of the thesis there are still several unknown parameters required to build a model that would satisfactorily describe the acoustical behaviour of contrast agent scatterers. Along with technological limitations, the limited amount of scientific studies are the prime reasons for this deficiency in experimental data.

An experimental set-up designed to assess the acoustic properties of contrast agents should ideally provide a wide range of beam settings with respect to frequency (say 0.01-20MHz), acoustic pressure (0.01-3MPa), and pulse length (1-10 cycles). Ideally each could be changed independently. This would allow a rigorous assessment of the acoustical properties of different agents, and consequently specify the settings for optimal imaging. Subsequently the assessment of the fundamental and harmonic components, generated by the microbubble non-linear oscillation and received in the backscatter signal, would provide valuable knowledge on the complexity of the interaction of the microbubbles with the ultrasonic field. Thus it would be possible to assemble a more complete theoretical model which would explain the behaviour of the microbubbles.

Unfortunately modern transducer technology alone provides an obstacle to achieving those goals. The spectral sensitivity of transducers has to date been the biggest problem, and in order to obtain results in the whole scattered spectrum the solution to date has been to use more than one transducer (De Jong et al 1993).

This chapter introduces a system that could stand as a reasonable compromise of the ideal system described above. It is based on an HDI3000 ATL scanner

(Advanced Technology Laboratories, Bothell, WA, USA), which is perhaps amongst the most technologically advanced ultrasound systems and which provides wide and flexible external control of frequency, acoustic pressure and pulse length. In this chapter the experimental set-up is presented, and the next chapter deals with the results using a contrast agent (DMP115).

9.2 Materials and methods

9.2.1 The set-up

Figure 9.1 illustrates the set-up. Various suspensions of particles were insonated using an HDI3000 ATL scanner, which was connected to a PC through its serial port. The tank is described in section 2.2.1.1. The ECG lead was connected to a pulse generator (Phillips PM5705), which was gated using the "timer PC" of the set-up used in previous chapters (Figure 2.1). The pulses generated and transmitted to the ECG lead were 1msec in duration, had 0.5Hz repetition frequency, and 5Volts amplitude. The timer was set to allow only 5 pulses to be transmitted to the ECG lead.

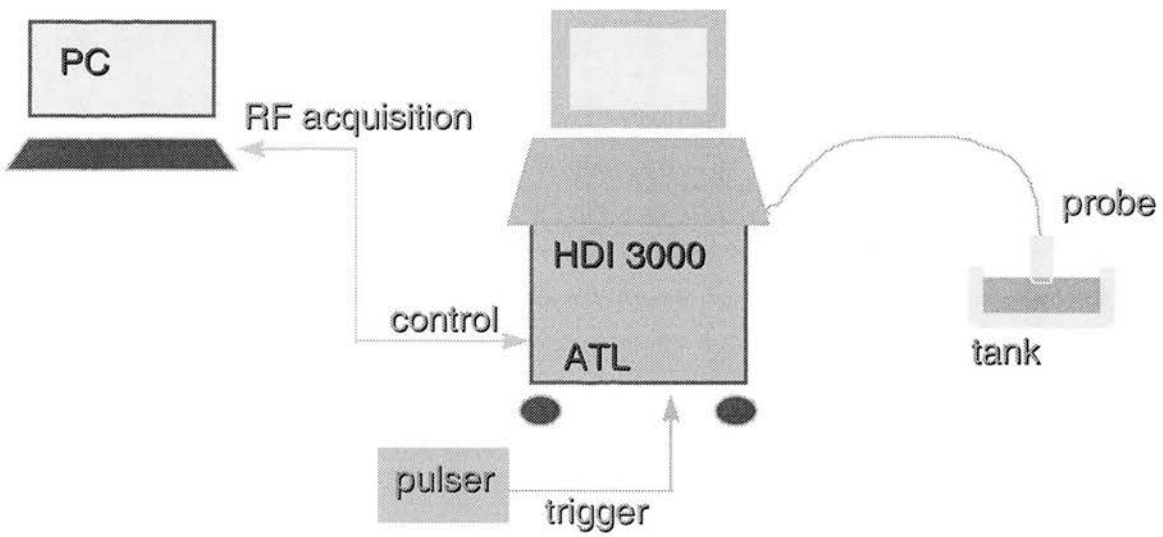

Figure 9.1 The set-up. Suspensions of particles were insonated using an HDI3000 ATL scanner, which was controlled by a PC. A pulse generator was connected to the ECG lead in order to acquire triggered frames. Data were stored in the PC for processing and analysis.

9.2.1.1 The scanner and the controlling set-up

The scanner provided a large range of settings. The transmit frequency for the two phased array probes (P3-2 and P5-3) ranged from 1.17-4.28 MHz, the

mechanical index (MI) from 0.1-0.7 (as displayed on the monitor), and the pulse length from 2-10 cycles. The different ultrasound fields were controlled by the PC, shown in Figure 9.1, using Labview 5.1 graphical programming software (National Instruments, Austin, Texas, USA). The programmes were supplied by ATL and were appropriately modified for the purposes of these experiments. The modifications mainly included the beam forming at different frequencies and pulse lengths. The MI was controlled by the scanner's keyboard. The graphical interface, provided by the controlling software, is shown in Figure 9.2. With this software, as seen in the figure, it was possible to control the frequency, the pulse length, the focal length (in the figure "xmt.zone" is 1 when the focal length is at 4cm), the offset position of the region of interest (in the figure "rf.offset" notes the distance in number of digitised points). The amount of transmitted information was also given (bytes at serial port), as was the full text of the transmitted information displayed in the "output string" box.

The digitisation rate of the scanner was 20MHz, therefore, taking into account the speed of sound in water, the 1024 points shown in Figure 9.2 (rf.offset) were equivalent to 4cm offset depth. The number of data points acquired was 256 for each line, equivalent to 1cm depth. This information was acquired for 96 lines in each frame, which was the preset line density. Therefore the acquired ROI for a frame was 96 lines wide, 1cm long beginning at 4cm from the probe. After freezing the scanner, a buffer would temporarily collect the above data over the last 90 frames.

Calibration of the scanner was performed using a PVDF needle hydrophone with 0.2mm diameter (Precision Acoustics Ltd, England). The sensitivity of the hydrophone, as certified by NPL calibration, varied significantly over the above range of frequencies. The points in Figure 9.3 illustrate the sensitivity certified by the NPL, and a 6^{th} order fit was performed. The equation shown in Figure 9.3 was used to calculate the sensitivity at different frequencies.

The centre frequency and the bandwidth at 6dB down from the peak were measured for all the different ultrasound fields generated by the scanner using a spectrum analyser (TF2370, Marconi Instruments Ltd). All the transmitted beams at different pulse-lengths, acoustic pressures, and transmit frequencies were visually

inspected in the display of the spectrum analyser, and those that did not provide a satisfactory bell shaped spectrum and a distinct centre frequency were not used in the experiments. Figure 9.4 illustrates the bandwidth versus frequency at all different pulse lengths of the beams used in the experimental procedure. These data were input to a statistical programme (similar to Script 6.1 and Script 6.2), and run in the SAS statistical software, in order to model the bandwidth as a function of the frequency and the pulse length. The outcome provided the equation:

$$\mathbf{bw} = 0.072 + 0.969\,\mathbf{f} / \mathbf{c} \qquad (9.1)$$

where **bw** is the bandwidth at 6dB down from the peak amplitude, **f** the centre frequency in MHz, and **c** the number of cycles in a pulse. The regression coefficient was 0.98.

Figure 9.2 Graphical interface of a Labview 5.1 programme, designed to control the HDI3000 beam shape. The control included the frequency, pulse length, focal length (xmt.zone=1 refers to the second focal distance which is 4cm), offset distance of ROI (rf.offset) in number of digitised points. The full text of transmitted information through to the scanner was shown in the "output string" box, while the "bytes at serial port" were also stated.

Figure 9.5 illustrated the calibration of acoustic pressure of the scanner, using this hydrophone, at a 6-cycle pulse length. The peak negative pressure measured at 4.5cm was plotted against frequency. The different graphs showed the calibration at different MIs, ranging from 0.1-0.7. The frequency ranged from 1.17-3.02MHz for

the P3-2 probe, and from 2.75-4.28MHz for the P5-3. The sensitivity peaked at 2.52MHz for the P3-2 probe and at 3.54MHz for the P5-3. The calibration was also performed at the 2, 3, 4, 8, and 10-cycle pulses, which were used in the following experiments.

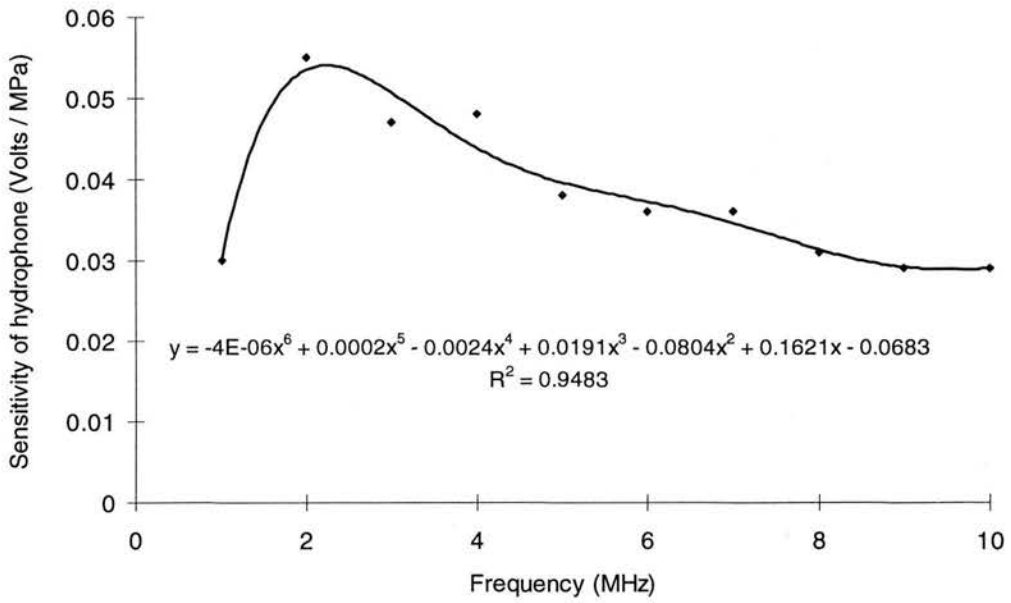

Figure 9.3 Sensitivity of the PVDF (0.2mm) hydrophone (Precision Acoustics, England) in Volts/MPa plotted against frequency. The points in the graph illustrate the calibration of the hydrophone by the National Physical Laboratory. A 6th order fit was performed in order to predict the sensitivity of the hydrophone at any desired frequency.

9.2.1.2 The data acquisition

Data could be acquired from the buffer of the scanner using a Labview programme. A typical interface is shown in Figure 9.6. This programme was also supplied by ATL and modified for the purposes of the experiments, and it was possible to acquire any part of the data available in the buffer. The data and their FFT were displayed in the Labview programme. Recognisable RF patterns and FFT curves facilitated the acquisition. For example signals from single scatterers were expected to be short and separated. The FFT of all signals were expected to have similarities to that of the transmitted pulse, such as bandwidth, as this was specified in the calibration. This way the transmitted beam characteristics were tested. The data were saved in an ASCII format in the hard disc of the PC.

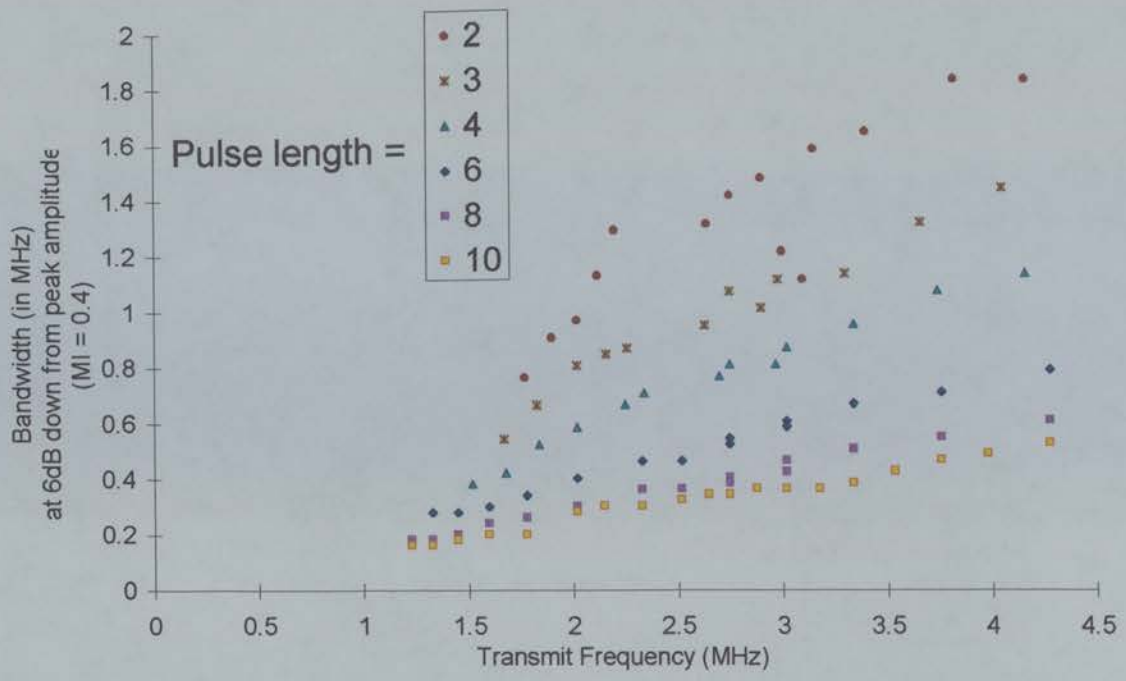

Figure 9.4 The bandwidth of the spectrum of the transmit pulse was measured at 6dB down from peak amplitude for both probes. Here it is plotted versus transmitted frequency at different pulse lengths. Note that increase in frequency or (and) shortening of the pulse increases the bandwidth. A model that describes the bandwidth as a function of the frequency and the pulse length was built from these data and is shown in equation 9.1.

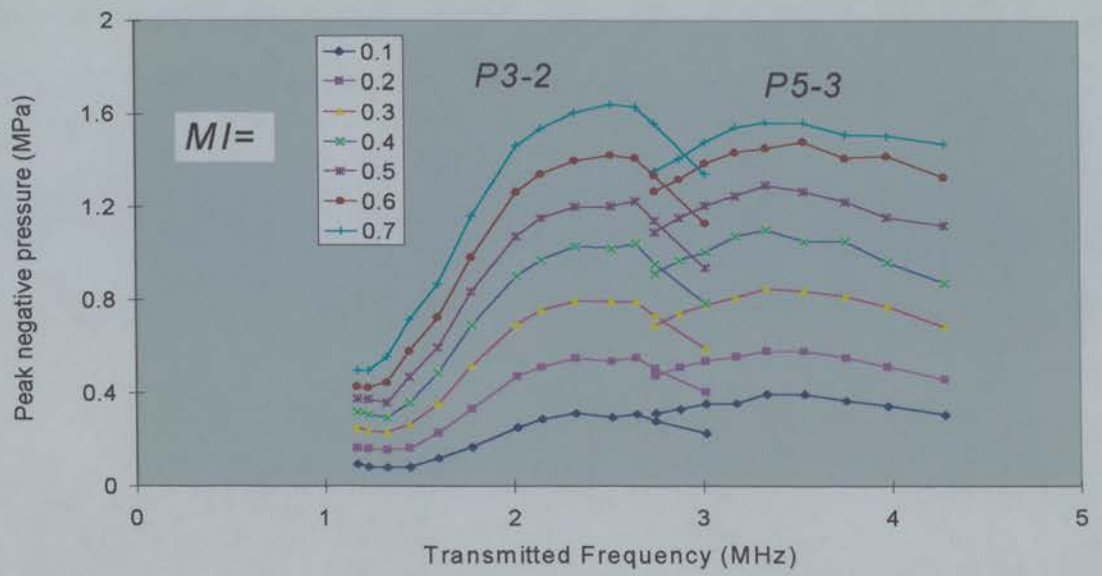

Figure 9.5 Calibration of the HDI3000 using a PVDF needle hydrophone. The pulse length was 6 cycles. The frequency ranged from 1.17-3.02MHz for the P3-2 probe, and from 2.75-4.28MHz for the P5-3 probe. The peak negative pressure, measured at 4.5cm from the probe, was plotted against frequency, and was grouped in the seven different MI settings ranging from 0.1-0.7.

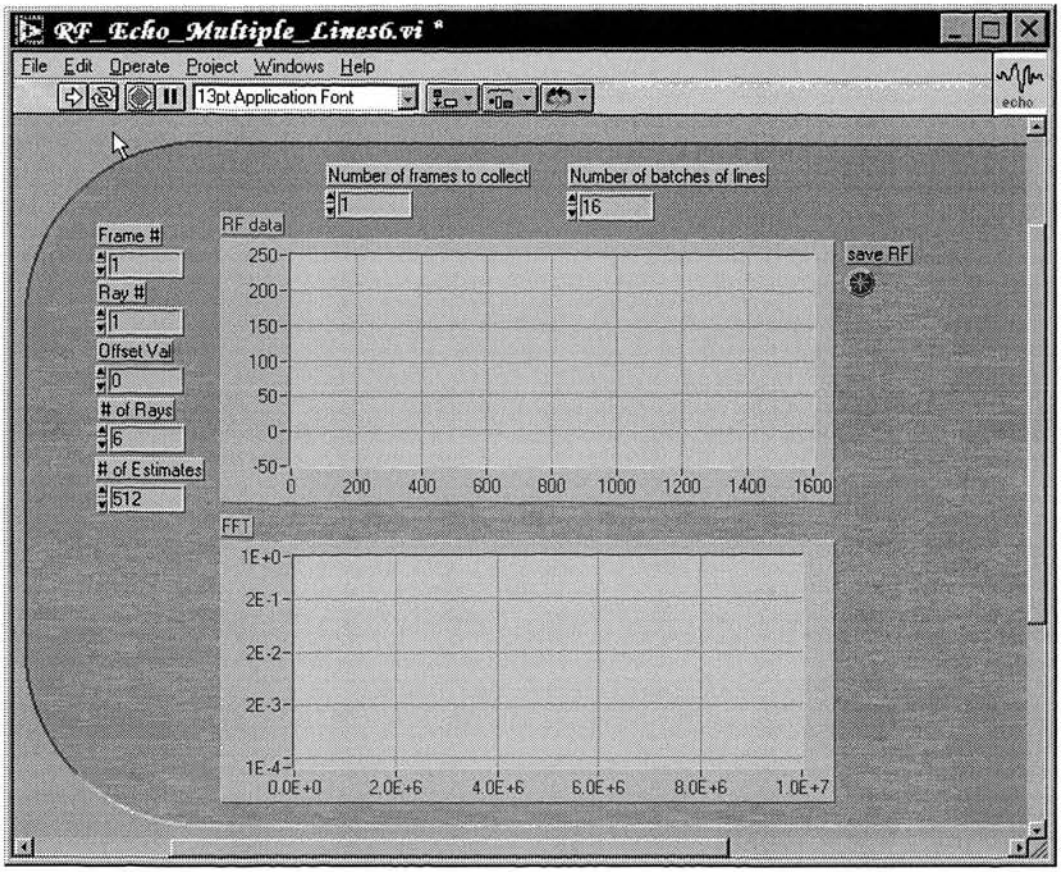

Figure 9.6 Interface of the Labview programme that was used for data acquisition from the scanner. The data, that were temporarily stored in the buffer, were 1cm deep by 96 lines ROIs from the last 90 frames before freezing the scanner. The programme enabled acquisition of any part of this data. The data was also saved in an ascii format at the hard disc of the PC. A display of the data and their FFT was also provided as criteria for correct acquisition.

9.2.2 The data processing

9.2.2.1 Image reconstruction

The collected data were in 96-lines-by-256-points format. The IDL 5.0.2 programming software (Research Systems, Boulder, Colorado, USA) was used to reconstruct the image data. The reconstruction algorithm was developed in the Department of Medical Physics, and was used only for visualisation purposes. A typical image is displayed in Figure 9.11. The image reconstruction was primarily used for visual inspection of the data for artefacts (see last paragraph of section 8.2.3.2).

9.2.2.2 Backscatter calculations

The backscatter information was extracted using a Matlab programme (Appendix A). The data were digitally filtered with an elliptic band-pass filter with the following characteristics:

1) To remove the DC offset (14^{th} order, 0.01dB passband ripple width, 70dB stopband loss), and
2) To filter out the fundamental (7^{th} order, 0.01dB passband ripple width, 70dB stopband loss),
3) To filter out the 2^{nd} harmonic (8^{th} order, 0.01dB passband ripple width, 70dB stopband loss), and
4) To filter out the 3^{rd} harmonic (8^{th} order, 0.01dB passband ripple width, 70dB stopband loss) frequency components of the signal.

The window used for the first filter was from 600kHz-9MHz, while for the rest it was centred at the corresponding frequency and was 1MHz wide. Graphical illustrations of the amplitude response of the above four filters are shown in Figure 9.7 for 2MHz centre frequency of the fundamental. Figure 9.7c was magnified in three different ways to produce Figure 9.8. The passband ripple was approximately 1/1000 of the amplitude response (Figure 9.8a) which, according to the definition of Johnson et al (1980), gave a passband ripple width of 0.009dB. The stopband was set at 70dB down from the passband, which is equal to the 0.32×10^{-3} of the amplitude of the passband. As seen in Figure 9.8b, the stopband amplitude did not exceed the above value. The transition width (distance between stopband and passband in the frequency domain) was not more than 200kHz (Figure 9.8c). Johnson et al (1980) pointed out the superiority of the elliptic filter over all other filters, since it has the shortest transition width for a given order and allowable pass- and stopband deviations. The filters were also tested by processing the results of the following experiments and performed satisfactorily.

After the data have been filtered appropriately, a Hilbert transform is applied. The average square value of the resulting data provides the intensity of the appropriate backscatter component (either the whole RF, or fundamental, 2^{nd}, 3^{rd} harmonics).

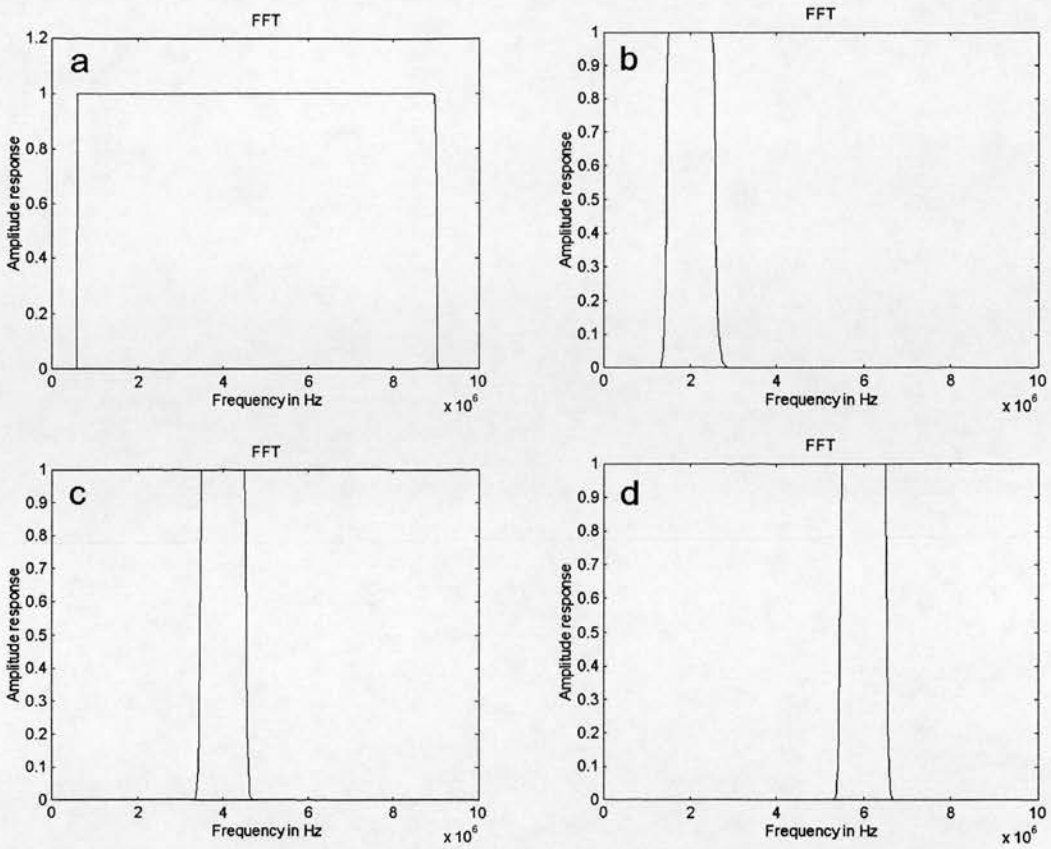

Figure 9.7 Plot of the amplitude of the elliptic bandpass filter for the extraction of the signals at particular frequency windows. ***a*** The passband window was 600kHz-9MHz, and of the order 14. This filter aimed in cancelling out the DC offset, and reducing the noise at high frequencies. ***b*** The passband window is 1MHz centred at the fundamental (also transmitted) frequency (2MHz), and the order was 7. This filter was intended to isolate the fundamental component of the signal. ***c*** the passband was the same as ***b***, but was centred at the 2nd harmonic frequency (twice the value of the fundamental). The order was 8, and was designed to isolate the 2nd harmonic component of the signal. ***d*** Same as ***c***, apart from the centre frequency of the window which was at the 3rd harmonic frequency (three times the value of the fundamental), and was designed to isolate the 3rd harmonic component of the signal. All filters provided a passband ripple of 0.01dB, and a 70dB attenuation for the stopband.

9.2.3 Testing the system

9.2.3.1 Gain linearity assessment

A section of reticulated foam was inserted in the tank with hot water, for degassing purposes. The tank was scanned at 2.15MHz (maximum sensitivity of P3-2 probe) and 2-cycle pulses. The maximum and minimum MI settings were applied. The gain was varied from 5 to 75dB, and data from the ROI described above were collected. The RF average backscatter intensity was calculated and plotted versus the gain (Figure 9.9). It is obvious from the graph that a linear relationship between backscatter intensity and gain existed between 15 and 55dB. 55dB gain was the choice for all the experiments that followed, as it was the maximum applied gain that

would provide linear backscatter intensity for the foam, and the backscatter intensities from the contrast microbubbles were at much lower level of intensity than the foam. Furthermore the materials used (contrast agent, and test materials) provide lower backscatter levels, and the maximum MI was 0.7.

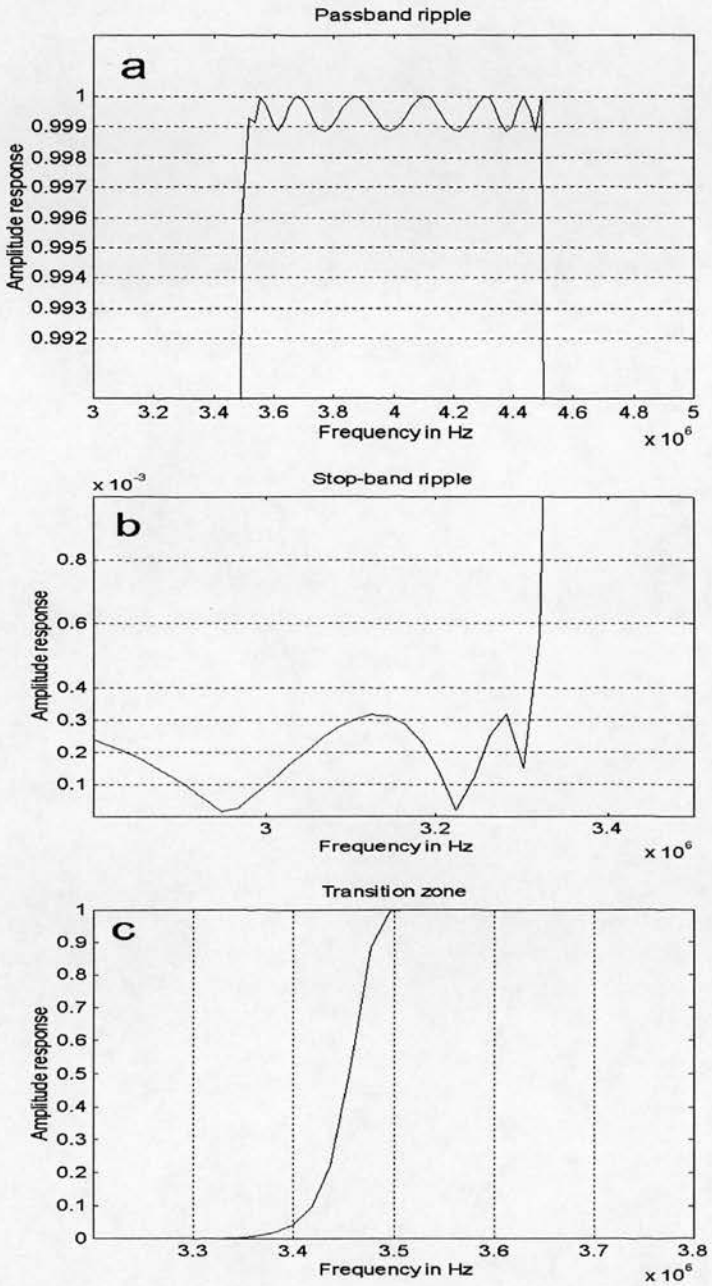

Figure 9.8 Detailed plots of the amplitude response of the filter illustrated in Figure 9.7c. The 2nd harmonic was centred at 4MHz with 1MHz window (3.5-4.5MHz). ***a*** The ripple of the passband was not more than 0.009dB(= $-20\log_{10}(0.9989)$) (passband ripple width as defined by Johnson et al (1980)). ***b*** The stopband amplitude was at 70dB(= $-20\log_{10}(0.32\text{x}10^{-3})$) lower than the passband. ***c*** The transition width (distance between passband and stopband in the frequency domain) was 200kHz. As shown in plot ***b*** the stopband ends around 3.3MHz, and in ***c*** the passband starts at exactly 3.5MHz. The elliptic filter performs better than any other filter (Johnson et al (1980)).

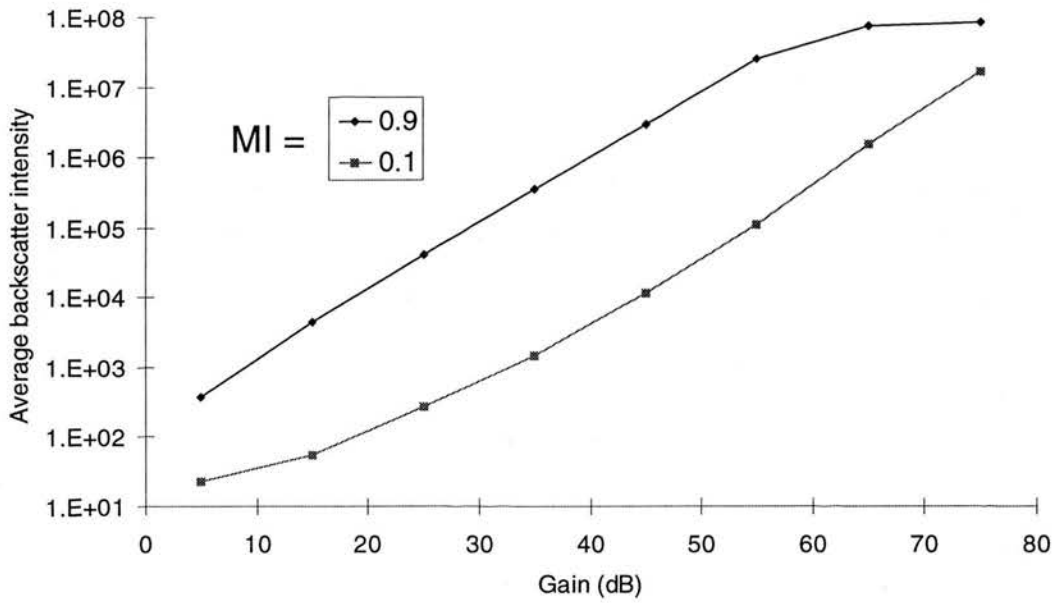

Figure 9.9 Average backscatter intensity of 1cm ROI of reticulated foam plotted against gain (in dB) for two different MI settings (0.1 and 0.9). Both graphs were linear between 15 and 55dB gain.

Reconstructed frames are shown in Figure 9.10 for two different positions of the probe, at 4cm+, and at 5cm from the bottom of the tank.

9.2.4 Imaging materials

Because of the increased control of the ultrasonic beam shape, due to the range of available settings, an extended normalisation approach was essential compared to earlier chapters. In principle, normalisation was previously considered essential in order to a) compensate for the changes in the beam shape (at different acoustic pressures), including those caused by non-linear propagation, and b) provide a comparison with a linearly scattering material of similar (high) particle density and size distribution, that also behaves acoustically in a similar manner to blood. In the last chapter it was shown that the scattering cross-section of two contrast agents increased linearly with acoustic pressure. However this conclusion could only be an approximation, since it was not a direct comparison of individual scatterers of similar size, and therefore did not represent a quantifiable difference in the scattering cross-

section between Orgasol® particles and contrast agent scatterers. The very low echoes scattered from the Orgasol® particles did not allow visualisation of individual scatterers, which meant that those echoes were mostly below the noise level. Therefore, in order to produce a suspension that would be effective for normalisation purposes, it was necessary to use a high concentration of particles.

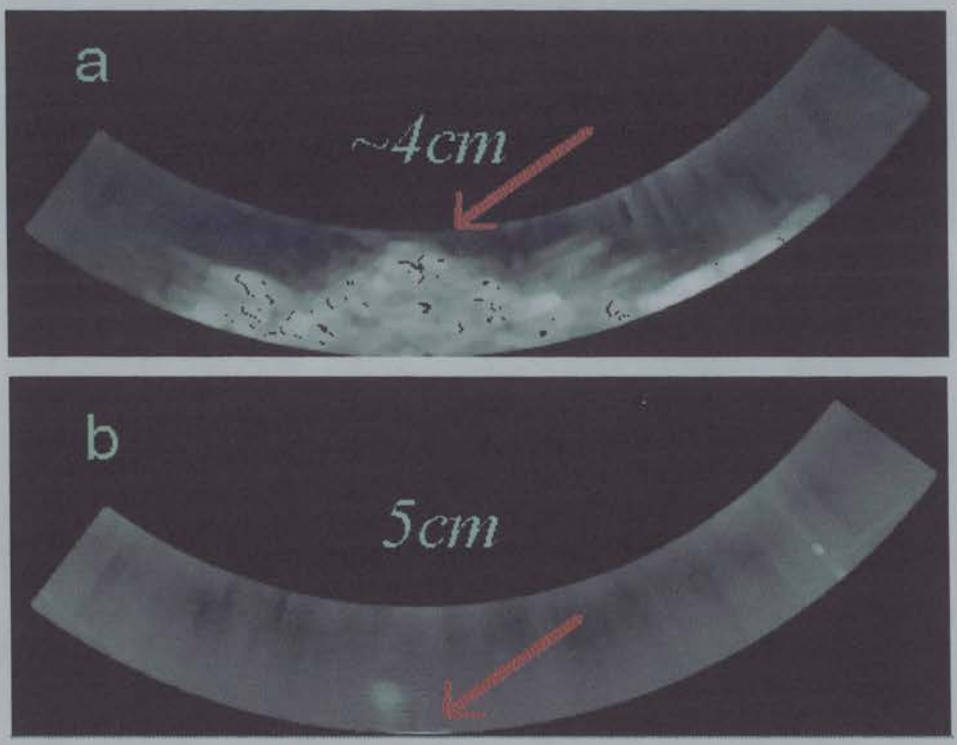

Figure 9.10 Reconstructed RF frames at 2.02MHz in order to verify the offset distance was as specified by the rf.offset variable in the interface of the controlling software of Figure 9.2 (4cm), as well as the depth of the ROI (1cm). **a** The bottom of the tank was at a little more than 4cm away from the probe, and the tip of a notch in the bottom of the tank is at the top of the ROI pointed with the arrow. **b** The bottom of the tank is placed 5cm away from the probe, and can just be seen at the bottom of the ROI (arrow). The DC offset was not filtered out before reconstruction.

In the experiment described in the next chapter an effective comparison between solid particles, and contrast agent scatterers was attempted. Unfortunately it was impossible to find particles of similar size distribution to intravenous contrast agents, which would scatter echoes above the noise level of this system. The proposed solution was to use particles of a larger size, which still could be considered as Rayleigh scatterers. Hence their sizes were much smaller than a wavelength. Although, the comparison between such particles and contrast agent bubbles was not ideal, it was nevertheless a direct one between two Rayleigh scatterers.

Two materials were used as test materials: a) The suspension of Orgasol® scatterers of 5μm diameter, as defined in paragraph 2.2.2.2, and b) A gelatine suspension of Eccosphere®. Eccosphere® (New Metals & Chemicals Ltd, Essex, UK) are hollow glass spheres of a median size of 55μm. 0.5gr of Eccosphere® was added to one litre of sterile water and was left for a day. 200ml of that suspension was added to 200ml boiling water and two sachets of cooking gelatine. Note that this gelatine was the only anechoic one amongst those that were tested (Agar, thrombin, etc). The resulting suspension was stirred for 30min, introduced in the tank using a test sieve of 90μm aperture (model 200sbw.090, Endecotts Ltd, London, UK), which would consequently remove the larger spheres from the suspension. The suspension was then stored in a refrigerator for at least six hours. The Eccospheres® have a 0.2gr/ml particle density and therefore float in water, which made the suspensions extremely difficult to reproduce. The gelatine suspension was sufficiently stable for over a week, by means of normalised backscatter, sufficient time to acquire all the measurements. The concentration of particles was unknown, but the objective was (a) to have a concentration that would make individual particles distinguishable in an ultrasound scan, and (b) to have a stable gelatine suspension during the course of all the measurements were fulfilled. These particles were the smallest size that would scatter sufficient signals to be detected by the scanner at all different combinations of settings.

RF frames were acquired for both materials at all the settings using the P3-2 probe, and for the suspension of Orgasol also using the P5-3 probe. Frames at a particular setting were also acquired every 30min, to assess possible time variations of backscatter of either material.

9.3 Results

An example of a reconstructed frame for both materials is displayed in Figure 9.11. The transmit frequency was 2.02MHz, the pulse contained 2 cycles, and the MI was set at 0.5. The data were filtered using a passband window 600kHz-9MHz, and then were reconstructed. The Orgasol® scatterers seem more uniformly suspended than the Eccospheres® suspension. The latter were more diluted, and individual

scatterers can possibly be identified in the figure. Reconstruction of the RF was performed for each acquisition in order to find artefacts. Only two frames of the Orgasol® suspension were found to have a high backscattering spot like an air bubble, and were not used in the analysis.

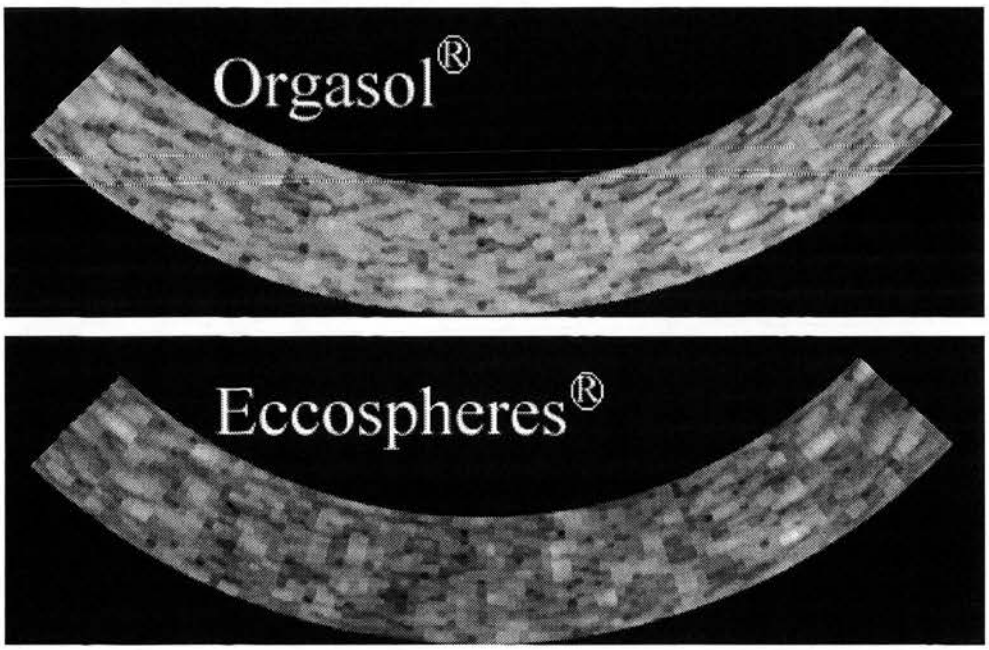

Figure 9.11 Image reconstructed RF data for the water suspension of Orgasol®, and the gelatine suspension of Eccospheres®. Frequency=2MHz, MI=0.5, and cycles=2.

Examples of calculated average backscatter intensity from the ROI are shown in Figure 9.12 for the Orgasol® suspension, and in Figure 9.13 for the Eccosphere® suspension. The acquisitions were made using an 8-cycle pulse. Figures (a) referred to MI=0.1 and figures (b) to MI=0.6. The complete signal, fundamental, 2nd harmonic, and 3rd harmonic backscatter intensities were plotted versus frequency. In the case of the 2nd and 3rd harmonics the points are plotted only if a visible peak occurs at that particular frequency in the corresponding FFT plots. 3rd harmonic signals were not apparent at MI=0.1 in either material. Note that each point refers only to one acquisition. Even though the data were plotted on a logarithmic backscatter intensity scale, it is noticeable that the variability was, at first glance, relatively low. All the plotted lines demonstrated spectral patterns with very low variability. The spectral patterns of the fundamental intensities (and obviously the whole RF) for example of both materials, resembled those of the calibration shown in Figure 9.5 (the peak negative pressures were displayed in a linear scale). The lowest

values of 2nd and 3rd harmonic intensities, in these figures, were just above the noise level of the two probes.

The range of acoustic pressures displayed a very low variation amongst different pulse lengths (<5%). Also the transmit frequencies were very similar at all the different pulse length settings. For 4 or more cycle pulses the frequency range (centre frequency of the pulse) was identical for all pulse lengths. This range narrowed for pulse lengths shorter than 4 cycles long (about 0.5MHz for 2-cycle pulses). Therefore, at a specific pulse length the calculation of the average backscatter intensity (of the fundamental frequency component of the backscatter signals) would represent an estimation of the level of backscatter, and could be used for comparison between different pulse lengths. These values were plotted in Figure 9.14 versus pulse length, as well as those that were compensated for the time variability of the suspension (see last paragraph of section 9.2.4). Figure 9.14a refers to the Orgasol® suspension and Figure 9.14b to the Eccosphere® suspension. A calculation of normalised intensities with the square of the peak negative pressure was also included in this plot (for both variability compensated and non-compensated data) in order to compensate for the spectral sensitivity of the transducers. A squared amplitude value has a linear relationship with an intensity value, and the latter was shown to be linear with the backscatter of similar suspensions (Figure 2.4).

As shown in Figure 9.14, the small time variability of both materials was compensated effectively, and the backscatter level of both materials displayed a linear relationship between the backscatter intensity and the pulse length with very high regression coefficients, which was expected for linear scatterers. The increase in pulse length increases proportionally with the intensity of the transmitted pulse. Therefore the echoes, scattered from linear scatterers, should be proportional to their increase of intensity. Normalising the average values of intensity with the square of peak negative pressure was equivalent to normalising with the transmitted intensity, and showed that the true variability of the data was very low. The regression coefficient of the linear fit was greater than 0.99 for both materials. For the rest of the chapter the backscatter intensity of both materials refers to the compensated for time variability backscatter intensity.

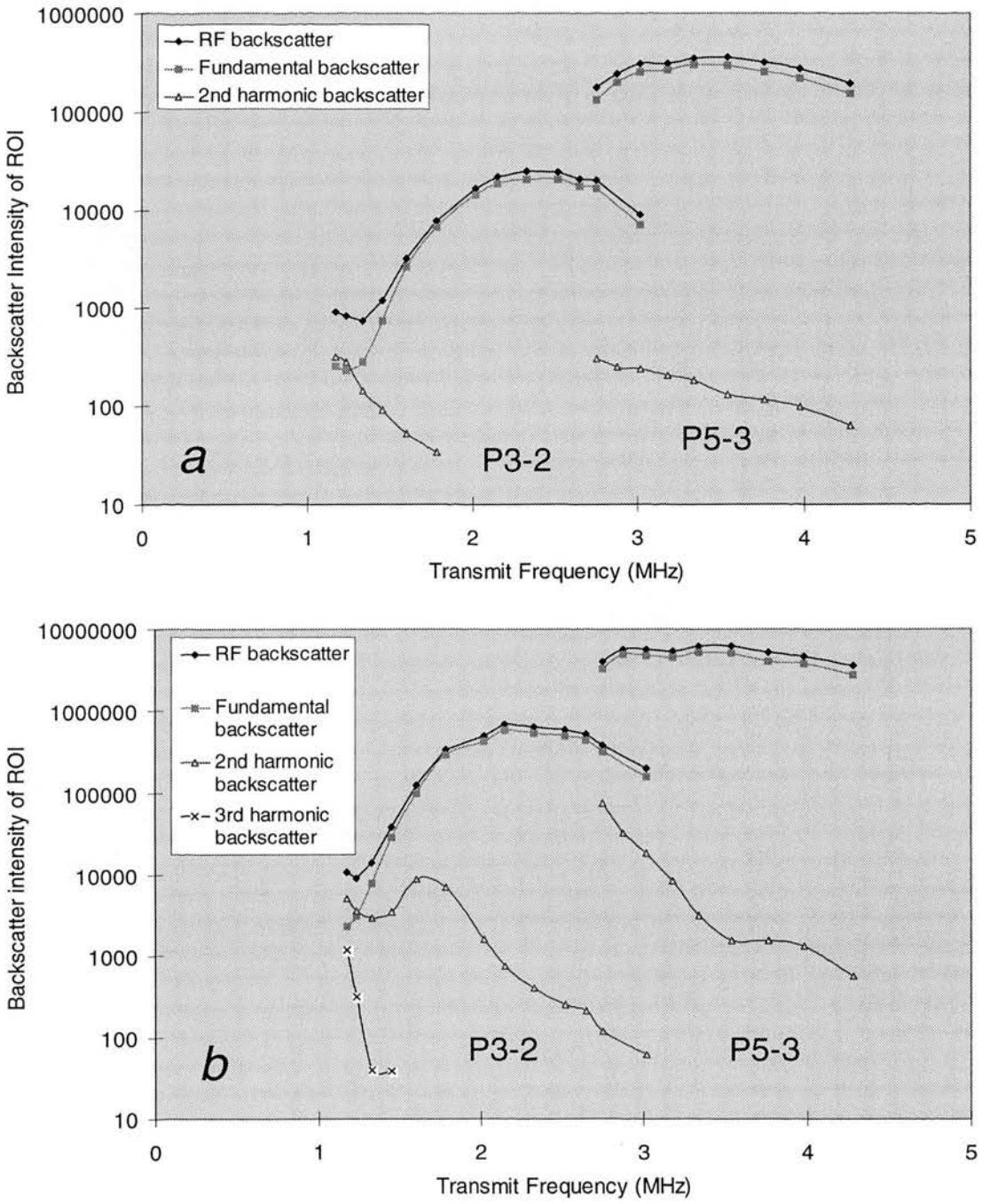

Figure 9.12 Backscatter intensity of the whole RF, fundamental, 2nd, and 3rd harmonic components versus frequency for the Orgasol® suspension. Points were displayed when visually distinct peaks were witnessed when the whole signal was plotted in the frequency domain. The transmitted pulse was an 8-cycle one, and the MI was (***a***) 0.1, and (***b***) 0.6.

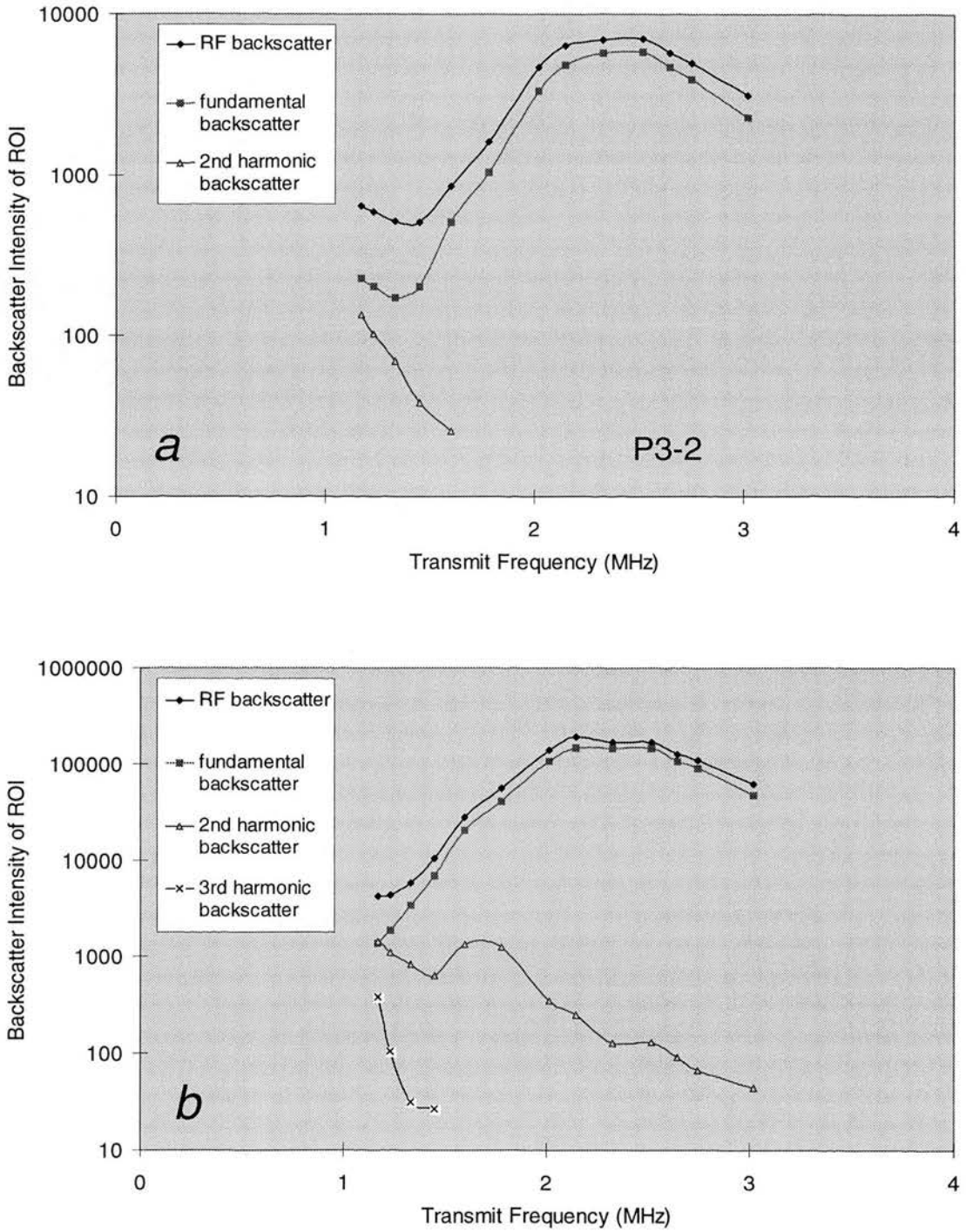

Figure 9.13 Backscatter intensity of the whole RF, fundamental, 2nd, and 3rd harmonic components versus frequency for the Eccosphere® suspension. Points were displayed when distinct peaks were witnessed when the whole signal was plotted in the frequency domain. The transmitted pulse was an 8-cycle one, and the MI was (***a***) 0.1, and (***b***) 0.6.

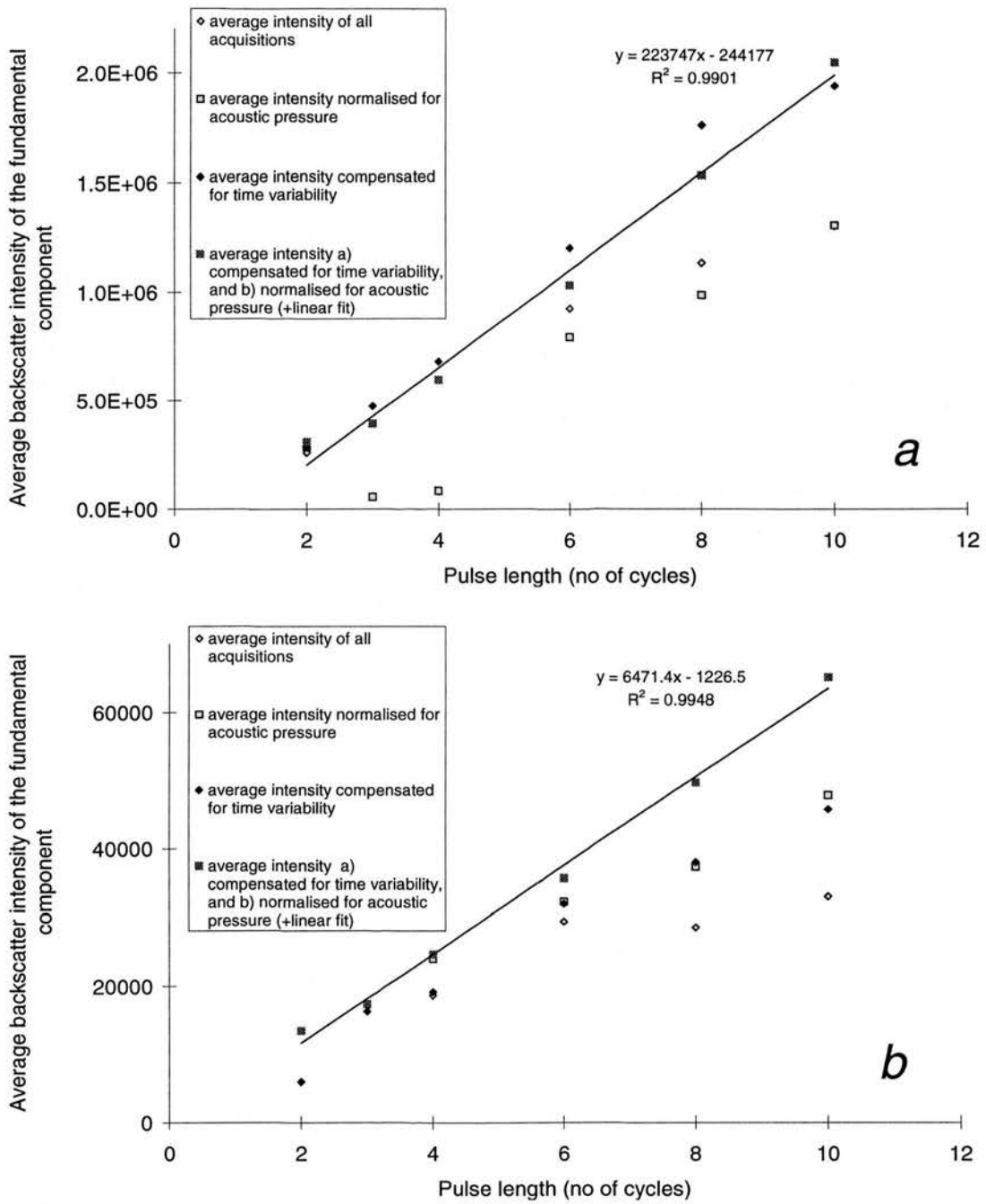

Figure 9.14 Average backscatter intensity versus pulse length. Four different calculations of intensity were displayed for comparison. The measured one, one which compensated for the time variability of the suspensions, one which normalised for the intensity of the transmitted pulse, and one which both compensated and normalised. The latter showed a near perfect linear relationship between backscatter intensity and pulse length for both the Orgasol® (***a***) and Eccosphere® (***b***) suspensions.

The FFT of the echoes showed that above 6-cycle pulses, the bandwidth was suitably small for extracting individual spectral components from those signals. This agreed with the calibration (Figure 9.4). The fundamental and harmonic components

were clearly separated, and also the transmit frequency could be approximately considered as a single frequency, instead of a range of frequencies that centre at the transmit frequency value. The ratio of backscatter intensity to the number of cycles was plotted versus peak negative pressure in Figure 9.15a for the P5-3 probe, and in Figure 9.15b for the P3-2 probe, for the Orgasol® suspension. The figures contain scattered data plots categorised in terms of frequency. Power fits showed high regression coefficients at a 2nd degree relationship between backscatter intensity and peak negative pressure which was an expected result, and agreed with Figure 2.4. The trends provided a higher regression coefficient for the P5-3 probe. The results for the P3-2 probe were similar for the Eccosphere® suspension.

The increase in the number of cycles in each pulse was responsible for the linear increase of backscatter intensity, because it provided a linear increase in the transmitted intensity. In a similar manner, an increase of frequency gives a linear decrease on the backscatter intensity. Increase in frequency means an inversely proportional decrease of the wavelength, which causes a linear decrease of transmitted intensity due to the reduction of the length of the pulse. It is therefore expected that by increasing the frequency, an inversely proportional decrease in the transmitted intensity occurs. Likewise, the intensity of the scattered echoes will also decrease in the same manner. The backscatter intensity was normalised for those two parameters, as well as the peak negative pressure.

$$\mathbf{nB = B * f / c * p^2} \qquad (9.2)$$

where **nB** was the normalised backscatter intensity, **B** the backscatter intensity, **f** the transmit frequency in MHz, **c** the number of cycles in a pulse, and **p** the peak negative pressure in MPa. Note that the above normalisation did not resemble the one proposed in equation 2.1 (p23). The normalised backscatter intensity was plotted versus transmit frequency in Figure 9.16 for different transmitted peak negative pressures (probe P3-2). The figures for both materials reveal a pattern similar to that of the sensitivity of the probe shown in Figure 9.5, as well as a slight increase of the normalised backscatter with peak negative pressure. However, the Eccosphere® suspension (Figure 9.16a) showed a very small variability within each frequency, i.e. the **nB** at each frequency did not vary much for different acoustic pressure and pulse

lengths. This low variability was not seen in the Orgasol® suspension in Figure 9.16b apart from the 3 lowest transmit frequencies.

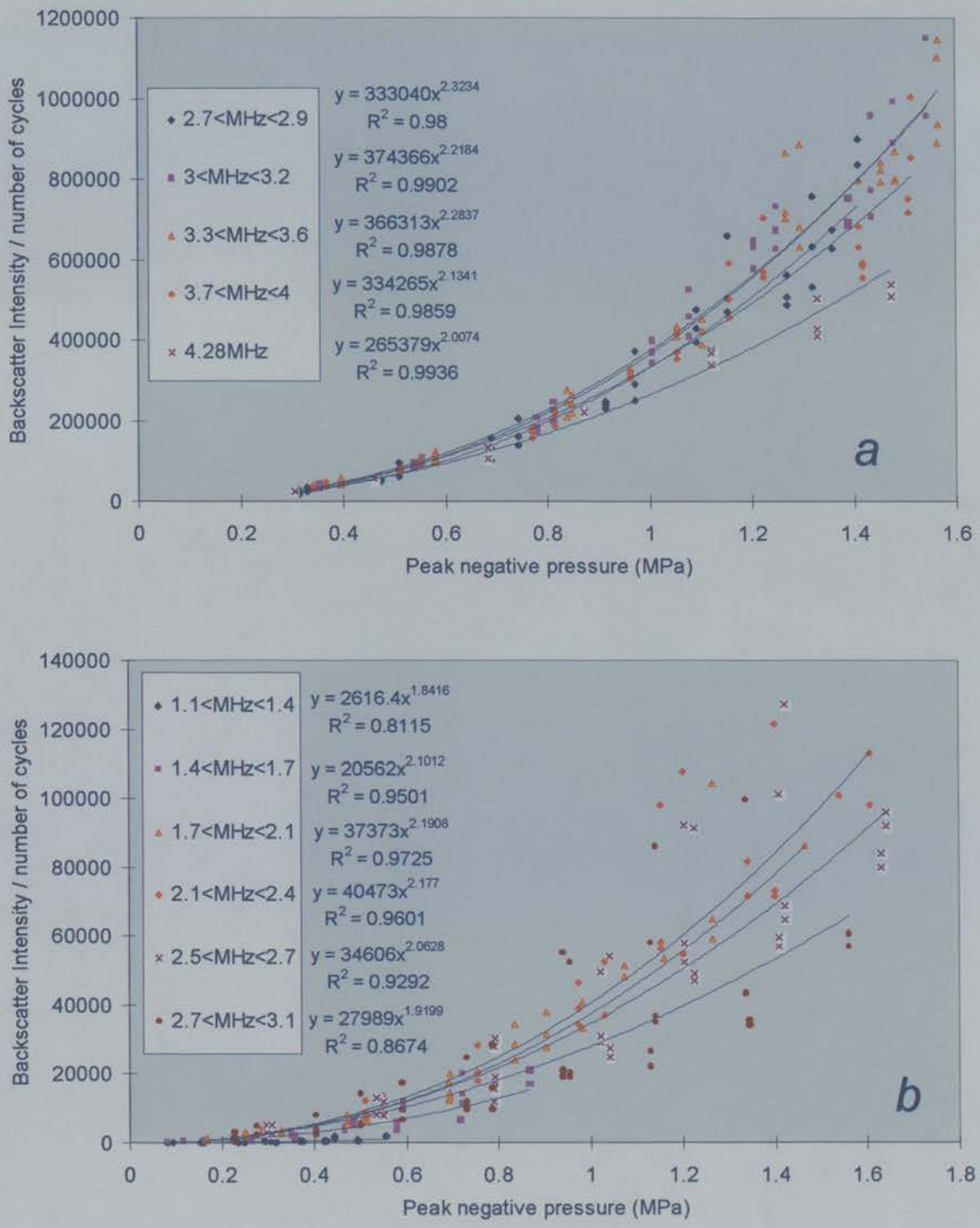

Figure 9.15 Ratio of backscatter intensity to pulse length plotted versus peak negative pressure (for pulse length > 6 cycles) for the suspension of Orgasol®. **a** probe P5-3, and **b** P3-2. Note that the relationship between the ratio and the peak negative pressure tended to be of a power of 2, with particularly high regression coefficients.

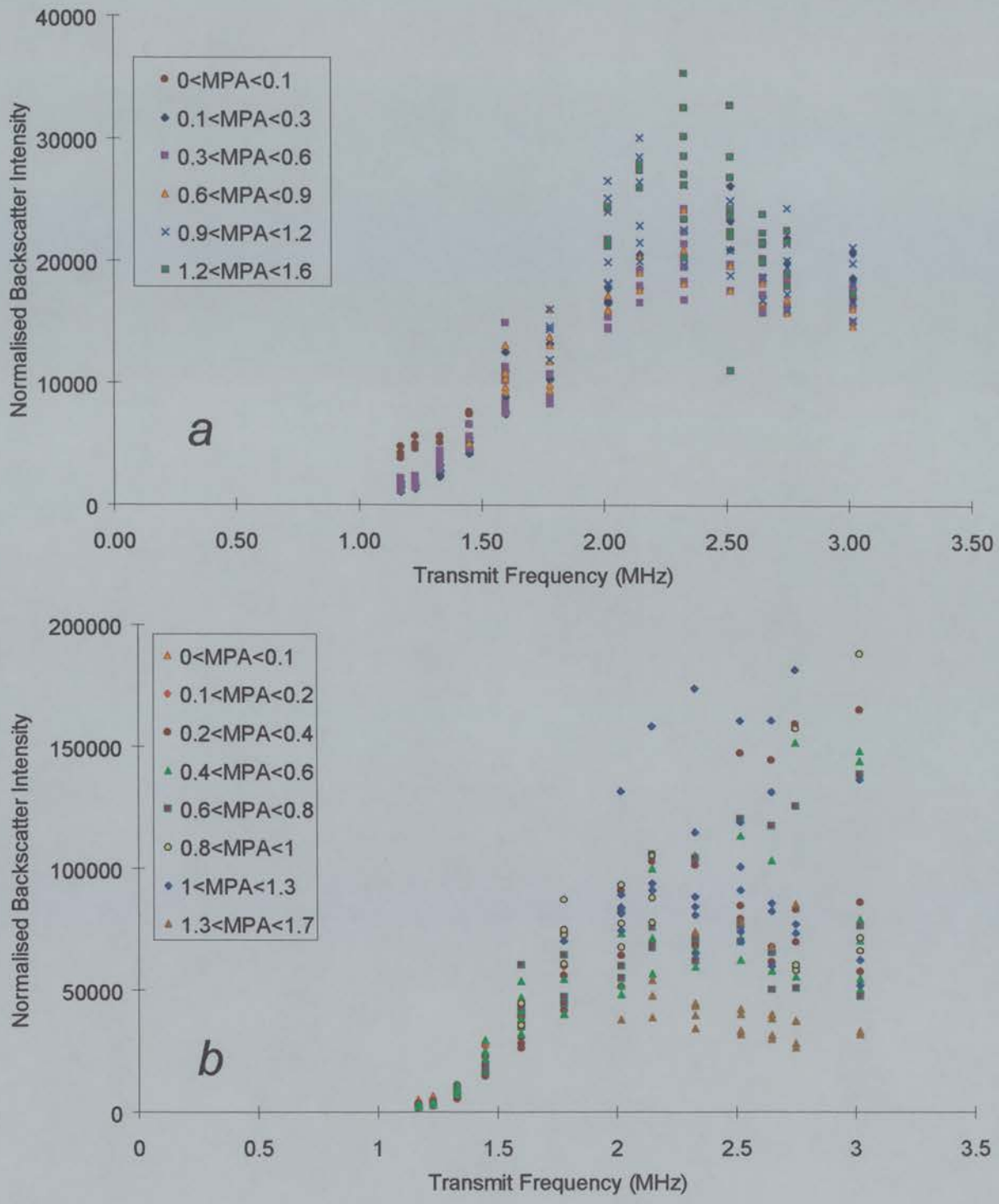

Figure 9.16 Normalised backscatter intensity for the Eccosphere® (a) and Orgasol® (b) suspensions, as compensated by equation 9.2, versus transmit frequency. Note that the pattern of the spectral sensitivity of the probe was preserved, if we compare this plot with Figure 9.5.

9.4 Discussion

This chapter presented an advanced version of an experimental ultrasonic system with expanded capabilities, compared to the one used in the previous chapters. The wide range of settings needed a more elaborate calibration, an expanded analysis tool, in addition to a better characterisation of the reference materials that will be used in the next chapter. An overall assessment of the system and its limitations will be part of the discussion in the next chapter, when a contrast agent will be investigated.

A second harmonic could be detected for the highest transmit frequency of this system. In Figure 9.12b and in Figure 9.13b the second harmonic was detected at 6MHz for the P3-2 probe, and at 8MHz for the P5-3 probe (note that those figures were plotted versus transmit frequency). Third harmonic signals were isolated which denotes the high sensitivity of the system.

The approach employed in these experiments was to perform one acquisition at each setting, and not to repeat acquisitions. It was expected that the wide range of settings would provide a quantitatively useful summary of the properties of the materials used. Figure 9.12, Figure 9.13 and Figure 9.14 further display the low variability of the data. The data points (resulting from single acquisitions) followed specific patterns, as discussed in the results' section, and this applies to all the data for both materials.

With the help of the calibration, the backscatter intensity was normalised by means of equation 9.29.29.29.2. A dependency of the intensity on the 4^{th} power of frequency, which is typical of Rayleigh scatterers (Morse and Ingard, 1968) should then be expected in Figure 9.16 from both scatterer suspensions. Chen and Zagzebski (1996) measured a $\mathbf{f^{3.8\pm0.1}}$ frequency dependence of 42μm Sephadex spheres below 5MHz. After using a 90μm pore sieve to insert the gelatine suspension of Eccosphere® into the tank, it was expected that the mean size of the particles would be lower than the initial 55μm. A high order relationship between normalised backscatter and frequency occurred up to around 2MHz, but above that frequency a different behaviour was observed similar perhaps to the sensitivity spectrum of Fig. 2. This illustrates that there are several parameters which could not be fully

compensated. Figure 9.16a showed that the normalisation, despite failing to normalise (hence show the scattering properties of the material) for different frequencies, it was effective within most frequencies for the Eccosphere® suspension. There is a noticeable difference on the scatter of the data between the Eccosphere® and the Orgasol® suspensions. The Orgasol® normalised data demonstrated a higher variability at each frequency compared to the Eccosphere®. Therefore equation 9.2 worked pretty well in normalising for the beam shape at each frequency for most frequencies separately for the latter suspension, and was unable to compensate for the variation of beam shape perhaps amongst the different transmit frequencies. It is strongly suggested that the variability of response amongst different settings is caused primarily by the change of beam shape at different frequencies. This conclusion was drawn by graphical information displayed by the Eccosphere® suspension. The Orgasol® suspension did not provide good compensation of settings by means of equation 9.2 within each frequency. It is speculated that the intensity dependence of a linear scatterer on pulse length, frequency, and acoustic pressure exists only if the number density of scatterers is low and they do not interfere.

It was difficult to assess the parameters that affect the backscatter intensity values at different settings. The use of all the acquisitions of both materials, for normalising contrast backscatter is expected to fully compensate for all the different aspects of the field. It was shown in this chapter that this would be very difficult to achieve otherwise by doing a very detailed calibration.

9.5 Conclusion

A new system for the investigation of contrast agents was presented and evaluated in this chapter. It provided a wide range of settings, transmit pulses between 2-10 cycles, a frequency range 1-4.5MHz transmit and 1-8MHz receipt, and acoustic pressure 0.08-2MPa. This allowed the extraction of the fundamental, 2nd and 3rd harmonic components of the signal. Two scattering suspensions were presented, which are going to be used to normalise the echoes from contrast agent suspensions. It was very difficult, to characterise those materials, and to assess their behaviour in the acoustic field. This proved that in order to extract useful information from the

contrast echoes, normalisation should be performed with the assistance of the above two materials, which would compensate for all variations of the ultrasonic field at different settings.

10 Chapter Ten: Study of DMP115

10.1 Introduction

The last chapter described a powerful *in vitro* set-up for the characterisation of contrast agents. Table 10.1 lists the in-vitro investigations by other workers performed with contrast agents together with the settings used in each experiment. It is evident that the system described in the previous chapter provided the widest range for each individual beam parameter (frequency, acoustic pressure, pulse length).

The aims of the system were to: 1) assess the value of a detailed in-vitro investigation of the physical properties of a contrast agent, 2) assess the requirements for the system used for such an investigation, 3) contribute towards the assessment of the optimal settings for contrast imaging, and 4) learn more about the physical properties of contrast agents. The contrast agent used to perform the study reported in this chapter was DMP115.

10.2 Materials and methods

10.2.1 Imaging protocol

The system was presented, calibrated, and tested in the previous chapter. The full range of settings is used in the experiments of the present chapter. The contrast agent used was DMP115. 7μl of the agent was inserted in 100ml of sterile water and mixed using a magnetic stirrer. 100μl of that suspension was introduced in the tank, which contained 300ml of sterile water. The concentration of the agent in the tank (10^9 bubbles/ml in the vial) was calculated to approximately 23 bubbles/ml of suspension in the tank. Note the difference compared to the concentration used in chapter 8 which was 7.5 bubbles/ml. The concentration here was specified using the same criterion as in chapter 8, i.e. on the basis of distinguishing individual contrast agent scatterers. It can be speculated that the scanner used in this present study (HDI3000, ATL), being newer and more technologically advanced, it would provide with a thinner beam slice than that of the previous scanner (UM9, ATL). The

suspension was stirred for 30sec, and the first triggered frame was captured and stored in the PC (Figure 9.1).

Table 10.1 *Papers in-vitro investigation of contrast agents*

Author	*Transmit frequency (MHz)*	*acoustic pressure (kPa)*	*pulse length (no of cycles)*	*Contrast agent*	*Format of results*
De Jong 1992	1, 2.25, 3.5, 5, 7.5	- (1)	1	Albunex	a
Schrope 1992	2.5, 5	36	cw	Levovist	f, h
Schneider 1992	2.25, 7.5	- (1)	1	Polymeric	rf
De Jong 1993	1, 2.25, 5, 10	- (1)	1	Albunex	rf
Schrope 1993	2.25, 5	20	cw	Levovist	f, h
De Jong 1994	1, 2	25, 50	3	Albunex	f, h
Chang 1996	1.5-5 (0.5 step)	10-80	cw	Albunex, FSO69	f, h
Krishna 1997	1, 2, 4, 5	0-1400	10	Albunex, FSO69	f, h
Wei 1997	2.7, 5.5, 7.5	1000, 700	1	Albunex, FSO69	f, h
Wu 1998	2.5	1000	1	Albunex	a, v
Moran 1998	~4	1400	1	Quantison™ Myomap™	rf
Morgan 1998	2.4, 5, 6	60-3200	1, >6	Albunex, FSO69, MP1950	f, h
Frinking 1998	2, 5, 10	50, 100	1	Quantison™, Myomap™, Albunex	rf, h, a
Marsh 1998	- (bd)	- (1)	square	Albunex	
Dayton 1999	0.5, 2.25, 5.6	120-3200	1, >6	Albunex, Optison, MP1950	f, h
Frinking 1999	0.5, 1	100, 1600	10	Quantison™	f, h
Krishna 1999	2	50-300	5, 10	Optison	h, s

The acoustic pressures that are not stated give the number of different acoustic pressures in brackets. (cw) stands for continuous wave transmission. (bd) stands for broadband transmission. Abbreviations for the format of results: (rf) for radiofrequency, (f) for fundamental, (h) for 2nd harmonic, (s) for subharmonic, (a) for attenuation, (v) for phase velocity. The settings refer to all the range used in each study, but does not imply that these

fully overlap. Usually a very small overlap between settings, for example the range of frequencies and acoustic pressures, occurred.

10.2.2 Analysis of data

Image reconstruction was performed using the IDL software described in the previous chapter. Visualisation of all data was necessary in order to search for artefacts that would corrupt of the results of these experiments.

After acquisition the RF data from each frame were signal processed, as described in the previous chapter, by means of an elliptic filter to extract the fundamental, 2nd or 3rd harmonic components, or simply to reject the DC offset and extract the whole RF signal. A Hilbert transform was performed after separation of the target component (for example 2nd harmonic), and the average backscatter intensity was calculated for the specific component. The ratio of the intensities of contrast to the reference material (suspension of Orgasol® or the gelatine suspension of Eccospheres®) formed the (2nd harmonic) component's normalised backscatter. Figure 10.1 illustrates the fundamental and 2nd harmonic normalised backscatter in the frequency domain. The data were acquired at the maximum MI (0.7), 1.45MHz transmit frequency, and a pulse length of 8 cycles. The filter for both frequencies provided a 1 MHz passband. The fundamental component was centred on 1.45MHz, and the harmonic component at 2.9MHz. The backscatter intensity of the fundamental frequency component for DMP115 was equivalent to the area with margins under the DMP115 FFT curve, the 0.95 and 1.95MHz gridlines, and the frequency axis (the light grey and black area centred on 1.45MHz). The backscatter intensity of the fundamental frequency component for the suspension of Eccospheres® was equivalent to the area under the Eccospheres® FFT curve, the 0.95 and 1.95MHz gridlines, and the frequency axis (the black area centred on 1.45MHz). The ratio of the two intensities gives the fundamental normalised backscatter intensity. Likewise, the 2nd harmonic component of the backscatter intensity of DMP115 was the light grey area centred on 2.9MHz. For the Eccospheres®, the 2nd harmonic was the black area centred on the same frequency. The ratio of these two intensities gives the 2nd harmonic normalised backscatter intensity.

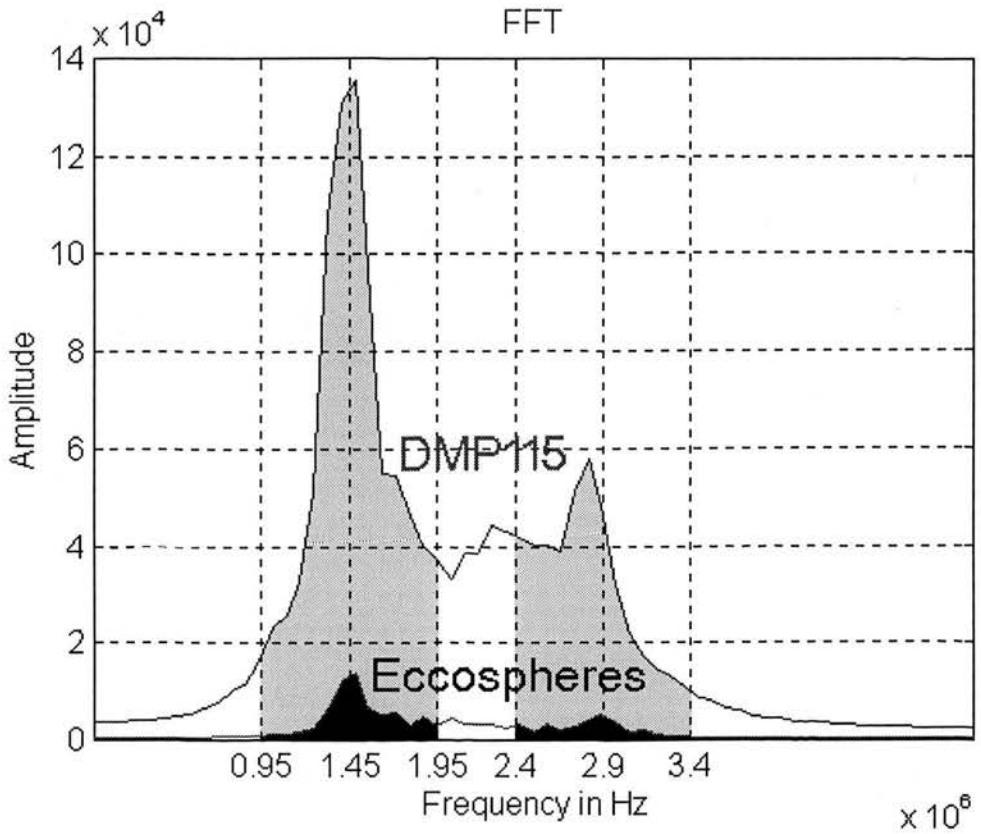

Figure 10.1 Amplitude of the signal of the contrast agent DMP115, and the suspension of Eccospheres® in the frequency domain. The principle of the calculation of normalised backscatter at different parts of the spectrum is illustrated. Acquisition was performed MI = 0.7, 1.45MHz transmit frequency, and 8-cycle pulse. The filter for both fundamental and 2nd harmonic frequencies provided a 1 MHz passband. The fundamental component was centred at 1.45MHz, and the harmonic component at 2.9MHz. The backscatter intensity of the component of the fundamental frequency for DMP115 was equivalent to the light grey and black area centred at 1.45MHz. The backscatter intensity of the component of the fundamental frequency for the suspension of Eccospheres® was equivalent to only the black area centred at 1.45MHz. The ratio of the two intensities gives the fundamental normalised backscatter intensity. Likewise, the 2nd harmonic component of the backscatter intensity of DMP115 was the light grey and the black areas centred at 2.9MHz, and for the Eccospheres® only the black area centred at the same frequency. The ratio of those two intensities gives the 2nd harmonic normalised backscatter intensity.

Note that if we assume that:

$$I_{DMP115} = I_{DMP115}^{(1)} + I_{DMP115}^{(2)} + I_{DMP115}^{(3)} + \ldots \quad (10.1)$$

where I_{DMP115}, $I_{DMP115}^{(1)}$, $I_{DMP115}^{(2)}$, and $I_{DMP115}^{(3)}$ are the overall backscatter intensity and the individual intensities of the fundamental, 2nd and 3rd harmonic respectively for DMP115, and also:

$$I_{ECCO} = I_{ECCO}^{(1)} + I_{ECCO}^{(2)} + I_{ECCO}^{(3)} + \ldots \quad (10.2)$$

where I_{ECCO}, $I_{ECCO}^{(1)}$, $I_{ECCO}^{(2)}$, and $I_{ECCO}^{(3)}$ are the overall backscatter intensity and the individual intensities of the fundamental, 2nd and 3rd harmonic respectively for the suspension of Eccospheres®, it is evident that:

$$\frac{I_{DMP115}}{I_{ECCO}} \neq \frac{I_{DMP115}^{(1)}}{I_{ECCO}^{(1)}} + \frac{I_{DMP115}^{(2)}}{I_{ECCO}^{(2)}} + \frac{I_{DMP115}^{(3)}}{I_{ECCO}^{(3)}} + \ldots \qquad (10.3)$$

This means that the sum of the normalised backscatter of each component need not necessarily be equal to the normalised backscatter of the whole signal.

Hence the normalised backscatter of different spectral parts of the signal were the physical quantities used to assess the enhancement of the agent with respect to a reference material. In this instance, the Orgasol® suspension of scatterers (a material acoustically very similar to human blood), was used as reference material.

10.3 Results

10.3.1 Images

Image reconstruction for the acquisition at 1.17MHz transmit frequency, 8-cycle pulse length, and 0.426MPa peak negative pressure, was performed for the whole RF signal (600kHz-9MHz), and for the fundamental, 2nd and 3rd harmonic frequency components of the signal. These images are displayed in Figure 10.2. Also in Figure 10.2, the average amplitude, over the ROI, is plotted in the frequency domain. The different spectral regions are shaded to show the spectral content of each of the reconstructed images. Since the transmit frequency was at its minimum value (1.17MHz), it was expected that the 2nd harmonic signal would be at a frequency where the transducer was more sensitive (see also Figure 9.5). Therefore, the amplitude of the different frequency components of the signal, as displayed in Figure 10.2, did not represent the relationship between these components as emitted by the contrast bubbles. Thus, the reconstructed image that contained all the spectral information looked "noisy", since it consisted of fundamental and harmonic information. The rest of the images looked clearer. Improvement of both lateral and axial resolution was apparent, for images composed of increasing frequency components. Improved lateral resolution was due to the narrowing of the beam at harmonic frequencies (Ward et al, 1997). A small improvement in axial resolution

observed in the same study was suggested to be "due to the fact that the greatest harmonic generation occurs where the fundamental pressure is highest" (Ward et al, 1997). Also, much of the clutter that appears in ordinary B-mode is removed in 2nd harmonic images and structures are easier to distinguish, which gave the impression of improved resolution (Ward and Whittingham, 1999)

As explained above, care was taken in order to avoid air bubbles and artefacts that would distort the frame backscatter information. Fortunately, only 5 images were found to have big structures, which were suggestive of air bubbles, and were rejected on this account from further analysis. However it was useful to observe the frames for the fundamental and 2nd harmonic spectral windows in two of those acquisitions. In Figure 10.3, the image reconstruction of the fundamental suggested that there was a larger air bubble in line 86, as indicated by the arrow in the figure. The figure is in a three column format. In the first, the image reconstruction is shown. In the second, the particular line of interest is shown, and the third depicts the scaled log-compressed demodulated line as it was used for reconstruction. The display of that line in the time domain showed a strong reflection, and the scaled log-compressed display further showed that the amplitude was at a maximum for that structure, something commonly observed for larger scatterers like air bubbles. The 2nd harmonic image did not seem to have a strong reflection at that particular line. The size was similar, as was the resolution, but the scaled log-compressed line showed an amplitude which was not maximum. This made the structure even more difficult to distinguish in the harmonic image.

Figure 10.4 had a similar format to Figure 10.3. The fundamental image showed a structure similar to the previous one (arrow) in line 83. The structure was 12-cycle long as shown in the display of the line, and was of maximum amplitude for that image, as shown in the log-compressed display of the line. However, the 2nd harmonic image showed 3 separate structures similar to those in the rest of the image (arrow). The display of the line at the 2nd harmonic frequency showed clearly the 3 structures, with the one in the middle destructively interfering with the other two. The distance between the middle of each structure was 7-8 cycles, which is approximately half the pulse length for the second harmonic component (8-cycle

transmit pulse gives a 16-cycle pulse for the 2nd harmonic). The third column of that figure also showed that the amplitude of the signal in that line was almost at maximum compared to the rest of the frame. This translated to more non-linear behaviour (from the 3 scatterers) when compared with the large scatterer of the previous figure. It is unlikely for a large air bubble to resonate and display a non-linear behaviour at that frequency, where contrast microbubbles display non-linear motion and emit harmonic signals. This is suggested to be the case for those two figures.

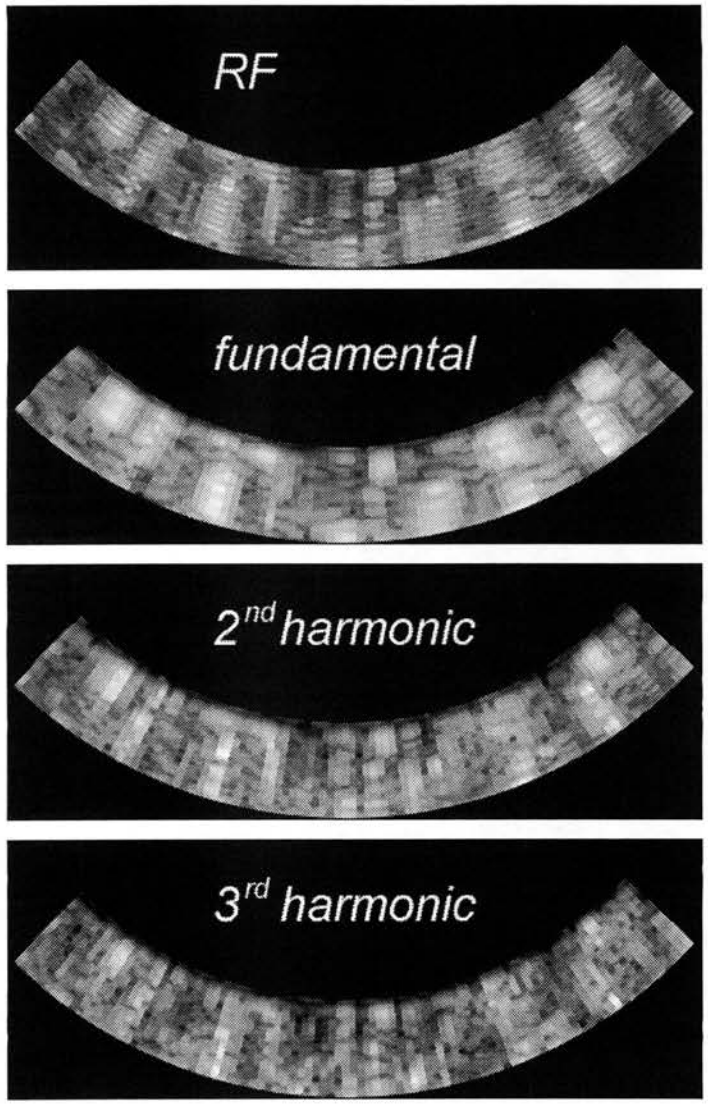

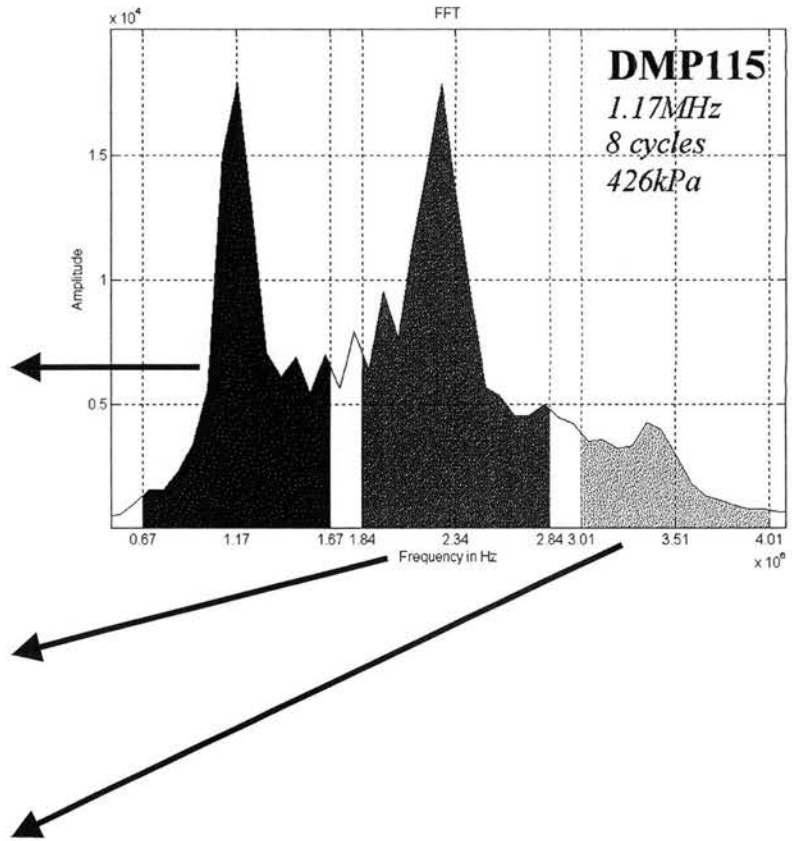

Figure 10.2 Image reconstructed data for the whole RF (window = 0.6-9MHz), fundamental, 2nd, and 3rd harmonic spectral regions (windows = 1MHz). The transmit pulse had 1.17MHz frequency, 8-cycle length, and 426kPa peak negative pressure. The FFT of the RF was displayed above and the different spectral regions used for reconstruction are shaded. It was apparent that the higher the harmonic, the more both lateral and axial resolutions improved. See text for details.

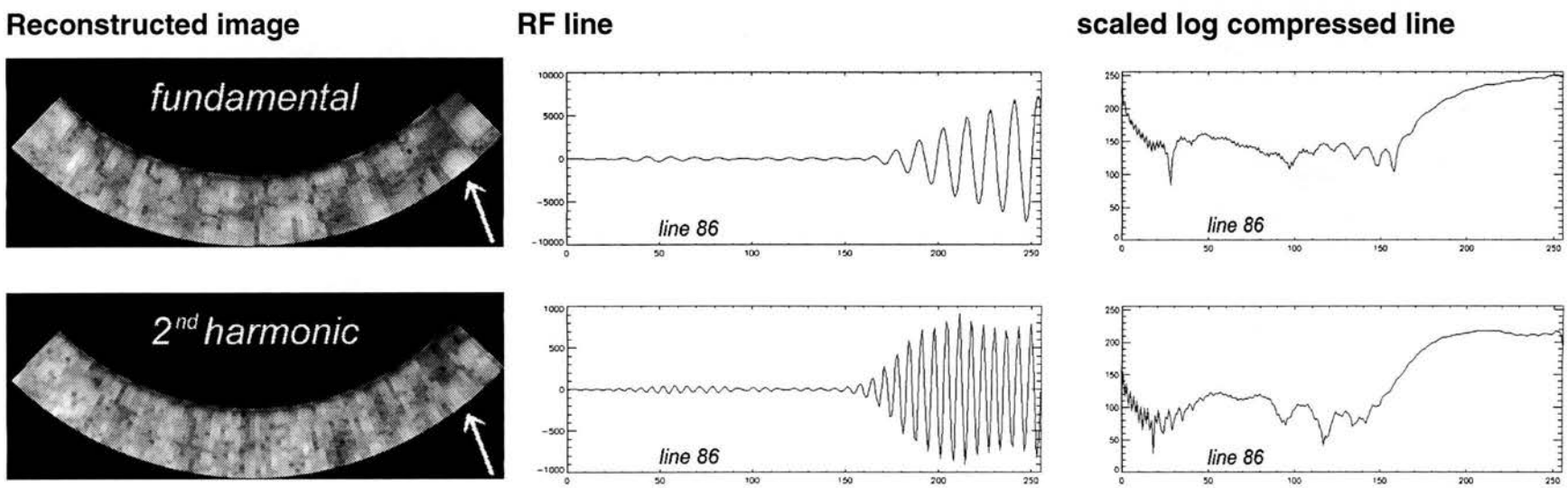

Figure 10.3 The acquisition of a frame at 1.60MHz transmit frequency, 0.49MPa peak negative pressure, and 8-cycle pulse. The first row referred to the fundamental, and the second row to the 2nd harmonic components of the signal. The first column shows the reconstructed image, the second shows the filtered RF at the 86th line, and the third column the scaled log compressed 86th line as it was used for the reconstruction. The arrows in images of the first column point at the 86th line. Neither the fundamental nor the 2nd harmonic show any difference in resolution at that line. The scaled log compressed image suggested that the fundamental amplitude was maximised at that line (compared to the rest of the image), while the same was not true for the 2nd harmonic. The size of the structure and the reduced 2nd harmonic emission suggested an artefact similar to an air bubble (see text for detailed discussion).

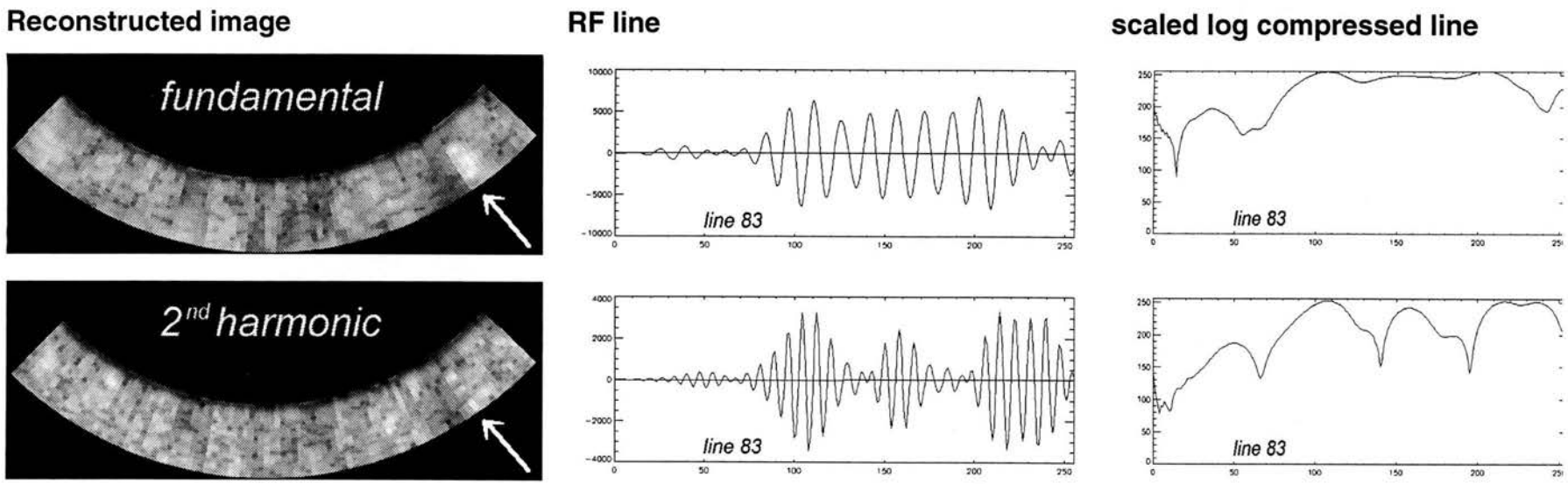

Figure 10.4 The acquisition of a frame at 1.33MHz transmit frequency, 1.34MPa peak negative pressure, and 8-cycle pulse. The first row referred to the fundamental, and the second row to the 2nd harmonic components of the signal. The first column shows the reconstructed image, the second shows the filtered RF at the 83th line, and the third column the scaled log compressed 83th line as it was used for the reconstruction. The arrows in images of the first column point at the 83th line. The 2nd harmonic displayed a notable difference in resolution at that line. Three small structures were resolved, while it was impossible to distinguish them in the fundamental mode. The scaled log compressed image suggested that both the fundamental and 2nd amplitude was maximised at that line (compared to the rest of the image). The small size of the structures and the large 2nd harmonic emission suggested that they were contrast agent microbubbles.

10.3.2 Data analysis

Inspection of the FFT of all the data showed that there were very few frames with significant 3rd harmonic signals. The frequency bandwidth of the system was the limiting factor in receiving 3rd harmonic signals at frequencies above 4.5MHz (1.45MHz transmit frequency). Images constructed on the whole spectrum of the signal produced images with speckle patterns more than in any other individual frequency component (Figure 10.2). Furthermore, the fundamental or 2nd harmonic windows of the spectrum provided significant enhancement of signal to noise ratio, compared to the whole RF for most of the spectrum (Figure 10.5). The 3rd harmonic signals were at noise level above 1.6MHz transmit frequency and therefore excluded from further analysis. For the above reasons, the experimental analysis was focused on the fundamental and 2nd harmonic components of the signals. Most importantly, those two components are primarily related to the type of oscillation the contrast bubble demonstrate (Burns, 1996), since scattered echoes that do not contain harmonic components are considered to belong to linear bubble oscillation motion, and scattered echoes that contain harmonic components emerge from non-linear motion. Non linear bubble oscillation is related to 2nd harmonic emission, while the absence or significant reduction of harmonic signals is associated with linear oscillation.

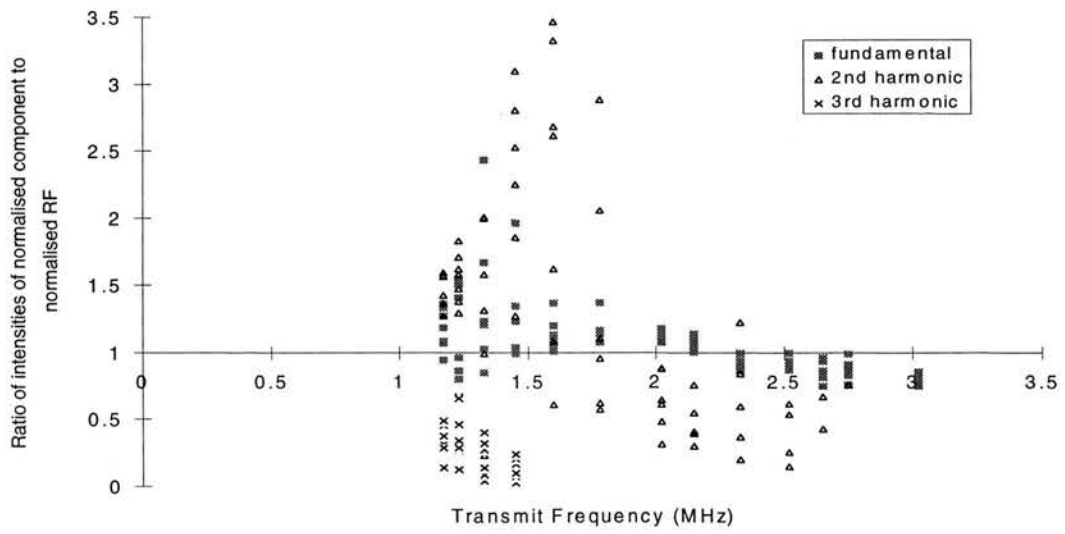

Figure 10.5 Ratio of normalised backscatter (at either fundamental, 2nd or 3rd harmonic) to RF normalised backscatter. All acquisitions were done using an 8-cycle pulse.

The dependence of the normalised 2nd harmonic component of DMP115 on (transmit) frequency, is shown in Figure 10.6. Each point in those plots referred to one setting. The measurements using two different pulse lengths at 3 and 6 cycles were displayed. There were distinct peaks of the harmonic component at a frequency below 2MHz. However, for the 3-cycle pulse, the peak can be located at around 1.7MHz, while for the 6-cycle pulse the peak was located at 1.45MHz. Table 10.2 shows the frequencies at which peak normalised backscatter was observed for the fundamental and the 2nd harmonic. The results refer to the normalisation with Orgasol®. The normalisation with the Eccosphere® suspension provided identical results. There was a distinct tendency of decrease in the frequency where the peak was observed, when the pulse length was increased. This tendency was associated with the bandwidth offered by the different pulse lengths. Equation 9.1 showed that the bandwidth is proportional to the frequency and inversely proportional to the number of cycles. Longer pulses provide narrower bandwidths, and above 6 cycles there was an agreement in the frequency of the peak response (Table 10.2). The shorter pulses provided peak response at a higher transmit centre frequency, which also included spectral information of lower and higher frequencies. Therefore the frequencies that provided peak normalised backscatter for larger pulse lengths, were included in the spectra emitted by the shorter pulse lengths. The observation that this happens at higher frequencies is explained by the fact that the peak sensitivity of the probe is at even higher frequency (~2.3MHz).

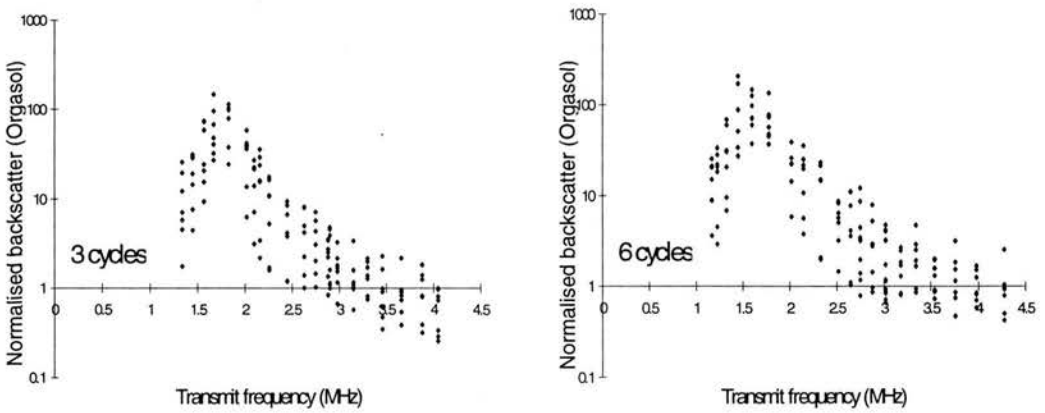

Figure 10.6 2nd harmonic normalised (with Orgasol®) backscatter. All the data acquired for 3 and 6-cycle pulses were displayed. The normalised backscatter peak was close to 1.8MHz and to 1.45, for the 3- and 6-cycle data respectively. See text for details.

Table 10.2 *Observed peak normalised backscatter at different pulse lengths*

Pulse length	fundamental (transmit frequency at peak in MHz)	2nd harmonic (transmit frequency at peak in MHz)
2	1.90	1.77
3	1.83	1.67-1.83
4	1.68	1.68
6	1.78	1.45
8	1.60	1.45
10	1.60	1.45

The dependence of the fundamental and the 2nd harmonic normalised backscatter on (transmit) frequency, was plotted for the two ways of normalisation in Figure 10.7 and Figure 10.8 successively. In both figures (a) was the plot of the fundamental and (b) the 2nd harmonic normalised backscatter versus transmit frequency. The results for the two different probes were plotted in different patterns in Figure 10.7. The data captured using 6, 8, and 10-cycle pulses at all acoustic pressures were shown in the graphs. This illustrated the normalised spectrum of those materials. Those pulse lengths were selected due to the narrow bandwidth of the backscatter signals at both the fundamental and 2nd harmonic windows.

Differences between the two normalising approaches were not noticeable from this display. Peak enhancement of the normalised backscatter was located between 1.6-1.8 MHz (transmit frequency) for the fundamental frequency component, and between 1.4-1.6 MHz for the 2nd harmonic frequency component. Figure 10.7 demonstrated a very good overlap between the normalised data from the two probes, which proved the effectiveness of the normalisation approach used in the analysis.

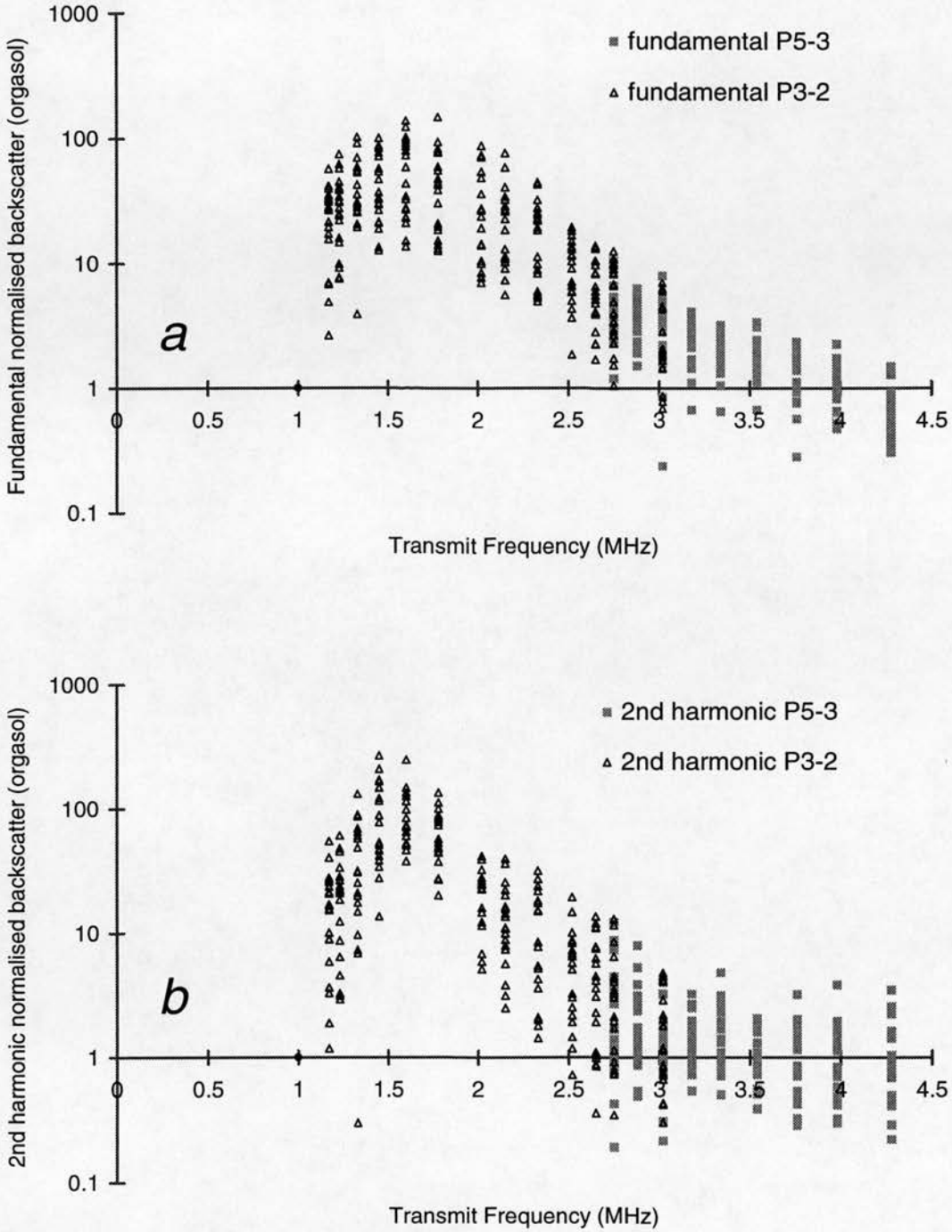

Figure 10.7 Normalised (in terms of the Orgasol® suspension) backscatter (***a***) for the fundamental, and (***b***) for the 2nd harmonic plotted versus transmit frequency. The data were captured using 6-, 8-, and 10-cycle pulses (and all the different acoustic pressures), using both probes. The fundamental normalised backscatter peaked at around 1.6MHz, while the 2nd harmonic at around 1.45MHz. Data from the two probes overlap, suggestive of the successful normalisation approach.

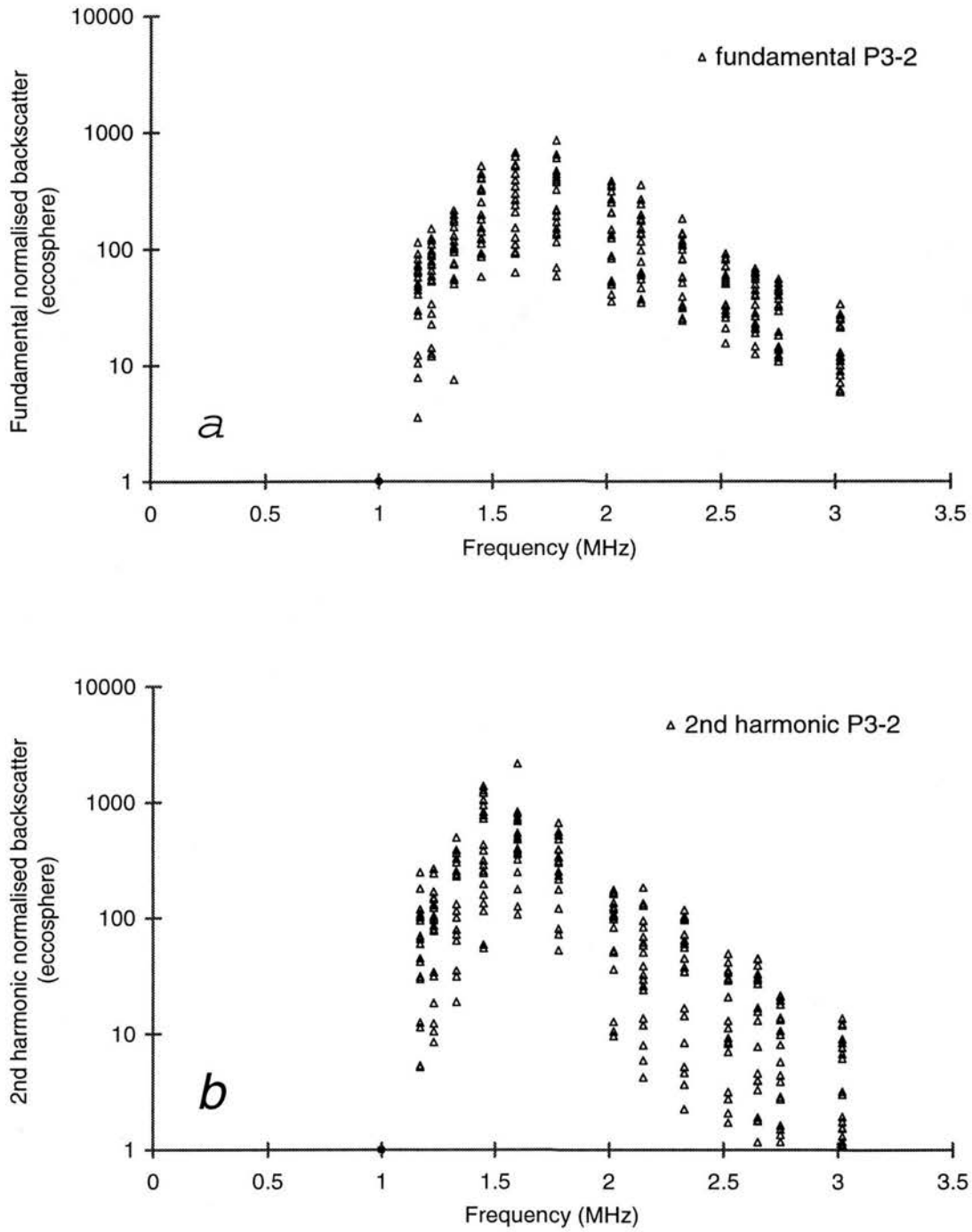

Figure 10.8 Normalised (in terms of the Eccosphere® suspension) backscatter (***a***) for the fundamental, and (***b***) for the 2nd harmonic plotted versus transmit frequency. The data were captured using 6-, 8-, and 10-cycle pulses, using both probes. The fundamental normalised backscatter peaked at around 1.6MHz, while the 2nd harmonic at around 1.45MHz. These values were very similar for the Orgasol® normalisation.

Figure 10.9 plotted the normalised backscatter versus incident acoustic pressure for different frequencies, (a) for the fundamental, and (b) for the 2^{nd} harmonic components. Normalised values of backscatter for the 2^{nd} harmonic component were only displayed if both the contrast agent and normaliser provided information above the noise level, at a particular setting. The fundamental normalised backscatter followed a positive linear relationship to acoustic pressure below 2.75MHz. For frequencies above 2.75MHz there was no correlation between fundamental normalised backscatter and acoustic pressure. The slope of the linear fits was maximum at frequencies similar to those that demonstrated peak enhancement in Figure 10.7a and Figure 10.8a.

The behaviour of the 2^{nd} harmonic normalised backscatter was different. There was a definite maximum at acoustic pressures around 0.5MPa, which was more pronounced at the frequencies which demonstrated peak enhancement in Figure 10.7b and Figure 10.8b.

The normalised backscatter for all different acoustic pressures and frequencies was averaged for each pulse length and was plotted as a measure of the level of the backscatter at different pulse lengths (Figure 10.10). This figure referred to Eccosphere® normalised data. This averaging could only be suggestive of the contribution of the pulse length to backscatter, rather than directly quantifying the effect. The percent standard deviation of these average values was around 100%, since the normalised backscatter from all different frequencies and acoustic pressures were used to calculate the average. The different scatter plots referred to fundamental and 2^{nd} harmonic, and also high (>0.6MPa) and low (<0.4MPa) acoustic pressures, in an effort to explain the maximum 2^{nd} harmonic at around 0.5MPa. It was evident from Figure 10.10 that at high acoustic pressures the average normalised backscatter at both modes did not demonstrate any correlation with the pulse length, while the opposite happened at low acoustic pressures. The harmonic component demonstrated a regression coefficient equal to 0.98, and the fundamental for pulse lengths above 3 had a regression coefficient equal to 0.87. In that figure, the linear fit was shown at low acoustic pressures by the solid lines, and at high acoustic pressures by the dashed lines.

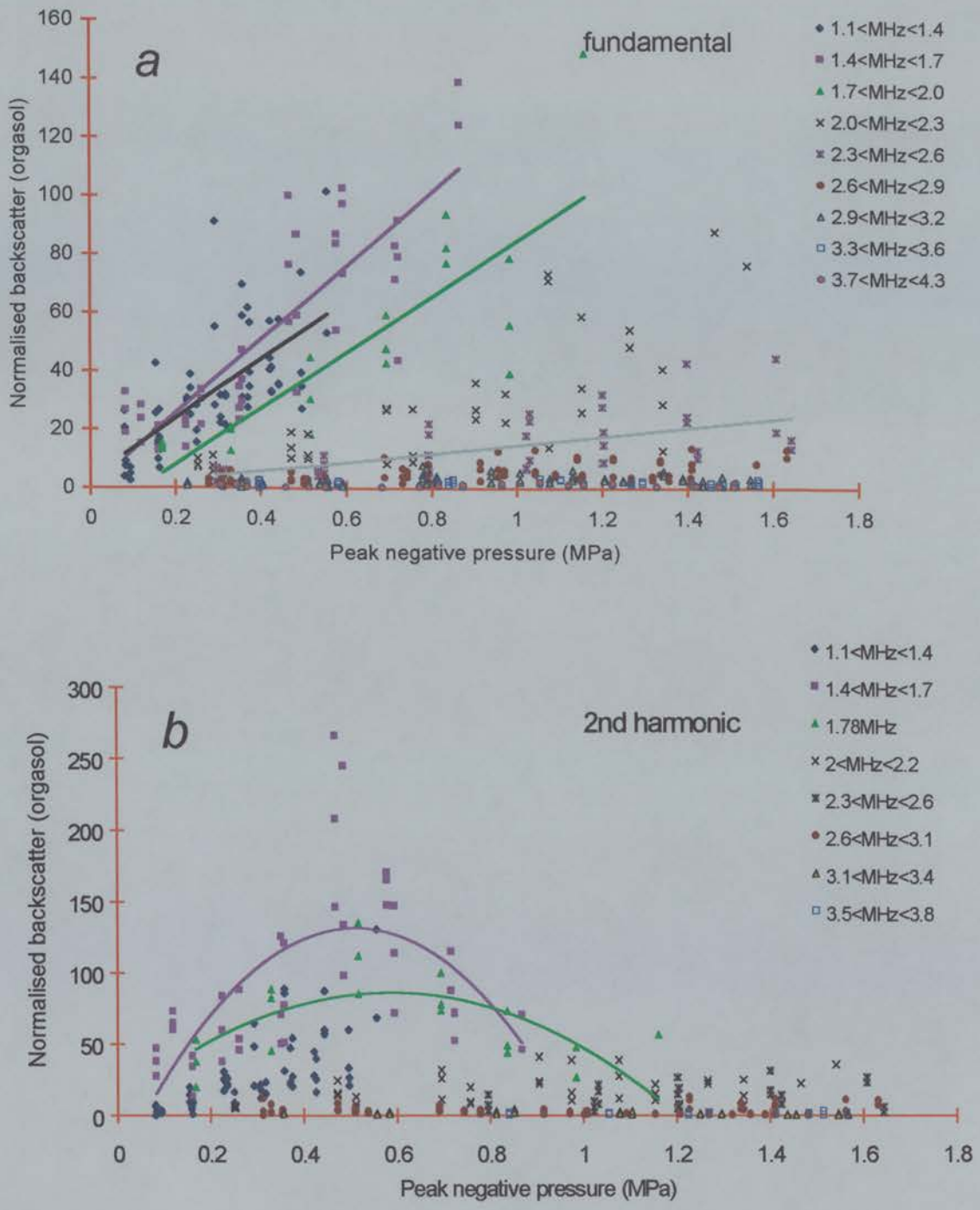

Figure 10.9 Normalised backscatter (in terms of Orgasol®) (**a**) for the fundamental, and (**b**) for the 2nd harmonic, plotted versus peak negative pressure grouped in frequency. Data for the 2nd harmonic were not plotted if they did not contain information above noise (for both contrast and normaliser). The fundamental normalised backscatter increased linearly with increasing peak negative pressure, and the gradient was maximised at the peak frequency. The 2nd harmonic normalised backscatter did not follow similar behaviour. There was a distinct peak at around 0.5MPa, also associated with the peak frequency.

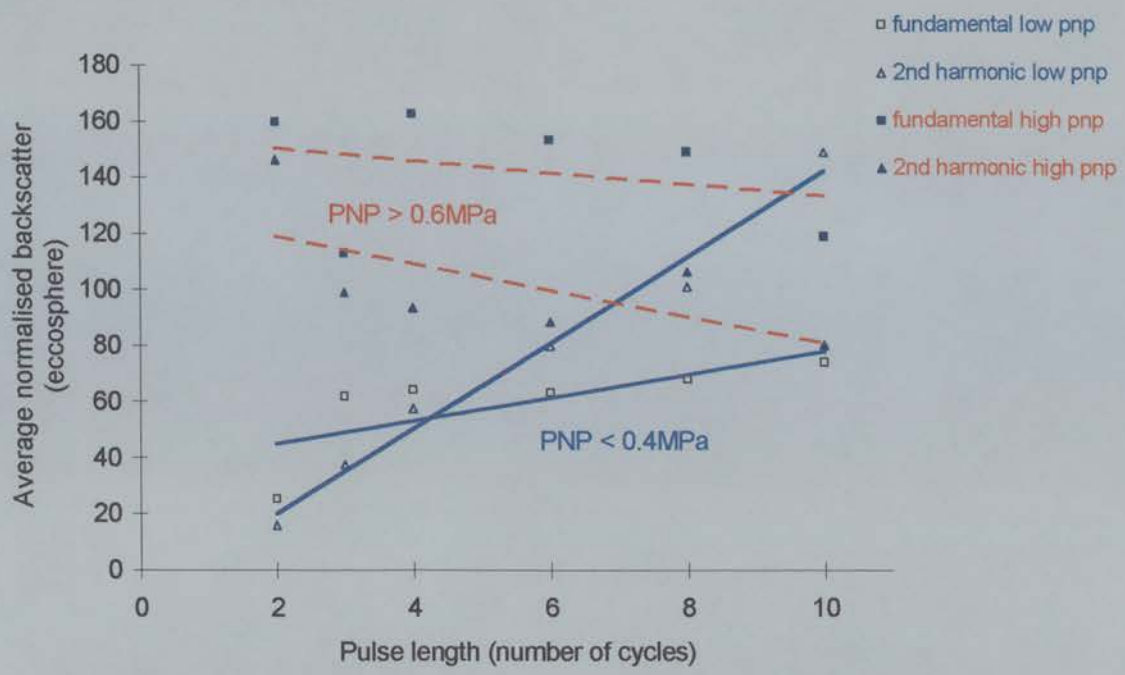

Figure 10.10 Average fundamental (squares) and 2nd harmonic (triangles) normalised backscatter plotted versus pulse length. The average data were grouped in low <0.4MPa (empty points) and high >0.6MPa (filled points) peak negative pressure (PNP). This averaging aimed at illustrating the level of normalised backscatter at different pulse lengths. Lines were fitted to the data and demonstrated the lack of correlation between the average of normalised backscatter and the pulse length at high acoustic pressures, and the strong positive correlation (especially for the 2nd harmonic) between the average normalised backscatter and the pulse length at low acoustic pressures. The general impression was that at low acoustic pressures only the backscatter for both components was increasing with increasing pulse length. This suggests that the oscillation is driven by the pulse at those pressures, and therefore the bubbles were not destroyed. See text for details.

It was also very interesting to see the dependence of the ratio of the two normalised quantities (2nd harmonic/ fundamental), as well as the comparative effect of the two normalising media. It was found that for high acoustic pressure >0.6MPa the fundamental normalised backscatter was at higher levels than the 2nd harmonic enhancement at low acoustic pressures, up to 10dB (Figure 10.11a and b). The opposite happened for low acoustic pressures <0.6MPa. At those acoustic pressures, the harmonic normalised backscatter provided more enhancement. It can also be seen from this figure that the frequencies varied slightly according to normalising medium. Figure 10.11a showed that the 2nd harmonic component was higher than the fundamental between 1.3 - 1.8MHz (probe P3-2) and 2.3 - 3.2MHz (probe P5-3) for acoustic pressure below 0.6MPa. The range in the P3-2 probe in Figure 10.11b was between 1.1 - 1.8MHz.

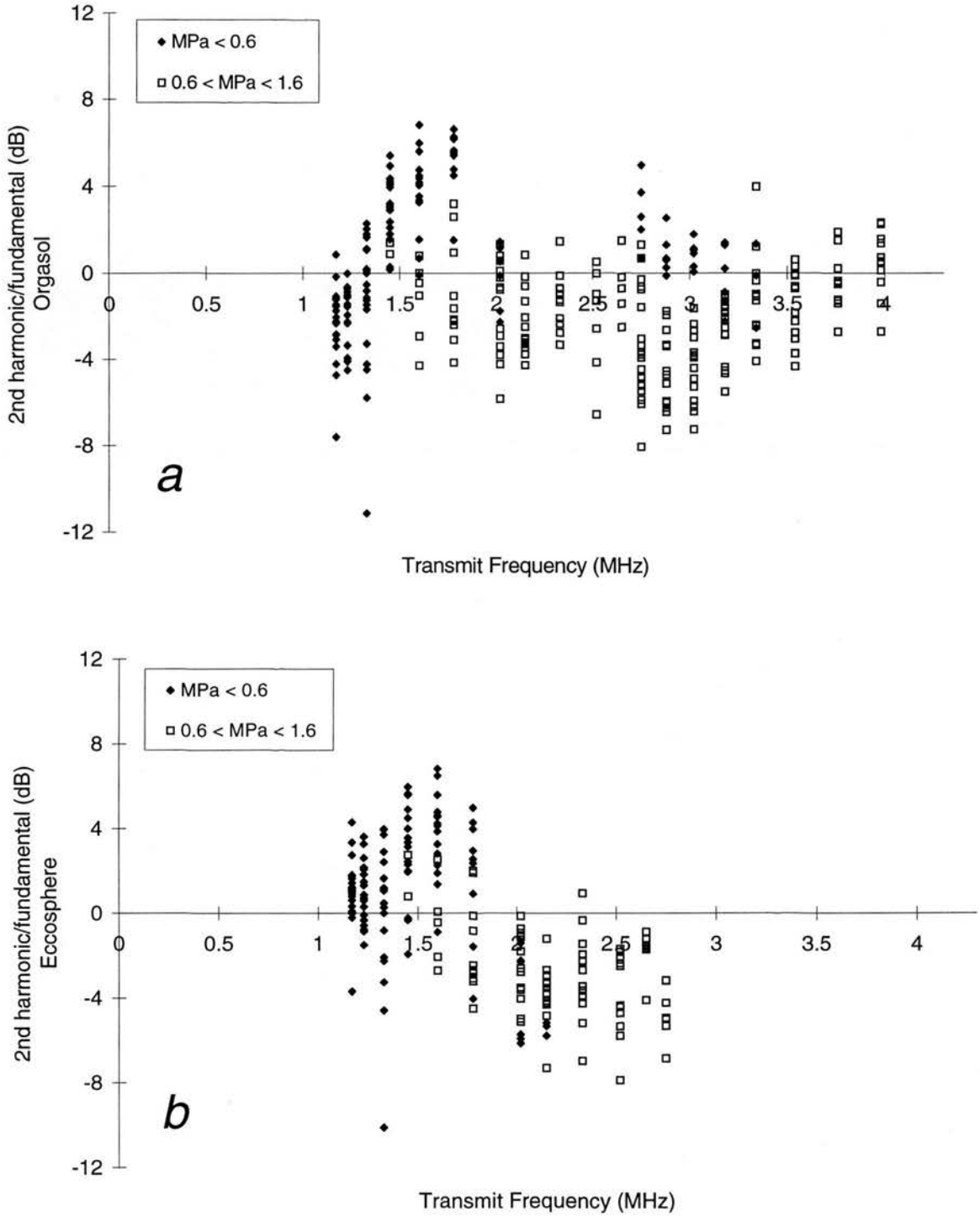

Figure 10.11 Ratio of 2nd harmonic to fundamental normalised backscatter (***a***) for the Orgasol® and (***b***) for the Eccosphere® normalisation plotted versus transmit frequency. Acoustic pressures below 0.6MPa provided enhanced 2nd harmonic compared to the fundamental, and acoustic pressure above 0.6MPa provided enhanced fundamental. The Eccosphere® normalisation seemed more efficient in the lower frequencies.

10.4 Discussion

The investigation of DMP115 using this system provided interesting results. These have been presented in a concise manner which was thought as most appropriate for the particular set of data. The initial aims of this chapter were to: 1) assess the value of a detailed in-vitro investigation of the physical properties of a contrast agent, 2) assess the requirements for the system used for such an investigation, 3) contribute towards the assessment of the optimal settings for contrast imaging, and 4) learn more about the physical properties of contrast agents. The discussion of the results presented in the following sections will now address these four points.

10.4.1 Analysis

This study specified the optimal settings for an in-vitro contrast investigation with DMP115. Figure 10.6 demonstrated the similarity of the spectral shape of the 2^{nd} harmonic normalised backscatter for 3 and 6-cycle pulses, and justified the approach of the experimental protocol to perform one acquisition at each setting.

A closer look at the graphs referring to both fundamental and 2^{nd} harmonic at all pulse lengths produced Table 10.2. It was shown that the increase in the number of cycles in each pulse was associated with a decrease of the frequency of the peak normalised backscatter at both fundamental and 2^{nd} harmonic up to 6 cycles, where the frequency of the peak became fixed at one value. This denoted a higher degree of precision since changes of 0.1 – 0.2MHz in the frequency of the peak were observable from those plots, despite the high variability of the data. Pulse lengths below 4 cycles were considered unsuitable to extract accurate 2^{nd} harmonic and fundamental information (Table 10.2).

Figure 10.12 displays the average spectrum of the frames captured using similar frequencies, at the 6 different pulse lengths. The 3 longer pulses (6, 8, and 10 cycles) demonstrate distinct spectral peaks at the fundamental and the 2^{nd} harmonic frequencies. Therefore the bandpass filter used would be efficient in extracting each one of those components, as can be seen by the dark areas resulting from the filtering process (Figure 10.12). In the shorter pulses (2, 3, and 4 cycles) the fundamental component overlapped the 2^{nd} harmonic, and it was therefore difficult to assess the

amount of the 2nd harmonic content of the filtered signal. This demonstrated that the optimal pulse length for an in-vitro contrast investigation should be longer than 6 cycles.

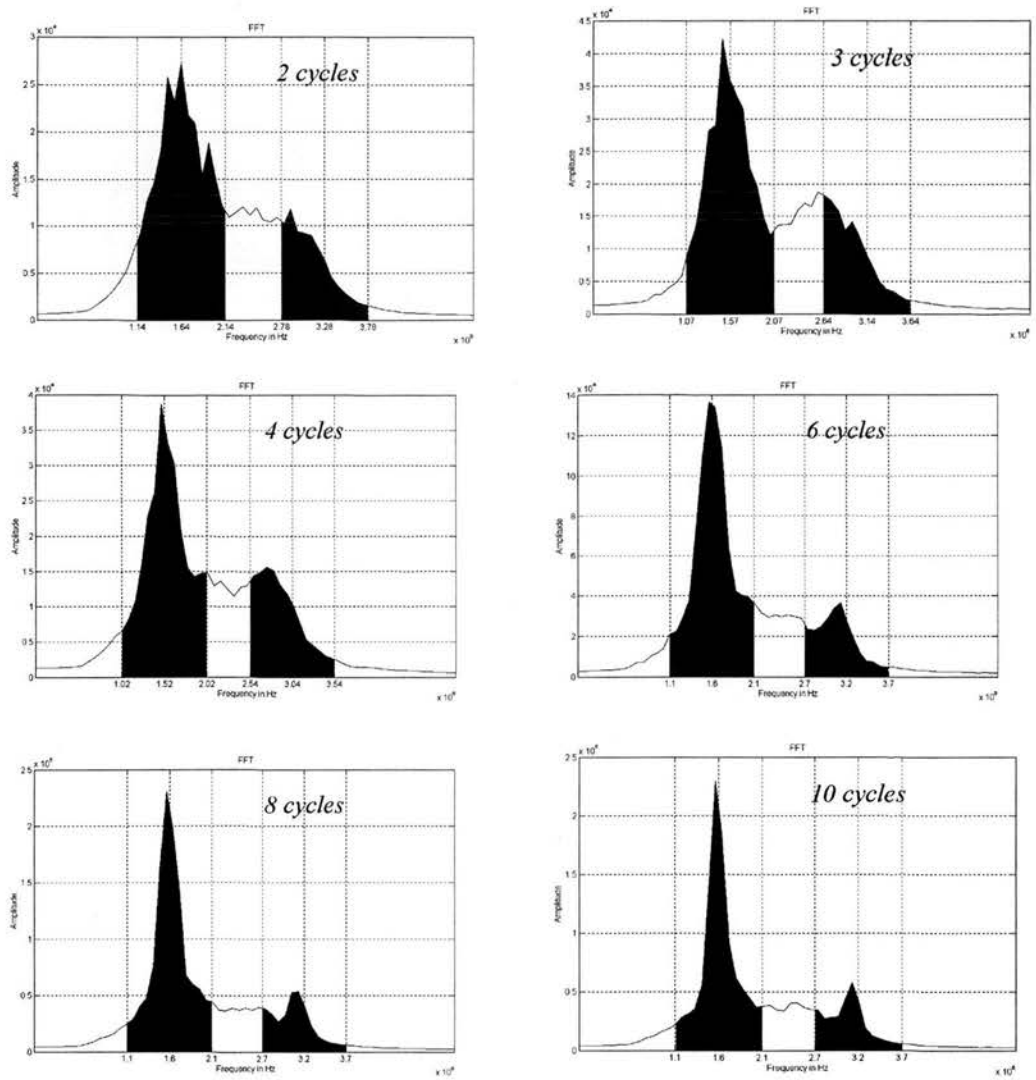

Figure 10.12 Typical average spectra at all the used pulse lengths. The dark areas illustrated the fundamental and 2nd harmonic components as the corresponding filters extracted them. At 2, 3, and 4 cycles the 2nd harmonic signal overlap with the fundamental and it is difficult to filter out the 2nd harmonic component. At 6, 8, and 10 cycles the overlap between the two components was minimised, there was a distinct peak at the 2nd harmonic frequency, and it was possible to extract the 2nd harmonic component.

The system provided an unprecedented range of facilities. DMP115 demonstrated an optimal frequency for the fundamental around 1.8MHz transmit frequency, and for the 2nd harmonic around 1.5MHz transmit frequency. It also was shown that the largest possible acoustic pressure would be optimal in the fundamental mode, and acoustic pressures around 0.5MPa were optimal for the

harmonic mode of imaging. This was in agreement with the calculations performed by Chin and Burns (1997) where maximum 2nd harmonic cross-section occurs at 0.5MPa. Furthermore, at high acoustic pressures (>0.6 MPa), the pulse length did not significantly enhance the backscatter in any mode, while its increase at low acoustic pressure (<0.4 MPa) enhanced the fundamental and even more so the harmonic normalised backscatter. Furthermore, the settings that gave enhanced harmonic or fundamental modes were shown to be very distinct. Low acoustic pressures favoured the harmonic mode and high acoustic pressures favoured the fundamental. These results pointed that optimal imaging was achieved in 2nd harmonic at around 0.5MPa peak negative pressure, 1.5MHz transmit frequency, and 10-cycle pulses. These results can not be directly implemented in in-vivo imaging, since such an environment was not simulated in these studies. The resonant frequency of a bubble is proportional to the square root of ambient pressure (Miller, 1981), which might alter the frequency response for the fundamental and the 2nd harmonic.

The interactions between contrast agent and ultrasound have been witnessed visually (Dayton et al. 1999). In that paper, encapsulated bubbles of similar structure to DMP115 demonstrated a non-linear oscillation at 0.4MPa acoustic pressure. Here, a strong positive correlation between the level of normalised backscatter (either fundamental or 2nd harmonic) and the pulse length was demonstrated for acoustic pressures below 0.5MPa, while there was no correlation displayed between the level of normalised backscatter and pulse length at higher than 0.6MPa acoustic pressure (Figure 10.10). This was suggestive of a predominant destruction mechanism for the bubbles at the higher acoustic pressures. Visual observation of bubbles being destroyed with a single pulse at 1.3 MPa agrees with this suggestion (Morgan et al, 1998). At the lower acoustic pressures the pulse still seemed to be driving the oscillation of most of the encapsulated bubbles. The results also showed peak 2nd harmonic signals at around 0.5MPa (Figure 10.9a), while a steady increase of the fundamental with increasing acoustic pressure was displayed at all frequencies (Figure 10.9b). It is suggested that the shell provided restriction in the oscillatory motion of the bubbles of DMP115, which resulted in enhancement of the non-linear scattered signals. Dayton et al (1999) reported a higher contraction than expansion

for the oscillating encapsulated bubbles, which was highly indicative of the contribution of the shell to a non-linear motion. Therefore it might be possible that as soon as the shell was destroyed and the bubble was liberated, there was not as much restriction in the expansion of the bubbles, which means that the motion might be less non-linear. Hence the dominance of the fundamental over the 2nd harmonic at high acoustic pressures (Figure 10.11), which is in agreement with Morgan et al (1998) who found that at high acoustic pressure (>0.5MPa) the ratio of the harmonic to fundamental did not further increase, a behaviour displayed at low acoustic pressures. Chin and Burns (1997) predicted that above 0.5MPa, the energy is transferred to higher harmonics, which contradicts the above speculation. The set-up is limited in testing that calculation.

In conclusion the present study suggested a mechanism for the motion of the DMP115 bubbles.

Further to this, a different approach in the assessment of fundamental and 2nd harmonic components of contrast agents was introduced. The ratio I_{DMP115} / I_{ECCO} in formula 10.3 is equal to the ratio of scattering cross-section of the DMP115 and Eccosphere®, but the ratios of the intensities of the individual components of the different harmonics in that formula do not have the same physical meaning. A harmonic intensity component for a linear scatterer would represent the reflection of waves created by non-linear propagation. The corresponding harmonic intensity component for the contrast agent bubble would be the sum of the reflected intensity at the harmonic frequency and the harmonic emission generated by the non-linear oscillation of the bubbles. Therefore a direct physical meaning can not be given to the ratio of the intensities in a harmonic component. Despite these facts, the approach of normalisation offered an independent way of studying the fundamental and 2nd harmonic components, and can potentially be used in building a model that describes the oscillatory motion of contrast bubbles.

10.4.2 Limitations

10.4.2.1 The normalising procedure

The aim in using normalised backscatter was to compensate for all the beam parameters, and to use particles that could be used as a reference and perform a direct

comparison with contrast agent bubbles. However it is impossible to perform a direct comparison of a contrast bubble with a solid bubble of similar size. The Orgasol® particles and any solid particles of subcapillary size were not scattering enough ultrasound to be identified individually. Therefore their suspension was high in concentration and had similar properties to the blood mimicking fluid. The Orgasol® suspension was used as a reference material. Nevertheless, at low frequencies, with reduced system sensitivity, the echoes coming from the Orgasol® suspension were indeed low, and the increase of the normalised backscatter from 1.17-1.6MHz at very low acoustic pressure (0-0.4MPa) was to the 8^{th} power of the frequency. This was very high compared to the 4^{th} power frequency dependency of the scattering cross-section of Rayleigh particles, which strongly suggests that the Orgasol® suspension was not suitable at that range of settings.

Using the Eccosphere® particles solved this problem. By having an average size of 55μm, they provided a Rayleigh scatterer that also scattered sufficiently so that each could be seen individually. Figure 10.11 showed that the two normalising approaches were in disagreement at the low frequency range. The Orgasol® normalised backscatter provided an underestimation compared to the Eccosphere® normalised backscatter, mainly because the fundamental frequency component in the Orgasol® suspension at those frequencies was close to that of noise. The Eccosphere® normalised backscatter showed that the normalised 2^{nd} harmonic was higher than the normalised fundamental backscatter at the lowest used frequencies (Figure 10.11b).

10.4.2.2 The scanner

The large variation of sensitivity from P3-2 probe dictated a considerably large concentration of particles in the Eccosphere® suspension, and therefore individual particles were not distinguishable at the most sensitive frequencies.

The same applied to the contrast agent. In order to visualise a few bubbles at the lowest sensitivity settings, and also to have one concentration protocol, the most sensitive of settings provided images in which bubbles could not be seen individually.

The spectral shape of the normalised backscatter was almost identical for both Eccosphere® and Orgasol® (Figure 10.7 and Figure 10.8), which implies that the

sensitivity of the system affected all the materials in a similar manner. Similar conclusions can be extracted from Figure 10.11. The small difference of plots (a) and (b) at the lower frequencies was explained in the previous section.

Another drawback that relates both to the system and to using solid particles was that the 2nd harmonic signals collected from them were very low. Even though the probe would be sensitive enough (P3-2 at 4MHz) to collect 2nd harmonic signals from the contrast agent at high frequencies, the signals from the solid particles would be at noise level. Therefore the normalised values for those frequencies were underestimated since the 2nd harmonic component of the normaliser would lie lower than noise. Those values were not displayed in the figures.

Another important limitation of the system was that the settings at the low sensitivity end of the transducers could not overlap with those at the higher sensitivity range. In particular, the probe P3-2 provided very low sensitivity for frequencies below 1.5MHz, and it was therefore impossible to insonate the agent by using high acoustic pressures (>0.6MPa). Even though it is not considered that it significantly affected the outcome of the particular study, wider band transducers would be desirable.

10.4.2.3 The processing

The most important limitation of the processing of the data was the filtering. The used filter was a 1MHz window elliptic filter which proved reliable over the range of different frequencies, in terms of passband ripple and width, and stopband attenuation. However, there was no available information in the literature on the optimisation of such a filter. The optimal width of the filter is expected to be variable over the range of different frequencies. At 6, 8, and 10 cycles, Figure 10.12 demonstrated that the 2nd harmonic component was clearly isolated from the fundamental. Both the fundamental and the 2nd harmonic components were inside the limits of the passband of the corresponding filters. However, as the pulse length increased, there was an increasing additional spectral information that did not belong to the fundamental or the 2nd harmonic components, and was inside the passband of the filters. For example the filtering of fundamental or 2nd harmonic was almost ideal at the 6-cycle spectrum, while at the 10-cycle one there was additional noise and

information that was included in the passband. Hence the filtering in the 6-cycle spectrum was more efficient that the one in the 10-cycle one.

Of course at different frequencies this balance can be reversed. The simple criterion applied here (1MHz window) aimed at including all the useful spectral information in the passband. Future studies should be performed with optimal filtering.

10.5 Conclusion

An elaborate system for the study of the interaction of individual contrast bubbles with the ultrasonic beam was evaluated in this chapter with the use of DMP115. A detailed analysis of the behaviour of the fundamental and 2^{nd} harmonic components proved that preliminary in-vitro experiments are necessary in order to assess the optimal imaging settings for a contrast agent. DMP115 displayed high harmonic signals at transmit frequencies around 1.5MHz, and fundamental signals around 1.6MHz. A peak for the harmonic signals was also found at acoustic pressures of around 0.5MPa, while the fundamental component of the signal increased with increasing acoustic pressure. The length of the pulse also proved important at low acoustic pressures, in particular for the 2^{nd} harmonic. This strongly suggested that the bubbles remained encapsulated at low acoustic pressures, while at high acoustic pressures, free bubbles were witnessed that did not oscillate in non-linear fashion to the same extent as the encapsulated ones. Despite the many limitations involved in this study, this system provided a novel and efficient tool in the investigation of the physical properties of the contrast agents.

11 Chapter Eleven: Conclusions

11.1 Conclusions from the thesis

The initial aims of this thesis were outlined in paragraph 1.4.1, and here the degree of fulfilment of those aims is discussed.

11.1.1 The set-up

Chatpers 2 and 9 evaluated the two systems used in this thesis and illustrated the high sensitivity and reproducibility. These features were further confirmed in most experimental chapters. The experiments in chapter 1 dealt with very small variations of acoustic pressure, frame rate, and focal length. The echoes from the contrast agent suspensions were modelled as a function of those parameters providing high regression coefficients and significance, which illustrated the capability of the system in demonstrating the properties of different agents in small variations of settings.

Chapter 9 presented an experimental set-up that provided an unprecedented range of settings (Table 10.1).

11.1.2 Stability of contrast agents

11.1.2.1 Effect of pO_2 of the suspension

Levovist, that contains air, displayed a fast decay in degassed suspensions at very low acoustic pressures, while DMP115 (perfluorocarbon), Quantison™ (air), and Myomap™ (air) proved stable (chapter 4). Increased acoustic pressure showed that Quantison™ and Myomap™, which are also air-filled, decayed faster in degassed suspensions than in gas-saturated suspensions (chapter 5). This demonstrated the advantage of DMP115, which is filled with a non-soluble gas. This suggested that the difference between the three agents that contain air lay in the different coating. Quantison™ and Myomap™ have a robust coating while Levovist has a very thin one.

It is therefore suggested in order to achieve higher reproducibility in-vivo, where variable gas levels co-exist, to use contrast agents that contain non-soluble gases.

11.1.2.2 Effect of ultrasound

Dayton et al (1999) report their microscopical observations of bubble destruction. The different mechanisms were a) gradual gas diffusion, b) formation of defects in the coating, c) fragmentation of bubble, and d) rapid destruction.

In this thesis the ultrasonic beam proved to be responsible for the decay of all the agents used. The exponential fit was accurate in demonstrating the decay of DMP115 at all acoustic pressures (chapters 4, 5, and 1). The homogeneity of the images for all the range of acoustic pressures in chapter 5 (Figure 5.1) was due to the slow diffusion of the gas of this agent. Note that all the microbubbles of DMP115 in the field of view interacted with the ultrasound beam in the same fashion (Figure 8.5a). The possible mechanisms for the destruction of those bubbles are probably similar at different acoustic pressures, and had an increasing effect with the increase of acoustic pressure.

Quantison™ had a negligible destruction of bubbles at low acoustic pressures. The appearance of a small population of free bubbles was caused by the ultrasonic beam at pressures greater than 0.69MPa (chapter 8). It is strongly suggested that the encapsulated air leaked out of the robust coating. It was observed using a videotape recording that the free bubble diffused in a single frame (chapter 5). The number of the microbubbles that were destroyed in a single frame did not exceed the 8% of the total number in the field of view at any acoustic pressure (Figure 8.5b). Increasing acoustic pressure increased the proportion of free bubbles in the suspension suggesting that the acoustic pressure was related to increasing gas leak for lower degree of defect in the coating of the bubbles. It was also shown that for the vast majority of the bubbles more than a single insonation was needed to create the necessary leak in the coating (Figure 6.5b). Myomap™ was very similar to Quantison™.

11.1.3 Quantitation of continuous imaging and the Overall Backscatter

The destruction of the agents when exposed to ultrasound is the reason for the reduced enhancement of imaging in continuous mode.

The Overall Backscatter was defined as the integral of the decay of the contrast over time of insonation (chapter 5), and physically represents the backscatter that can be obtained by all the scatterers in suspension. It showed differences in the decay of Quantison™ and Myomap™ in different pO2 impossible to distinguish using the comparison of the decay constants (Figure 5.4). The improved definition of the Overall Backscatter in the frame domain instead of the time domain, showed that it can accurately and reproducibly characterise the echoes from contrast agents and provide better sensitivity than backscatter intensity in continuous imaging. The Overall Backscatter is a promising physical quantity that could be adapted for use in quantitative measurements in-vivo.

11.1.4 Optimisation of contrast imaging

Contrast enhanced imaging in qualitative but even more in quantitative studies requires a constant relationship between Backscatter and Concentration. If this relationship could be assessed, then useful indices representative of flow might be measured (Kaul et al, 1989). It was shown that using high concentration of contrast might provide two major obstacles in this effort (chapter 7):

1) Different acoustic pressures might provide a variable degree of interference between the scattered echoes from the microbubbles, which alters the relationship between backscatter and concentration.
2) Different acoustic pressure and bubble concentrations provide attenuation patterns, which can not be predicted and corrected for.

Microbubbles with thin coating (Levovist, DMP115) provided ideal contrast enhancement at low acoustic pressure (<0.5MPa) at all imaging modes.

11.1.5 Understanding of the bubble-beam interaction

In chapter 3 DMP115 and Levovist which are agents with a thin coating, demonstrated higher reflectivity (Figure 3.1), than Quantison™ and Myomap™ that have much thicker coating. The damping provided by the shell to the oscillation of the microbubbles was shown to be significant at low acoustic pressures.

It is important to preserve a linear relationship between the backscatter and the concentration of the microbubbles in order to investigate their backscatter properties (chapter 7).

The study of individual bubbles showed that their scattering cross-section is linearly proportional to peak negative pressure (chapter 8), which implies increasing amplitude of their oscillation with increase of peak negative pressure. The backscatter of different agents becomes very similar at very high acoustic pressures, which suggested that free bubbles were created above 0.6MPa peak negative pressure. Contrast agents with robust shells provide high levels of enhancement only when the microbubbles are liberated from the shell (Quantison™).

At low acoustic pressures (<0.5MPa), and at dominant resonance (around 1.5MHz for DMP115), microbubbles with flexible coating oscillate non-linearly, but it is questionable whether this continues to happen at higher acoustic pressures where free bubbles are formed. The 2nd harmonic component at high acoustic pressures is significantly reduced, but it is argued that the energy is transferred to higher harmonics (Chin and Burns, 1997).

11.2 The in-vitro contrast test

The understanding of contrast microbubbles and the subsequent modelling of them would also assist in the identification of optimal settings for ultrasonic contrast imaging. It is however necessary to carry out some preliminary in-vitro investigation before using contrast agents in-vivo. This thesis outlined the most significant aspects of this investigation. The recommended in-vitro tests, mostly resulting from this thesis, for an agent are:

1) Stability in the physical (gas level, ambient pressure, viscosity, temperature), and chemical environment.
2) Stability in the ultrasonic field and in combinations of different environments. Performance in continuous imaging.
3) Efficiency. Proportion of strong scatterers in a population of contrast microbubbles.
4) Performance in fundamental and harmonic (including higher harmonics) domains at different beam settings.

11.3 Future research

It is very important to establish an efficient and complete frame of tests for ultrasonic contrast agents. A system that can incorporate all the different tests mentioned above, and subsequently simulate an in-vivo environment for contrast microbubbles would be the natural way forward from this thesis.

In the effort to accumulate enough information for the interaction of ultrasound with the bubbles, and subsequently model their oscillatory motion, it is necessary to focus on different sizes of bubbles and understand their behaviour. De Jong and Hoff (1993) use different filters in order to isolate microbubbles with different size distributions.

It would also be desirable to minimise the "width" of each instrument setting in a particular insonation. This includes narrow frequency bandwidth, as well as narrow acoustic pressure width. Practically this would mean investigating the microbubbles that are positioned in the spatial peak of an ultrasonic beam. If the exact beam characteristics become known, the normalisation might not be necessary.

Improvement of the transducer technology would be welcome in the quantitative assessment of contrast agents. Broader band transducers would facilitate the investigation of additional spectral signatures, and would probably introduce new approaches in ultrasonic contrast imaging.

Further research is needed on the evaluation of the Overall Backscatter as an in-vivo physical quantity.

References

Albrecht T, Blomley MJK. Contrast agents add new dimension to sonography. Diag Im Eur 1997; 0: 21-33.

Anderson AL, Hampton LD. Acoustics of gas-bearing sediments I. Background. J Ac Soc Am 1980; 67: 1865-1888.

Armitage P, Berry G. Ch.10 Multiple Measurements. In: Statistical Methods in Medical Research. Blackwell Science Ltd, 1996 (3rd edition): 321.

Atkins PW. Physical chemistry. Oxford University Press, 1994.

Ayida G, Harris P, Kennedy S, Seif M, Barlow D, Chamberlain P. Hysterosalpingo-contrast sonography (HyCoSy) using Echovist-200 in the outpatient investigation of infertility patients. Br J Radiol 1996; 69: 910-913.

Barnhart J, Levene H, Villapando E, Maniquis J, Fernandez J, Rice S, Jablonski E, Gjoen T, Tolleshaug H. Characteristics of Albunex: Air-filled albuming microspheres for echocardiography contrast enhancement. Invest Radiol 1990; 25: S162-S164.

Bauer A, Becker G, Krone A, Frohlich T, Bogdahn U. Transcranial duplex sonography using ultrasound contrast enhancers. Clin Radiol 1996; 51(S1): 19-23.

Bauer A, Schlief R, Zomack M, Urbank A, Niendorf HP. In "Advances in echo imaging using contrast enhancement" (Eds. Nanda NC, Schlief R, Goldberg BB) Kluwer Academic Publisher, Dodrecht, The Netherlands, 1997.

Bleeker HJ, Shung KK, Barnhart JL. Ultrasonic characterization of Albunex, a new contrast agent. J Ac Soc Am 1990; 87: 1792-1797.

Brayman AA, Azadniv M, Makin IRS, Miller MW, Carstensen EL, Child SZ, Raeman CH, Meltzer Rs, Everbach EC. Effect of a stabilized microbubble echo contrast agent on hemolysis of human erythrocytes exposed to high intensity pulsed ultrasound. Echocardiography 1995; 12: 13-21.

Burkard ME, Van Liew HD. Simulation of exchanges of multiple gases in bubbles in the body. Respir Physiol 1994; 95: 131-145.

Bijnens B, Herregods M, Nuyts J, Vandeweghe G, Suetens P, Van de Werf F. Acquisition and processing of the radio-frequency signal in echocardiography: a new global approach. Ultrasound Med Biol 1994; 20: 167-176.

Broillet A, Puginier J, Ventrone R, Schneider M. Assessment of myocardial perfusion by intermittent harmonic power doppler using SonoVue, a new ultrasound contrast agent. Invest Radiol 1998; 33: 209-215.

Burns PN, Powers JE, Hope Simpson D, Uhlendorf V, Fritzsch T. Harmonic imaging and Doppler using microbubble contrast agents: a new method for contrast imaging. Ultrasound Med Biol 1994; 20: S73 (Abstract).

Burns PN. Harmonic imaging with ultrasound contrast agents. Clin Radiol 1996; 51: 50-55.

Carr DH. Contrast media. Churchill Livingstone, London UK, 1988.

Chang PH, Shung KK, Levene HB. Quantitative measurements of second harmonic doppler using ultrasound contrast agents. Ultrasound Med Biol 1996; 22: 1205-1214.

Chen JF, Zagzebski JA. Frequency dependence of backscatter coefficient versus scatterer volume fraction. IEEE trans UFFC 1996; 43: 345-353.

Chin CT, Burns PN. Predicting acoustic response of a microbubble population for contrast imaging. IEEE Ultrasonics Symp Proc 1997; 2: 1557-1560.

Christiansen C, Vebner AJ, Muan B, Vik H, Haider T, Nicolaysen H, Skotland T. Lack of an immune response to Albunex, a new ultrasound contrast agent based on air-filled albumin microspheres. 1994; 104: 372-378.

Church CC. The effects of an elastic solid surface layer on the radial pulsations of gas bubbles. J Ac Soc Am 1995; 97: 1510-1521.

Correas JM, Quay SD. Echogen emuslion: a new ultrasound contrast agent based on phase shift colloids. Clin Radiol 1996; 51: 11-14.

Correas J, Lafortune M, Burns PT, Pourcelot L. Detection of renal artery stenosis with B-mode enhancement after administration of a US contrast agent. Radiology 1996; 201(P): 201.

Dalecki D, Raeman CH, Child SZ, Francis CW, Meltzer RS, Carstensen EL. Hemolysis *in vivo* from exposure to pulsed ultrasound. Ultrasound Med Biol 1997; 23: 307-313.

Dayton PA, Morgan KE, Klibanov AL, Brandenburger GH, Ferrara KW. Optical and acoustical observations of the effects of ultrasound on contrast agents. IEEE trans UFFC 1999; 46: 220-232.

De Jong N, Ten Cate FJ, Lancee CT, Roelandt JRTC, Bom N. Principles and recent developments in ultrasound contrast agents. Ultrasonics 1991; 29: 324-330.

De Jong N, Hoff L, Skotland T, Bom N. Absorption and scatter of the encapsulated gas filled microspheres: theoritical considerations and some measurements. Ultrasonics 1992; 30: 95-103.

De Jong N, Hoff L. Ultrasound scattering properties of Albunex microspheres. Ultrasonics 1993; 31: 175-181.

De Jong N, Ten Cate FJ, Vletter WB, Roelandt JRTC. Quantification of transpulmonary echocontrast effects. Ultrasound Med Biol 1993; 19: 279-288.

De Jong N, Cornet R, Lancee CT. Higher harmonics of vibrating gas-filled microspheres. Part one: simulations. Ultrasonics 1994; 32: 447-453 (a).

De Jong N, Cornet R, Lancee CT. Higher harmonics of vibrating gas-filled microspheres. Part two: measurements. Ultrasonics 1994; 32: 455-459 (b).

Epstein PS, Plesset MS. On the stavility of gas bubbles in liquid-gas solutions. J Chem Phys 1950; 18: 1505-1509.

Feinstein SB, Cheirif J, Ten Cate FJ, Silverman PR, Heidenreich PA, Dick C, Desir RM, Armstrong WF, Quinones MA, Shah PM. Safety and efficacy of a new transpulmonary ultrasound contrast agent: initial multicenter clinical results. J Am Coll Cardiol 1990; 16: 316-324.

Fowlkes JB, Carson PL. Systems for degassing water used in ultrasonic measurements. J Ac Soc Am 1991;90:1197-1200.

Frinking PJA, de Jong N. Acoustic modeling of shell-encapsulated gas bubbles. Ultrasound Med Biol 1998; 24: 523-533.

Frinking PJA, de Jong N, Cespedes EI. Scattering properties of encapsulated gas bubbles at high ultrasound pressures. J Ac Soc Am 1999; 105: 1989-1996.

Goldberg BB. Ultrasound contrast agents. Maria Dunitz, London, UK, 1997.

Goldberg BB, Liu JB, Burns PN, Merton DA, Fosberg F. Galactose-Based Intravenous Sonographic Contrast Agent: Experimental Studies. 1993; 12: 463-470.

Gramiak R, Shah P. Echocardiography of the aortic root. Invest Radiol 1968; 3: 356-366.

Gramiak R, Shah P, Kramer DH. Ultrasound Cardiography: Contrast Studies in Anatomy and Function. Radiology 1969; 92: 939-948.

Jayaweera AR, Edwards N, Glasheen WP, Villanueva FS, Abbott RD, Kaul S. *In vivo* myocardial kinetics of air-filled albumin microbubbles during myocardial contrast echocardiography. Comparison with radiolabeled red blood cells Circ Res 1994; 74: 1157-1165.

Johnson DE, Johnson JR, Moore HP. A handbook of active filters. Prentice-Hall, NJ, USA, 1980.

Johnson R. Latest clinical developments with Quantison™. 2nd Thoraxcentre European Symposium on Ultrasound Contrast Imaging, Rotterdam, the Netherlands. January 1997. (Abstract)

Kaul S, Kelly P, Oliner JD, Glasheen WP, Keller MW, Watson DD. Assessment of regional myocardial blood flow with myocardial contrast two-dimensional echocardiography. J Am Coll Cardiol 1989; 13: 468-482.

Keller MW, Segal SS, Kaul S, Duling B. The behavior of sonicated albumin microbubbles within the microcirculation: A basis for their use during myocardial contrast echocardiography. Circ Res 1989; 65: 458-467.

Koenig K, Meltzer RS. Effect of viscosity on the size of microbubbles generated for use as echocardiographic contrast agents. J Cardiovasc Ultrasonography 1986; 5: 3-4.

Krishna PD, Newhouse VL. Second harmonic characteristics of the ultrasound contrast agents Albunex and FSO69. Ultrasound Med Biol 1997; 23: 453-459.

Landini L, Mazzarisi A, Iraca D, Slavadori M, Benassi A. On-line two-dimensional evaluation of ultrasonic integrated backscatter. J Biomed Eng 1987; 9: 341-344.

Leen E, Angerson WJ, Warren HW, O'Gorman P, Moule B, Carter EC, McArdle CS. Improved sensitivity of colour Doppler flow imaging of colorectal hepatic metastases using galactose microparticles: a preliminary report. Br J Surg 1994; 81: 252-254.

Leighton TG. The acoustic bubble. Academic Press, London UK, 1994.

Lerski RA, Duggan TC, Christie J. A simple tissue-like ultrasound phantom material. Br J Radiol 1982; 55: 156-157.

Lindner JR, Kaul S. Insights into the assessment of myocardial perfusion offered by different cardiac imaging modalities. 1995; 2: 446-460.

Lindner JR, Firschke C, Wei K, Goodman NC, Skyba DM, Kaul S. Myocardial perfusion characteristics and hemodynamick profile of MRX-115, a venous echocardiographic contrast agent, during acute myocardial infarction. J Am Soc Echocard 1998; 11: 36-46.

Livett AJ, Preston RC. A comparison of the AIUM/NEMA, IEC and FDA (1980) definitions of various acoustic output parameters for ultrasonic transducers. Ultrasound Med Biol 1985; 11: 793-802.

Martin RP. Myocardial Contrast Echocardiography: A Light in the (Heart of) Darkness. J Am Coll Cardiol 1989;13:857-859.

McDicken WN. Diagnostic Ultrasonics. Churchill Livingstone, Edinburgh UK, 1991.

Medwin H. Counting bubbles acoustically: a review. Ultrasonics 1977; 15: 7-13.

Miller DL. Ultrasonic detection of resonant cavitation bubbles in a flow tube by their second-harmonic emissions. Ultrasonics 1981; 19: 217-224.

Miller DL, Thomas RM. Ultrasound contrast agents nucleate inertial cavitation *in vitro*. Ultrasound Med Biol 1995; 21: 1059-1065.

Miller DL, Thomas RM. Contrast-agent gas bodies enhance hemolysis induced by lithotripter shock waves and high-intensity focused ultrasound in whole blood. Ultrasound Med Biol 1996; 22: 1089-1095.

Miller DL, Gies RA. Enhancement of ultrasonically-induced hemolysis by perfluorocarbon-based compared to air-based echo-contrast agents. Ultrasound Med Biol 1998; 24: 285-292.

Missouris CG, Allen CM, Balen FG, Buckenham T, Lees WR, MacGregor GA. Non-invasive screening for renal artery stenosis with ultrasound contrast enhancement. J Hypert 1996; 14: 519-524.

Moran CM, Sutherland GR, Anderson T, Riemersma RA, McDicken WN. A comparison of methods used to calculate ultrasonic myocardial backscatter in the time domain. Ultrasound Med Biol 1994; 20: 543-550.

Moran CM, Anderson T, Sboros V, Sutherland GR, Wright R, McDicken WN. Quantification of the enhanced backscatter phenomenon from an intravenous and an intra-arterial contrast agent. Ultrasound Med Biol 1998; 24: 871-880.

Mor-Avi V, David D, Akselrod S, Bitton Y, Choshniak I. Myocardial regional blood flow: quantitative measurement by computer analysis of contrast enhanced echocardiographic images. Ultrasound Med Biol 1993; 19: 619-633.

Morgan KE, Dayton PA, Kruse DE, Klibanov AL, Brandenburger GH, Ferrara KW. Changes in the echoes from ultrasonic contrast agents with imaging parameters. IEEE trans UFFC 1998; 45: 1537-1548.

Morrison DC. Medical ultrasonics: A computer analysis of echoes from soft tissues. Ph.D. thesis, University of Edinburgh. 1979.

Morse PM, Ingard KU. Theoretical acoustics. McGraw Hill, New York, USA, 1968.

Nanda CN, Schlief R. Advances in echo imaging using contrast enhancement. Kluwer Academic publishers, Dodrecht, The Netherlands, 1993.

Ophir J, Parker KJ. Contrast agents in diagnostic ultrasound. Ultrasound Med Biol 1989;15:319-333.

Padial LR, Chen MH, Vuille C, Guerrero JL, Weyman AE, Picard MH. Pulsatile pressure affects the disappearance fo echocardiographic contrast agents. J Am Soc Echocard 1995; 8: 285-292.

Parks TW, Burrus CS. Digital Filter Design. John Wiley & Sons, London,1987.

Porter TR, Xie F. Transient myocardial contrast after initial exposure to diagnostic ultrasound pressures with minute doses of intravenously injected microbubbles. Circulation 1995;92:2391-2395.

Porter TR, Xie F, Kricsfeld D, Armbruster RW. Improved myocardial contrast with second harmonic transient ultrasound response imaging in humans using

intravenous perfluorocarbon-exposed sonicated dextrose albumin. J Am Coll Cardiol 1996;27:1497-1501.

Preston RC. Hydrophone-based measurements on a specific acoustic pulse part 1: Field characterisation. In: Preston RC, ed. Output measurements for medical ultrasound. London: Springer-Verlag, 1991:91-105.

Ramnarine KV, Nassiri DK, Hoskins PR, Lubbers J. Validation of a new blood-mimicking fluid for use in doppler flow test objects. Ultrasound Med Biol 1998;24:451-459.

Rijsterborgh H, Mastik F, Lancee CT, Verdouw P, Roelandt J, Bom N. Ultrasound myocardial integrated backscatter signal processing: frequency domain versus time domain. Ultrasound Med Biol 1993;19: 211-219.

Roelandt J. Contrast Echocardiography. Ultrasound Med Biol 1982; 8: 471-492.

Rovai D, Lombardi M, Mazzarisi A, Landini L, Taddei L, Distante A, Benassi A, L' Abbate A. Flow quantitation by radio frequency analysis of contrast echocardiography. Int J Card Im 1993;9:7-19.

Rovai D, DeMaria AN, Lombardi M, Marini C, Schneider J, L'Abbate A. In "Advances in echo imaging using contrast enhancement" (Eds. Nanda NC, Schlief R, Goldberg BB) Kluwer Academic Publisher, Dodrecht, The Netherlands, 1997.

Rubio R, Berne RM. Regulation of coronary blood flow. Prog Cardiov dis 1975; 18: 105-122.

Sahn DJ, Walker KW, Willians M, Crume M, Giraud GD, Grauer SE, Pantely GA. "Intrument factors and strategies for limiting and taking advantage of bubble destruction" 2nd Thoraxcenter European Symposium on Ultrasound Contrast Imaging, 23-24 January 1997.

Sebba F. Microfoams-An unexploited colloid system. J Colloid Interface Sci 1971; 35: 643-646.

Schlief R. Ultrasound contrast agents. Curr Op Radiol 1991; 3: 198-207.

Schlief R, Schurmann R, Balzer T, Somack M, Niendorf HP. "Saccharide based contrast agents" In: Nanda N, Schlief R (editors) "Advances in echo imaging using contrast enhancement" Kluwer Academic Publishers, London UK, 1993.

Schneider M, Bussat P, Barrau MB, Arditi M, Yan F, Hybl E. Polymeric microballoons as ultrasound contrast agents. Physical and ultrasonic properties compared with sonicated albumin. Invest Radiol 1992;27:134-139.

Schrope BA, Newhouse VL, Uhlendorf V. Simulated capillary blood flow measurement using a nonlinear ultrasonic contrast agent. Ultrasonic Im 1992; 14: 134-158.

Schrope BA, Newhouse VL. Second harmonic ultrasonic blood perfusion measurement. Ultrasound Med Biol 1993; 19: 567-579.

Schwarz KQ, Bezante GP, Chen X. When can doppler be used in place of integrated backscatter as a measure of scattered ultrasound intensity? Ultrasound Med Biol 1995; 21: 231-242.

Schwarz KQ, Bezante GP, Chen X, Schlief R. Hemodynamic effects of microbubble echo contrast J Am Soc Echocard 1996; 9: 795-804.

Sebba F. Microfoams-An unexploited colloid system. J Colloid Interface Sci 1971; 35: 643-646.

Simpson DH, Chin CT, Burns PN. Pulse inversion doppler: A new method for detecting nonlinear echoes from microbubble contrast agents. IEEE trans UFFC 1999; 46: 372-382.

Solbiati L, Arsizio B, Crespi L, Rizzatto G. Three-dimensional power Doppler with an intravascular echo enhancement agent and second harmonic imaging in radio-frequency ablation of liver metastases. Radiology 1996; 201(P): 196.

Stecher PG."The Merck index" an encyclopedia of chemicals & drugs. Rahway N.J. USA: Merck & Co Inc, 1968.

Tiemann K, Becher H, Bimmel D, Schlief R, Nanda NC. Stimulated acoustic emission. Echocardiography 1997; 14: 65-69.

Uhlendorf V, Hoffmann C. Nonlinear acoustical response of coated microbubbles in diagnostic ultrasound. 1994 IEEE Ultrasonics Symp Proc 1994; 3: 1559-1562.

Unger E, Shen D, Fritz T, Kulik B, Lund P, Wu GL, Yellowhair D, Ramaswami R, Matsunaga T. Gas-filled lipid bilayers as ultrasound contrast agents. Invest Radiol 1994; 29: S134-S136.

Unger E, Fritz T, McCreery T, Sahn D, Barette T, Yellowhair D, New T. "Liposomes as myocardial perfusion ultrasound contrast agents" In: Goldberg BB (ed.) "Ultrasound Contrast Agents" Martin Dunitz Ltd, London UK, 1997.

Van Liew HD, Burkard ME. Bubbles in circulating blood: stabilization and simulations of cyclic changes of size and content. J Appl Physiol 1995; 79: 1379-1385 (a).

Van Liew HD, Burkard ME. Behaviour of bubbles of slowly permeating gas used for ultrasonic imaging contrast. Invest Radiol 1995; 30: 315-321 (b).

Villanueva FS, Glasheen WP, Sklenar J, Jayaweera AR, Kaul S. Successful and reproducible myocardial opacification during two-dimensional echocardiography from right heart injection of contrast. Circulation 1992; 85: 1557-1564.

Villanueva FS, Glasheen WP, Sklenar J, Kaul S. Characterization of spatial patterns of flow within the reperfused myocardium by myocardial contrast echocardiography. Implications in determining extent of myocardial salvage. Circulation 1993; 88: 2596-2606.

Vuille C, Nidorf M, Morrissey RL, Newell JB, Weyman AE, Picard MH. Effect of static pressure on the disappearance rate of specific echocardiographic contrast agents. J Am Soc Echocard 1994; 7: 347-354.

Ward B, Baker AC, Humphrey VF. Nonlinear propagation applied to the improvement of resolution in diagnostic medical ultrasound. J Ac Soc Am 1997; 101: 143-154.

Ward B, Whittingham T. Tissue harmonic imaging: what is it and how does it work? BMUS Bull 1999; 7: 7-14.

Webb S. The physics of medical imaging. Adam Hilger, Bristol UK, 1988.

Wei K, Skyba DM, Firschke C, Jayaweera AR, Lindner JR, Kaul S. Interactions between microbubbles and ultrasound: *In vitro* and *in vivo* observations. J Am Coll Cardiol 1997; 29: 1081-1088.

Wei K, Jayaweera AR, Firoozan S, Linka A, Skyba DM, Kaul S. Quantification of Myocardial blood flow with ultrasound-induced destruction of microbubbles administered as a constant venous infusion. Circulation 1998; 97: 473-483.

Wells PNT. Biomedical ultrasonics. Academic Press, London UK, 1977.

West JB. Best and Taylor's physiological basis of medical practice. Williams & Wilkins, London, UK, 1985.

Wiencek JG, Feinstein SB, Walker R, Aronson S. Pitfalls in Quantitative Contrast Echocardiography: The Steps to Quantitation of Perfusion. J Am Soc Echocardiog 1993;6:395-416.

Williams DD, Miller RR. An instrument fro on-stream stripping and gas chromatographic determination of dissolved gases in liquids. Anal Chem 1962;34: 657-659.

Wilson B, Shung KK, Hete B, Levene H, Barnhart JL. A feasibility study on quantitating myocardial perfusion with Albunex, an ultrasonic contrast agent. Ultrasound Med Biol 1993; 19: 181-191.

Wu J, Tong J. Experimental study of stability of a contrast agent in an ultrasound field. Ultrasound Med Biol 1998; 24: 257-265.

Appendix A: Matlab programme

```
filename = input('Enter the name of the file: ','s');        input the filename, number of lines, frames, and batches
nbRays = str2num(input('Enter the number of rays: ','s'));
nbframes = str2num(input('Enter the number of frames: ','s'));
nbbatches = str2num(input('Enter the number of batches: ','s'));
namecode = filename(:,1);                                    decode the encoded settings from the filename
cyclescode = filename(:,2);
frequencycode = filename(:,3);
micode = str2num(filename(:,4));
numbercode = filename(:,5);
for q = 1:6
        if q == 6
                cycles = setstr(51);
        elseif  q == 5
                cycles = setstr(97);
        else
                cycles = setstr(48+2*q);
        end
frequencytable = [1.17 1.23 1.33 1.45 1.6 1.78 2.02 2.15 2.33 2.52 2.65 2.75 3.02 3.18 3.28 3.48 3.05 3.0 3.1 2.75 2.88 3.02
3.18 3.34 3.54 3.76 3.98 4.28 4.53 4.16;
                1.2 1.29 1.41 1.52 1.68 1.84 2.02 2.15 2.25 2.34 2.56 2.7 2.97 3.07 3.14 3.27 3.05 3.0 3.1 2.75 2.88
3.02 3.18 3.34 3.52 3.74 3.98 4.16 4.32 4.16;
                1.17 1.34 1.45 1.57 1.67 1.83 2.02 2.1 2.16 2.26 2.45 2.63 2.9 2.97 3.07 3.18 3.05 3.0 3.1 2.75 2.88
2.98 3.15 3.3 3.46 3.66 3.88 4.05 4.28 4.16;
                1.17 1.23 1.52 1.64 1.77 1.9 2.02 2.08 2.12 2.16 2.3 2.2 2.48 2.64 2.7 2.86 3.05 3.0 3.1 2.75 2.8 2.9
3.04 3.15 3.24 3.4 3.6 3.82 3.96 4.16];
                                                             insert transmit frequencies
finalfilename = sprintf('%s%s%s%dha1.txt',namecode,cycles,numbercode,nbframes); fprintf('%s',finalfilename);
fid = fopen(finalfilename,'r+');                             insert results filename
if fid == -1
        fid = fopen(finalfilename,'w');
end
status = fseek(fid,0,'eof');
fprintf(fid,'%s','mi/freqency');
if cycles == '4'                                             choose the row from the frequency table that corresponds to each pulse length
        r = 2;
elseif cycles == '3'
        r = 3;
```

```
elseif cycles == '2'
        r = 4;
else
        r = 1;
end

for j = 1:30                                    loop for frequency
        if j <= 26                              set the frequency code carried on the filename

                frequencycode = setstr(j+96);
        else
                frequencycode = setstr(j+22);
        end
        batchfileNames = sprintf('%s%s%s%d%s%da.txt',namecode,cycles,frequencycode,micode,numbercode,nbframes);
        fid = fopen(batchfileNames, 'r');       open data file to check for its existence of the
                                                particular transmit frequency
        if fid == -1
                fid = fopen(batchfileNames,'w');
                status = fclose(fid);
                delete(batchfileNames);
                flag1(j) = 0;
        else
                status = fclose(fid);
                fid = fopen(finalfilename,'r+');
                if fid == -1
                        fid = fopen(finalfilename,'w');
                end
                status = fseek(fid,0,'eof');
                fprintf(fid,'%s',frequencytable(r,j));
                flag1(j) = -1;
        end
end
for i = 1:7                                     loop for MI
        micode = i;
        fid = fopen(finalfilename,'r+');
        if fid == -1
                fid = fopen(finalfilename,'w');
        end
        status = fseek(fid,0,'eof');
        fprintf(fid,' \n%d',i);

        for j = 1:30                            loop for transmit frequency
                if j <= 26
                        frequencycode = setstr(j+96);
```

```
else
        frequencycode = setstr(j+22);
end
batchfileNames=sprintf('%s%s%s%d%s%da.txt',namecode,cycles,frequencycode,micode,numbercode,nbframes);
fprintf('%s',batchfileNames);      input the value –1 for missing files in the results file
fid = fopen(batchfileNames, 'r');
if fid == -1
        fid = fopen(batchfileNames,'w');
        status = fclose(fid);
        delete(batchfileNames);
        if flag1(j) == -1      set flags for missing data files
                fid = fopen(finalfilename,'r+');
                if fid == -1
                        fid = fopen(finalfilename,'w');
                end
                status = fseek(fid,0,'eof');
                fprintf(fid,' %d', flag1(j));
                status = fclose(fid);
        end
else
        status = fclose(fid);
        secfr = frequencytable(r,j)*2000000;      calculate 2nd harmonic frequency
        [b,a] = ellip(8,0.01,70,[secfr-500000 secfr+500000]*2/20000000);
                                                  calculate elliptic filter array
        [H,w] = freqz(b,a,512);                   plot filter in frequency domain
        table = zeros(256, nbRays * nbbatches);
        for k = 1:nbbatches                       loop for every batch
                s = setstr(k+96);
batchfileNames=sprintf('%s%s%s%d%s%d%s.txt',namecode,cycles,frequencycode,micode,numbercode,nbframes,s
);                                                open data file
                fprintf('%s',batchfileNames);
                fid = fopen(batchfileNames, 'r');
                [table1] = fscanf(fid,'%f');
                status = fclose(fid);
                nbEstimates = size(table1,1)/nbRays;
                for l = 1:nbRays
table(:,l+(k-1)*nbRays) = filter(b,a,table1((l-1)*nbEstimates+1:l*nbEstimates));
                                                  load filtered frame data to table
                end
        end
```

```
                    [n,m] = size(table);
                    Hilberttable = zeros(n,m);
                    for p = 1:m
                    Hilberttable(:,p) = Hilbert2(table(:,p));      apply Hilbert transform
                    end
                    Hilberttable = abs(Hilberttable);              rectify table
                    for l = 0:(nbbatches-1)
                            res1 = 0;
                            count1 = 0;
                            HilbertIB(l+1) = 0;
                            for p = 1:nbRays
                                    for k = 1:n
                                    res1 = res1 + (Hilberttable(k,p + l * nbRays))^2;
                                            count1 = count1 +1;
                                    end

                            end
                    HilbertIB(l+1) = res1 / count1;   calculate backscatter intensity at each
                                                      point
                    end
                    totalHilbertIB = mean(HilbertIB)               calculate average backscatter
                                                                   intensity
                    fid = fopen(finalfilename,'r+');
                    if fid == -1
                            fid = fopen(finalfilename,'w');
                    end
                    status = fseek(fid,0,'eof');
                    fprintf(fid,' %e',totalHilbertIB);             download to results file
                    status = fclose(fid);
            end
    end
end
end
```

Appendix B: List of publications

Papers

V Sboros, CM Moran, T Anderson, SD Pye, IC Macleod, AM Millar, WN McDicken. "Evaluation of an experimental system for the in-vitro assessment of ultrasonic contrast agents" Ultrasound in Medicine and Biology (in press).

Abstracts

V Sboros, CM Moran, T Anderson, SD Pye, KAA Fox, WN McDicken. "Studying the behaviour of individual contrast agent scatterers" Echocardiography, Vol 15, No. 8 (part 2), pp. S102, 1998.

Conference presentations

1) V Sboros, CM Moran, T Anderson, A Criton, M Averkiou, WN McDicken. "A system for the study of individual Contrast Agent Scatterers" The Physics and Technology of Ultrasound, March 30-31, 1999, York, England.
2) V Sboros, CM Moran, T Anderson, KAA Fox, WN McDicken. "Setting up an ultrasonic scanner for contrast myocardial perfusion studies" European Society of Cardiology, August 22-26, 1998, Vienna, Austria (poster).
3) V Sboros, CM Moran, IC Macleod, WB Geake, DH Glass, AM Millar, T Anderson, GR Sutherland, WN McDicken. "The effect of varying both the partial pressure of oxygen in the surrounding solution and acoustic pressure on a variety of myocardial contrast agents: An in-vitro study based on integrated backscatter analysis." European Society of Cardiology, August 24-28, 1997, Stockholm, Sweden (poster).
4) V Sboros, CM Moran, IC Macleod, WB Geake, DH Glass, AM Millar, T Anderson, GR Sutherland, WN McDicken. "An investigation of ultrasonic contrast agents' backscattering properties when introduced into solutions with

varying oxygen levels and different ultrasonic pressures." 2nd Thoraxcenter European Symposium on Ultrasound Contrast Imaging, 23-24 January, 1997, Rotterdam, The Netherlands.

5) V Sboros, CM Moran, IC Macleod, DH Glass, AM Millar, GR Sutherland, WN McDicken. "An in-vitro comparison of ultrasonic contrast agents when introduced into solutions with varying oxygen levels." British Medical Ultrasound Society 28th annual scientific meeting, 11-13 December, 1996, Edinburgh, Scotland.